THE REDUCTION AND DISSOLUTION OF MANGANESE(III) AND (IV) OXIDES BY ORGANICS

Thesis by

Alan Thomas Stone

In Partial Fulfillment of the Requirements

for the Degree of

Doctor of Philosophy

California Institute of Technology

Pasadena, California

1983

(Submitted January 4, 1983)

PREFACE

This thesis begins with a review of the chemistry pertinent to the study of the dissolution of manganese oxides by organics (Chapters 2, 3, and 4). The reader primarily interested in the experimental results should go directly to Chapter 5.

Chapter	
1	INTRODUCTION
2 3 4	CHEMICAL REVIEW
5 6 7 8	EXPERIMENTAL DESIGN AND RESULTS
9	CONCLUSIONS

ACKNOWLEDGEMENTS

I wish to thank my advisor James J. Morgan for directing his attention towards my project and my welfare, and for allowing me freedom and flexibility in research. I would also like to thank those who encouraged me to enter this work: my mother, my father, Rena Zafiriou, and George Helz.

A number of fellow students and associates contributed to this work through their advice, support, and friendship: Howard Liljestrand, Jim Young, Jim Hunt, Steve Johnston, Windsor Sung, Scott Boyce, Bruce Faust, Roger Bales, Connie Senior, and many others. Michael Barcelona and Simon Davies provided direction and much encouragement.

Michael Hoffmann, Fred Anson, George Rossman, and John List kindly served on my examining committees. Michael Hoffmann's continual support and interest is greatly appreciated. Robert Koh helped with computational problems, both in person and indirectly through the program MAGIC. George Rossman, Roger Aines, Heinz Lowenstam, and Sten Samson assisted me in characterizing manganese oxides, and their help and enthusiasm was appreciated.

Discussions with researchers from other institutions, especially Walter Schneider, David Waite, and William Sunda were quite helpful.

The staff of Keck Labs went to great lengths to assist with whatever problems arose, especially Elaine Granger and Joan Matthews.

I would like to thank my family for following my progress, and also Marty Gould, Dan Zwillinger, and the Alams (Alam, Natasha, and Mishi), close friends who always welcomed my company.

Financial support from the Jessie Smith Noyes Foundation Fellowship, Union Oil of California, and the President's Fund is gratefully acknowledged.

ABSTRACT

Although it is known that manganese oxides are solubilized by reduction in anoxic waters, the chemical processes are poorly understood. A study of the reduction and dissolution of manganese oxide suspensions by twenty-seven organic substrates that have chemical structures similar to those of natural organics was undertaken to determine the rates and mechanisms of the solubilization reactions.

Dissolution of suspensions by hydroquinone in the pH range 6.5 < pH < 8.5 is described by the following experimental rate law:

$$\frac{d[Mn^{2+}]}{dt} = k_1\{H^+\}^{0.46}[HQ]^{1.0}(Mn_T-[Mn^{2+}])$$

where $[Mn^{2+}]$ is the amount of dissolved manganese, [HQ] is the hydroquinone concentration, and Mn_T is the initial amount of manganese oxide. The apparent activation energy of the reaction was found to be +37 kJ/mole. The Mn(III,IV) oxide suspension was prepared by oxidizing a $Mn(OH)_2$(s.) suspension with oxygen, and has a composition characterized by $MnO_{1.66}$. Suspension particles were between 0.2 and 1.0 microns in diameter. Calcium and phosphate were found to inhibit the dissolution reaction, by adsorbing on the oxide surface.

Dihydroxybenzenes and methoxyphenols dissolved the suspensions at appreciable rates. Of the aliphatic substrates examined, only ascorbate, oxalate, and pyruvate dissolved the oxide. Dissolution by

marine fulvic acid was found to be photocatalyzed.

A model was developed to explain the observed rate dependence and the relative reactivity of different organic substrates. The model assumes that complexes between substrate and surface sites form prior to electron transfer and dissolution. The pH dependence is not explained by this model; involvement of H^+ in the dissolution of reduced surface sites may be responsible for the observed fractional order with respect to H^+.

TABLE OF CONTENTS

Chapter TABLE OF CONTENTS (Continued) Page

Chapter TABLE OF CONTENTS (Continued) Page

Chapter TABLE OF CONTENTS (Continued) Page

LIST OF TABLES

LIST OF TABLES (Continued)

LIST OF FIGURES

Figure LIST OF FIGURES (Continued) Page

Figure LIST OF FIGURES (Continued) Page

Figure LIST OF FIGURES (Continued) Page

Figure LIST OF FIGURES (Continued) Page

Figure LIST OF FIGURES (Continued) Page

CHAPTER 1

INTRODUCTION

1.1 General Comments

Three oxidation states of manganese are found in natural waters: II, III, and IV. The relative stability of each oxidation state depends upon the oxidation potential (E_h) and the pH. Figure 1.1 shows that for solutions in equilibrium with atmospheric oxygen (the upper dashed line), $MnO_2(s)$ predominates. For fully anoxic solutions (the lower dashed line), Mn^{II} species predominate: Mn^{2+} and $Mn(OH)_2(s)$ in carbonate-free waters, Mn^{2+} and $MnCO_3(s)$ in the presence of carbonate. Mn^{III} phases (such as MnOOH(s)) and phases containing manganese in more than one oxidation state (such as $Mn_3O_4(s)$) can be formed at intermediate oxidation potentials.

When E_h-pH conditions are changed, manganese is transformed into the phase most stable under the new conditions, provided that suitable reaction pathways exist. Consider, for example, the following reactions:

1.1 $$MnOOH(s) + e^- + 3H^+ \rightleftharpoons Mn^{2+} + 2H_2O$$

1.2 $$MnO_2(s) + 2e^- + 4H^+ \rightleftharpoons Mn^{2+} + 2H_2O.$$

Addition of excess reductant to waters containing $MnO_2(s)$ and MnOOH(s) causes the forward reaction to occur, while oxygenation of anoxic solution results in reaction in the opposite direction. The

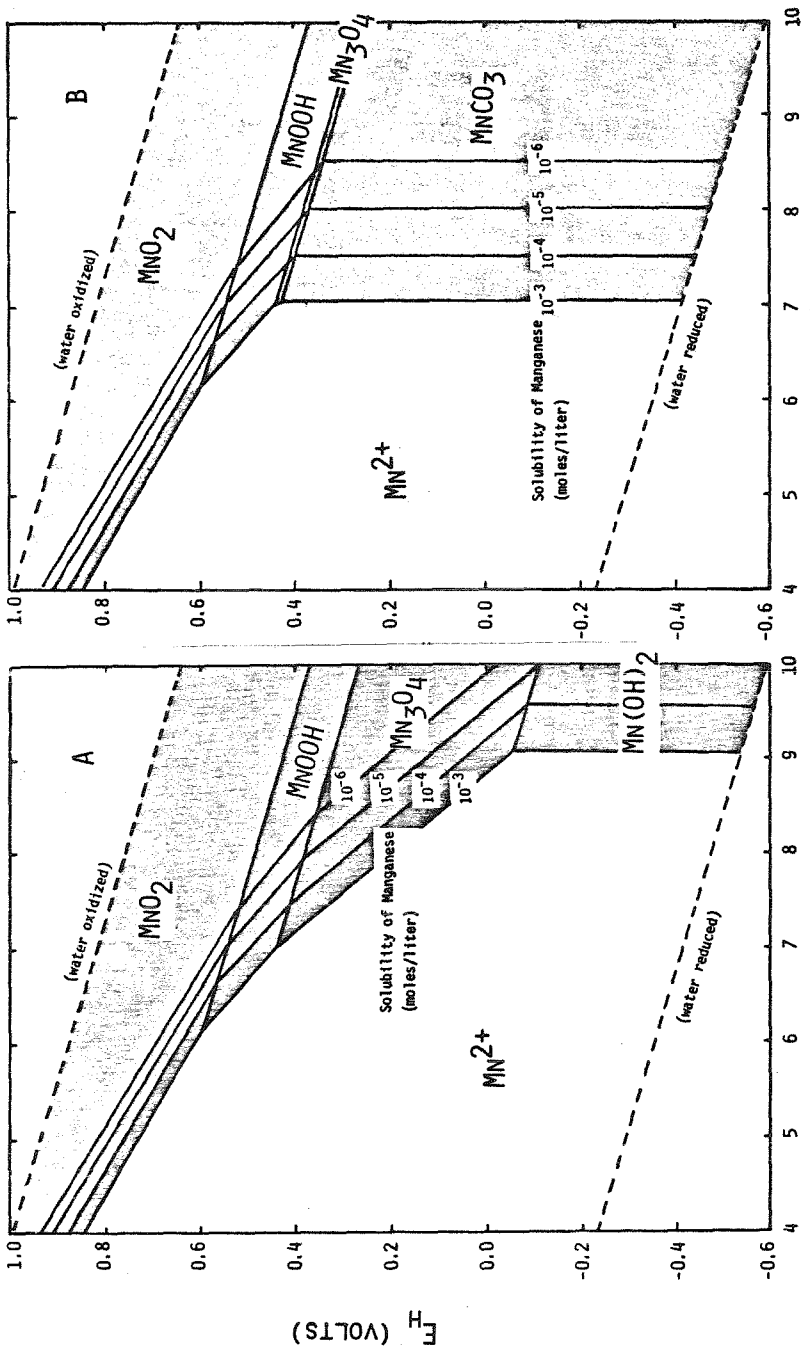

Figure 1.1 E_h-pH diagrams for (A) the Mn-H_2O system at 25^oC, 1 atm., and for (B) the Mn-CO_2-H_2O system in equilibrium with $10^{-3.5}$atm. CO_2. Solid phases considered are pyrochroite ($Mn(OH)_2(s)$), rhodochrosite ($MnCO_3(s)$), hausmannite ($Mn_3O_4(s)$), manganite (MnOOH(s)), and pyrolusite ($MnO_2(s)$).

forward reactions form dissolved Mn^{2+}, greatly increasing the mobility of manganese.

The equilibrium states of manganese are relatively well known (Bricker, 1965) and most recent work has focused instead on the rates at which redox reactions such as 1.1 and 1.2 occur. Oxygenation of Mn^{2+} to manganese (III) and (IV) oxides has been studied extensively both in the laboratory and under natural conditions. Rate laws for the oxygenation reaction have been formulated, and the effects of surfaces and complexing agents on the reaction rate explored (Morgan, 1964; Wilson, 1980; Sung, 1981). Bacterial mediation of the oxygenation reaction in natural waters has been postulated (Emerson et al., 1979, 1982).

The reverse reaction, in contrast, is little understood, and has been examined in only a few qualitative studies (see Section 4.6). This thesis examines the reduction and dissolution of manganese oxides by organics in detail. In the chapters that follow, factors that affect the rate of dissolution under natural conditions are systematically explored, so that predictions can be made concerning the mobility of manganese in different environmental situations.

1.2 Redox Reactions in Natural Waters

Changes in free energy (ΔG) for reduction of different natural oxidants differ considerably. Consider, for example, the following four reactions (Stumm and Morgan, 1981):

		E^o(pH 0.0)	$E^{o\prime}$(pH 7.0)
1.3	$\frac{1}{4}O_2(s) + H^+ + e^- = \frac{1}{2}H_2O$	+1.229 volt	+0.815 volt
1.4	$\frac{1}{2}MnO_2(s) + 2H^+ + e^- = \frac{1}{2}Mn^{2+} + H_2O$	+1.229	+0.401
1.5	$MnOOH(s) + 3H^+ + e^- = Mn^{2+} + 2H_2O$	+1.50	+0.257
1.6	$FeOOH(s) + 3H^+ + e^- = Fe^{2+} + 2H_2O$	+0.945	-0.297

For oxidants commonly found in natural waters, the energy yield per mole of of electrons (at pH 7.0) decreases in the order oxygen > manganese oxides $\tilde{>}$ nitrate > iron oxides > sulfate (Stumm and Morgan, 1981). If suitable reaction pathways are available, the strongest oxidant is consumed first, followed by the next strongest member of this series. In systems containing abundant organic substrate that are sealed off from the atmosphere, oxygen is depleted, followed by other oxidants in turn. In sediments where oxygen availability is limited by diffusion from overlying waters, oxidants are consumed at increasing depth in the order outlined above (Froelich et al., 1979). Thus, once oxygen is depleted, manganese oxides are the strongest oxidants, providing the greatest energy yield per mole of available reductant.

If the overall free energy for reaction of an oxidant with a reductant is negative, the reaction is thermodynamically favorable, regardless of whether or not stronger oxidants are available. Kinetics are therefore important. If reduction of the strongest oxidant is quite slow, other oxidants may be consumed. Situations may exist where iron and manganese oxides are reduced, despite a significant oxygen concentration.

1.3 Solubilization of Manganese Oxides in Nature

Iron and manganese oxides are reduced and dissolved in anoxic systems when enough natural organic substrate is available. High levels of Fe^{II} and Mn^{II} are undesirable in water supplies since they stain fixtures and laundry upon oxygenation, and are associated with the growth of microorganisms (O'Connor, 1971). Removal is performed by oxidation to insoluble oxides, followed by filtration (O'Connor, 1971).

A number of situations exist where Mn(III) and Mn(IV) oxides, formed in oxygenated environments, come in contact with oxygen-depleted, organic-rich waters. In Saanich Inlet (British Columbia) and the Black Sea, restricted circulation results in anoxic bottom waters. In both cases, a manganese oxide particulate layer is formed some distance above the oxic-anoxic boundary (Spencer and Brewer, 1971; Emerson et al., 1979). Manganese oxide particulates that settle into the anoxic zone are reduced and dissolved. Mn^{2+} formed in this manner moves upward by advection and diffusion until the oxygen concentration is high enough for reoxidation. In this way the particulate layer is continually regenerated.

More frequently, the oxic-anoxic boundary is found within the sediment column. Organic detritus is incorporated into the sediment, and diffusion of oxygen is not sufficient to maintain oxic conditions below a certain depth. Once oxygen is depleted, manganese oxides are reduced and dissolved; dissolved manganese increases with increasing depth until limited by the solubility of rhodochrosite, $MnCO_3(s)$

(Li et al., 1969). Dissolved manganese diffuses upward until the oxygen concentration is high enough to reoxidize it. An enriched layer of manganese oxides is formed within the oxic layer by this process. The depth at which this layer forms depends upon the oxygen profile in the sediment, the rate of diffusion of dissolved manganese, and the rate of the oxygenation reaction (Froelich et al., 1979). These enriched crust and surface layers are not only important to manganese geochemistry, but also influence the distribution of trace metals such as cobalt, copper, and zinc (Murray and Brewer, 1977). Manganese oxides readily adsorb trace metals from seawater (Balistrieri and Murray, 1982).

Profiles of dissolved oxygen and manganese in pore waters, and of solid phase manganese oxides are shown schematically in Figure 1.2 (Froelich et al., 1979). The slopes of the profiles, as well as the depth of the manganese oxide enriched layer, reflect a steady-state condition. Changes in bottom water oxygen concentration or in the flux of organic matter to the sediment cause a shift in the profiles and the formation of a new steady-state. Movement of the oxic-anoxic boundary upward to shallower depths may submerse the oxide crust within a region of active reduction (Froelich et al., 1979).

The time required to reach a new steady-state after movement of the oxic-anoxic boundary was estimated by Froelich et al. (1979) using the depths of relict crusts and gradients of dissolved species in pore waters. It was found that pore water profiles in deep-sea sediments readjust to a 10 cm shift in the oxic-anoxic boundary in about a year,

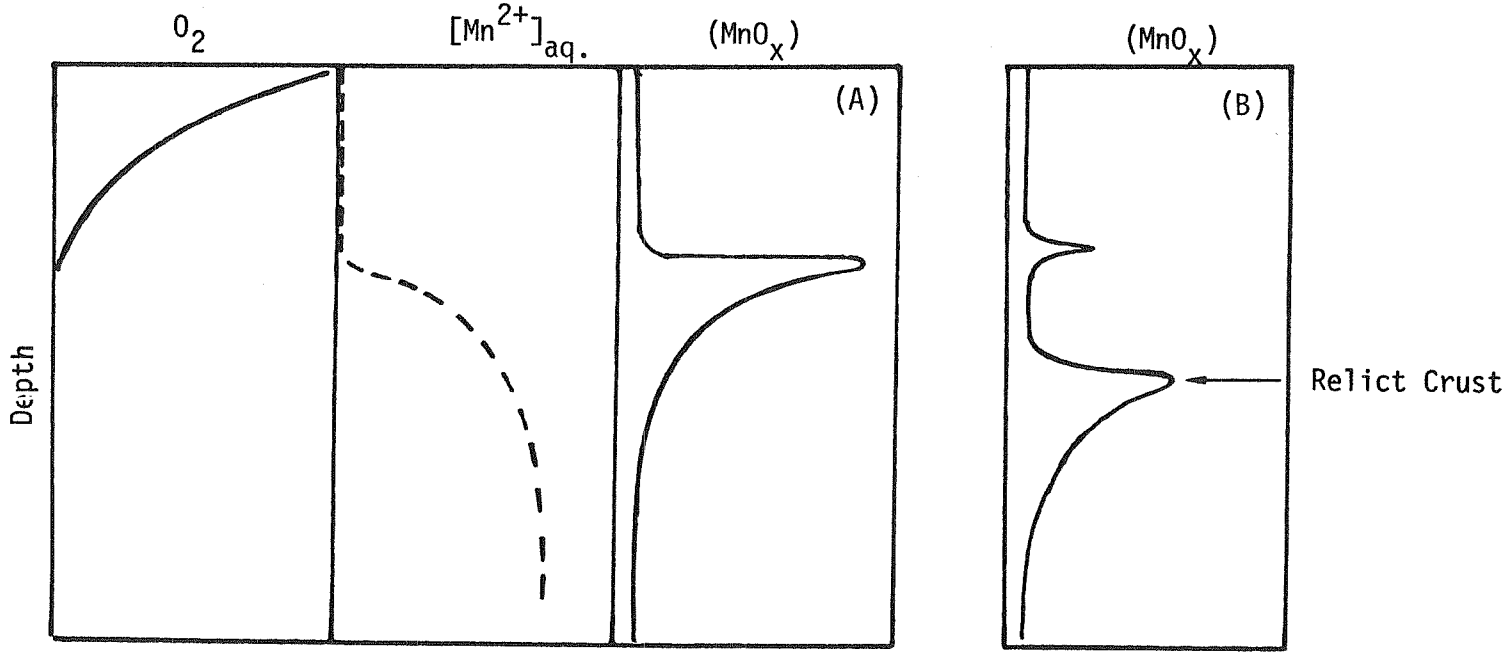

Figure 1.2 Pore water profiles of dissolved oxygen and manganese, and of solid manganese oxide at steady-state in a marine sediment (A). (B) shows a relict crust not yet at steady-state with the pore water profiles shown to the left. (Adapted from Froelich et al., 1979).

but that solid oxide layers take on the order of a 700 years to readjust. Their results imply that reduction and dissolution of manganese oxides in deep-sea sediments are extremely slow. The flux of organic detritus to deep-sea sediments is small, and therefore the organic matter content in such sediments is low.

Near-shore sediments receive a greater input of organic matter than deep-sea sediments, which may cause dissolution to occur more quickly. Balzer (1982) covered Baltic Sea sediment with a plexiglas bell jar, preventing downward diffusion of oxygen. The sediment originally contained a 3 cm thick manganese oxide enriched layer. In the course of a 100-day experiment, the oxic-anoxic boundary moved progressively upward as oxygen was depleted, and sulfide appeared in the bell jar. Dissolved manganese increased throughout the study, but accelerated when dissolved oxygen dropped to below 70% of its original value. After 100 days under the bell jar, the manganese oxide enriched layer was no longer present; reduction and dissolution were fast enough in this situation to completely dissolve the manganese oxides.

Near-shore crusts are dissolved more quickly than crusts in deep-sea sediments. Slow rates of dissolution in deep-sea sediments are probably caused by low amounts of organic detritus in the sediment, but other factors, such as the mineralogy of the oxides or their surface area, may also be responsible.

1.4 Natural Organic Compounds

The ability of natural organic compounds to reduce manganese oxides depends upon their chemical structure. Natural organics are

found in varying stages of decomposition of the source biological material (Stumm and Morgan, 1981). Oxidative degradation and polymerization reactions transform most simple biological molecules into complex structures. For this reason, the fraction of organic compounds having structures that are readily identified is small.

A number of metabolites and other biological molecules have been identified in natural waters and sediments, including amino acids, carbohydrates, lipids, heterocyclic compounds, vitamins, phenols, and quinones (Degens, 1965; Cranwell, 1975). Monosaccharides and sugar acids (uronic acids) are produced in large amounts by marine algae and are readily identified in marine sediments (Mopper and Larsson, 1978; Mopper et al., 1980). Biological compounds decompose at different rates, and some are sufficiently refractory (inert to reaction) that they are used as markers of the source material (Barnes and Barnes, 1978). Fatty acids, hydrocarbons, and pigments are commonly used for this purpose (Barnes and Barnes, 1978).

Organic matter in marine sediments is derived from settled particles, and has considerable resistance to chemical oxidation (Barcelona, 1980). Dissolved organics in pore waters are formed from in situ microbial reaction with insoluble organic detritus. Low molecular-weight metabolites such as formic, acetic, n-butyric, and iso-butyric acids have been measured at concentrations exceeding 2.0×10^{-4} M in reducing pore waters, and may make up as much as half of the total dissolved organic carbon (Barcelona, 1980). Glycolic, lactic, oxalic, and succinic acids have also been identified in

reducing sediments (Peltzer and Bada, 1981). These simple metabolites may be important reductants of inorganic species in sediments (Barcelona, 1980).

Many studies have attempted to identify structures of simple organics present in trace amounts in natural waters. Pitt et al. (1975) identified a variety of compounds in primary and secondary domestic sewage plant effluents, including hydroxybenzoic acids, phenol, p-cresol, catechol, o-phthalic acid, succinic acid, and oxalic acid. Although only a fraction of the total dissolved organic carbon, their structures may be similar to the uncharacterized fraction.

Humic substances, formed by oxidative degradation and polymerization of natural organics, are the predominant organic compounds in most environmental systems. The reader is referred to the reviews by Schnitzer and Kahn (1972,1978) and Gjessing (1976) for a complete description of their chemical and physical properties.

Humic acid is the fraction of humic substances that is soluble in dilute base but insoluble in acid, and fulvic acid is the fraction soluble in both acid and base (Steelink, 1977). Because of their large molecular weight (300-2000 for fulvic acids, 500- 100,000 for humic acids), characterization is difficult (Steelink, 1977). Chemical degradation by acid or base hydrolysis, or $KMnO_4$ or alkaline $CuSO_4$ oxidation breaks the macromolecules into smaller fragments that can be separated and identified (Christman and Ghassemi, 1966; Schnitzer and Kahn,1972; Liao et al., 1982). These studies indicate that humics contain a core structure of phenols and phenolic acids such

as hydroxybenzoic acids, vanillic acid, syringic acid, 3,4-dihydroxybenzoic acid, 3,5-dihydroxybenzoic acid, resorcinol, and catechol (Norwood et al., 1980). These aromatic groups are linked together by short, saturated aliphatic chains, possibly at 3 or more positions on the aromatic ring (Liao et al., 1982).

1.5 Reduction of Inorganic Species by Natural Organics

Natural organic compounds have been shown to reduce a variety of inorganic species. Soil fulvic acids reduce Hg(II) to Hg(0), Fe(III) to Fe(II), and I_2 to I^- (Skogerboe and Wilson, 1981). Reduction of $VO_3^-(V^V)$ to $VO^{2+}(V^{IV})$ by humic acid has been observed using ESR and shown to involve the formation of free radicals, probably semiquinones (Goodman and Cheshire, 1975; Wilson and Weber,1979; Senesi et al.,1977).

Iron and manganese oxides are reduced in anoxic waters, presumably by reaction with natural organics. Some laboratory and field studies have attempted to verify that these reactions do occur. Previous research on the reduction of manganese oxides by organics are reviewed in Section 4.6. Oxygenation of solutions containing iron and humic substances involves oxidation of Fe(II) to Fe(III) by oxygen, followed by reduction of Fe(III) to Fe(II) by organics. Theis and Singer (1974) showed that the rate of Fe(III) generation upon oxygenation is lowered by the presence of organic reductants, including humic materials. Miles and Brezonik (1981) found that iron increased the consumption of oxygen by lake humics. Reduction of Fe(III) to Fe(II) by lake humics was found to be photocatalyzed. In surface waters, iron is continually

cycled between the two oxidation states, catalyzing the oxidation of the humic material.

1.6 Applications

Listed below are a number of research areas which could benefit from the proposed study of dissolution of manganese oxides by organics.

(i) Geochemical fluxes of trace metals and radionuclides.

Reductive dissolution controls dissolved manganese concentrations in situations where oxides come in contact with anoxic waters. Dissolution not only mobilizes iron and manganese from ferromanganese oxides, but also other trace metal and radionuclides adsorbed on oxide surfaces or present as lattice impurities. Knowledge of rates of oxidation and dissolution at oxic-anoxic boundaries could be used to predict locations of enriched crusts in sediments.

(ii) Manganese availability to organisms.

Manganese must be in a dissolved form before uptake by organisms can occur, most likely as $Mn^{2+}(aq)$ (W. Sunda, pers. comm.). In many situations, the dissolution reaction will determine the concentration of $Mn^{2+}(aq)$ and therefore the bioavailability of manganese.

(iii) Removal of iron and manganese from water supplies.

Dissolved iron and manganese in organic-rich, anoxic waters are frequently removed by oxidation to insoluble oxides followed by

settling or filtration. Chlorine and oxygen are the most common oxidizing agents. If the concentration of reactive organics is quite high, continual reduction and dissolution may prevent oxide formation, and thwart removal.

(iv) The formation of humic material.

Oxidation by iron and manganese oxides may be an important degradative pathway for natural organics, and may influence the overall structures of the oxidized products that result. The persistence of some organics in natural systems may be determined by how quickly they are oxidized by these oxides.

(v) Corrosion

The slow step in the corrosion of many metals is not oxidation of the metal, but rather dissolution of a protective layer of oxide. Research into the dissolution of manganese oxides may provide insight into the dissolution of other oxides as well.

1.7 Organization of this Research

Manganese oxides are reduced and dissolved in situations where oxygen is depleted and the concentration of natural organics is high, greatly increasing the mobility of manganese. It is known that natural organics reduce a variety of inorganic species, including iron and manganese oxides. Many different chemical structures are present in natural organics, which differ considerably in reactivity. The rates and mechanism of reduction and dissolution of manganese oxides by a

variety of organics must be determined if the solubilization of manganese oxides under natural conditions is to be understood.

Chapters 2, 3, and 4 provide a chemical basis for understanding this reaction. The oxidation of organics in aqueous solution is reviewed, with particular attention given to oxidations by Mn(III) solute complexes. Reactions at oxide surfaces are then examined, highlighting differences between surface reactions and reactions in homogeneous solution.

Chapters 5 through 8 are the experimental portion of this thesis. The preparation and characterization of manganese oxide suspensions are described in Chapter 5, and Chapter 6 outlines procedures followed in the dissolution experiments. Reactions between hydroquinone and manganese oxide suspensions and the effects of prevalent chemical conditions on reaction rate are examined in Chapter 7. Chapter 8 discusses reduction and dissolution by a variety of organic substrates, including marine fulvic acid.

Experimental results are summarized in Chapter 9. The solubilization of manganese oxides in natural situations is discussed in light of these results.

CHAPTER 2

OXIDATION OF ORGANICS

2.1 Introduction

Organics having widely varying structures are present in natural waters, and their reactivity towards oxidation vary considerably. This chapter reviews ways in which organic compounds are oxidized in aqueous solution. Relationships between structure and reactivity are considered, so that organics that are most likely to reduce manganese oxides can be distinguished from organics inert to reaction.

Oxidation of natural organics by metal ion oxidants can dramatically change their structure. These reactions may be important in catalyzing the oxygenation of organics in natural waters and the formation of humic compounds from simple biological molecules.

2.2 Homolytic and Heterolytic Reactions

Organic compounds are oxidized through either the elimination of hydrogen or the replacement of hydrogen by a more electronegative element, typically oxygen (Sheldon and Kochi,1981). Considerable modification of the structure of an organic compound can occur following the initial oxidation step.

Two classes of oxidation reactions, homolytic and heterolytic, can be defined (Waters, 1964). Homolytic reactions disrupt electron-pairs by transferring a single electron from reductant to oxidant. The first oxidation product of a homolytic reaction is a reactive free-radical intermediate with an unpaired electron. Homolytic electron transfer

continues in a series of reactions until all unpaired electrons are eliminated. Dimerization, disproportionation, and chain reactions are characteristic of free radical reactions. Radical reactions are typically fast and require low activation energies (Waters, 1964). Oxidants in homolytic reactions are either free-radicals themselves or compounds containing atoms that can accommodate unpaired electrons.

Heterolytic reactions, in contrast, transfer electron pairs intact. Product molecules contain only complete electron pairs and are considerably less reactive than the intermediates formed by homolytic processes (Waters, 1964). Reaction rates are considerably lower, corresponding to higher activation energies. Heterolytic oxidants are electrophilic species that capture exposed electron pairs of oxygen, nitrogen, or sulfur containing groups, or pi-electrons of double-bonded compounds (Waters, 1964).

2.2A. Radical Reactions

Once generated by homolytic oxidation, radical reactions may propagate in a number of ways until termination reactions consume unpaired electrons, eliminating the reactive radical species. Typical radical reactions are listed in Table 2.1 (Waters and Littler, 1965). Reactions (2),(3), and (4) produce one radical for every radical consumed, and can therefore propagate many times and generate a variety of radical species before termination. Termination reactions ((5),(6),(7),and (8)) require combination of two radicals or electron transfer between the radical and a metal ion to eliminate unpaired electrons.

Table 2.1: Typical Radical Reactions

(Adapted from Waters and Littler, 1965)

Initiation Reactions

(1) Formation of free radicals by homolytic oxidation

$$M^{(n+1)+} + R\text{-}H \longrightarrow M^{n+} + R^{\bullet} + H^{+}$$

Propagation Reactions

(2) Reaction with oxygen

$$R^{\bullet} + O_2 \longrightarrow ROO^{\bullet}$$

$$ROO^{\bullet} + R\text{-}H \longrightarrow ROOH + R^{\bullet}$$

(3) Reaction with organics inert to (1)

$$R^{\bullet} + R'\text{-}H \longrightarrow R\text{-}H + R'^{\bullet}$$

(4) Polymerization

$$R^{\bullet} + R \longrightarrow R\text{-}R^{\bullet}$$

Termination Reactions

(5) Dimerization

$$R^{\bullet} + R^{\bullet} \longrightarrow R\text{-}R$$

(6) Disproportionation

$$R^{\bullet} + R^{\bullet} \longrightarrow R^{-} + R^{+}$$

(7) Oxidation of inorganic ions

$$R^{\bullet} + M^{(n-1)+} \longrightarrow R^{-} + M^{n+}$$

(8) Reduction of inorganic ions

$$R^{\bullet} + M^{(n+1)+} \longrightarrow R^{+} + M^{n+}$$

A variety of different radical reactions compete to determine the eventual distribution of oxidized products. Propagation reactions (2),(3), and (4) are unimolecular with respect to free radical concentration, but termination reactions (5) and (6) are bimolecular. The rates of termination reactions therefore increase relative to rates of propagation reactions as radical concentrations are increased. Polymerization, for example, is more extensive when radical concentrations are low. Termination reactions typically have low activation energies, so propagation reactions must also have low activation energies if propagation is to occur (Huyser, 1970). When the concentration of metal ions capable of reactions (7) or (8) is high, radicals are quickly quenched, and little propagation occurs.

2.2B. Structure/Reactivity Relationships

Molecular configuration and substituent groups influence the oxidation rate of organic substrates. In heterolytic oxidation reactions, charge separation accompanies formation of the activated complex. Molecules in which the developing charge is delocalized by resonance or reduced in magnitude by inductive effects are more readily oxidized.

Substituent groups containing atoms of different electronegativities create bond dipoles. Field effects arise from the interaction of the partial charge separation of the bond dipole with charge separation developing at another site in the molecule (Carey and Sundberg, 1977). Inductive effects arise when the bond dipole of a substituent group causes the polarization of neighboring bonds, which

in turn polarize bonds in their vicinity. In general, polar substituents influence reactivity through field effects, rather than inductive effects (Carey and Sundberg, 1977).

Ring substituents dramatically affect the reactivity of benzenoid compounds, because of their influence on electron distribution in the aromatic ring. Alkyl, alkoxy, and hydroxy substituents are electron-donating groups which activate reaction of the ring with electrophiles. Hydroxy and alkoxy groups are capable of resonance interaction with the ring, and are therefore particularly strong ring activating groups. Carbonyl groups such as aldehyde, ketone, ester, or carboxylic acid substituents are electron-withdrawing, and not capable of resonance. They are therefore deactivating. Nitro substituents are very strong electron-withdrawing groups, and strongly deactivate the ring towards reaction with electrophiles (Carey and Sundberg, 1977).

Homolytic reactions may involve abstraction of hydrogen atoms ($H^{\cdot}$) from reductant molecules. The reaction rate reflects the C-H bond dissociation energy of the group providing the hydrogen atom (Carey and Sundberg, 1977), because the bond is partially broken in the transition state. The ease of aliphatic hydrogen atom abstraction increases in the order primary < secondary < tertiary, reflecting relative C-H bond strengths. Vinyl and phenyl groups aid the abstraction of hydrogen atoms (Carey and Sundberg, 1977).

Many free-radical reactions are influenced by polar substituents in a manner similar to heterolytic reactions. Charge separation during activated complex formation, although smaller than in heterolytic

reactions, may be responsible for this effect. It is more likely, however, that polar substituents change bond-dissociation energies, which affects the ease of hydrogen atom abstraction (Carey and Sundberg, 1977).

2.3 Homolytic Oxidation of Phenolic Compounds

Most oxidations of phenolic compounds begin by generation of free radical species. Factors that influence the rate of radical formation therefore determine how quickly phenolics can be oxidized. The activation enthalpy ($\Delta H^{\ddagger}$) of any reaction cannot be lower than the overall enthalpy of reaction , $\Delta H_{rxn.}$ (Carey and Sundberg, 1977). When radical formation is highly endothermic, H is therefore large. This makes the activation energy large, and the reaction rate correspondingly low (Carey and Sundberg, 1977). A substrate that strongly stabilizes an unpaired electron generated by oxidation encourages electron transfer earlier in the reaction sequence because less molecular reorganization is required to reach the transition state. The activation energy is therefore lowered by stabilization of the product (Purcell and Kotz, 1977).

Abstraction of a hydrogen atom from phenols forms phenoxy radicals stabilized by resonance that distributes the unpaired electron over the entire aromatic ring (Figure 2.1). Ring substituents can further stabilize the phenoxy radical. Resonance structures drawn in Figure 2.1 for the phenoxy radical place the unpaired electron at the oxygen and at ortho- and para-carbons on the aromatic ring. ESR measurements identify these sites as having high spin density (localization of the

electron at these positions) , with density at the oxygen atom and para-carbons being twice that at ortho-carbons (Musso,1967).

Electron-donating ring substituents increase the stability of the radical. Alkyl substituents, for example, lower the spin density of the ring, thereby stabilizing the radical (McDonald and Hamilton, 1973). In addition, substituents can block intermolecular reactions by shielding high spin density sites on the ring. This is discussed in more detail in Section 2.5.

2.4 Dihydroxybenzenes

Dihydroxybenzenes are particularly reactive towards oxidation. Oxygen anions at ortho- or para-positions provide the best resonance stabilization for phenoxy radicals; ESR measurements of ortho- and para- semiquinone radicals indicate that 60 to 65% of the spin density is localized on the oxygen atoms (McDonald and Hamilton, 1975). Semiquinone radicals are unusually stable, and ortho- and para-dihydroxybenzenes are easily oxidized. ESR measurements of meta-semiquinone radicals, in contrast, indicate that 82% of the spin density is distributed in the aromatic ring (McDonald and Hamilton, 1973). Resonance stabilization that is possible in ortho- and para-substituted radicals is not possible for meta-substituted ones. The reactivity of meta-dihydroxybenzenes is not much greater than monophenols, and they are oxidized more slowly than ortho- and para-dihydroxybenzenes (Musso, 1967).

Oxidation of ortho- and para-semiquinones by an additional equivalent forms the corresponding quinone (Figure 2.2). The overall

Figure 2.1 Resonance forms of the phenoxy radical.

(Mihailovic and Cekovic, 1971)

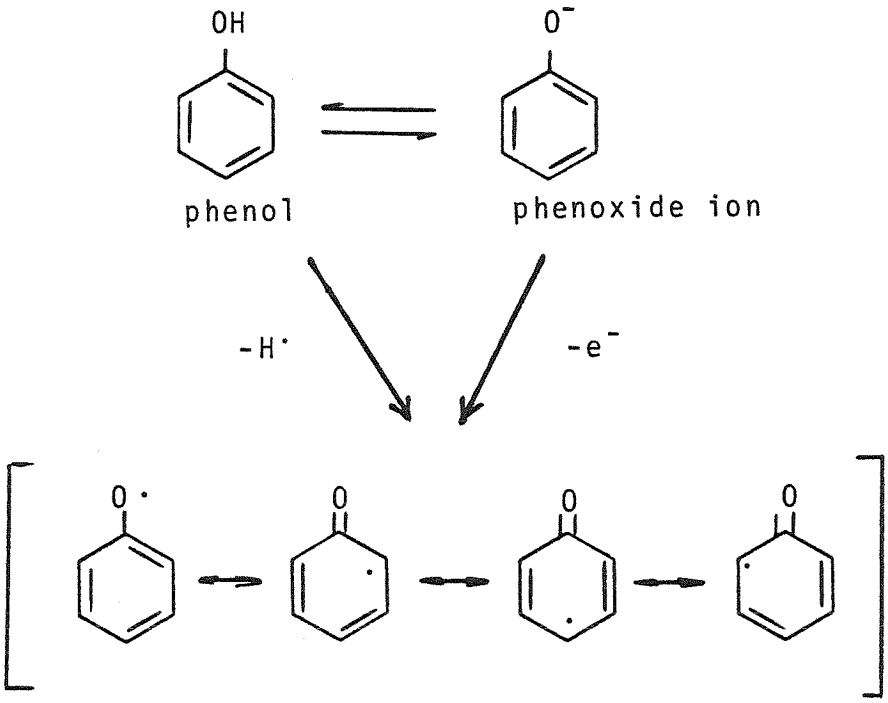

Figure 2.2 Redox States of Dihydroxybenzenes.

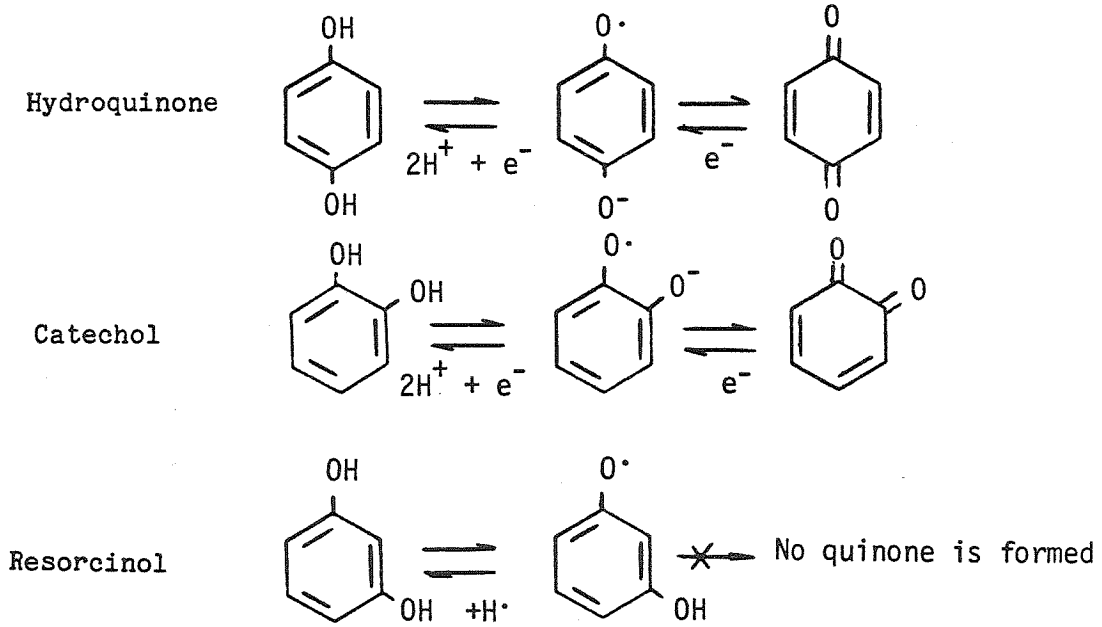

free energy of forming quinones from semiquinones is quite low, and conversion upon addition of oxidant is quite rapid (Musso, 1967). This is responsible in part for the enhanced reactivity of ortho- and para-dihydroxybenzenes. Radicals generated from meta-dihydroxybenzenes cannot be oxidized to quinone products.

The oxidation of hydroquinones and catechols to form quinones is sufficiently facile that irreversible side reactions are minimized, and standard redox potentials can be defined. Table 2.2 lists standard and half-wave potentials for half-cell reactions written as:

$$\text{Quinone} + 2H^+ + 2e^- = \text{Dihydroxybenzene}.$$

Decreasing values of E^o indicate an increase in the strength of the reductant. Hydroquinone has a slightly lower E^o than catechol, and is therefore a stronger reductant. Half-wave potentials of orcinol and resorcinol (for the phenoxy radical/dihydroxybenzene redox couple) are higher than for catechol and hydroquinone, and therefore the overall free energy of the oxidation reaction is lower.

Redox and protonation equilibria for hydroquinone are listed in Table 2.3. At pH 7, hydroquinone is a neutral species and the semiquinone radical is an anion (equations 1,2, and 3). Two semiquinone radicals can react to form hydroquinone and p-benzoquinone, by the disproportionation reaction (equation 5). The equilibrium constant for (5) is quite low, meaning that the concentration of semiquinone radicals at equilibrium is quite low. Ring substituents

Table 2.2 Standard and Half-Wave Potentials of Dihydroxybenzenes

The electrode reaction is:

Quinone + $2H^+$ + $2e^-$ = Dihydroxybenzene E^o

Dihydroxybenzene	E^o (vs. SHE)	$E_{1/2}$*
Hydroxyhydroquinone	.594 (2) volts	- volts
Hydroquinone	.699 (1)	.560 (1)
2,5-Dihydroxybenzoic Acid	.77 (3)	-
Catechol	.792 (1)	.600 (1)
3,4-Dihydroxybenzoic Acid	.883 (2)	-
4-Nitrocatechol	.95 (3)	-
Orcinol **	-	.700 (1)
Resorcinol **	-	.800 (1)

(1) H. Musso and H. Dopp (1967)

(2) W.A. Clark (1960)

(3) Mentasti and Pelizzetti (1976)

* Half-Wave Potential at pH = 0.

** $E_{1/2}$ is for the reaction:

(Phenoxy Radical + e^- = meta-Dihydroxybenzene)

Table 2.3 Hydroquinone Protonationation and Redox Equilibria

(1)	$H_2Q = HQ^- + H^+$	pKa1 = 10.1	Serjeant and Dempsey (1979)
(2)	$HQ^- = Q^{2-} + H^+$	pKa2 = 11.06	" "
(3)	$HQ^{\cdot} = Q^{\cdot -} + H^+$	pKa = 3.7	Smith and Carrington (1967)
(4)	$H_2Q = Q + 2H^+ + 2e^-$	E^o = .699 v.	Musso and Dopp (1967)
(5)	$H_2Q + Q = 2Q^{\cdot -} + 2H^+$	$\log_{10}K$ = -20.43	Bishop and Tong (1965)

where H_2Q = Hydroquinone

$Q^{\cdot -}$ = Semiquinone Radical Anion

Q = p-Benzoquinone

change the magnitude of the disproportionation constant by changing the relative stability of the three oxidation states. Electronegative substituents increase the stability of the semiquinone radical anion with respect to disproportionation (Bishop and Tong, 1965). At pH's above 11, the disproportionation reaction is quite fast (Bishop and Tong, 1965). Disproportionation at neutral pH values is commonly assumed to be slower than reaction of semiquinone radicals with oxidant species (Ono et al., 1977).

In alkaline solution, hydroxide ion adds to p-benzoquinone by both a reversible and an irreversible reaction (Musso, 1977) as illustrated in figure 2.3. Irreversible addition forms trihydroxybenzene (A), which has a lower potential than hydroquinone (Table 2.2). It reacts quickly with oxidant to form hydroxybenzoquinone, product (B) (Musso, 1967). Because of reactions (1) and (2) of Figure 2.3, hydroquinone consumes more than two equivalents of oxidant when oxidized in alkaline solution.

2.5 Coupling Reactions

Only ortho- and para- semiquinone radicals can react with oxidant or disproportionate to form stable quinones; for other phenoxy radicals, other reactions consume the unstable radical. Addition of the phenoxy radical to unreacted substrate, to another phenoxy radical, or to oxidized product is frequently observed. Coupling reactions, as they are termed, can form a complex mixture of oxidation products.

Alkaline potassium ferricyanide ($K_3Fe(CN)_6$) is a commonly used one-electron oxidant. Figure 2.4 illustrates the products formed

Figure 2.3 Addition of hydroxide ion to p-benzoquinone.

(From Musso, 1967)

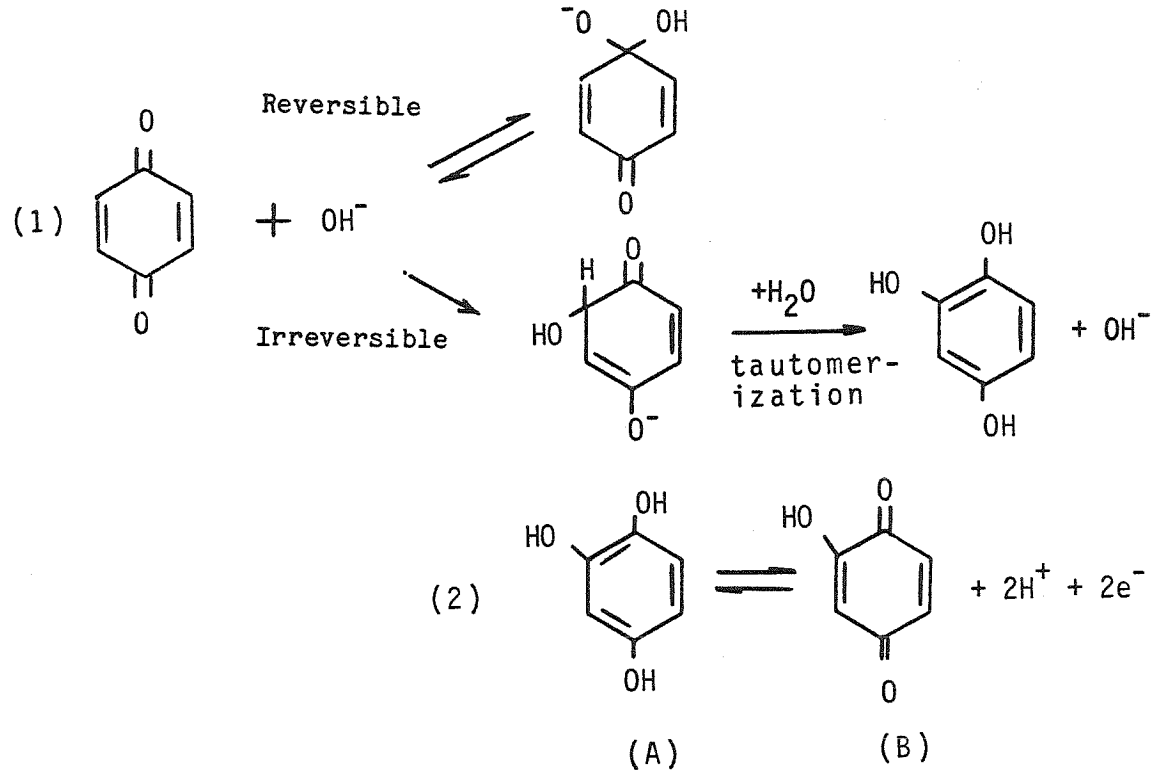

Figure 2.4 Oxidation of p-cresol by alkaline $K_3Fe(CN)_6$.

(Musso, 1967)

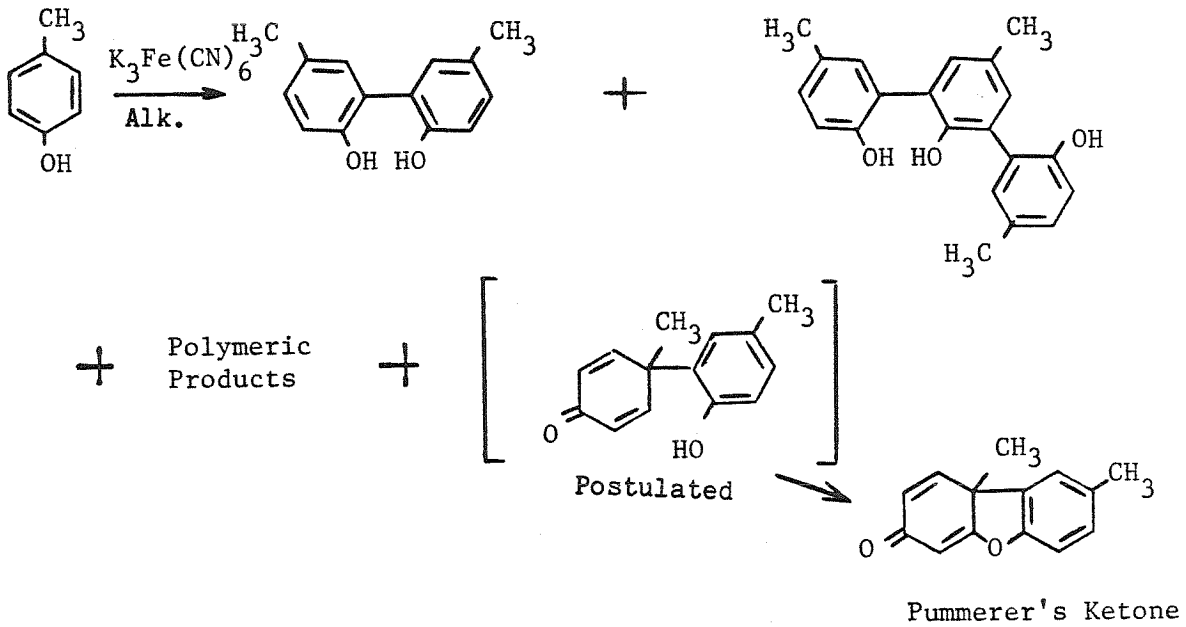

Figure 2.5 Oxidation of Orcinol by $K_3Fe(CN)_6$.

(Musso et al., 1965)

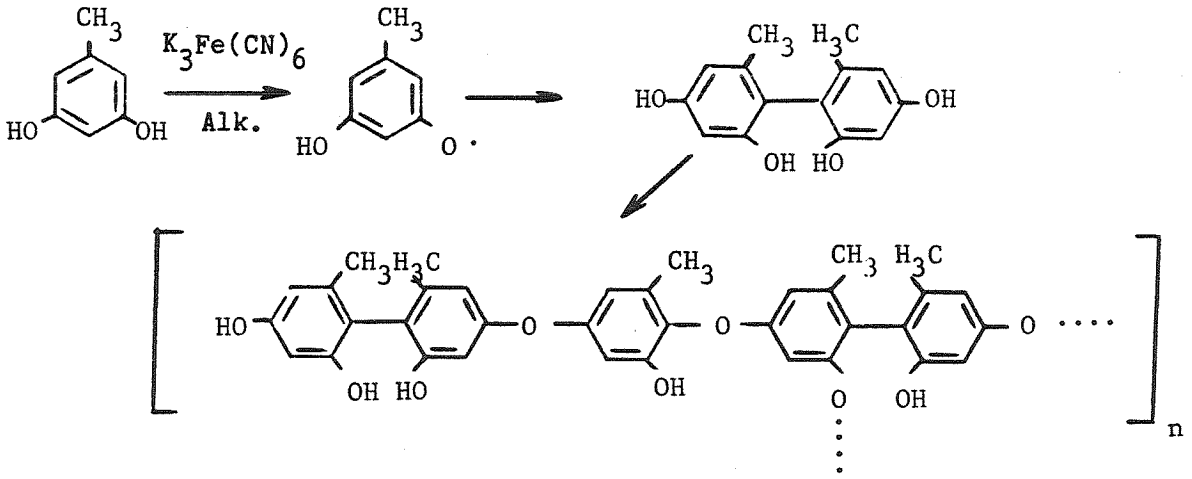

when p-cresol is oxidized by this reagent (Musso, 1967). Dimers linked through the phenolic oxygen, or through ortho- or para- ring positions are formed. Further oxidation of the dimer can lead to intramolecular coupling, forming compounds such as Pummerer's ketone. Polymerization occurs when dimers formed by coupling are themselves oxidized and coupled.

As mentioned in Section 2.3, meta-hydroxybenzenes cannot form quinone oxidation products, but react in a manner analogous to monohydroxy phenols. Figure 2.5 illustrates products formed by oxidation of 3,5-dihydroxytoluene (orcinol). Dimeric and polymeric products are formed (Musso et al., 1965), just as in the oxidation of monophenols.

Figure 2.6 lists products that can be formed by coupling two phenoxy radicals (Musso, 1967). Dimers may form by pairing of two radicals, or by radical addition onto non-radical substrate molecules (Mihailovic and Cekovic, 1971). Coupling between two phenoxy oxygens to form the peroxide dimer (3) has been postulated, but such products have never been identified. The density of the unpaired electron is greatest at the para-carbon on the aromatic ring, and para-coupled products do in fact predominate (Musso, 1967). Tautomerization of the coupled products (4 through 7) forms fully aromatic products (8 through 12), which may themselves become oxidized (Musso, 1967).

A variety of phenoxy radical dimerization products have been observed (Mihailovic and Cekovic, 1971), and are illustrated in Table 2.4. Ortho- and para-carbons are the most reactive sites for coupling

Figure 2.6 Coupling of phenoxy radicals.

(Musso, 1967)

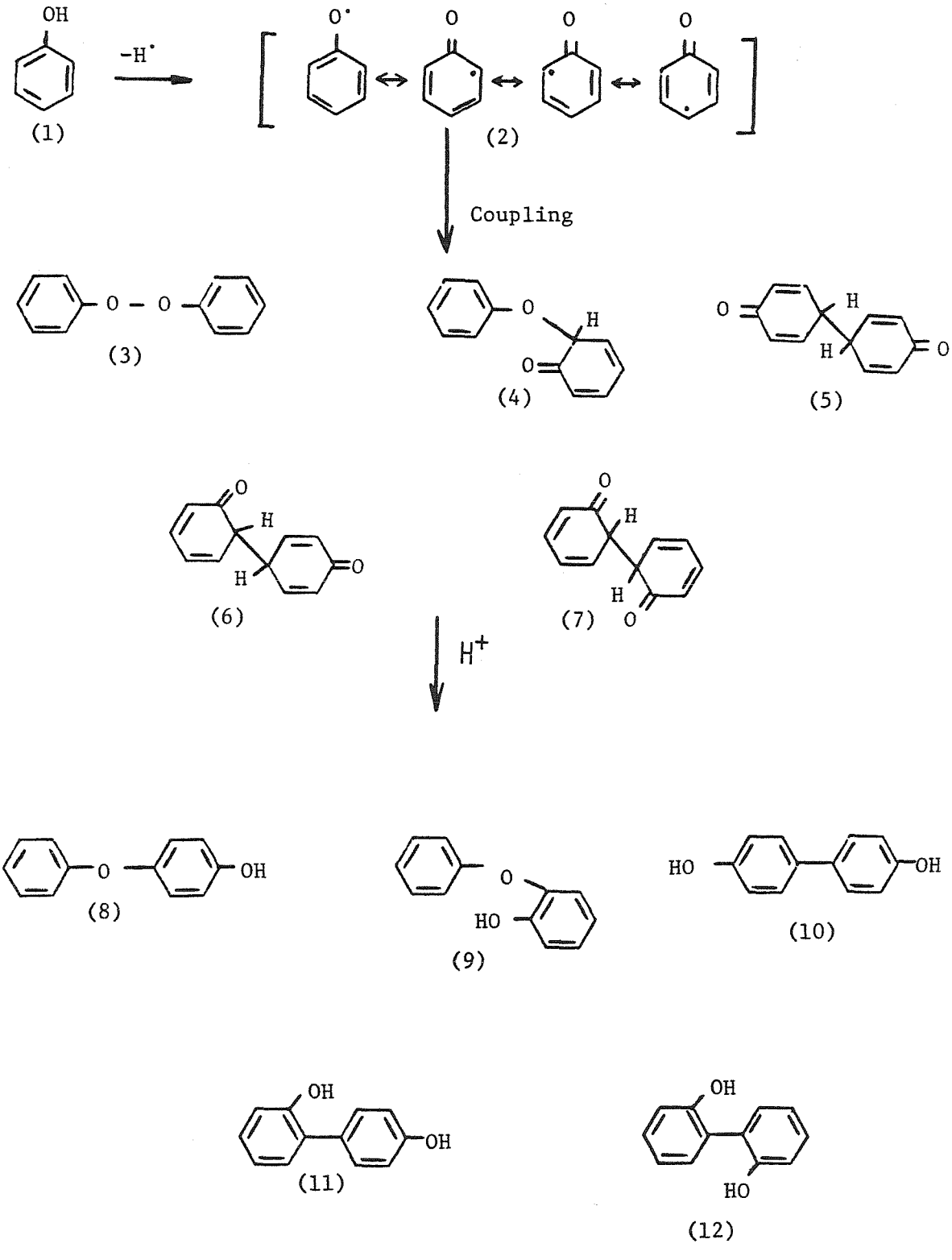

Table 2.4 Phenoxy Radical Dimerization Products.

(Mihailovic and Cekovic, 1971)

(1) Carbon-Carbon Coupling of Aromatic Carbons.

ortho-ortho: Species (7) in Figure 2.6
ortho-para: " (6) " " "
para-para: " (5) " " "

(2) Carbon-Carbon Coupling of Substituent α-Carbon Atoms (Hindered phenols)

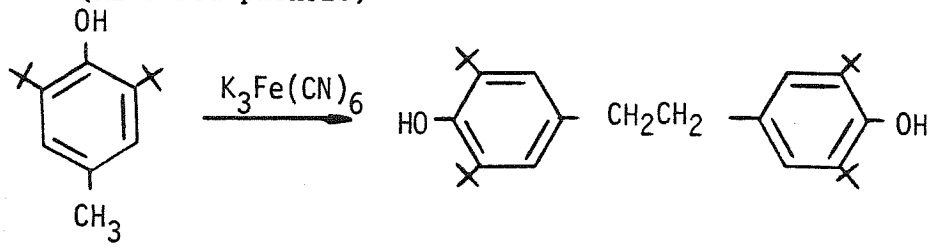

(3) Carbon-Carbon Coupling of Substituent β-Carbon Atoms (Hindered phenols)

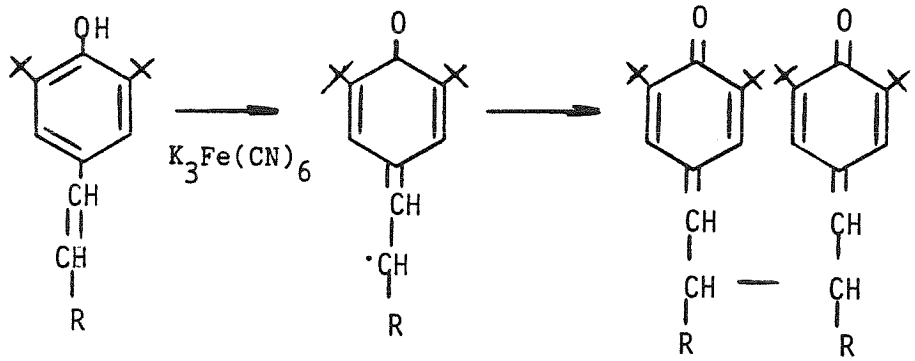

(4) Carbon-Oxygen Coupling between an Aromatic Carbon and Phenoxy Oxygen.
(Hindered phenols)

Species (4) in Figure 2.6.

(5) Oxygen-Oxygen Coupling between Phenoxy Oxygens.

(Never observed experimentally).

(Continued)

Table 2.4 (Continued)

(6) Formation of Charge-Transfer Complexes.
(Hindered phenols)

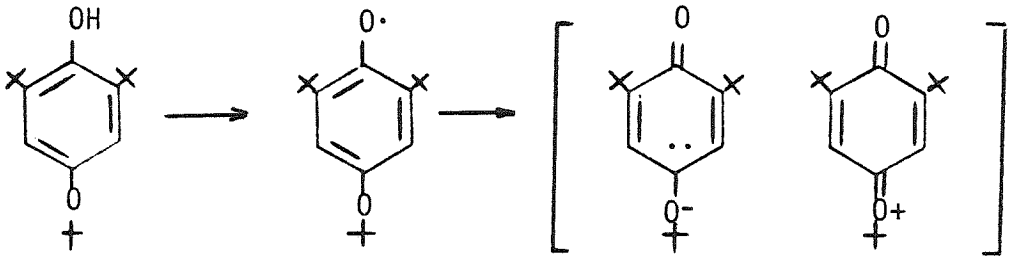

(Operative in only special cases)

because the unpaired electron is centered at these positions. The yield of products coupled through other sites is high only when the ortho- and para- sites have been sterically blocked (Musso, 1967). Substitution by bulky tert-butyl groups at ortho- and para- positions, for example, effectively prevents coupling at those sites. Compounds in which ortho- and para- positions are sterically blocked are called "hindered" phenols. The half-life of hindered phenols is higher than non-hindered analogs, since only less active sites are available for reaction (Musso, 1967).

2.6 Concluding Remarks

The reactivities of organic compounds toward oxidation are a function of chemical structure, and differ considerably. Functional groups may alter the reaction rate and the overall free energy of reaction by influencing the stabilities of the transition state and the oxidized product. The reactivity of natural organic compounds with manganese oxides depends upon the relative amounts of different chemical structures present; this will differ in samples from different locations.

Oxidations of organics by manganese oxides are most likely homolytic reactions, and therefore a variety of radical pathways are involved. Partially oxidized intermediates may be formed which are also reactive with manganese oxides. Product structures depend upon the oxidant used, the relative concentrations of organics and oxidant, and the pH. Manganese oxides may initiate coupling and polymerization reactions of organics in some natural systems, possibly leading to the

formation of humic compounds.

No additional generalizations can be made concerning the oxidation of organic compounds without considering characteristics of the oxidant. Reaction rates, and to some extent product structure, depend upon the oxidant employed and the mechanism of the electron transfer reaction. The next chapter examines these topics in detail, by focusing on the oxidation of organics by Mn(III) species.

CHAPTER 3

OXIDATION BY MANGANESE (III)

3.1 Introduction

Reduction and dissolution of manganese oxides begin by electron transfer from reductant molecules to Mn(III) and Mn(IV) oxide surface sites. Little is known about electron transfer at oxide surfaces, and this chapter begins, therefore, by examining the oxidation of organics by metal ion solute species, particularly Mn(III) complexes. Oxidation by Mn(III) solute complexes may occur via a mechanism similar to the mechanism of the surface reaction. Differences between the two oxidants do exist, however; the coordinative environments are different, and surface Mn(III) sites may be influenced by neighboring oxide sites.

The chemistry of Mn(III) species in solution and their reactions with organic reductants are reviewed in this chapter. By comparing the chemistry of Mn(III) solute species to Mn(III) oxide surface sites, generalities can be made concerning the reaction at oxide surfaces.

3.2 Oxidation of Organics by Metal Complexes

3.2A. Oxidation Mechanisms

Homolytic oxidation of organic compounds may occur via three possible mechanisms, as outlined by Littler (1970). In the non-bonded mechanism, the inner coordination shell of the metal ion remains intact, and electron transfer occurs without direct bond formation between the metal center and the organic substrate. This mechanism is analogous to outer-sphere electron transfer between metal complexes

(see Purcell and Kotz, 1977). Correlation between the overall free energy of reaction and the oxidation rate are sometimes observed (Kochi, 1973), for reasons outlined in Section 3.2C. Oxidation by substitution inert complexes occurs through non-bonded mechanisms, since inner-sphere ligands cannot be displaced by organic substrate.

Bonded mechanisms involve replacing a ligand of the inner coordination sphere with organic substrate prior to electron transfer, so that electron transfer occurs through a metal-ligand bond. Bonded mechanisms predominate when the metal complex is labile and the organic substrate is capable of complexing the metal ion (Littler, 1970).

Another mechanism, hydrogen-atom transfer, may occur when the ligands of the inner coordination sphere of the metal complex can accept hydrogen atoms from organic substrates. Hydrogen-atom abstraction is a low energy pathway for oxidizing organic species since charge separation in the transition state is minimized. In aqueous solution, charged species are readily solvated by water molecules, and therefore hydrogen-atom transfer is less favored over other mechanisms than in nonpolar solvents. Hydrogen-atom transfers are known to occur between free radicals and organics and have been postulated in reactions with metal complexes (Littler, 1970).

3.2B. Influence of Oxidant on Product Distribution

The reaction mechanism can influence the structure of oxidized products (McDonald and Hamilton, 1973). Consider, for example, the oxidation of 2-napthol by alkaline $K_3Fe(CN)_6$ and by $FeCl_3$ in neutral or acidic solution (Figure 3.1). $Fe(CN)_6^{3-}$ is

Figure 3.1 Oxidation of 2-napthol by $K_3Fe(CN)_6$ and $FeCl_3$.
(McDonald and Hamilton, 1973)

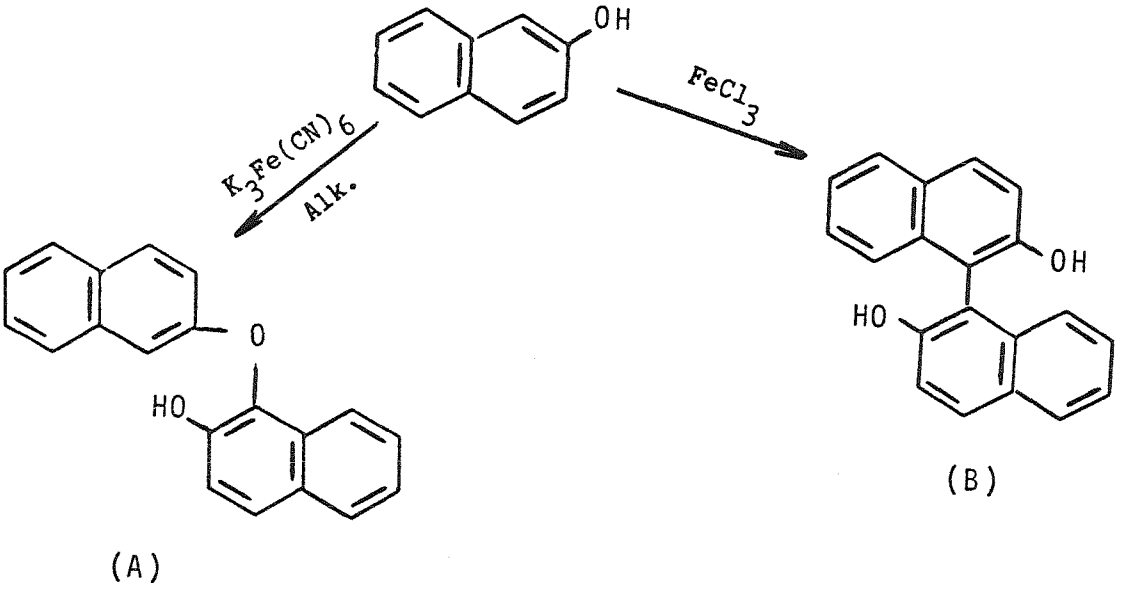

(A) (B)

substitution inert, and therefore binding between the metal ion and organic reductant prior to reaction cannot occur. Product (A) forms by coupling between the phenoxy oxygen and an ortho-carbon, the two most reactive sites of the radical species formed by one-electron oxidation (McDonald and Hamilton, 1973). $FeCl_3$, in contrast, can readily exchange chloride for another ligand. Fe^{III} binds strongly to oxygen donor ligands, and forms a complex with 2-napthol prior to electron transfer. If Fe^{III} is still complexed to 2-napthol when coupling occurs, the phenoxy oxygen is blocked, and only carbon-carbon coupling is possible (McDonald and Hamilton, 1973). Product (B) forms because the pathway to form (A) is blocked. In the case of 2-napthol, then, the product formed by the bonded mechanism differs from the product of the non-bonded mechanism.

3.2C. Oxidation Mechanism and Rate

Small differences in the structure of the oxidant complex or organic reductant often alter the rate of the redox reaction, because of changes in the energy of the transition state. The rate-limiting steps of each of the three general mechanisms discussed in Section 3.2A. are different. The way in which the reaction rate is changed when the organic structure is changed is, therefore, different for each of the mechanisms.

In reactions occurring via bonded mechanisms, the metal ion and organic reductant are chemically bonded to one another in the precursor complex. Considerable bond formation and rearrangement is necessary to reach the transition state. For this reason, the activation enthalpy

that accompanies bond transformations is the dominant contribution to the activation energy (Littler, 1970). The relative ability of organic substrates to complex oxidant metal ions can be estimated from stability constants with other, non-oxidizing metal ions. Organic reductants that form strong complexes are expected to react more quickly, because the concentration of precursor complex is higher. As in all electron transfer reactions, some distortion of oxidant and organic reductant structure is necessary for electron transfer to occur. Complex formation may distort the reactants in a favorable manner, and increase the reaction rate (Littler, 1970). Because of the number of different interactions that contribute to the activation energy, the rates of bonded mechanism reactions are difficult to predict.

The hydrogen-atom transfer mechanism involves partial dissociation of the hydrogen-substrate bond in forming the transition state (Littler, 1970). The bond dissociation energy (Section 2.2B.) is therefore an important contributor to the activation energy. Correlations between bond dissociation energies and relative reaction rates may exist for the oxidation of organic compounds of similar structure, when this mechanism is dominant (Littler, 1970).

The activation energy for oxidation via non-bonded mechanisms, in contrast, does not depend on energies of bond dissociation and formation, since no bonds are created prior to electron transfer (Littler, 1970). For outer-sphere reactions of this kind, the activation energy is comprised of three terms: the electrostatic

energy accompanying approach of the reactants (if they are charged), the energy required to distort the structures of the reactants to allow for electron transfer, and the energy necessary to reorder solvent molecules (Cotton and Wilkinson, 1980).

Outer-sphere electron transfer reactions between metal ions have been carefully studied, and a theory has been developed for predicting reaction rates in some cases. To illustrate this theory, consider the following reactions:

3.1 $M_A^{3+} + {}^*M_A^{2+} \longrightarrow M_A^{2+} + {}^*M_A^{3+}$

$$\text{Rate} = k_1[M_A^{3+}][M_A^{2+}].$$

3.2 $M_B^{3+} + {}^*M_B^{2+} \longrightarrow M_B^{2+} + {}^*M_B^{3+}$

$$\text{Rate} = k_2[M_B^{3+}][M_B^{2+}].$$

These are self-exchange reactions, for which the rates of electron transfer between oxidized and reduced forms are measured, usually by isotopic methods (Cotton and Wilkinson, 1980). Next, consider a cross-reaction between two different metal species:

3.3 $M_A^{3+} + M_B^{2+} \longrightarrow M_A^{2+} + M_B^{3+}$

$$\text{Rate} = k_{12}[M_A^{3+}][M_B^{2+}]$$

$$K_{12} = \frac{k_{12}}{k_{21}} = \text{The equilibrium constant for equation 3.3.}$$

For certain cross-reactions, the energy required to distort each

reactant in forming the transition state is the same as the energy required for this step in the self-exchange reactions. When this is true, Marcus-Hush theory predicts that the rate constant k_{12} for the cross- reaction can be calculated from the following equations (Purcell and Kotz, 1977):

3.4 $$k_{12} = (k_1 k_2 K_{12} f)^{1/2}$$

$$\log f = (\log K_{12})^2 / 4 \log(k_1 k_2 / z^2)$$

where z is a measure of the collision frequency.

The activation energy of the cross reaction contains a thermodynamic contribution from the overall free energy of the reaction ($\Delta G_{12} = -RT \ln K_{12}$) and a contribution derived from the rates of the corresponding self-exchange reactions (k_1 and k_2). This latter contribution is a measure of the distortion necessary in each reactant to form the activated complex. If changes in self-exchange rates (k_1 and k_2) are small compared to changes in the free energy of the reaction (K_{12}), then a linear relationship between $\log k_{12}$ and ΔG_{12} may exist (Purcell and Kotz, 1977).

If the energies required to distort reactant molecules to form the transition state are different from the energies required in the self-exchange reaction, then equation 3.4 is no longer valid. For this reason, Marcus-Hush theory fails to predict relative rates for many outer-sphere cross reactions.

A linear relationship between $\log(k_{12})$ and ΔG_{12} is not adequate proof of an outer-sphere mechanism. Other chemical properties can also be functions of ΔG_{12}, and may influence the reaction rate. If rates of self-exchange are known or can be estimated, then the slope of $\log(k_{12})$ against ΔG_{12} can be calculated and compared to the slope predicted from equation 3.4. Agreement between these two values is further proof of an outer-sphere mechanism.

Marcus theory can be extended to include reactions between metal ions and organics via non-bonded mechanisms (Littler, 1970). For these reactions, however, it is less likely that the energies required to distort the organics in forming the transition state will be the same in both the self-exchange and cross reactions. Rates of self-exchange for organics having electron-withdrawing or electron-donating substituents may vary considerably. Marcus theory has been shown, however, to predict relative oxidation rates of catechols and hydroquinones by Fe(III) substitution-inert complexes (Mentasti and Pelizzetti, 1976, 1977).

In somes cases, oxidation of organics by metal ions via a bonded mechanism may also show a linear relationship between the log of the rate constant and the overall free energy. Consider, for example, the oxidation of different organics by the same metal ion oxidant; the potential of the oxidant couple is the same for all reactions, and therefore relative differences in ΔG_{12} depend only on the potential of the organic redox couple (Red. + ne^- = Ox.). Adding electron-withdrawing substituents to the organic molecule raises the

potential, and decreases the stability of metal-organic complexes. The reaction rate via a bonded mechanism is therefore slower with stronger electron-withdrawing substituents. In some cases, the decrease in reaction rate may be proportional to the increase in potential, resulting in a linear free energy relationship, even though the reaction has a bonded mechanism.

It is difficult to assign mechanisms for metal ion-organic redox reactions on the basis of rate data alone. Although a relationship between rate and overall reaction free energy makes a non-bonded mechanism more likely, it is not proof that this is the correct mechanism, since bonded and hydrogen-atom transfer mechanisms may also give similar relationships. On the other hand, lack of a linear free energy relationship does not exclude a non-bonded mechanism.

3.3 The Chemistry of Mn^{III}

Mn^{III} in aqueous solution readily hydrolyzes and disproportionates:

3.5 $$Mn^{3+} + 2H_2O = \gamma\text{-MnOOH(s)} + 3H^+ \qquad \log K = 0.63 \text{ (Bricker, 1965)}$$

3.6 $$2Mn^{3+} + 2H_2O = MnO_2(s) + Mn^{2+} + 4H^+ \qquad \log K = 19.1 \text{ (Latimer, 1952)}$$

In concentrated acid containing excess Mn^{II}, disproportionation is quite slow, and Mn^{III} is meta-stable (Rosseinsky, 1963). Mn^{III} is a strong oxidant, as shown by the potential of the Mn^{III}/Mn^{II} couple:

3.7 $Mn^{III} + e^- = Mn^{II}$ $E^\circ = +1.56$ v. in 3 M $HClO_4$ (Latimer, 1952)

Mn^{III} can be further stabilized by adding complexing agents that form stronger complexes with Mn^{III} than with Mn^{II}. Because Mn^{II} is a poor complex former relative to Mn^{III}, a number of ligands can be used for this purpose (Cotton and Wilkinson, 1980). Sulfate and pyrophosphate readily complex Mn^{III}, and therefore lower the potential of equation 3.7:

Medium	E°(volts)	Reference
3M $HClO_4$	1.56	Latimer (1952)
H_2SO_4	1.51	"
$H_4P_2O_7$	1.15	Waters and Kolthoff (1948)

The potential of the Mn^{III}/Mn^{II} couple in pyrophosphate media is a complex function of pH, because of protonation and deprotonation of the pyrophosphate ligands (Drummond and Waters, 1955). Mn^{III} complexes with organic ligands generally degrade by oxidation of the coordinated ligands (Cotton and Wilkinson,1980).

3.4 Oxidation by Mn^{3+} and $MnOH^{2+}$

3.4A. $Mn^{3+}/MnOH^{2+}$ Equilibria

Mn^{III} can be generated in strong acid solutions containing excess Mn^{2+} electrolytically or by reduction of permanganate (Davies, 1969). Measurable amounts of the first hydrolysis product,

$MnOH^{2+}$, are present even in strongly acidic solution (Wells, 1965):

3.8 $\quad Mn^{3+} + H_2O = MnOH^{2+} + H^+ \qquad K_H = 0.88.$

K_H for Mn^{III} is considerably larger than for other first-row trivalent transition metals (Wells, 1965). Mn^{III} has a d^4 ($t_{2g}^3 e_g^1$) electronic configuration, one electron away from the stable d^5 ($t_{2g}^3 e_g^2$) "half shell" configuration. Hydroxide ion is a more polarizable ligand than water, and therefore greater delocalization of electrons onto the metal center is possible when Mn^{III} is hydrolyzed. For this reason, the enthalpy of reaction 3.8 is particularly small, causing K_H to be large (Wells, 1965).

Hydrolysis affects the rate of oxidation reactions, since Mn^{3+} and $MnOH^{2+}$ interact differently with substrate. For reactions that proceed via a bonded mechanism, the rate of ligand exchange of the metal complex can be rate-limiting. Mn^{III} complexes have exchange rates higher than complexes of most other trivalent metals because of Jahn-Teller distortion (Diebler and Eigen, 1966), which labilizes axial-coordination positions. Hydroxide ligands bind metals more strongly than water, however, causing the exchange rate for $MnOH^{2+}$ to be slower than for Mn^{3+}. A partial blocking effect is felt in reactions with $MnOH^{2+}$, since there are only five rapidly exchanging coordinative positions, instead of the six with Mn^{3+} (Davies et al., 1968). Reactions that require complex formation with organic

substrate prior to electron transfer are therefore faster when the amount of hydrolysis is decreased.

If oxidation occurs by hydrogen-atom transfer, then $MnOH^{2+}$ should be more reactive than Mn^{3+}, since the hydrogen atom is more readily accepted by the hydrolyzed species. Transfer of a hydrogen atom to $MnOH^{2+}$ reduces the metal center by one equivalent and transforms the hydroxide ligand into water (Davies et al., 1968).

For the reasons outlined above, $MnOH^{2+}$ should be the active oxidant in Mn^{III} solutions when the substrate contains abstractable hydrogen atoms and is not a strong complex former (Davies, 1969). When the organic reductant complexes strongly, or is not oxidized by hydrogen-atom abstraction, then Mn^{3+} should be the active species. In practice, it is difficult to distinguish the relative rates of reaction with Mn^{3+} and $MnOH^{2+}$ because of the effects of other protonation equilibria (Mentasti et al., 1975). Formation of metal-organic complexes lowers the pK_a of the organic substrate, an effect that can't be conveniently accounted for. Thus, an increase in reaction rate upon increasing acidification does not necessarily mean that Mn^{3+} is more reactive than $MnOH^{2+}$.

3.4B. Oxidation of Organics by Mn^{3+} and $MnOH^{2+}$

The oxidation of alcohols with Mn^{III} in perchlorate media has been shown to occur by a bonded mechanism. Methanol, ethanol, and n-propanol form complexes of the form $Mn^{3+}(ROH)_{aq.}$ and $Mn^{3+}(RO^{-})_{aq.}$ (or $Mn^{3+}OH^{-}(ROH)_{aq.}$) prior to oxidation, based on spectral information (Wells and Barnes, 1968).

Isopropanol, sec-butanol, and cyclohexanol are also oxidized, but there is no spectral or kinetic evidence of complex formation (Wells and Davies, 1967; Wells, Barnes, and Davies, 1968). Long chains and branching appear to sterically hinder complex formation, despite increased electron availability as chain length and branching are increased (Wells and Barnes, 1968).

The reaction between alcohols and Mn^{III} generates radicals. The oxidation of isopropanol, for example, is first-order with respect to Mn^{III} and substrate concentration, and thought to proceed by the following mechanism (Wells and Davies, 1967):

3.9 $$Mn^{III} + (CH_3)_2CHOH \xrightarrow{k_1} Mn^{II} + (CH_3)_2\dot{C}OH + H^+$$

3.10 $$Mn^{III} + (CH_3)_2\dot{C}OH \xrightarrow{k_2} Mn^{II} + (CH_3)_2CO + H^+$$

$$k_2 >> k_1$$

The overall stoichiometry of the reaction is:

3.11 $$2Mn^{III} + (CH_3)_2CHOH = 2Mn^{II} + (CH_3)_2CO + 2H^+$$

Rapid polymerization of acrylonitrile added to the reaction solution confirms that radicals are generated in this reaction. The reaction rate is insensitive to acidity (Wells and Davies, 1967).

Pinacol and α-hydroxybutyric acid, unlike the organics discussed above, are bidentate ligands, and therefore capable of chelating

Mn^{III}. Both alcohols have been shown to form complexes with Mn^{III} prior to electron transfer, and measured reaction rates are significantly greater than with other alcohols (Wells and Barnes, 1971A and 1971B). One molecule of pinacol reacts by a radical mechanism to form two molecules of acetone (Wells and Barnes, 1971A). Oxidation of α-hydroxybutyric acid, in contrast, generates carbon dioxide as well as acetone (Wells and Barnes, 1979B).

Wells and Kuritsyn (1970) and Davies and Kustin (1969) examined the oxidation of hydroquinone by Mn^{III} in acid perchlorate medium. In both investigations, the observed reaction stoichiometry is:

3.12 $$2Mn^{III} + QH_2 = 2Mn^{II} + Q + 2H^+$$

where QH_2 = Hydroquinone

and Q = Quinone.

UV spectra show consumption of hydroquinone and production of p-benzoquinone without the formation of side products (Davies and Kustin, 1969). The rate is first order with respect to $[Mn^{III}]_{aq.}$ and $[QH_2]$, and independent of $[Mn^{II}]$. Reaction rate decreases as acidity is increased, caused either by protonation reactions of the Mn^{III}/hydroquinone complex (Wells and Kuritsyn, 1970) or by formation of $MnOH^{2+}$ that reacts at a faster rate (Davies and Kustin, 1969). Additional information is required to decide which of the two explanations is correct.

Complex formation prior to electron transfer can be observed using

fast spectroscopic techniques. Wells and Kuritsyn (1970) observed that absorbance of the reaction solution at 470 nm (the wavelength of maximum absorbance by Mn^{III}) initially rose, then decreased as Mn^{III} was consumed. The mechanism proposed by Wells and Kuritsyn (1970) is presented in Table 3.1. The rate-limiting step is electron transfer within the Mn^{III}/hydroquinone complex, forming a semiquinone radical that is quickly consumed by oxidant. The reaction has an activation energy of 59±3kJ/mole (Wells and Kuritsyn, 1970).

The oxidation of catechol by Mn^{III} in perchlorate medium was studied by Mentasti et al. (1975). Reaction stoichiometry is consistent with the formation of o-benzoquinone by two one-equivalent oxidation steps, as was observed for the reaction with hydroquinone. The reaction was first-order with respect to $[Mn^{III}]$ and [Catechol], and reaction rate decreased upon increasing acidity. Once again, the experimental results are not sufficient to determine whether or not the acidity dependence is caused by hydrolysis of Mn^{III}, or by protonation of the Mn^{III}/organic substrate complex. Similar results were obtained for the oxidation of substituted catechols and catecholamines with Mn^{III} in perchlorate medium (Pelizzetti et al., 1975).

3.5 Oxidation by Mn^{III} Sulfate and Pyrophosphate Complexes

Mn^{III} pyrophosphate and sulfate complexes in acidic solution are particularly convenient for studying the oxidation reactions of organics. The reader is referred to the reviews by Waters and Littler (1965) and Kemp (1972) for detailed information concerning oxidation by

Table 3.1 Oxidation of hydroquinone by $Mn^{3+}/MnOH^{2+}$.

Wells and Kuritsyn (1970)

$$Mn^{3+} + H_2O \overset{K_H}{\rightleftharpoons} MnOH^{2+} + H^+$$

$$Mn^{3+} + QH_2 \overset{\beta_1}{\rightleftharpoons} MnQH_2^{3+}$$

$$MnOH^{2+} + QH_2 \overset{\beta_1'}{\rightleftharpoons} MnQH^{2+} + H_2O$$

$$MnQH_2^{3+} \overset{K_1}{\rightleftharpoons} MnQH^{2+} + H^+$$

$$MnQH_2^{3+} \xrightarrow{k_a} Mn^{II} + HQ\cdot + H^+ \qquad \text{slow}$$

$$MnQH^{2+} \xrightarrow{k_a} Mn^{II} + HQ\cdot \qquad \text{slow}$$

$$Mn^{III} + HQ\cdot \xrightarrow{k_b} Mn^{II} + Q + H^+ \qquad \text{fast}$$

where QH_2 = Hydroquinone
$HQ^{\cdot}$ = Semiquinone Radical
Q = p-Benzoquinone

these complexes. The potential of the Mn^{III}/Mn^{II} couple in pyrophosphate solution is lower than in sulfate solution (Section 3.3), and therefore Mn^{III} pyrophosphate is a weaker oxidant. Reduction of Mn^{III} pyrophosphate involves loss of a pyrophosphate ligand (Drummond and Waters, 1955):

3.13 $$Mn(H_2P_2O_7)_3^{3-} + e^- = Mn(H_2P_2O_7)_2^{2-} + H_2P_2O_7^{2-}$$

The potential is a complex function of pH, because of protonation and deprotonation of the pyrophosphate ligands.

Oxidations of organic substrates by Mn^{III} sulfate and pyrophosphate proceed in most cases via bonded mechanisms. Loss of one coordinated ligand occurs prior to complex formation with substrate. Electron transfer from the substrate to Mn^{III} occurs within this complex (Kemp and Waters, 1964C). Dissociation of the complex releases organic radicals and Mn^{II} into solution. The rates of most oxidation reactions by Mn^{III} complexes are independent of $[Mn^{II}]$, but there are important exceptions, as discussed later.

Radical formation can be detected in a number of ways. Free radicals reduce added mercuric chloride (Drummond and Waters, 1953B) and initiate polymerization of acrylamide, acrylonitrile (Benson, 1976), or vinyl cyanide (Drummond and Waters, 1953B). Sufficiently high concentrations of radicals can be measured directly using ESR (Benson, 1976).

Table 3.2 summarizes the ability of Mn^{III} sulfate and

Table 3.2 Reactivity of aliphatic substrates with Mn^{III} sulfate and pyrophosphate complexes

Substrates Oxidized	Substrates Not Oxidized
Lactic Acid	Fumaric Acid
Pyruvic Acid	Carboxylic Acids (RCOOH)
Malonic Acid	Saturated Alcohols (Ethanol, tert-butanol)
Propionaldehyde	
Unsaturated Alcohols (Allyl and crotyl alcohols)	

pyrophosphate complexes to oxidize different classes of aliphatic substrates. In general, oxidation proceeds at an appreciable rate if the radical intermediates generated are stabilized by resonance or by electron-donating substituents, or if non-radical products of high stability are formed in the electron transfer step. Increasing the stability of intermediates lessens the structural rearrangement necessary for electron transfer to occur, and therefore lowers the activation energy of the reaction. Abstraction of a hydrogen atom from a saturated alcohol, for example, forms a radical that is not stabilized by delocalization. The reaction is therefore quite slow. Oxidation of unsaturated allyl alcohol, in contrast, occurs at an appreciable rate, because the unpaired electron of the radical is extensively delocalized (Drummond and Waters, 1958):

$$\left[CH_2{=}CH{-}\dot{C}HOH \longleftrightarrow \dot{C}H_2{-}CH{=}CHOH\right]$$

The unsaturated carbon-carbon double bond of fumaric acid is a site of high electron density, but it is not readily oxidized by Mn^{III} complexes because removal of an electron does not form a resonance stabilized radical (Drummond and Waters, 1953A).

Propionaldehyde is oxidized by Mn^{III} sulfate and pyrophosphate; Figure 3.2 gives the proposed mechanism (Drummond and Waters, 1953A, 1955). Two tautomeric forms exist in solution (A and B), which equilibrate by means of reactions (1) and (2). Oxidation of the enol form (B) generates a radical stabilized by resonance, as shown

Figure 3.2 Oxidation of propionaldehyde by Mn^{III} pyrophosphate and sulfate.

A. Y. Drummond and W. A. Waters
J. Chem. Soc. (1953):435-443.
" " " (1955):497-504.

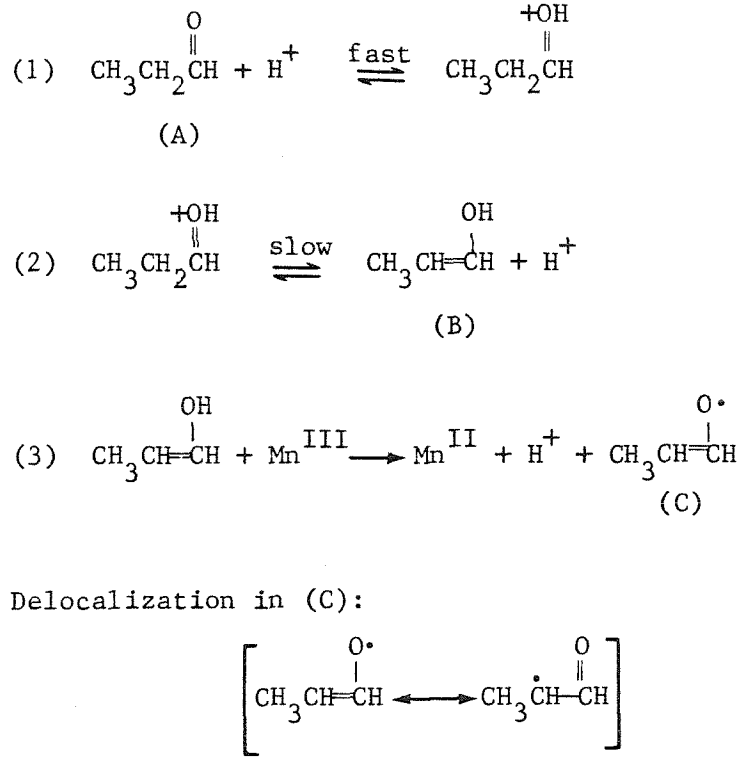

in equation (4). The oxidation rate of enolizable aldehydes and ketones is dependent upon the rate of enol formation (reaction 2), and is independent of [Mn^{III}] (Drummond and Waters, 1953A, 1955).

Formic acid and formaldehyde are not enolizable, and much less reactive towards Mn^{III} complexes; oxidation by Mn^{III} sulfate is quite slow, and oxidation by Mn^{III} pyrophosphate has not been observed (Kemp and Waters, 1964A). Inhibition by Mn^{II} led Kemp and Waters to postulate a mechanism for the oxidation of formic acid and formaldehyde that depends upon complexation and reaction with the small amount of Mn^{IV} formed by disproportionation.

Oxidation of 1,2-glycols, glycollic acid, pyruvic acid, lactic acid, oxalic acid, and malonic acid is enhanced by formation of cyclic complexes between Mn^{III} and substrate (Drummond and Waters 1953A, 1954, 1955; Levesley and Waters, 1955; Kemp and Waters, 1964B, 1964C). Decomposition of cyclic complexes of pyruvate and lactate generates carbon dioxide and radical intermediates (Drummond and Waters, 1955). Figure 3.3 shows the proposed mechanism for pyruvic acid oxidation. Electron transfer and carbon dioxide formation occur through a concerted mechanism. The thermodynamic free energy associated with carbon dioxide formation lowers the overall energy required to form products in the rate-limiting step (2).

Oxidation of malonic acid by Mn^{III} pyrophosphate occurs by a mechanism quite different from the ones described above. Drummond and Waters (1954) noted that the reaction was inhibited by Mn^{II}, but accelerated by addition of acrylonitrile, which consumes free radicals.

Figure 3.3 Oxidation of pyruvic acid by Mn^{III}pyrophosphate

---

A. Y. Drummond and W. A. Waters
J. Chem. Soc. (1955): 497-504

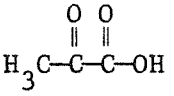

Pyruvic acid

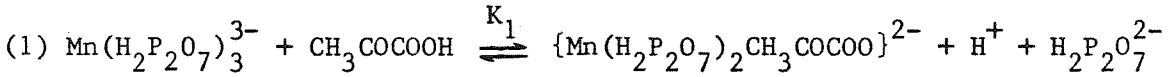

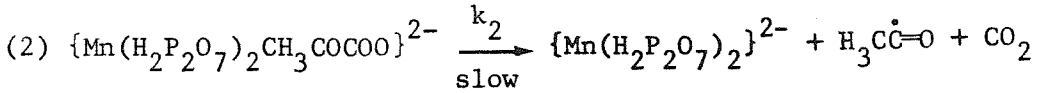

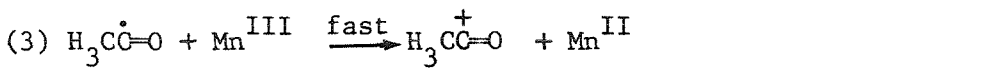

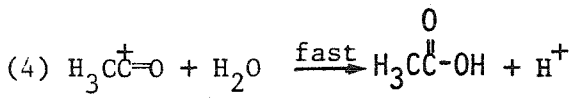

Electron-Transfer via step (2):

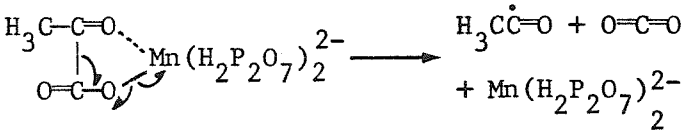

Of particular interest was the observation that oxidation of organic substrates inert to oxidation by Mn^{III} such as ethanol was induced by malonic acid, presumably through reaction with malonate radical. On the basis of this information, Drummond and Waters (1954) postulated mechanism (A), shown in Figure 3.4. Inhibition by Mn^{II} is accounted for by writing the electron transfer reaction (2) as reversible. Increasing $[Mn^{II}]$ shifts the equilibrium of reaction (2) to the left, lowering the reaction rate. Removal of radical ions by reaction with acrylonitrile shifts reaction (2) to the right, accelerating the consumption of Mn^{III}.

Oxidation of malonic acid by Mn^{III} sulfate was investigated by Kemp and Waters (1964C) for comparison. Mn^{III} sulfate is a considerably stronger oxidant than Mn^{III} pyrophosphate, and therefore reaction (2) of mechanism (A) should much more strongly favor product formation. In fact, although malonate radical can oxidize Mn^{II} in pyrophosphate solution, it probably cannot in sulfate solution, since the potential of Mn^{III}/Mn^{II} in sulfate solution is too high. Reaction (2) should be written as irreversible when Mn^{III} sulfate is the oxidant, and no dependence on $[Mn^{II}]$ should be observed.

The experimental results, however, show that Mn^{III} sulfate follows the same rate law as Mn^{III} pyrophosphate, and that reaction rates are quite similar. For this reason, mechanism A was discarded, and mechanism B, involving the formation of a Mn^{IV} malonate complex, was proposed for the reaction with both oxidants (Kemp and

Figure 3.4 Oxidation of malonic acid by Mn^{III} sulfate and pyrophosphate.

Drummond and Waters, J. Chem. Soc. (1954): 2456-2467
Kemp and Waters, J. Chem. Soc. (1964): 1489-9493

Mechanism (A):

(1) $Mn^{III} + CH_2(COOH)_2 \overset{fast}{\rightleftharpoons} CH_2(COOH)_2 \cdot Mn^{III}$

(2) $CH_2(COOH)_2 \cdot Mn^{(III)} \overset{slow}{\rightleftharpoons} \cdot CH(COOH)_2 + Mn^{II} + H^+$

(3) $Mn^{III} + \cdot CH(COOH)_2 + H_2O \longrightarrow Mn^{II} + HOCH(COOH)_2 + H^+$

Mechanism (B):

(1) $Mn^{III} + CH_2(COOH)_2 \overset{fast}{\rightleftharpoons} CH_2(COOH)_2 \cdot Mn^{III}$

(2) $CH_2(COOH)_2 \cdot Mn^{III} + Mn^{III} \overset{slow}{\rightleftharpoons} CH_2(COOH)_2 \cdot Mn^{IV} + Mn^{II}$

(3) $CH_2(COOH)_2 \cdot Mn^{IV} \longrightarrow Mn^{II} + \text{products}$

(4) $CH_2(COOH)_2\ Mn^{IV} + Mn^{III} \longrightarrow Mn^{II} + Mn^{III} + \text{products}$

Resonance of complex:

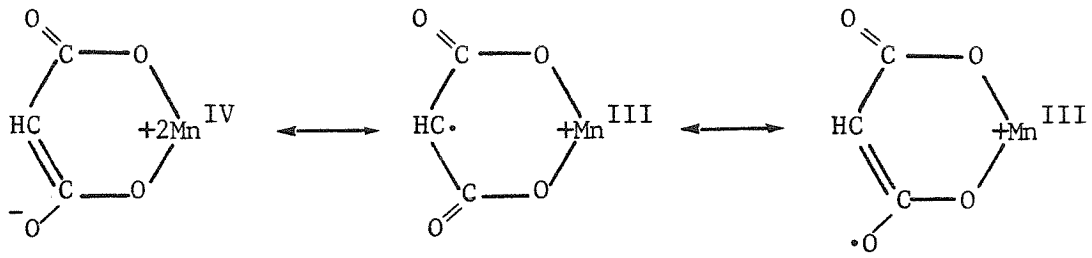

Waters, 1964C). The observed rate law is consistent with either step (3) or step (4) reacting to form products. Resonance forms show that intramolecular electron transfer is quite facile, and is responsible for the special characteristics that have been observed for this system.

Oxidation reactions of Mn^{III} pyrophosphate and sulfate outlined above all proceed through bonded mechanisms. In most cases, the electron transfer reaction forms radicals, which have been observed by a number of techniques.

3.6 Predictions Concerning the Reactivity of Manganese Oxide Surfaces

Considerable information has been collected concerning the oxidation of organic compounds by Mn^{3+}, $MnOH^{2+}$, Mn^{III} sulfate, and Mn^{III} pyrophosphate in acidic solution, as outlined in preceding sections. This section examines whether oxidation by Mn^{III} oxide surfaces should be expected to resemble oxidation by Mn^{III} solute species. If the reactions are similar, predictions can be made concerning the reactivity of solid manganese oxide surfaces, and the relative rate of oxidation of different organic substrates.

For reactions that proceed via a bonded mechanism, the following complex formation reactions with substrate HA can be envisioned:

3.14 $$Mn^{3+} + HA = MnA^{2+} + H^{+}$$

3.15 $$MnOH^{2+} + HA = MnA^{2+} + H_2O$$

3.16 $\equiv MnOH + HA = \equiv MnA + H_2O$

HA is the fully protonated organic substrate and surface sites are denoted by (≡). Reactions 3.14 and 3.15 represent formation of a complex between the organic substrate and Mn^{III} solute species, and reaction 3.16 represents formation of a surface complex (see Section 4.2). Written in this manner, solute and surface complexes form in the same manner. The stability of the three complexes will be different, because other ligands bound to Mn^{III} influence the strength of the Mn-A bond. Neighboring surface groups may cause steric constraints to be more severe for formation of surface complexes. Complex formation at surface sites may be different with chelating organics, since two coordinative positions may not be available at one Mn^{III} surface site. Chelating ligands may actually bind two adjacent sites on the surface. Thus, while a surface reaction proceeding through a bonded mechanism resembles the corresponding reaction with Mn^{III} solute species, the reaction rate may be significantly different. Some organic substrates are oxidized more quickly by Mn^{III} solute complexes than others. The trend in reactivity of organic substrates should be the same for oxidation by Mn^{III} surface sites, in that bonding interactions are similar.

Next, consider oxidation proceeding by hydrogen-atom transfer:

3.17 $Mn^{3+} + HA = Mn^{2+} + A^{\cdot} + H^{+}$

3.18 $MnOH^{2+} + HA = Mn^{2+}\text{-}OH_2 + A^{\cdot}$

3.19 $\equiv MnOH + HA = \equiv MnOH_2 + A^{\cdot}$.

Section 3.4 discussed differences in reactivity between Mn^{3+} and $MnOH^{2+}$. Hydrogen-atom abstraction by the oxide surface should most resemble reaction with $MnOH^{2+}$.

The rates of reaction via non-bonded mechanisms depend upon the amount of distortion in each substrate necessary before electron transfer can occur, and upon the overall free energy of the reaction. The oxide surface is a considerably weaker oxidant, because the potential of the $MnOOH(s)/Mn^{2+}$ couple (at neutral pH) is considerably lower than that of Mn^{III}/Mn^{II} in acidic solution. Oxidation of the same substrate by non-bonded mechanisms may therefore be slower when the oxide surface is the oxidant. The relative reactivities of organic substrates with Mn^{III} solute complexes and with oxide surface sites should be the same for bonded mechanism reactions with Mn^{III} solute complexes and with oxide surface sites.

Most oxidations by Mn^{III} solute complexes that have been studied involve bonded mechanisms. It is likely that oxidations by Mn^{III} surface sites also occur by bonded mechanisms, because similar interactions between organic reductant and oxidant are involved. The relative reaction rates, however, may be quite different.

CHAPTER 4

REACTIONS AT OXIDE SURFACES: ADSORPTION, ELECTRON-TRANSFER, AND DISSOLUTION

4.1 Introduction

In the dissolution of manganese oxide particles by organic reductants, only changes in bulk solution can be easily measured. By carefully taking into account interactions between bulk solution and oxide surface, however, some knowledge of the surface reaction can be obtained. The entire reaction sequence can be separated into the following steps:

1. Diffusion of organic substrate into the boundary layer
2. Formation of a surface complex between the adsorbate and oxide (possibly an activated complex)
3. Charge transfer within the surface complex
4. Desorption of oxidized organic substrate
5. Movement of reduced Mn(II) from the crystal lattice to the adsorbed layer
6. Desorption of Mn^{2+}
7. Diffusion of products away from the surface.

Any of these steps may be rate-limiting, depending on the activation energy required and the prevalent chemical conditions. Reactions in which diffusion of either reactants to the surface or products away from the surface is rate limiting are transport controlled. All other reaction steps are chemically controlled.

This chapter presents theories about the mechanism of the heterogeneous reaction and ways in which the true mechanism can be discerned. Experimentally determined reaction rates and their dependence on solution conditions can help distinguish between different possible mechanisms. The results of previous laboratory experiments will be examined in light of the mechanisms discussed. Subsequent chapters will describe how the dissolution reactions studied in this work fit into this reaction scheme.

4.2 Adsorption of Anions

4.2A. Equilibrium Descriptions

Anions adsorb onto oxide surfaces in response to both electrostatic and chemical forces. The electrostatic contribution to adsorption is caused by charged surface layers that disturb the distribution of charged solute species near the oxide/water interface. The energy associated with the formation of surface complexes, which includes changes in solvation energy, makes up the chemical contribution (Hingston, 1981). The hydrophobic effect (Stumm and Morgan, 1981) can be considered part of the chemical term, since collection of hydrophobic molecules at interfaces minimizes the chemical free energy of the system. Three charged layers make up the interface: a surface layer of potential- determining ions associated with the solid lattice, a layer of chemically bound (specifically adsorbed) ions, and a diffuse layer of electrostatically held counterions (Stumm and Morgan, 1981). Potential determining ions are components of the solid phase which can also exchange with the bulk

solution. Specifically adsorbed ions, in contrast, are not components of the solid phase although chemically bound to the surface.

Non-specific adsorption is dependent upon the oxide surface charge. A surface charge arises from protonation equilibria of the amphoteric oxide surface. The pH_{IEP} is defined as the pH at which the oxide is neutral. In the absence of specifically adsorbing ions, this pH is termed the pH_{zpc} (zero proton condition). Non-specific adsorption cannot alter the pH_{IEP} of the oxide, since ions are not adsorbed when the surface is either neutral or of the same sign. Non-specific adsorption of anions does not occur above the pH_{IEP}.

Specific adsorption, in contrast, can occur despite unfavorable surface charge, because of the chemical bonding energy gained in surface complex formation. Specific adsorption can therefore shift the pH_{IEP}. Solvation energies may be important since specifically adsorbed ions, unlike ions in the diffuse layer, have lost part of their hydration shell (Hingston, 1981). Specific adsorption of anions is modelled as a ligand exchange reaction in which hydroxyl surface groups of the oxide are replaced by adsorbate molecules that bind directly to the metal centers on the surface (Stumm et al., 1981). Al^{III}, Mn^{III}, Mn^{IV}, and Fe^{III} surface sites are hard Lewis acids, and should therefore bind strongly to hard Lewis bases such as oxyanions and fluoride (Schindler, 1981).

Two experimental observations support the idea that some anions are bound in the inner sphere of metal ions on the surface (Stumm et al., 1980). If inner-sphere surface complexes are formed, their

formation constants should be proportional to corresponding inner sphere-solute complexes. This correlation is observed when surface complex formation constants for the binding of organic ligands to aluminum oxide surfaces are compared to Al^{3+} solute complexes (Kummert and Stumm, 1980). It has also been observed that the acidity of polyprotic ligands increases upon adsorption. Adsorption of salicylic acid on aluminum oxide, for example, lowers pK_{a2} (of the aromatic hydroxy proton) by 6.8 units (Kummert and Stumm, 1980). Enhancement of acidity by this magnitude requires close association with the metal center and would not be observed if ligand and metal were separated by one or more water molecules (Stumm et al., 1980). Both results confirm that specifically adsorbed anions are bound in the inner sphere of surface metal centers.

The adsorption of a monoprotic ligand onto an oxide surface can be modelled using the formation constants defined in equations (1) through (4) in Table 4.1 (Stumm et al., 1980). Concentrations of surface species are written as {≡X} in units of (moles of sites)/liter. $K^S_{a1(intr)}$ and $K^S_{a2(intr)}$ are surface constants defined in terms of the hydrogen ion concentration at the oxide surface ($[H^+]_i$). $[H^+]_i$ is related to the bulk hydrogen ion concentration by:

$$4.1 \qquad [H^+]_i=[H^+]_b e^{F\psi/RT}$$

where ψ is the surface potential. Equation (1) in Table 4.1 represents the surface ligand exchange reaction in which the hydroxide group is replaced by the adsorbed anion.

Table 4.1 Adsorption of a Monoprotic Ligand

(1) $\equiv SOH + HA = \equiv SA + H_2O \qquad K^s_{SA} = \dfrac{\{\equiv SA\}}{\{\equiv SOH\}[HA]}$

(2) $\equiv SOH_2^+ = \equiv SOH + H^+ \qquad K^s_{a1} = \dfrac{\{\equiv SOH\}[H^+]}{\{\equiv SOH_2^+\}}$

(3) $\equiv SOH = \equiv SO^- + H^+ \qquad K^s_{a2} = \dfrac{\{\equiv SO^-\}[H^+]}{\{\equiv SOH\}}$

(4) $HA = H^+ + A^- \qquad K_a = \dfrac{[A^-][H^+]}{[HA]}$

(5) $S_T = \{\equiv SOH_2^{+3}\} + \{\equiv SOH\} + \{\equiv SO^-\} + \{\equiv SA\}$

$$= \{\equiv SOH\}\left(\frac{[H^+]}{K^s_{a1}} + 1 + \frac{K^s_{a2}}{[H^+]} + K^s_{SA}[HA]\right)$$

(6) $$A_T = [HA] + [A^-] + \{\equiv SA\} = [HA]\left(1 + \frac{K_a}{[H^+]} + K^s_{SA}\{\equiv SOH\}\right)$$

(7) $$\log\{\equiv SA\} = \log K^s_{SA} + \log\{\equiv SOH\} + \log[HA]$$

(8) $$\{\equiv SA\} = \frac{K^s_{SA} S_T A_T}{\left(\dfrac{[H^+]}{K^s_{a1}} + 1 + \dfrac{K^s_{a2}}{[H^+]} + K^s_{SA}[HA]\right)\left(1 + \dfrac{K_a}{[H^+]} + K^s_{SA}\{\equiv SOH\}\right)}$$

Taking the log of the equilibrium constant K_H for equation (1) results in equation (7). The concentration of surface complex {≡SA} is highest when the sum (log{≡SOH} + log[HA]) is maximized. Taken separately, log{≡SOH} is highest in the pH range $pK^s_{a1} < pH < pK^s_{a2}$ and log [HA] in the range $pH < pK_a$. When the pK_a of the ligand is between pK^s_{a1} and pK^s_{a2}, the maximum amount of adsorption occurs in the range $pK^s_{a1} < pH < pK_a$. When the pK_a is outside this range the full equation written in terms of $[H^+]_i$ (equation 8) can be used to find the pH dependence. The adsorption maxima for ligands with high pK_a values is spread over a broad pH range compared to those with low pK_a values. The amount of ligand adsorbed at a given pH will be small for ligands with large values of pK_a, however, since the ligand is effectively tied up in the protonated form.

Stability constants of surface complexes between phosphate and goethite (pH_{zpc} 7.8) are presented in Table 4.2 (Sigg and Stumm, 1980). Equations (4) and (5) represent the formation of binuclear complexes in which one phosphate anion binds to two surface sites. Adsorption of phosphate is constant over a wide pH range, in contrast to the adsorption of fluoride and sulfate, which drops off dramatically above pH values of 6. Successive deprotonation of phosphate as pH increases allows it to compete effectively with hydroxide ions for the metal centers.

A number of studies have measured the stability of oxide surface complexes with organic ligands. Davis and Leckie (1978) and Kummert

Table 4.2: Adsorption of Phosphate onto Goethite (Sigg and Stumm, 1980).

	log K
(1) $\equiv FeOH + H_3PO_4 = \equiv FePO_4H_2$	9.5
(2) $\equiv FeOH + H_3PO_4 = \equiv FePO_4H^- + H_3O^+$	5.1
(3) $\equiv FeOH + H_3PO_4 = \equiv FePO_4^{2-} + 2H^+ + H_2O$	-1.5
(4) $2\equiv FeOH + H_3PO_4 = \equiv Fe_2PO_4H + 2H_2O$	8.5
(5) $2\equiv FeOH + H_3PO_4 = \equiv Fe_2PO_4^- + H^+ + H_2O$	4.5
(6) $\equiv FeOH_2^+ = \equiv FeOH + H^+$	-6.4
(7) $\equiv FeOH = \equiv FeO^- + H^+$	-9.25

and Stumm (1980) studied compounds that have functional groups similar to natural organics, and are similar to compounds used in this work. In both studies the procedure outlined in Table 4.1 is successful in predicting the pH dependence of adsorption. Davis and Leckie (1978) found that 3,4-dihydroxybenzoic acid (3,4-diOH) is strongly adsorbed on amorphous iron oxide over a wide pH range, in contrast to the adsorption of salicylic acid, which drops off above a pH of 6. The ortho hydroxy groups of 3,4-diOH are responsible for this enhancement. Kummert and Stumm (1980) measured the adsorption of benzoic, phthalic, and salicylic acids as well as catechol on alumina (pH_{zpc} 7.8). In agreement with the treatment in Table 4.1, the amount of adsorption decreased as the pH was increased with all the ligands except catechol. The pK_{a1} of catechol is the highest in this group of ligands, and an increase in pH allows the surface to compete more effectively with protons for the anion.

Adsorption studies with humic materials are complicated by the distribution of molecular size, functional groups, and charge within the sample. Adsorption of natural organics has been studied on oxides of manganese (Dempsey, 1981), iron (Tipping, 1981A, 1981B), and aluminum (Davis and Gloor, 1981; Parfitt et al., 1977). In each case, adsorption of humics in the absence of other specifically adsorbing ions decreased with increasing pH. This finding, as well as IR studies by Parfitt et al. (1977), indicates that functional groups having low pK_a values (such as carboxyl groups) are responsible for adsorption.

Different molecular weight fractions have been shown to have different affinities for the alumina surface (Davis and Gloor, 1981). Organics having molecular weights in excess of 1000 are adsorbed most readily. Between 20 and 60% of the total dissolved organic carbon was not adsorbed, regardless of the alumina dose. This fraction has a low affinity for oxide surfaces.

Addition of Ca^{2+} and Mg^{2+} enhances the adsorption of humic substances on oxides (Tipping, 1981B and Dempsey, 1981). When $5x10^{-3}$M Ca^{2+} is added, the amount of adsorption actually increases with increasing pH; this is the reverse of the pH dependence observed absence of Ca^{2+} and Mg^{2+} (Dempsey, 1981). Both oxide and organics are negatively charged in these experiments, and the divalent cations may enhance adsorption by partially neutralizing the negative charge on the humic molecules (Dempsey, 1981).

4.2B Kinetics of Adsorption/Desorption

The adsorption of a number of anions on oxide surfaces is only partially reversible, and rates of adsorption and desorption are sometimes quite slow (Schindler, 1981). Rates of anion adsorption are more dependent on the character of the lattice metal ions than cation adsorption since anions are bound directly to the metal ions while cations are bound to surface hydroxyl groups.

Many experiments have determined the time necessary for adsorption reactions to come to equilibrium (or pseudo-equilibrium). Fluoride adsorption onto goethite is complete within five minutes, but phosphate adsorption requires 48 hours to reach its maximum level (Sigg and

Stumm, 1981). In a similar manner, adsorption of oxalate onto goethite takes two hours, while benzoic acid takes two weeks (Parfitt et al., 1977). Oxalate binds strongly to goethite and can form binuclear surface complexes. Benzoic acid in contrast, has low affinity for the oxide surface (Parfitt et al., 1977).

The influence of the lattice metal ions on the rate of adsorption was examined by Yates and Healy (1975). Rates of adsorption of nitrate, sulfate, and phosphate on an Fe^{III} oxide were compared to those on a Cr^{III} oxide. Cr^{III} and Fe^{III} solute complexes have approximately the same stabilities, but Cr^{III} ligand exchange occurs at a much slower rate. Adsorption on Cr^{III} oxides should therefore be slower than on Fe^{III} oxides. The adsorption experiments verified this prediction. Ligand exchange on both oxides was much slower than exchange between solute complexes (Yates and Healy, 1975).

The Elovich Equation, originally developed for the adsorption of gases onto solid surfaces, has been applied to rates of adsorption from aqueous solution. The derivation is based on the assumption that activation energy (E) increases linearly with increasing surface coverage (Hayward and Trapnell, 1964):

$$4.2 \qquad E = E_o + a\theta$$

where θ is the fraction of surface sites occupied by adsorbate molecules. The Elovich Equation for adsorption onto a non-uniform

surface is found by integrating over a collection of area elements, each of which has a uniform surface. At low surface coverage, the equation is written as:

$$4.3 \quad \frac{d\theta}{dt} = ae^{-\alpha\theta/RT}$$

The constant α/RT represents the magnitude of the activation energy, and (a) is a constant which relates to the initial reaction velocity (Hingston, 1981).

Atkinson et al. (1971, 1972) derived a form of the Elovich Equation to model isotope exchange and applied it to the exchange of ^{32}P-labelled orthophosphate on goethite. Experimental exchange rates were first order with respect to Fe^{III}-phosphate surface complexes, and showed little dependence on free phosphate concentration. Acid and base catalysis were observed, causing a minimum in the exchange rate at pH 9.0. The half-life for exchange was dependent on pH, with values from 25 minutes to 12 hours measured between pH values of 2.6 and 12.

4.3 The Surface Site-Binding Model

In this section a model is developed for the heterogeneous dissolution reaction based upon the formation of complexes between surface sites and organic substrate prior to electron transfer. Adsorption and desorption reactions affect the reaction rate by determining the concentration of surface complex species. Dissolution changes the number of reactive surface sites and their availability.

Changes brought about by different reaction schemes are considered. The pH dependence arises from surface site and substrate protonation equilibria.

4.3A General Model, Constant Number of Surface Sites

This section and section 4.3B are based on a treatment by Castellan (1971) of decomposition of molecules on a surface. Consider the following reaction:

$$4.4 \qquad \equiv SOH + HA \underset{k_{-1}}{\overset{k_1}{\rightleftharpoons}} \equiv SA + H_2O$$

$$4.5 \qquad \equiv SA \xrightarrow{k_2} P$$

where ≡SOH and ≡SA are surface species. The product P is formed by first-order reaction of the surface complex ≡SA. For the moment, ignore protonation equilibria, and assume that all surface sites are either ≡SOH or ≡SA. Next, define the following quantities:

$$4.6 \qquad S_T = \{\equiv SOH\} + \{\equiv SA\} = \text{(Total surface sites)/liter}$$

$$4.7 \qquad \theta_A = \frac{\{\equiv SA\}}{S_T} = \text{Fraction of sites bound to } A^-.$$

It is assumed that the total number of surface sites is constant, which is a reasonable assumption near the start of the reaction. The rate law is therefore:

4.8 $$\text{Rate} = \frac{d[P]}{dt} = k_2\{\equiv SA\} = k_2 S_T \cdot \theta_A$$

Next, apply the steady-state condition to the concentration of surface complex sites:

4.9 $$\frac{d\{\equiv SA\}}{dt} = k_1[HA]\{\equiv SOH\} - k_{-1}\{\equiv SA\} - k_2\{\equiv SA\} = 0$$

The fraction of sites bound to A^- can be found by dividing equation 4.9 by S_T:

4.10 $$k_1[HA](1-\theta_A) - k_{-1}\theta_A - k_2\theta_A = 0$$

4.11 $$\theta_A = \frac{k_1[HA]}{k_1[HA] + k_{-1} + k_2}$$

Combining the results of equation 4.11 with 4.8 gives the rate equation in terms of the adsorbate concentration in solution:

4.12 $$\frac{d[P]}{dt} = k_2 S_T \theta_A = \frac{k_1 k_2 S_T[HA]}{k_1[HA] + k_{-1} + k_2}$$

The reaction rate is directly proportional to the total concentration of surface sites.

There are two principal limiting cases of equation 4.12.

Case 1: The surface reaction is much faster than adsorption and desorption. Under these conditions, $k_2 >> k_1[HA] + k_{-1}$

and 4.12 reduces to:

$$4.13 \qquad \frac{d[P]}{dt} = k_1 S_T [HA]$$

The rate of product formation is equal to the rate of adsorption of HA. The reaction is first order with respect to adsorbate concentration.

Case 2: The surface reaction is much slower than adsorption and desorption. In this case $k_2 << k_1[HA] + k_{-1}$ and the amount of HA bound on the surface can be defined by a stability constant:

$$4.14 \qquad K^s_{SA} = \frac{k_1}{k_{-1}}$$

Equation 4.12 then becomes:

$$4.15 \qquad \frac{d[P]}{dt} = \frac{k_1 k_2 S_T [HA]}{k_1[HA]+k_{-1}} = \frac{k_2 S_T K^S_{SA}[HA]}{K^S_{SA}[HA] + 1}$$

The rate of reaction is therefore dependent upon the adsorption isotherm that defines the equilibrium adsorption of HA on the oxide surface. When the surface coverage is low, $K^S_{SA}[HA] << 1$ and the rate becomes:

$$4.16 \qquad \frac{d[P]}{dt} = k_2 S_T K^S_{SA}[HA]$$

The order with respect to adsorbate concentration is again 1.0. At high surface coverage, $K^{S}_{SA}[HA]>>1$ and the reaction becomes zero order:

4.17 $$\frac{d[P]}{dt} = k_2 S_T$$

The order with respect to adsorbate concentration in this case is a function of the substrate loading. When the adsorbate concentration is low, the reaction is first-order, but as the concentration is increased, the order become less than one and finally zero, when the surface is saturated with adsorbate.

Two limiting cases result in rate laws that have a first-order dependence on adsorbate concentration. If the surface reaction is faster than adsorption and desorption, the reaction is first-order regardless of adsorbate concentration. If the surface reaction is slow, the reaction is first-order only at low adsorbate concentrations; the order becomes less than one at higher adsorbate concentrations.

4.3B. Competition for Surface Sites.

Next, consider the situation in which a second adsorbate (HB) binds surface sites but does not react to form product. In this case, the system is defined by reactions 4.4 and 4.5, and an additional reaction:

4.18 $$\equiv SOH + HB \underset{k_{-3}}{\overset{k_3}{\rightleftharpoons}} \equiv SB + H_2O$$

The following definition is also needed:

4.19 $$\theta_B = \frac{\{\equiv SB\}}{S_T} = \text{Fraction of sites bound to } B^-$$

Equation 4.9 therefore becomes:

4.20 $$k_1[HA](1-\theta_A-\theta_B) - k_{-1}\theta_A - k_2\theta_A = 0$$

and the reaction rate is:

4.21 $$\frac{d[P]}{dt} = \frac{k_1 k_2 S_T(1-\theta_B)[HA]}{k_1[HA] + k_{-1} + k_2}$$

θ_B is not constant but changes as the amount of free surface changes, and depends upon the relative rates of adsorption and desorption of both HA and HB. The addition of HB, however, clearly blocks sites from reaction with HA. Consider the following two special cases:

Case 1: The adsorption/desorption reactions of HA and HB are faster than the surface reaction of ≡SA. In this case, the equilibrium constants K_{SA} and K_{SB} define the concentration of surface ≡SA species:

4.22 $$\theta_A = \frac{K^S_{SA}[HA]}{1 + K^S_{SA}[HA] + K^S_{SB}[HB]} \qquad K^S_{SB} = \frac{k_3}{k_{-3}}$$

and the rate expression becomes:

$$4.23 \qquad \frac{d[P]}{dt} = \frac{k_2 S_T K^s_{SA}[HA]}{1 + K^s_{SA}[HA] + K^s_{SB}[HB]}$$

The reaction rate is dependent upon the equilibrium distribution of surface species ≡SA and ≡SB.

Case 2: Consider the case in which the surface reaction is faster than adsorption/desorption reactions, and assume that the oxide surface is pre-equilibrated with HB prior to addition of HA. When the reaction begins, θ_B is given by:

$$4.24 \qquad \theta_B = \frac{K^S_{SB}[HB]}{1 + K^S_{SB}[HB]}$$

The initial reaction rate is given by:

$$4.25 \qquad \frac{d[P]}{dt} = \frac{k_1 k_2 [HA] S_T (1-\theta_B)}{k_1[HA] + k_{-1} + k_2} = \frac{k_1 k_2 [HA]}{k_1[HA] + k_{-1} + k_2} \left(\frac{S_T}{1 + K^s_{SB}[HB]} \right)$$

Under these conditions the initial rate is lowered in proportion to the amount of sites bound to HB before addition of HA.

Other cases can be considered in which adsorption of HB only partially blocks reaction at bound surface sites, or actually enhances the reaction. The influence of HB can be generalized by writing the experimental rate constant as a combination of terms (Bard and Faulkner, 1980):

$$4.26 \qquad k = k_o(1-\theta_B) + k_c \theta_B.$$

where k = Overall rate constant

k_o = Rate constant for sites not bound to B^-

k_c = Rate constant for sites bound to B^-.

For reactions in which adsorption by B^- blocks surface sites, $k_c=0$. When adsorption of B^- catalyzes the surface reaction, $k_c > k_o$.

4.3C Consumption of the Oxide

In an actual dissolution reaction, S_T does not remain constant but changes as the oxide is reduced and dissolved. S_T may change in a number of ways, depending upon the relationship between volume and surface area of the particle, and the rate in which surface groups are dissolved and new ones are exposed. In this section, ways in which S_T may change with time are considered, along with how these changes modify the reaction rate.

For simplicity, let P be the amount of dissolved manganese in solution. S_o and S_T are the number of sites available at t=0 and at time t. Two new quantities will also be used:

$(MnO_x)_o$ = The amount of Mn(III) and Mn(IV) in the solid oxide phase at t=0.

$(MnO_x)_t$ = The amount of Mn(III) and Mn(IV) in the solid oxide phase at time t. (The amount of undissolved manganese at time t.)

At any time during the reaction, the following relationship holds:

4.27 $$(MnO_x)_t = (MnO_x)_o - [P].$$

The amount of oxide remaining at time t is equal to the amount originally added minus the amount dissolved.

At any given time during the reaction, the ratio between oxide surface sites and remaining undissolved manganese can be calculated:

$$4.28 \quad f(t) = S_T/(MnO_x)_t = S_T/((MnO_x)_o - [P]).$$

This ratio represents the fraction of undissolved manganese that is found on the oxide surface. Since the reaction rate is proportional to S_T, the following equation can be written:

$$4.29 \quad \frac{d[P]}{dt} = k_2 S_T \theta_A = k_2 f(t)((MnO_x)_o - [P])\theta_A.$$

f(t) is a function of reaction time, and may change in a complex manner as the oxide is dissolved. If channels are etched into the oxide surface by the reaction, for example, the surface area to volume of remaining oxide increases, and f(t) therefore increases with time.

At the beginning of the reaction, the following relationship holds:

$$4.30 \quad S_o = f(0)(MnO_x)_o.$$

Doubling the amount of oxide added doubles the number of sites

available at t=0, regardless of the value of f(0). The initial reaction rate is therefore first-order with respect to oxide loading.

For some reactions, the surface to volume ratio of the oxide particles will remain approximately constant during dissolution, and f(t) is therefore constant. In this case, $S_T = f(MnO_x)_t$ and the reaction rate is directly proportional to the amount of remaining oxide, ($(MnO_x)_o$ - [P]).

The following cases illustrate ways in which the relationship between S_T and $(MnO_x)_t$ can change as the oxide is consumed.

Case 1: Assume that a certain fraction of manganese oxide groups are available for reaction at t=0, and are all equally reactive. Also assume that as these sites are consumed, no new ones are created. In this case, $S_o = f(0)(MnO_x)_o$ and:

4.31 $$S_T = f(0)(MnO_x)_o - [P] \ .$$

If the assumptions are strictly true, then dissolution ceases when [P] = $f(0)(MnO_x)_o$. In the presence of excess reductant, only a fraction of the total amount of manganese oxide, f(0), can be dissolved.

Case 2: Consider the situation where dissolution removes successive layers of Mn^{III} sites. Also assume that as each surface site is dissolved, a new one is exposed. If the particles are large enough,

the total number of available surface sites remains constant as the reaction progresses. If f(0) is the fraction of oxide sites at t=0, then:

4.32 $$S_T = S_o = f(0)(MnO_x)_o.$$

The reaction rate in this case is independent of the amount of manganese that has been dissolved.

Case 3: In some situations, only a fraction (g) of the sites that are dissolved are replaced by new surface sites. If the number of sites available at t=0 is equal to $f(0)(MnO_x)_o$, then S_T becomes:

4.33 $$S_T = f(0)(MnO_x)_o - g[P].$$

In this case, the dependence of the reaction rate on the amount of remaining oxide is considerably more complicated. The fraction g may be a function of time.

The rate may depend upon the amount of remaining oxide in different ways as well. Reductant molecules, for example, may in some cases diffuse through surface layers and react with inner oxide groups. If inward diffusion does occur, the concentration gradient that develops will influence the reaction rate.

4.3D. pH Dependence

Until now the protonation equilibria of surface and adsorbate species have been ignored. This is a good first approximation at pH values near the pH_{zpc} of the oxide surface and when the pH is below the pK_a of the adsorbate. To see the effect of pH, consider Table 4.1 along with equations 4.4 and 4.5. The assumption is made that protonation equilibria are faster than adsorption and desorption of HA, and faster than the surface reaction. Using the steady-state approximation, the concentration of surface sites bound to A^- is:

$$4.34 \qquad \{\equiv SA\} = \frac{k_1[HA]\{\equiv SOH\}}{k_1 + k_2}$$

If $\{\equiv SA\}$ is small compared to S_T and A_T, then:

$$4.35 \qquad [HA] = \frac{A_T}{\left(1 + \frac{Ka}{[H^+]}\right)} \qquad \text{and} \qquad \{\equiv SOH\} = \frac{S_T}{\left(\frac{[H^+]}{K^s_{a1}} + 1 + \frac{K^s_{a2}}{[H^+]}\right)}$$

The rate of reaction therefore becomes:

$$4.36 \qquad \frac{d[P]}{dt} = k_2\{\equiv SA\} = \frac{k_1k_2}{k_{-1} + k_2}\left(\frac{S_T}{\frac{[H^+]}{K^s_{a1}} + 1 + \frac{K^s_{a2}}{[H^+]}}\right)\left(\frac{A_T}{1 + \frac{Ka}{[H^+]}}\right)$$

When surface coverage by substrate is low, the pH dependence of the dissolution reaction is the same as for adsorption of substrate, shown in Table 4.1. The reaction rate is fastest when the product $[HA]\{\equiv SOH\}$

is at its maximum value. Conditions that lead to greater amounts of adsorbate being bound to the surface also result in faster reaction rates.

4.3E. Summary

A simple model has been developed that assumes that the dissolution rate depends upon the formation of surface complexes that subsequently react to form products. Once dissolution begins, the number of surface sites available for reaction changes, possibly in a complex manner. A change in pH changes the amount of substrate adsorbed on the surface, and therefore the reaction rate. The pH dependence of surface complex formation is easily found from substrate and surface site protonation equilibria.

4.4 The Dissolution Reaction

4.4A. Introduction

The rate of a dissolution reaction depends upon how fast component ions are released from the solid lattice and transported away from the surface. Dissolution is enhanced by surface chemical reactions that lower the energy required to break bonds between surface component ions and the solid lattice. Rates of dissolution of some solids depend upon the distribution of imperfections on the solid surface, which make some sites more reactive than others.

Some dissolution reactions are transport controlled. The slow step may be diffusion through a surface stagnant layer (Bard and Faulkner, 1980), through a partially leached oxide layer, or out of surface micropores (Pankow, 1978).

4.4B. Surface Chemical Reactions

Dissolution is accomplished by hydrating component ions with solvent molecules as the remaining bonds to the solid lattice are broken. An activated complex is envisioned, in which solute species (such as protons or complexing ligands) can take part, lowering the activation energy (Pankow, 1978). The rate is enhanced by increasing the stability of the solute complex and by lowering the energy of the bonds to the lattice. In this way, component ions are made more effective leaving groups.

Protonation of surface hydroxyl groups changes the rate of dissolution. As the amount of protonation of surface groups increases, the surface metal ions become increasingly hydrated:

4.37 $$\equiv MeO^{-} \longrightarrow \equiv MeOH \longrightarrow \equiv MeOH_2^{+}.$$

Me-O groups are bound to the solid lattice more strongly than Me-OH or $Me-OH_2$ groups, and are therefore released from the lattice more slowly (Valverde and Wagner, 1976). Components may leave the surface separately (as Me^{z+}, OH^{-}, and H_2O), or as hydroxo complexes ($MeOH^{(z-1)+}$, $Me(OH)_2^{(z-2)+}$, etc.) (Valverde and Wagner, 1976). Reactions that form these species at the surface are pH dependent, and therefore the rate of dissolution will be a function of pH.

Metal ions having high charge to radius ratios are tightly bound to their coordinated ligands and exchange them quite slowly (Purcell

and Kotz, 1976). Oxides of metals that exist in two or more oxidation states dissolve more quickly when surface groups are in the lower valence form, because the charge to radius ratio is smaller, weakening Me-O bonds to the lattice. Wuestite ($Fe_{1-\delta}O$) is a mineral which contains predominately ferrous iron (Fe^{II}) but which also contains an impurity of ferric iron (Fe^{III}) that increases as the iron deficit (δ) increases. The dissolution rate decreases as δ increases, since Fe^{III} is bound more strongly in the lattice and hydrates more slowly (Valverde and Wagner,1976).

An important observation concerning the effect of surface metal ion oxidation state was made by Pe'ligot (1844, 1845). Anhydrous $CrCl_3(s)$ crystals dissolve very slowly, but small additions of $CrCl_2(s)$ to solution significantly enhance the dissolution rate. The following reactions are thought to be responsible for the rate increase (Valverde and Wagner, 1976):

4.38 $Cr^{3+}(surface)+Cr^{2+}(aq.) = Cr^{2+}(surface)+Cr^{3+}(aq.)$

4.36 $Cr^{2+}(surface) \xrightarrow{fast} Cr^{2+}(aq.)$

4.37 $Cr^{3+}(surface) \xrightarrow{slow} Cr^{3+}(aq.)$

The water exchange rate of $Cr^{II}(H_2O)_6^{2+}$ is much faster than that of $Cr^{III}(H_2O)_6^{3+}$, and it is likely that hydration of surface groups will follow the same trend. The postulated reaction therefore enhances the rate by replacing a slowly dissolving

surface group by a quickly dissolved one. Cr^{2+} released to solution can then readsorb and continue the process.

The oxidation state of surface groups is dependent upon the oxidation potential in the overlying solution, because of equilibration reactions at the surface. Valverde (1976) observed that the dissolution rate of FeO, Fe_3O_4, Fe_2O_3 and CoO increased when the redox potential of the bulk solution was decreased by adding reducing agents. The redox potential can be set by adding an excess of both oxidant and reductant (such as V^{3+} and VO^{2+}) in the appropriate ratio. Increasing the ratio of V^{3+} to VO^{2+} lowered the redox potential of the solution, and increased the rate of dissolution. When this ratio was held constant but the sum of the two species ($[V^{3+}] + [VO^{2+}]$) was increased, the dissolution rate was also increased. This may have been caused by depletion of V^{3+} at the oxide surface, or by slow equilibration with the surface (Valverde, 1976). An increase in the sum accelerates the rate of equilibration reactions and increases the rate of diffusion into the depleted surface layer.

Studies of the reaction between dissolved, inorganic reductants and solid phase oxidants have provided some information concerning charge transfer at surfaces. Gordon and Taube (1962) studied the oxidation of U^{4+}(aq.) by ^{18}O labelled PbO_2(s) and MnO_2(s). Oxidation by either oxidant resulted in the formation of UO_2^{2+} ions containing two labelled oxygen atoms. This indicates that U^{4+} was specifically adsorbed on the oxide surface

prior to oxidation, possibly bridging between two surface oxide groups.

The oxidation of Cr^{2+}(aq.) by MnO_2, Mn_2O_3, PbO_2, Tl_2O_3, Co_2O_3, and CeO_2 was examined by Zabin and Taube (1964). In homogeneous solution, one-equivalent oxidants form only monomeric Cr^{3+}, but two-equivalent oxidants can also form binuclear Cr(III) species (Zabin and Taube, 1964). Two-equivalent oxides react by one equivalent, they reasoned, because two-equivalent reduction of a metal ion in the crystal lattice would be more disruptive than one-equivalent reduction, and is therefore less likely. The change in ionic radius in going from Mn^{IV} to Mn^{III}, for example, is less than going from Mn^{IV} to Mn^{II}. They postulated that the lattice site that is reduced is not necessarily the one closest to the adsorbed reductant, but may be some distance inside the lattice. Subsequent lattice reordering and electron transfer may concentrate reduced metal centers on the surface layer where they can dissolve.

Complexing agents can alter the dissolution rate by becoming involved in the formation of the activated complex (Pankow, 1978). The dissolution rate is enhanced when the ligand binds surface metal ions in a way that weakens remaining bonds to the lattice. Inhibition can occur if the surface complex formed with the ligand blocks dissolution of that site. Complexing agents may also act by simply lowering the component ion concentrations in overlying solution, increasing the degree of undersaturation (Valverde and Wagner, 1976).

Dissolution of CoO(s) and NiO(s) in acidic solution increases by a

factor of ten when the chloride ion concentration is increased from zero to 0.20M (Valverde, 1976). Complexation by chloride ion is responsible. In another example, phosphate has been found to inhibit the dissolution of iron oxides near neutral pH values, but accelerates dissolution in nitric acid (Stumm, Furrer, and Kunz, 1982). A possible explanation is that protonation transforms phosphate from a ligand forming surface complexes more stable than solute complexes to one in which the reverse is true.

Zutic and Stumm (1981) have shown that fluoride ion accelerates the dissolution of hydrous alumina in the pH range of 3 to 6. The effect of fluoride can be nullified by adding ligands that by themselves do not affect the rate of the dissolution reaction (such as citrate and oxalate). This blocking effect obeys an adsorption isotherm in that the dissolution rate decreases as blocking adsorbate concentration is increased until a limiting value is reached. The acceleration by fluoride is therefore dependent upon the fraction of surface sites that are occupied by fluoride.

4.4C. Surface Microstructure

It has been observed that crystals with few lattice imperfections dissolve quite slowly, but that crystals with more imperfections dissolve more quickly (Valverde and Wagner, 1976). Imperfections create small outcrops of oxide units that share fewer coordination positions with other units than those in a planar surface (Berner, 1980). Such outcrops or "kinks" are especially active sites for renewed crystal growth, dissolution of existing surface, or adsorption

of solution species, since these sites share fewer bonds to neighboring component ions, and are more exposed to overlying solution (Pankow, 1978). Berner (1980) and Pankow (1978) discuss crystal growth and dissolution as they relate to surface microstructure.

If the activation energy of the release of component ions into solution is high, dissolution is surface-reaction controlled. Surface microstructure is important for these reactions (Berner, 1980) because sites having lower activation energies react considerably faster than other sites. Dissolution of an entire surface may depend upon reaction at only a small fraction of the total number of sites (at kink sites, for example). Blocking these sites not only blocks their dissolution, but also hinders the development of new reactive sites. Thus small amounts of inhibitor can block dissolution of a considerable area.

The surface-site binding model in Section 4.3 assumed that all surface sites have the same free energy. According to this model, the rate of dissolution is proportional to the fraction of sites occupied by substrate, and the amount of inhibition is proportional to the fraction of sites occupied by inhibitor. The effect of surface microstructure on the rate of dissolution can be incorporated into this model by allowing a distribution of surface-site free energies. According to this model, particular sites (such as kinks) bind substrate more strongly than other sites. Reaction is therefore centered at such sites, which are continually regenerated as neighboring sites are dissolved. Adsorption of inhibitor onto the most reactive sites lowers the reaction rate by an amount greater than the

fraction of total surface sites bound to inhibitor.

4.4D. Transport-Controlled Reactions

The dissolution rate may be limited by either transport of reactants to the surface or of products away from the surface. Transport is dominated by diffusion, the movement of species in response to a gradient of chemical potential (Bard and Faulkner, 1980). Consider the case of a reaction limited by transport of lattice component ions away from the surface. The rate of diffusion depends upon the thickness (δ) of the surface stagnant layer within which component concentrations reach their saturated value. The flux of reactant through the stagnant layer is given by (Bard and Faulkner,1980):

$$4.41 \quad -J(x=0) = D(dC/dx)_{x=0}$$

where x is the distance away from the surface, J(x=0) is the flux of ions (in moles/cm^2sec) away from the surface, and D is the diffusion coefficient (in cm^2/sec). The concentration gradient (dC/dx) is equal to the component bulk solution concentration minus the surface concentration, divided by the stagnant layer thickness (in cm):

$$4.42 \quad (dC/dx)_{0<x<\delta} = (C_b - C_o)/\delta$$

substituting into equation 4.41 gives:

$$4.43 \quad -J(x=0) = D(C_b - C_o)/\delta$$

Given a surface area A (cm^2) in a volume V of solution, the change

in bulk solution concentration with time is:

$$4.44 \qquad dC/dt = -AD(C_b - C_o)/V\delta$$

When diffusion of component ions away from the surface is rate limiting, the surface component concentration is equal to the saturation concentration of components in contact with the solid phase ($C_o = C_s$). The diffusion coefficient D is known for a number of ions, having been determined by electrochemical methods.

Since A, V, C_b, and C_s can all be determined experimentally, values of δ can be calculated . The magnitude of δ is determined by the stirring rate, since vigorous stirring reduces the stagnant layer thickness. Values of δ calculated for stirred reactors are typically between .001 and .01 cm (Castellan, 1971). One test for transport control of reaction rate is to assume that equation 4.44 is valid and calculate the value of δ necessary for the observed rate. If δ is much larger than the range given above, it is unlikely that the reaction is transport controlled (Pankow, 1978). The other test for transport control is to measure the reaction rate at different stirring rates. If the reaction rate increases when the stirring rate is increased, then the reaction is transport controlled.

The situation becomes more complicated when the reaction rate is controlled by diffusion through partially leached oxide layers or out of micropores in the oxide surface. In these cases, changing the stirring rate will not significantly affect the diffusion layer thickness, so no rate dependence will be observed. The value of δ may

also be larger than the range given above. Examination of the apparent activation energy can sometimes be useful. If the activation energy is large (>20 kJ/mole, Pankow (1978)) then the reaction is clearly chemically controlled. An apparent activation energy below this value, however, does not necessarily mean that the reaction is transport controlled.

4.5 Influence of Temperature and Ionic Strength

4.5A Temperature

The Arrhenius Equation defines the influence of temperature on reaction rate in terms of an energy barrier ($\Delta E^{\ddagger}$) that must be met and the frequency (A) of attempts to surmount it (Bard and Faulkner, 1980):

$$k = Ae^{-\Delta E^{\ddagger}/RT} \qquad 4.45$$

$\Delta E^{\ddagger}$, the activation energy of the reaction, is related to the enthalpy of activation by the following equation:

$$\Delta H^{\neq} = \Delta E^{\neq} + \Delta(PV)^{\neq} \qquad 4.46$$

In an aqueous phase, $\Delta E^{\ddagger} >> \Delta(PV)^{\ddagger}$ and the energy barrier depends on the magnitude of the enthalpy of activation. Factoring an entropy term out of the frequency factor A provides an expression for temperature dependence in terms of $\Delta G^{\ddagger}$, the standard free energy of activation (Bard and Faulkner, 1980):

4.47 $$k = Ae^{-\Delta E^{\ddagger}/RT} = A'e^{\Delta S^{\ddagger}/R}\, e^{-\Delta H^{\ddagger}/RT}$$

$$= A'e^{-(\Delta H^{\ddagger} - T\Delta S^{\ddagger})/RT} = A'e^{-\Delta G^{\ddagger}/RT}$$

The apparent activation energy (E_{act}) is calculated from the temperature dependence of the experimental rate constant, and does not require knowledge of the rate-determining step. The apparent activation energy, however, may contain contributions from reactions that precede the rate-determining step (Adamson, 1976). This is best illustrated by considering a few limiting cases of equation 4.12 from section 4.3A.

Case 1: The surface reaction is much faster than adsorption and desorption. In this case,

4.48 $$k_2 >> k_1[HA] + k_{-1}$$

and

4.49 $$\frac{d[P]}{dt} = k_1 S_T[HA].$$

The apparent rate constant is equal to the rate constant for the adsorption step:

4.50 $$k_{app} = k_1.$$

Therefore,

4.51 $$Ae^{-E_{act}/RT} = Ae^{-\Delta E_1^{\ddagger}/RT}$$

and

4.52 $$E_{act} = E_1^{\ddagger}$$

The apparent activation energy for this situation is equal to the activation energy for the adsorption step.

Case 2: The surface reaction is much slower than adsorption and desorption. ($k_2 << k_1[HA] + k_{-1}$). At low surface coverage,

4.53 $$\frac{d[P]}{dt} = k_2 S_T K_{SA}^{s}[HA]$$

and

4.54 $$k_{app} = k_2 K_{SA}^{s}$$

In this case,

4.55 $$E_{act} = \Delta E_2^{\ddagger} + \Delta H_{ads}^{o}$$

The apparent activation energy is equal to the sum of the activation energy of the surface reaction and the enthalpy of adsorption. At high surface coverage,

4.56 $$\frac{d[P]}{dt} = k_2 S_T$$

and

4.57 $$E_{act} = E_2^{\ddagger}$$

In case 2, changing the substrate surface coverage changes the apparent activation energy. The significance of experimentally derived values of E_{act} must be judged in light of this result.

4.5B Ionic Strength and Solute Species

The transition state for reaction between two charged species can be considered an activated complex, which decomposes to form product:

4.58 $$A + B \rightleftharpoons m^{\ddagger} \longrightarrow \text{Products}$$

$$K_s = \frac{\{m^{\ddagger}\}}{\{A\}\{B\}} = \frac{[m]}{[A][B]} \frac{\gamma_m^{\ddagger}}{\gamma_A \cdot \gamma_B}$$

The reaction rate is proportional to the concentration of activated complex (Frost and Pearson, 1961):

4.59 $$\text{Rate } \alpha[m^{\ddagger}] = K_s[A][B]\left(\frac{\gamma_A\gamma_B}{\gamma_m^{\ddagger}}\right)$$

Ionic strength influences the reaction rate because it determines the values of the activity coefficients. The rate constant at a given ionic strength is related to the rate constant at infinite dilution (I=0) by the ratio of the activity coefficients:

4.60 $$k(I) = k(0)\frac{\gamma_A\gamma_B}{\gamma_m^{\ddagger}} \quad .$$

Estimates of the activity coefficients can be used to find how the rate

constant changes as the ionic strength is changed. Below an ionic strength of $5x10^{-3}M$, the Debye-Huckel Approximation can be used (Stumm and Morgan, 1981) and equation 4.60 becomes (Frost and Pearson, 1961):

$$4.61 \quad \ell nk = \ell nk_0 + 2Z_A Z_B \alpha \sqrt{\mu}$$

$$\alpha = 0.51x2.303$$

For the reaction of ions having like charge, the rate constant increases with increasing ionic strength. Equation 4.60 will accurately predict the experimentally derived ionic strength dependence if the identity and charge of all species involved in activated complex formation are known.

The Secondary Salt Effect is pertinent when the reaction is subject to acid or base catalysis. It is caused by changes in the dissociation constants of weak acids and bases as the ionic strength is increased (Frost and Pearson, 1961).

4.5C. Ionic Strength, Surface Charge, and Surface Species

The rates of surface chemical reactions depend upon the relative amount of surface sites occupied by adsorbate. Ionic strength influences the extent of adsorbate binding by altering the coulombic forces at the surface, the availability of surface sites, and the activity of solute species.

The standard free energy (ΔG^o) of adsorption of a charged species from bulk solution onto a charged surface can be written as the

sum of the chemical (ϕ) and electrostatic ($zF\Psi_\delta$) energy contributions (Stumm and Morgan, 1981):

4.62 $$\Delta\overline{G}^\circ = \phi + zF\psi_\delta$$

where F= Faraday's constant
and z= Ion charge.

δ is the distance from the oxide surface to the plane of adsorption and ψ_δ is the potential at that plane. Depending on the relative magnitude of the two terms, the chemical energy can overcome unfavorable electrostatics and make adsorption of ions onto a surface of unfavorable charge possible.

The electrostatic contribution can be treated separately by defining the concentration of solute species in the surface layer using the following equation (Stumm and Morgan, 1981):

4.63 $$[C^z]_x = [C^z]_{x=\infty}\, e^{-zF\psi_\delta/RT}$$

where $[C^z]_{x=\infty}$ = Species concentration at an infinite distance from the charged surface (bulk solution).

The potential at the plane of adsorption (ψ_δ) determines the concentration of ions in the surface layer and therefore the amount of adsorption. The potential, in turn, is determined by the surface charge and the distribution of space charge.

Models for the calculation of surface complex equilibria have been developed by Davis et al. (1978) and Schindler (1981). The equilibrium

state is found by simultaneously solving surface equilibria, electroneutrality, and charge-potential equations at constant ionic strength. When the ionic strength is changed, the surface charge (σ_o) changes, except at pH = pH_{zpc} (Davis et al., 1978). The potential at the plane of adsorption changes in response to the new surface charge. The effect of ionic strength on the surface charge-potential relationship must therefore be addressed. Yates et al. (1974) noted that surface charge densities for metal oxides are much larger than for classical Nernstian Hg(l) and AgI(s) surfaces for a given potential. They also noted that surface charge densities of metal oxides are quite symmetric above and below the pH_{zpc}, indicating that anions and cations of supporting electrolyte are adsorbed to the same extent on oppositely charged surfaces. On the basis of these observations they proposed that ion pairs are formed between supporting electrolyte ions and surface sites. The oxide surface charge is therefore balanced both by the distribution of counterions in the diffuse layer and by electrolyte ions bound in ion pairs on the surface.

The formation of surface ion pairs can be written as follows (Davis et al., 1978):

4.64 $\equiv MeO^- + Na^+ \rightleftharpoons \equiv MeO^- - Na^+$

4.65 $\equiv MeOH_2^+ + Cl^- \rightleftharpoons \equiv MeOH_2^+ - Cl^-$.

Electrostatic interaction and energies of solvation are the main considerations in ion pair formation. For this reason, binding

constants for equation 4.64 and 4.65 are approximately the same. As the ionic strength increases, equilibria 4.64 and 4.65 shift to the right, and more surface sites are in the ion pair form. Ion pair formation competes with the formation of surface complexes with adsorbate species (as shown in Table 4.1). An increase in ionic strength, therefore, reduces the amount of adsorbate bound to the surface.

4.6 Previous Laboratory Studies

4.6A. Dissolution Experiments

Reduction of manganese oxides by organics has been observed under a variety of chemical conditions. Commercial grade MnO_2 was reduced by tannic and gallic acids in a study by Hem (1965). Aliquots were removed from test solutions over a period of several months and filtered to determine the amount of dissolved manganese. No effort was made to exclude oxygen, and pH changed by substantial amounts as the reaction proceeded. From 10 to 100 mg/l of organic substrate were used, and starting pH values were between 4.5 and 9.5. The rate and extent of dissolution were greatest at low pH values and high organic substrate concentrations. A month or more was required for the dissolved manganese concentration to reach its final value.

A study of mineral dissolution by Baker (1973) determined that measurable amounts of pyrolusite (MnO_2) were dissolved within one hour in solutions of soil humic acid, salicylic acid, oxalic acid, pyrogallol, and alanine. The results are difficult to interpret, however, because of poor pH control. Adding acidic organic substrates

may have lowered the pH enough to accelerate the rate of dissolution. A study by Guy and Chakrabarti (1976) found this to be true; pyrogallol, gallic acid, tannic acid, and hydroquinone all dissolved more manganese dioxide at pH 2.1 than at pH 8.0.

Manganese oxides have been found to accelerate the formation of colored organic polymers from phenolic compounds (Larson and Hufnal, 1980). Transition metal ions and oxides were added to 0.1M phosphate solutions (pH 7.6) of catechol, gallic acid, 3,4-dihydroxybenzoic acid, 4-methylcatechol, caffeic acid, hydroquinone, guaiacol, resorcinol, and phenol. The amount of polymerization was monitored by measuring the absorbance at 360 nm. Mn^{2+} was found to slightly increase the rate of polymerization. Commercial grade manganese dioxide was the most effective reagent for accelerating the color development of catechol, increasing the extent of polymerization by 30 times. Color development was greatest for organics having ortho- phenolic groups and was lowest for meta- substituted compounds. This observation may in part reflect differences between the spectra of the oxidation products formed. Oxidized catechol, for example, may absorb more strongly at 360 nm than oxidized resorcinol.

4.6B. Photoreduction

Photoreduction of manganese oxides by marine humics has been demonstrated by Sunda et al. (1982). ^{54}Mn labelled manganese oxides were added to filtered seawater samples and exposed to sunlight. Dissolution was measured by determining ^{54}Mn activity in aliquots filtered with 0.2 micron nucleopore filters. The total amount of added

manganese oxide was 10^{-8}M, and the highest concentration of marine organics was 5mg/l.

Dissolution was observed in all experiments, and increased with increasing light intensity and humic acid concentration. Runs performed in the dark exhibited a linear increase in dissolved ^{54}Mn with time. In the presence of light, the rate of dissolution increased at first, then reached a constant value. Final reaction rates in sunlight were 7 to 8 times faster than in the dark.

These results indicate that the marine humics are more effective reductants after photoactivation. Sunda et al.(1982) suggest that photoactivation may involve the generation of reactive radicals from humic molecules.

4.6C. Radical Formation

Generation of radicals by reaction of manganese dioxide with hydroquinone was studied by Fukuzumi et al. (1973, 1975) and Ono et al. (1977). Radicals were formed by passing oxygen-free, alkaline (pH 9) solutions of hydroquinone (5 to 30 mM) through a small column of commercial MnO_2 reagent. The effluent was pumped into an ESR chamber. ESR measurements determined that the semiquinone radical anion ($Q^{\cdot -}$) was present in the column effluent, while protonated radicals ($HQ^{\cdot}$ and $H_2Q^{\cdot +}$) were not. These radicals have the following structures:

$Q^{\cdot -}$ 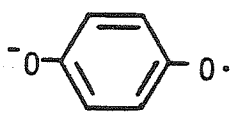

$HQ^{\cdot}$ 

$H_2Q^{\cdot+}$ 

The UV/visible absorbance spectrum of the semiquinone radical anion was measured and the following molar absorptivities calculated (Fukuzumi et al.,1973):

Wavelength(nm)	molar absorptivity ($x10^3$moles/liter/cm)	
430	5.4	
404	4.6	
371	3.7	shoulder
316	40.	
310	33.	shoulder

A reduction in flow rate through the MnO_2 column increased the concentration of semiquinone radical anion until a maximum value was reached, which was approximately 10% of the initial hydroquinone concentration (Fukuzumi et al., 1975). When the flow was turned off and oxygen allowed in, the radical decomposed by a first-order rate law, with a half-life greater than 120 minutes. The half-life in the absence of oxygen was even greater.

In a subsequent study, Ono et al.(1977) determined the following rate law by measuring the semiquinone radical anion concentration in samples removed from a stirred reaction vessel:

$$4.66 \qquad \frac{d[Q^{\cdot -}]}{dt} = k(b[QH_2]_0 - [Q^{\cdot -}])(c[MnO_2]_0 - [Q^{\cdot -}])$$

where $[QH_2]_0$ = Initial hydroquinone concentration

$[MnO_2]_0$ = Initial MnO_2 loading (gms/liter)

$k = 3.36 \times 10^2$ l/mole/minute.

The constants b and c were determined from the following relationships: when hydroquinone was in excess, $[Q^{\cdot -}]_{t=\infty} = c[MnO_2]_o$, and when manganese oxide was in excess, $[Q^{\cdot -}]_{t=\infty} = b[QH_2]_o$. The dependence of the reaction on temperature was studied in the range of 10 to 40^0C, and the activation energy calculated to be 33±2 kJ/mole (Ono et al., 1977).

The following mechanism was proposed for the reaction (Ono et al., 1977):

$$4.68 \qquad QH_2 + *MnO_2 \underset{k_{-1}}{\overset{k_1}{\rightleftharpoons}} HQ^{\cdot} + *MnO(OH)$$

$$4.69 \qquad QH_2 + *MnO(OH) \underset{k_{-2}}{\overset{k_2}{\rightleftharpoons}} HQ^{\cdot} + *Mn(OH)_2$$

$$4.70 \qquad {}^{\cdot}QH \underset{k_{-3}}{\overset{k_3}{\rightleftharpoons}} Q^{\cdot -} + H^+$$

(*) signifies surface species. Values of log k_3 and log k_{-3} were determined by Smith and Carrington (1967) to be 6.9±0.2 and 10.6±0.3 respectively. The pK_a of the semiquinone radical is,

therefore, 3.7. The rate-limiting step was found to be reaction 4.68, hydrogen-atom abstraction from hydroquinone. The authors assumed that reduction of *MnO(OH) sites generated by reaction 4.68 was quite fast.

The rates of Mn^{2+} and p-benzoquinone formation were not directly addressed in these studies. Fukuzumi et al. (1975) did note, however, that in acidic solution hydroquinone was converted completely to p-benzoquinone and that the amount of Mn^{2+} that was formed under these conditions was equal to $[QH_2]_o$.

4.7 Conclusions

The dissolution of manganese oxides by organics involved a number of separate steps, any of which may be rate-limiting. The rate-limiting step can be identified by using a number of different experimental results. The influence of the stirring rate on the reaction rate and the magnitude of the activation energy determine whether or not dissolution is transport limited. The surface site-binding model can be evaluated using the orders of the reaction with respect to substrate and hydrogen ion concentrations. Deviation from the rate-dependence predicted from this model indicates that other steps in the reaction sequence, such as release of Mn(II) from the crystal lattice, may be rate-limiting. Experimental rate information also shows how quickly new surface sites are generated as other sites are removed by dissolution.

CHAPTER 5

THE MANGANESE OXIDE SOLID PHASE

5.1 Introduction

A method has been developed for preparing manganese oxide suspensions in the laboratory that resemble natural manganese oxide phases. Chemical and physical parameters that influence the product mineralogy are considered in this chapter, and a procedure outlined that promotes the formation of trivalent manganese oxides. The method described involves oxygenation of $Mn(OH)_2(s)$ precipitated with ammonia at room temperature. Suspensions prepared by this method are stable with respect to settling over several months and are free of cationic impurities.

5.1A Mineralogy and Abundance of Natural Manganese Oxides

A variety of distinct mineralogical phases have been identified in manganese oxide particles, crusts, and coatings found in contact with natural waters. Many forms, however, are amorphous to X-ray diffraction analysis. In recent years infared (IR) spectra have been used to characterize samples of low crystallinity. Absorbance in the IR region depends on the short range ordering in the sample, making it well suited for the examination of amorphous material (Gadsden, 1975). IR is a particularly sensitive technique for studying hydrous minerals, including a number of important manganese oxides (Potter and Rossman, 1979A).

Manganese minerals of interest in this study are listed in Table 5.1. The phases todorokite, birnessite, and vernadite are predominant

Table 5.1 Manganese Oxide/Hydroxides (From Fleischer,1980)

From Fleischer (1980) and Burns and Burns (1979)

Pyrochroite	$Mn(OH)_2$
Manganosite	MnO
Hausmannite	Mn_3O_4
Partridgeite (Bixbyite)	Mn_2O_3
Groutite (α-MnOOH)	MnO(OH)
Feitknechtite (β-MnOOH)	MnO(OH)
Manganite (γ-MnOOH)	MnO(OH)
Birnessite (7 A Manganite)	$(Na,Ca,K)(Mn,Mn)Mn_6O_{14}\cdot 5H_2O$
Buserite (10 A Manganite)	Na Mn Oxide Hydrate
Pyrolusite (β-MnO_2)	MnO_2 (stoichiometric)
Ramsdellite	MnO_2 (")
Nsutite (γ-MnO_2)	$(Mn^{2+},Mn^{3+},Mn^{4+})(O,OH)_2$
Rancieite	$(Ca,Mn)Mn_4O_9\cdot 3H_2O$
Todorokite	$(Ca,Na,K)(Mn,Mn^{2+})Mn_5O_{12}\cdot xH_2O$
Vernadite (δ-MnO_2)	$(Mn^{4+},Fe^{3+},Ca,Na)(O,OH)_2\cdot nH_2O$

in marine systems (Burns and Burns, 1979). Birnessite is concentrated in hydrothermal crusts, todorokite in deep sea crusts and nodules. Studies to date suggest that slow oxidation of Mn^{2+} in ocean water forms vernadite (Burns and Burns, 1979). Biogenic formation of manganese oxides in seawater may also be significant; one species of marine bacteria has been found to form birnessite (D.W. Northfelt, G.R. Rossen, R.A. Rossen, and K.H. Nealson, pers. comm.).

IR analysis was used to identify manganese oxides in stream deposits by Potter and Rossman (1979B). Birnessite was predominant in most samples, and clay minerals were found necessary for its formation. Birnessite has also been identified in lake sediment ferromanganese nodules (Schoettle and Friedman, 1971). Potter and Rossman examined one oxide from an stream deposit lacking clay minerals, and it consisted of nsutite.

Identification of manganese oxide phases in natural particulate matter is quite difficult, often requiring indirect methods of study. Particulate manganese collected above the oxygen-hydrogen sulfide interface in Saanich Inlet has an average valence between +2.32 and +2.72, which indicates a predominance of partially oxidized phases (Emerson et al., 1982). Stumm and Giovanoli (1976) prepared artificial lake water and monitored the oxidation of added Mn^{2+}. After several months, long thin oxide needles were formed and identified as manganite (γ-MnOOH(s)) using X-ray diffraction. Manganese oxide particles collected from natural lake water, although X-ray amorphous, had the same needle-like morphology.

5.1B. Laboratory Studies of Mn^{2+} Oxidation

Both hausmannite ($Mn_3O_4(s)$) and feitknechtite (β-MnOOH(s)) have been identified in oxides freshly prepared by oxygenation of Mn^{2+} in slightly alkaline solution. Bricker (1965) oxidized Mn^{2+} by adding NaOH to solutions bubbled with oxygen, forming a mixture of the two phases. Sung (1981) identified feitknechtite as the product of Mn^{2+} oxygenation in bicarbonate solution. Both phases are transformed within a few months into manganite (γ-MnOOH(s)) (Feitknecht et al., 1962; Bricker, 1965; Stumm and Giovanoli, 1976). Stumm and Giovanoli (1976) have suggested that a similar sequence occurs in lake waters.

Precipitation of pyrochroite ($Mn(OH)_2(s)$) prior to oxygenation may favor feitknechtite formation. Feitknechtite has a crystal structure similar to pyrochroite, allowing oxidation to occur with a minimum amount of reordering (Bricker, 1965). Oxidation of pyrochroite to hausmannite, however, requires considerable reordering and will occur more slowly as a consequence. For this reason, rapid oxidation of pyrochroite may favor feitknechtite formation, whereas slow reactions allow reordering to hausmannite to occur. Oxygenation of solutions undersaturated with respect to pyrochroite may form a greater amount of hausmannite.

Feitknechtite and hausmannite are thus oxidation products of two competing reaction mechanisms. This implies that the relative yields of feitknechtite and hausmannite can be controlled by modifying the pyrochroite content of the Mn^{II} solution to be oxidized.

Temperature influences the relative amount of hausmannite and feitknechtite formed during oxygenation. Hem (1981) found that oxygenation near $0^{o}C$ formed only feitknechtite, while higher temperatures formed a mixture of the two phases. Between 25 and $37^{o}C$ hausmannite was the predominant product. Hem (1981) reasoned that both products result from oxidation of Mn^{II} hydrolysis species having structures similar to pyrochroite. The greater temperature dependence of hausmannite formation is caused by the additional amount of rearrangement necessary to form hausmannite from pyrochroite-like structures.

Manganite is the most highly oxidized product that can be formed from oxidizing Mn^{II} solutions of low alkalinity with oxygen or hydrogen peroxide (Bricker, 1965). Feitknechtite and hausmannite suspensions prepared by oxygenation convert to manganite upon standing several months. Stronger conditions or disproportionation reactions are necessary to make Mn^{IV} oxides at room temperatures. Giovanoli et al. (1970) formed Na-buserite by bubbling oxygen through suspensions of pyrochroite in 0.76M NaOH. Acidification of manganite, feitknechtite, or bixbyite disproportionates Mn^{III} into Mn^{II} and Mn^{IV} forming non-stoichiometric manganese dioxides (Giovanoli and Leuenberger, 1969).

A number of manganese oxide phases contain sites filled by mono- and divalent cations. Cation exchange can occur by replacing these cations by other cations of similar size, or by their replacement with H^{+}. Buser and Graf (1955) studied the exchange of radio-labelled

cations in layered Mn^{IV} manganites. Reaction half-lives varied from minutes for exchange into intermediate oxide layers to around 40 hours for exchange into the main oxide layers. The experiments of Giovanoli et al. (1975) illustrate such reactions with buserite minerals, which are particularly susceptible to loss of bound cations. Na-buserite was synthesized by oxidation of Mn^{II} in 3M NaOH. Cu,Zn,Ni,Co,Ca, and Mg-buserites were formed by washing the Na-buserite oxide and suspending it in 0.1M solutions of the corresponding metal nitrate. Exchange of Na^+ by transition metal ions causes the layer separation in the buserite lattice to change. The pH of acidic solutions in which buserites have been suspended gradually increases as the metal ions in the crystal lattice are exchanged for H^+. Loss of cations from the lattice can disrupt the mineral structure. Leaching of Na^+ from Na-buserite below pH 6.2 is sufficient to cause a collapse of the 10 Ångstrom layer separation of buserite to the 7 Ångstrom birnessite structure. Drying of Na-buserite in a vacuum also causes collapse to the birnessite structure (Burns and Burns, 1977). Potter and Rossman (1979A) found that the change from 10 Ångstrom to 7 Ångstrom layer spacing was caused by water loss alone. Loss of bound cations may simply change the degree of hydration.

The conclusions drawn from previous laboratory studies are that the preparation of a pure phase by oxidizing $Mn^{2+}(aq)$ is difficult, and that in most cases a non-stoichiometric oxide is formed.

5.2 Preparation of Manganese Oxide Suspensions

A procedure was sought that would produce a manganese oxide

suspension having as many of the following properties as possible:

A. Suspensions are stable with respect to settling over the entire study period (several months). Particles are a uniform size and a size convenient for study ($\sim$1 micron diameter).

B. Suspensions are prepared under conditions most resembling natural waters. The pH should be near neutrality, and oxygen should be the oxidant. In this way, surface charge, area, and reactivity are similiar to freshly precipitated natural oxides.

C. The oxide lattice is free of non-manganese cations and will not undergo cation exchange. This insures that the oxide structure does not undergo any major change as the pH is varied. Cation exchange of Mn^{II} must be avoided because release of Mn^{2+} into solution by cation exchange is indistinguishable from Mn^{2+} formed by reduction reactions.

D. The oxide is free of contamination by IR-absorbing species.

E. The oxide is a single phase. The reactivity of homogeneous particles is more uniform during dissolution than mixed phase particles that may have outer coatings of different reactivity. An oxide in which all manganese is in one oxidation state simplifies calculations of reaction stoichiometry based on dissolution reaction data.

5.2A General Considerations

The decision to use oxygen as the oxidant restricts the preparation to the following sequence:

$$Mn^{2+} \longrightarrow \text{Pyrochroite} \longrightarrow \begin{matrix}\text{Hausmannite}\\ \text{Bixbyite}\\ \text{Feitknechtite}\end{matrix} \longrightarrow \text{Manganite} \longrightarrow \text{Buserite}$$

Other oxides can be prepared by additional reactions, such as acidification of Mn^{III} oxides to form manganese dioxide by disproportionation. Mn^{II} is also formed in the disproportionation reaction, which complicates the interpretation of the dissolution experiments. The facile cation exchange of buserite, its conversion to birnessite in slightly acidic solution, and its inversion upon drying are all undesirable traits. Synthesis was therefore directed at forming Mn^{III} oxides. An additional advantage of using trivalent oxides is that every equivalent of Mn^{III} reduced releases one mole of Mn^{2+} to solution. The reaction can therefore be monitored by measuring $[Mn^{2+}]$. One-equivalent reduction of a tetravalent oxide, on the other hand, may form an insoluble Mn^{III} oxide, which does not change $[Mn^{2+}]$.

5.2B. Experimental Procedures

Reagents were chosen to minimize interference in product analysis. Stock solutions of $MnCl_2$ were used because chloride doesn't absorb in the IR. Ammonia was chosen as the source of alkalinity because its large ionic radius (compared to Na^+,K^+, etc.) may prevent its incorporation into the oxide phase. It was also felt that millimolar concentrations of Na^+, K^+, or Ca^{2+} might encourage the

formation of buserite. Any ammonium ion incorporated into the oxide product is easily identified in the IR spectrum of the washed product, because of its absorbance peak at 1398 cm^{-1} (Miller and Wilkins, 1952).

Solution pH (as controlled by ammonia concentration) controls the rate of the oxidation reaction (Morgan, 1967) and the solubility of pyrochroite (Figure 5.1). On the basis of Bricker's (1965) work, product distribution depends upon the rate of the oxidation reaction and upon whether pyrochroite saturation conditions exist. The surface charge of the forming oxide is dependent upon pH, and determines the amount of subsequent coagulation. The rate of mixing relative to the reaction rate may have a bearing on the particle size distribution by controlling localized supersaturation. Particular oxides may have surface characteristics that enhance oxidation on particle surfaces, creating fewer, larger particles.

Oxygenation experiments performed at pH's below pyrochroite saturation are illustrated by preparation B(1). Procedures followed in the preparation of B(1), as well as other preparations described in this section, are summarized in the Appendix. A solution containing 10mM of ammonia buffer (pH 8.4) was equilibrated with pure O_2 before addition of $MnCl_2$, so that local saturation of pyrochroite during mixing was avoided. Oxide particles produced during 9 hours of aeration coagulated and settled quickly, and adhered strongly to glass surfaces. All oxygenations at pH's below pyrochroite saturation ($5.0x10^{-4}$M Mn) produced particles that quickly settled and adhered

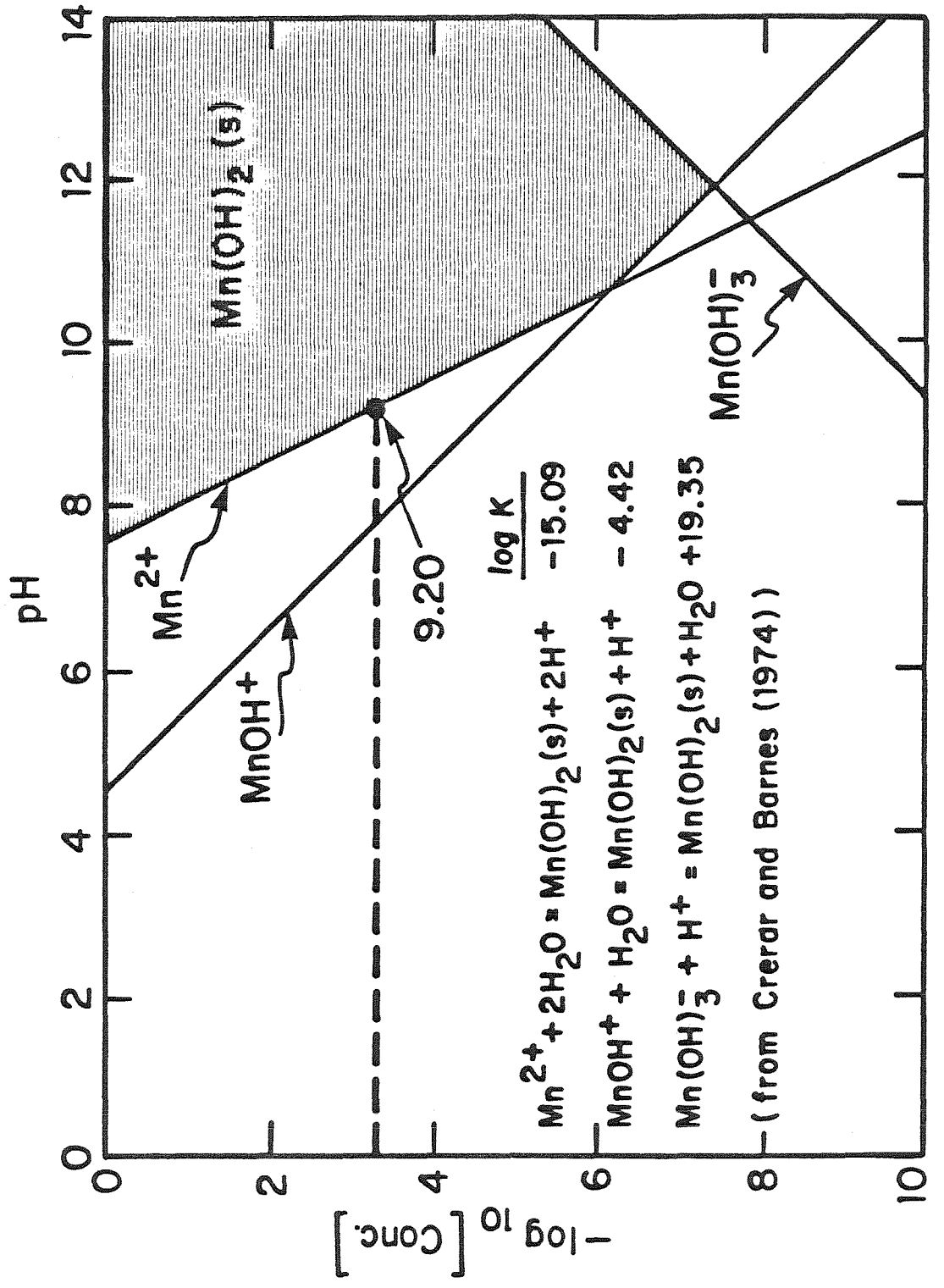

Figure 5.1 Solubility of pyrochroite, $Mn(OH)_{2(s)}$. The dashed line is drawn for $(Mn^{2+})_T = 5.0 \times 10^{-4}$M.

to surfaces.

Oxides can be produced in the range of pyrochroite saturation by either first forming a pyrochroite suspension under high purity (HP) nitrogen followed by oxygenation, or by raising the pH of an oxygen saturated solution quickly so that hydrolysis of Mn^{2+} and oxidation occur simultaneously. Sample N(2) was prepared by the latter procedure. A 3.7×10^{-2}M ammonia solution (pH 10.8) was equilibrated with pure oxygen and rapidly stirred with enough $MnCl_2$ to make a solution of 5.6×10^{-4}M Mn. Most of the oxide formed settled out during the first few days.

Formation of a pyrochroite suspension under nitrogen followed by oxygenation resulted in oxide suspensions of considerable stability with respect to settling. The preparation of oxide N(3) was begun by quickly adding enough $MnCl_2$ stock solution to 10mM ammonia (pH 10.4) to form a 3.76×10^{-4}M $Mn(OH)_2(s)$ suspension. Switching the purge gas from HP nitrogen to pure oxygen oxidized the finely dispersed pyrochroite suspension to a rich brown oxide suspension.

Suspensions N(3), N(7), N(8), and N(9) were all formed by this procedure and used in dissolution experiments and surface studies. Very high stirring rates (encouraging production of finely dispersed particles) and rapid introduction of oxygen were employed in all preparations. The procedure for preparing N(8) was different in that $MnCl_2$ stock solution was added in two steps, the first addition small and the second large. It was hoped that the resulting suspension would have fewer, larger diameter particles because of manganese from

the second addition condensing onto particles produced from the first.

5.3 Suspension Oxidizing Titer and Mn_T

5.3A. Experimental Details

Total manganese and oxidizing titer were determined using AAS and the leuco crystal violet colorimetric test. More accurate redox and complexometric titrations were also performed for comparison, and the results agree favorably. AAS determination of total manganese is described in section 6.3A.

The leuco crystal violet method of determining oxidizing titer described by Kessick et al.(1972), was followed. A suspension of manganese dioxide of known titer was used as standard, and prepared in the following manner. 400 mls of D_2H_2O (deionized,distilled water) and 25 mls of 0.20M ammonia were added to a 500 ml flask and bubbled with high purity nitrogen for one hour to remove oxygen. Addition of 6 mls of 0.10N $KMnO_4$ (Dilut-it standard) and 2 mls of 0.10M $MnCl_2$ (AR, Mallinckrodt) resulted in the formation of an oxide suspension. This suspension was purged with nitrogen for another half hour before 25 mls of 0.80M phosphate buffer solution (pH 7) were added to prevent further oxidation. The suspension was then diluted to 1 liter in a volumetric flask. This stock suspension contained 3.19×10^{-4}M Mn_T(total manganese) and 6.00×10^{-4}N oxidizing equivalents at a pH of 7.3.

Figure 5.2 shows absorbance plotted against relative dilution for the standard manganese dioxide suspension and for N(7). Both dilution plots show a linear increase in absorbance with increasing oxidizing

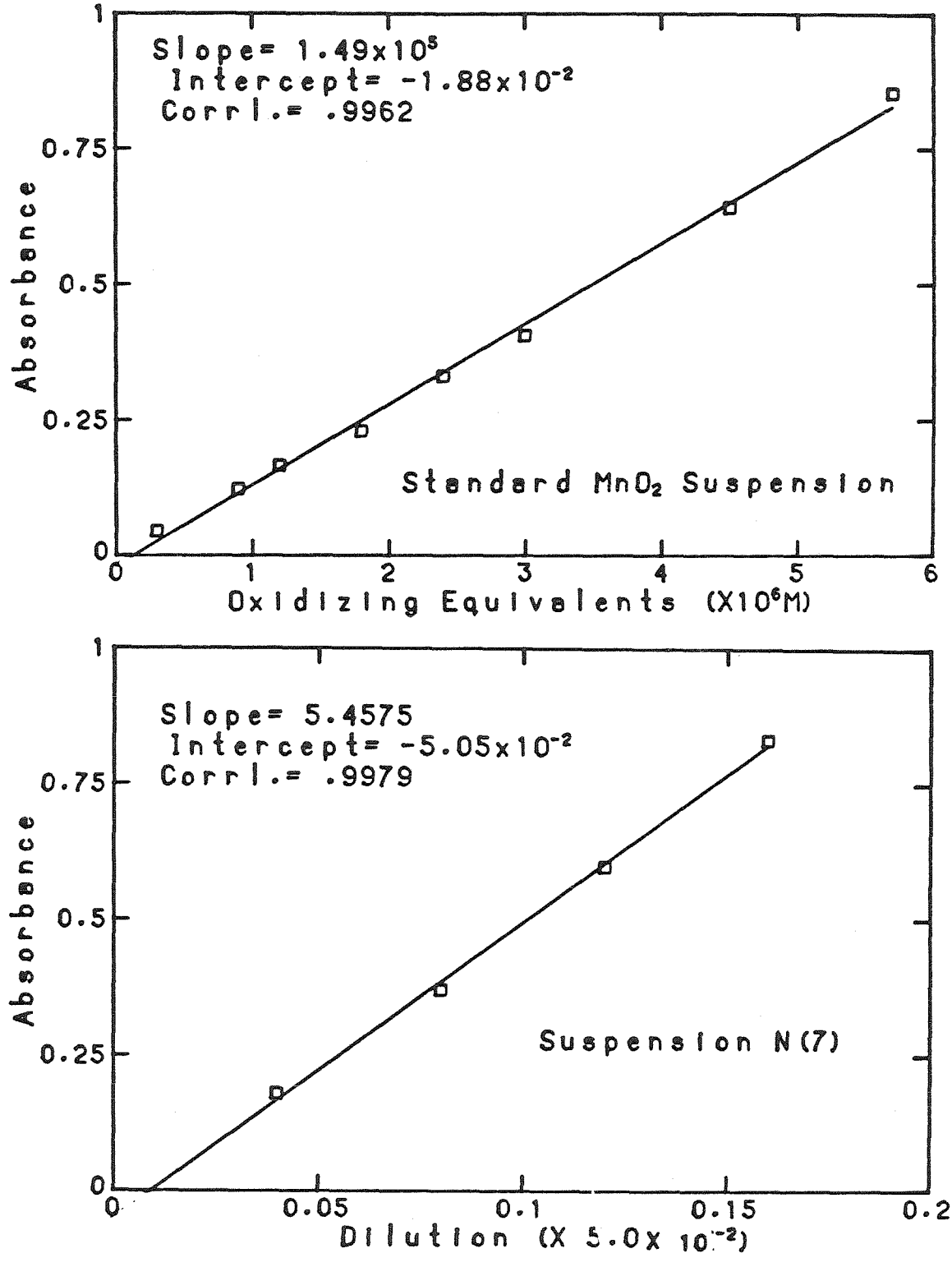

Figure 5.2 Absorbance of the Leuco Crystal Violet Reagent as a function of the concentration of oxide ir the test solution. Plot A is for manganese oxide prepared by oxidation of Mn^{2+} with permanganate, and Plot B for suspension N(7), prepared by oxidation of $Mn(OH)_2(s)$ with oxygen.

titer in accordance with Beer's law. Suspensions made by oxidizing $MnCl_2$ with oxygen consistently exhibited small, negative y-intercepts.

Procedures outlined by Schwarzenbach and Flaschka (1961) were followed to determine total manganese by complexometric titration. Manganese was reduced by excess ascorbate and titrated with EDTA using an Erio Black T indicator. Titrations were performed in a pH 10 ammonia buffer, with suspensions diluted so that the solubility of $Mn(OH)_2(s)$ was not exceeded.

Redox titration of oxidizing titer was performed by adding standardized oxalate in sulfuric acid to the suspension and titrating the excess with standardized $KMnO_4$. The method of McBride was used, as described in Skoog and West (1976). Values obtained from successive titrations agreed to within 2%.

5.3B. Oxidizing Titer and Mn_T: Results

Table 5.2 summarizes oxidizing titer and Mn_T determinations for three stock suspensions. Values determined by leuco crystal violet and AAS methods agree well with titration values. No overall trend with increasing age was observed except for a gradual decrease in Mn_T caused by settling of a fine oxide layer in the polyethylene storage bottles. Column E gives the overall oxidation state of the manganese in the oxide. If all manganese is either in the III or IV oxidation state, then 20 to 36% is present as Mn^{IV}. Although the oxides are primarily Mn^{III}, the amount of Mn^{IV} present is significant and will affect reaction stoichiometry.

Table 5.2 Oxidizing Titer and Mn_T Determinations

Suspension (A)	Age (B)	Mn_T (C)	Oxidizing Titer (D)	Oxid./Mnt (E)	Stoichiometry (F)
N(7)	10 days	5.12E-4M (AAS)	6.84E-4N (LCV)	1.337	$MnO_{1.67}$
	95	4.96E-4 (AAS)	6.32E-4 (LCV)	1.274	$MnO_{1.64}$
	204	4.60E-4 (EDTA)	6.23E-4 (Oxal)	1.356	$MnO_{1.68}$
N(8)	3 days	5.10E-4M (AAS)	6.45E-4N (LCV)	1.265	$MnO_{1.63}$
	88	4.94E-4 (AAS)	5.93E-4 (LCV)	1.200	$MnO_{1.60}$
	197	4.69E-4 (EDTA)	5.74E-4 (Oxal)	1.223	$MnO_{1.61}$
N(9)	66 days	4.61E-4M (EDTA)	5.90E-4N (Oxal)	1.280	$MnO_{1.64}$

5.4 X-Ray Diffraction

5.4A. Sample Preparation

Samples for B.E.T., X-ray diffraction, and IR analysis were all washed by the following procedure. 500 to 1000 mls of stock suspension were filtered with 0.2 micron, 47 mm nucleopore membrane filters. The oxide was rinsed three times with D_2H_2O then resuspended with about 75 mls of D_2H_2O and sonicated for 20 minutes. Filtration and sonication steps were then repeated two more times with each sample. Samples N(1), N(2), N(3), H(1), and H(2) were lypholized before analysis. Samples N(7) and N(8) were stored in D_2H_2O until IR analysis. Samples for B.E.T. and X-ray diffraction analysis were dried under an IR lamp and ground to a fine powder using a boron carbide mortar and pestle in toluene solvent.

5.4B. X-Ray Diffraction Analysis

X-ray diffraction lines were photographed using a 10 cm. diameter Debye-Scherrer (CIT Powder) camera. The back emulsion was removed from all negatives to minimize fluorescent background. Manganese oxide filtered, Fe K_α radiation (1.9373 Å) was used for most samples (28 hour exposure). One sample was also analyzed using vanadium filtered, Cr K_α radiation (2.291 Å).

5.4C. X-Ray Diffraction: Results

Table 5.3 lists the d-spacings calculated for all preparations described above, as well as for two additional ones, H(1) and H(2). These suspensions were prepared by oxidizing $MnCl_2$ solutions with hydrogen peroxide. Table 5.4 lists literature d-spacing values of

Table 5.3 X-Ray Diffraction Experimental Data

		d-Spacing (Å Angstroms)							
N(3)	8/10/81 Fe K	4.61 **	3.41	2.67 *	2.53	2.41 *	1.68	1.44	
N(3)	12/4/81 Cr K	4.63 **	3.44 *	2.69	2.52	2.41			
N(7)	4/24/82 Fe K	4.63 **	3.44	2.69 *	2.53 *	2.38 *	2.06	1.96	1.85
N(8)	4/24/82 Fe K	4.64 **		2.68 *	2.52 *	2.36 *		1.97	1.84
H(1)	1/21/82 Fe K	4.64 **	3.38	2.69 *	2.53 *	2.40 *			1.84
H(2)	1/21/82 Fe K	4.61 **		2.70 *					

** Brightest Line
* Bright Lines

Table 5.4A X-Ray Diffraction Reference Data

(Mn^{II} and Mn^{III} hydroxide/oxides)

	JCPDS Card*	d-Spacing (Ångstroms)							
Pyrochroite $Mn(OH)_2$	18-787	4.72 (90)	2.87 (40)	2.45 (100)	1.826 (60)	1.658 (40)	1.565 (30)	1.382 (20)	1.374 (20)
Manganosite MnO	7-230	2.568 (62)	2.223 (100)	1.571 (58)	1.340 (21)	1.283 (13)	.9938 (18)	.9074 (15)	.8554 (13)
Hausmannite Mn_3O_4	16-154	3.09 (50)	2.77 (90)	2.49 (100)	2.36 (40)	2.04 (40)	1.795 (50)	1.579 (50)	1.544 (80)
Partridgeite Mn_2O_3	24-508A	2.718 (100)	1.669 (13)	1.664 (13)					
Groutite α-MnOOH	12-733	4.20 (100)	2.81 (70)	2.67 (70)	2.38 (40)	2.30 (60)	1.737 (40)	1.695 (50)	1.608 (40)
Feitknechtite β-MnOOH	18-804	4.62 (100)	2.64 (50)	2.36 (20b)	1.96 (10b)				
Manganite γ-MnOOH	8-99	3.40 (100)	2.64 (60)	2.28 (50)	1.708 (40)	1.672 (30)	1.636 (40)	1.437 (30)	1.139 (40)
Manganite γ-MnOOH	18-805	3.41 (100)	2.65 (50)	2.41 (80)	2.28 (30)	2.20 (30)	1.781 (20)	1.675 (90)	1.435 (16)

* Joint Committee on Powder Diffraction Standards (1974)

Table 5.4B X-Ray Diffraction Reference Data

(Mn^{IV} oxides)

	JCPDS Card*	d-Spacings (Ångstroms)							
Na-Buserite	Giovanoli (1980)	10.11 (100)	5.07 (70)	2.59 (30)	2.50 (30)	2.47 (30)	2.39 (20)	2.31 (20)	2.29 (30)
Na-Birnessite (synthetic)	23-1046	7.09 (100)	3.56 (80)	2.51 (70)	2.42 (60)	2.21 (40)	2.15 (40)	1.47 (60)	1.43 (50)
Vernadite $MnO(OH)_2$	15-604	6.81 (30)	3.11 (60)	2.45 (20)	2.39 (100)	2.15 (60)	1.649 (30)	1.537 (40)	1.422 (40)
Nsutite γ-MnO_2	17-510	4.00 (95bb)	2.42 (65)	2.33 (70b)	2.13 (45)	1.635 (100)	1.603 (45b)	1.478 (25bb)	1.367 (40bb)
Todorokite	13-164	9.68 (100)	4.80 (80)	2.47 (20)	2.39 (40)	2.22 (20)	1.98 (20)	1.42 (30)	1.331 (50)
Pyrolusite β-MnO_2	12-716	3.14 (100)	2.41 (50)	2.13 (25)	1.98 (15)	1.63 (50)	1.56 (25)	1.43 (15)	1.31 (20)
Ramsdellite MnO_2	7-222	4.07 (100)	2.55 (100)	2.44 (70)	2.19 (70)	1.660 (80)	1.621 (80)	1.473 (80)	1.360 (80)

* Joint Committee on Powder Diffraction Standards (1974)

reference minerals for comparison.

The 4.62 Å line of feitknechtite is the strongest line in all oxides examined. This line, as well as those at 2.64, 2.36, and 1.96 Å confirm the presence of feitknechtite in all oxide samples. Feitknechtite is predominant even in oxides H(1) and H(2), products of hydrogen peroxide oxidation. The most prominent d-spacing line of manganite (3.41 Å), is present in 3 of the 5 oxides examined. Its absence in H(2), formed by adding NaOH to a solution of $MnCl_2$ and H_2O_2 indicates that using hydrogen peroxide alone does not ensure that manganite will be formed; higher pH's or temperatures than employed here are necessary to form a pure manganite phase.

The faintness of all observed lines suggests that the oxides have a low degree of crystallinity. The appearance and brightness of a line may be caused by higher crystallinity of a particular phase within the mixture and does not necessarily reflect the relative concentration of that phase.

X-ray diffraction analysis does little to help identify the 20 to 36% of manganese in the samples that is tetravalent, as determined by wet chemical techniques. The camera used can only record d-spacings smaller than 8.5 Å using Fe K_α radiation and 10.1 Å using Cr K_α radiation. The strongest lines of birnessite, nsutite, pyrolusite, and ramsdellite are within range using Fe K_α radiation, but were not observed. A line within the range 2.36 to 2.41 Å is observed in four of the five samples, and can be assigned as a weak feitknechtite line (2.36 Å) or as the most intense vernadite line (2.39 Å). None of the

other vernadite lines (although faint) were observed, making the assignment of this line to feitknechtite more reasonable. The most intense lines of buserite and todorokite are outside the measurable range of the camera. Their secondary lines, which lie within range, were not observed.

Feitknechtite was identified by X-ray diffraction in all five samples tested, and manganite in all samples except H(2) and N(8). No conclusion can be drawn based on X-ray diffraction data concerning the identity of the Mn^{IV} component.

5.5 IR Spectrometry

5.5A. Experimental Details

Oxide samples were pressed into potassium bromide (KBr) or thallous bromide (TlBr) pellets for IR analysis. KBr pellets were prepared by grinding 200 mg of KBr to a fine powder, drying KBr and sample oxide under an IR lamp, and dispersing 1 mg of sample in the KBr. Flat, 13 mm diameter pellets were pressed at 19,000 psi under vacuum. Pellets were protected from humidity before analysis. Spectra were measured against a KBr reference pellet using a Perkin-Elmer model 180 IR Spectrophotometer.

TlBr pellets were prepared for comparison with the KBr pellets. KBr is hydroscopic, and the preparation of KBr pellets can dehydrate the oxide sample. TlBr is non-hydroscopic and insoluble in water, so that moist samples can be dispersed in it, minimizing dehydration. Moist oxide (2.0 mg) was dispersed in 450 mg of finely ground TlBr (Harshaw Chemical Co., IR Red Grade). Pellets were made in a press

containing curved dies and pressed under vacuum at 19,000 psi. The use of a vacuum during pressing was unnecessary and may have caused partial dehydration of the sample. The IR spectrum of the pressed pellet was measured immediately against a TlBr reference pellet.

5.5B. IR Spectrometry: Results

Structural information concerning solid phases cannot be obtained directly from IR spectra, and identification depends upon the availability of reference spectra. Potter and Rossman (1979A) and Potter (1979) are the source of all reference spectra used in this study; absorbance peaks characteristic of each phase are summarized in Table 5.5. Table 5.6 lists the absorbance peaks measured for the solids prepared in this study. Interpretation of spectra will be difficult because no reference spectrum is available for feitknechtite, identified by X-ray diffraction in all samples. Absorbance bands of feitknechtite may overlap with those of other phases, such that assignment of absorbance bands cannot be made with confidence.

The IR spectra of N(7) and N(8) dispersed in KBr, and N(7) dispersed in TlBr are shown in Figure 5.3. All three spectra are quite similiar. Dehydration during KBr pellet preparation did not change the oxide structure.

As mentioned in section 5.2B., a peak at 1398 cm^{-1} establishes that ammonia is in the sample. Figure 5.4 indicates that ammonia was present in sample N(2), but absent in N(3). Raising the pH of an oxygen saturated solution by adding ammonia, therefore, incorporated ammonia into the solid. The absence of ammonia in N(3) indicates that

Table 5.5 IR Peaks of Reference Minerals (Potter, 1981)

(wavelengths given in cm^{-1})

Braunite		Groutite		Hausmannite	Manganite		Manganosite
221	477	293	1931	(246)	346	1087	313
246	515	325	2013	351	370	1119	466
278	550	358	2175	514	445	1149	658
312	611	497	2190	592	487	2068	
372	660	579	2695	617	>94	2665	
374	709	613	2825		613	3400	
411	948	995	3000		627	3525	
444		1027			730		

Partridgeite		Birnessite		Todorokite		
213	519	246	3352	243	590	3360-3390
251	570	330-360	3385-3435	305-310	617-635	3496-3502
270	604	420-460	3545-3550	379-388	748-763	
289	671	485-525		429-441	1593-1601	
335		555-575		457-459	1642-1649	
393		620-660		488	1685-1687	
438		740-755		508-518	2285	
494		1631-1645		549-554	3161-3186	

Rancieite	Buserite	Pyrolusite	Ramsdellite		Nsutite
425-456	359-362	335-340	270	3335	375-380
494-506	411-414	390-400	377	3389	476
623-633	475-477	535-615	476	3520	515-530
670-681	509-510	630-670	523		565-590
1643-1654	633	705-735	597		685-730
3200-3225			592		
3378-3397			750		
3546-3576			1640		

Table 5.6 IR Peaks of Oxide Preparations

(wavelength given in cm^{-1})

N(2)	N(3)	N(7)	N(8)	H(1)	H(2)
		275	279		
	325	320	320	(324)	324
(344)		348	349		
		371	380	375	
		425	(417)		
440					
	(504)	504	500	(505)	(492)
525	529	528	530	529	522
		578	580		
622	601	604	605	600	599
			(640)		
(749)	*	(735)		(727)	*
		(757)			
	813	814	813	816	
					833
		(890)	(890)		
	946	948	947	946	941
	1082	1069	1069	1067	1064
	(1109)			(1118)	
	1144			1146	(1150)
				(1244)	
				(1365)	
1398@					
				(1415)	
				1550	
1617	1636	1642	1646		
				(1711)	
	1862	1864	1865	1860	1859
			(1960)		
	2046				
		2152	2151	2160	2143
				2655	
	2760				
					2842
	2915				
				2979	
3000		3080	3070		
3155					
	3363				
		(3438)	(3438)	(3460)	3411
3508					

* Very weak shoulder @ Absorbance peak of NH_4^+

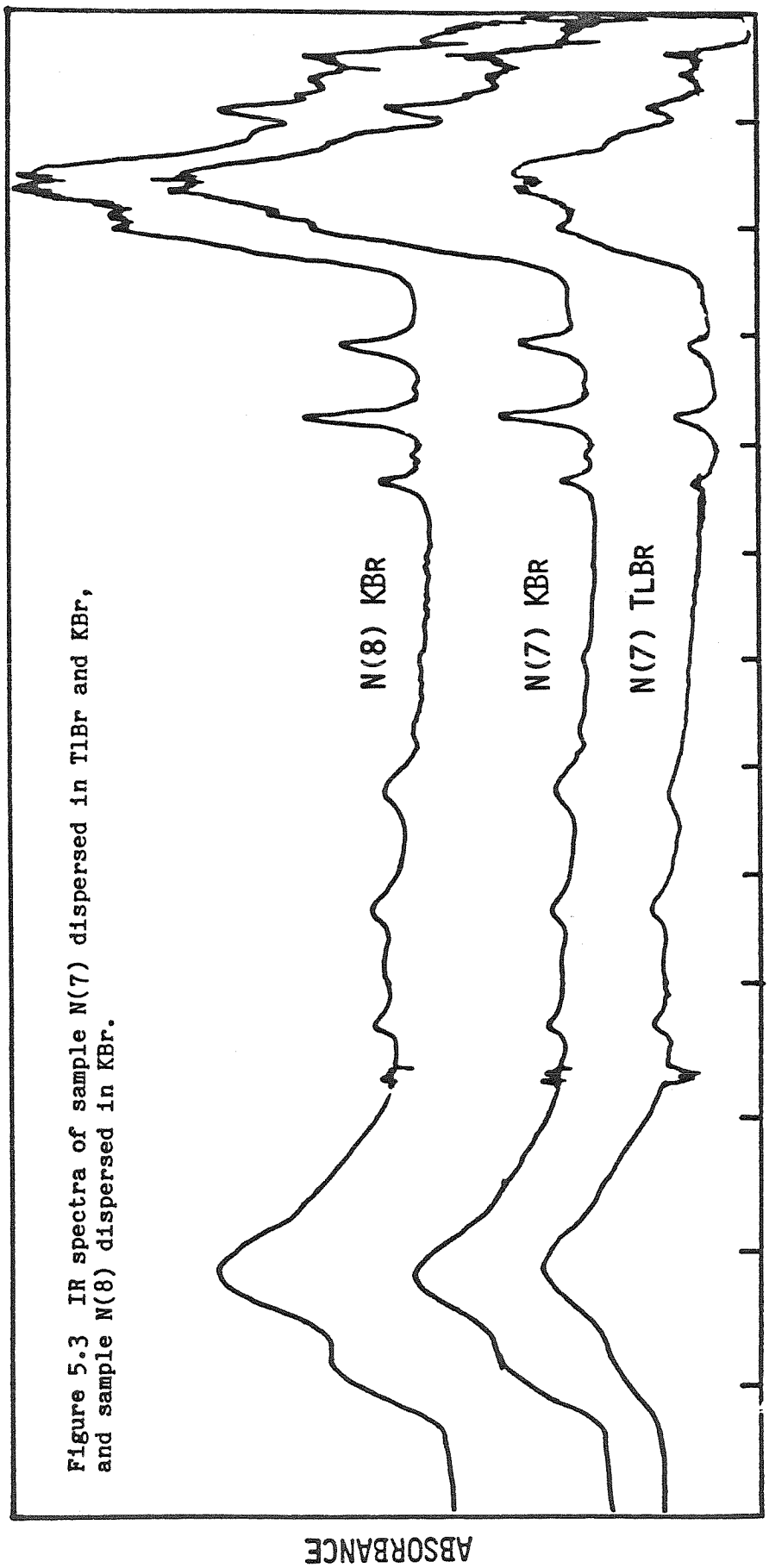

Figure 5.3 IR spectra of sample N(7) dispersed in TlBr and KBr, and sample N(8) dispersed in KBr.

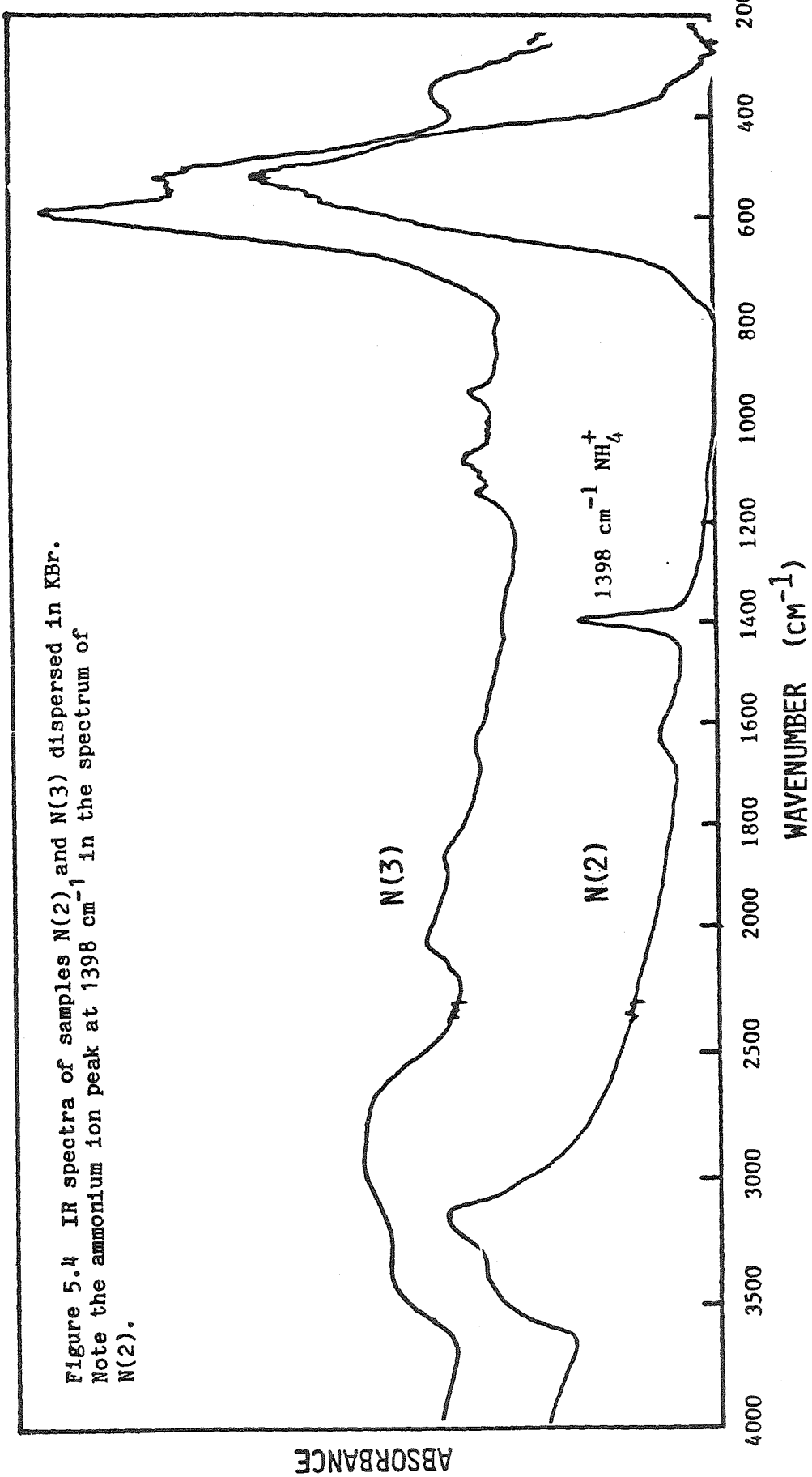

Figure 5.4 IR spectra of samples N(2) and N(3) dispersed in KBr. Note the ammonium ion peak at 1398 cm^{-1} in the spectrum of N(2).

formation of a pyrochroite suspension followed by oxygenation was successful in excluding ammonium ions.

Spectra of samples N(7) and N(8) contain features not present in any of the reference spectra. Three intense metal-hydroxide bands are observed at 813-816 cm^{-1}, 941-947 cm^{-1} and 1064-1069 cm^{-1}, and are quite distinct from the characteristic bands of manganite (1087,1119, and 1149 cm^{-1}) and groutite (995 and 1027 cm^{-1}). Manganite lines, although faint, do appear in the spectra of samples N(3) and H(1) (Figures 5.4,5.5, and 5.6). Groutite characteristic bands were not observed in any spectra. Figure 5.6 shows that, within the region characteristic of manganese- hydroxide groups (800-1200 cm^{-1}), relative peak heights vary considerably. This reflects varying amounts of different Mn-OH mineral phases, predominately feitknechtite and manganite, in the samples. Oxides such as N(2) prepared by raising the pH of oxygen-saturated $MnCl_2$ solutions do not absorb appreciably in this region (Figure 5.4). The three unknown absorbance bands described above are assigned to the phase feitknechtite, because of the identification of feitknechtite by X-ray diffraction, and because of their distinct position relative to reference manganite and groutite bands.

Although feitknechtite bands are easily distinguished from other oxides in the 800-1200 cm^{-1} region, they are not in the 200-800 and 1200-4000 cm^{-1} regions. Bands are observed within 100 cm^{-1} of the 2100 and 2700 cm^{-1} manganite hydroxyl bands, but cannot be assigned to manganite because of the unknown feitknechtite contribution

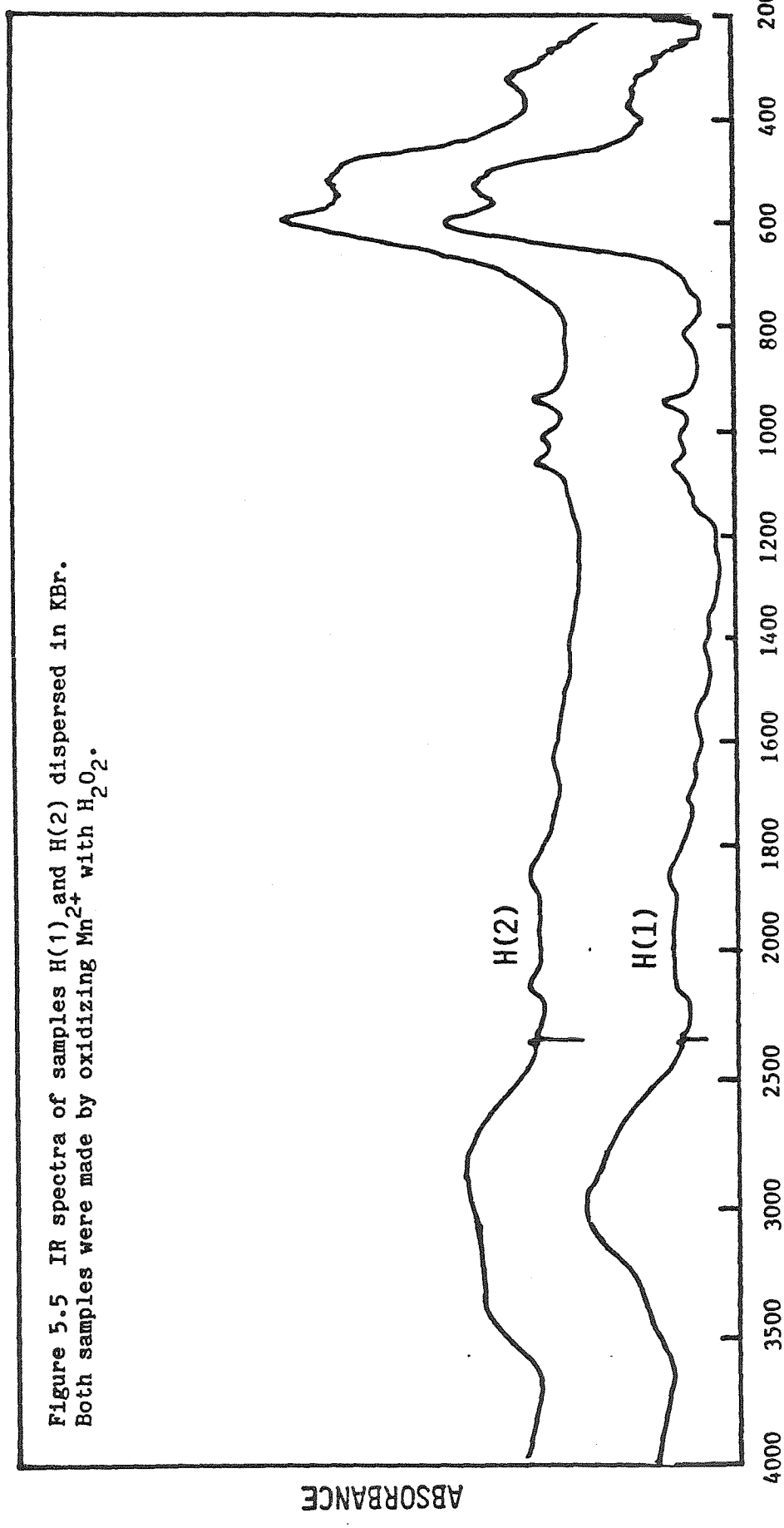

Figure 5.5 IR spectra of samples H(1)$_2$ and H(2) dispersed in KBr.
Both samples were made by oxidizing Mn^{2+} with H_2O_2.

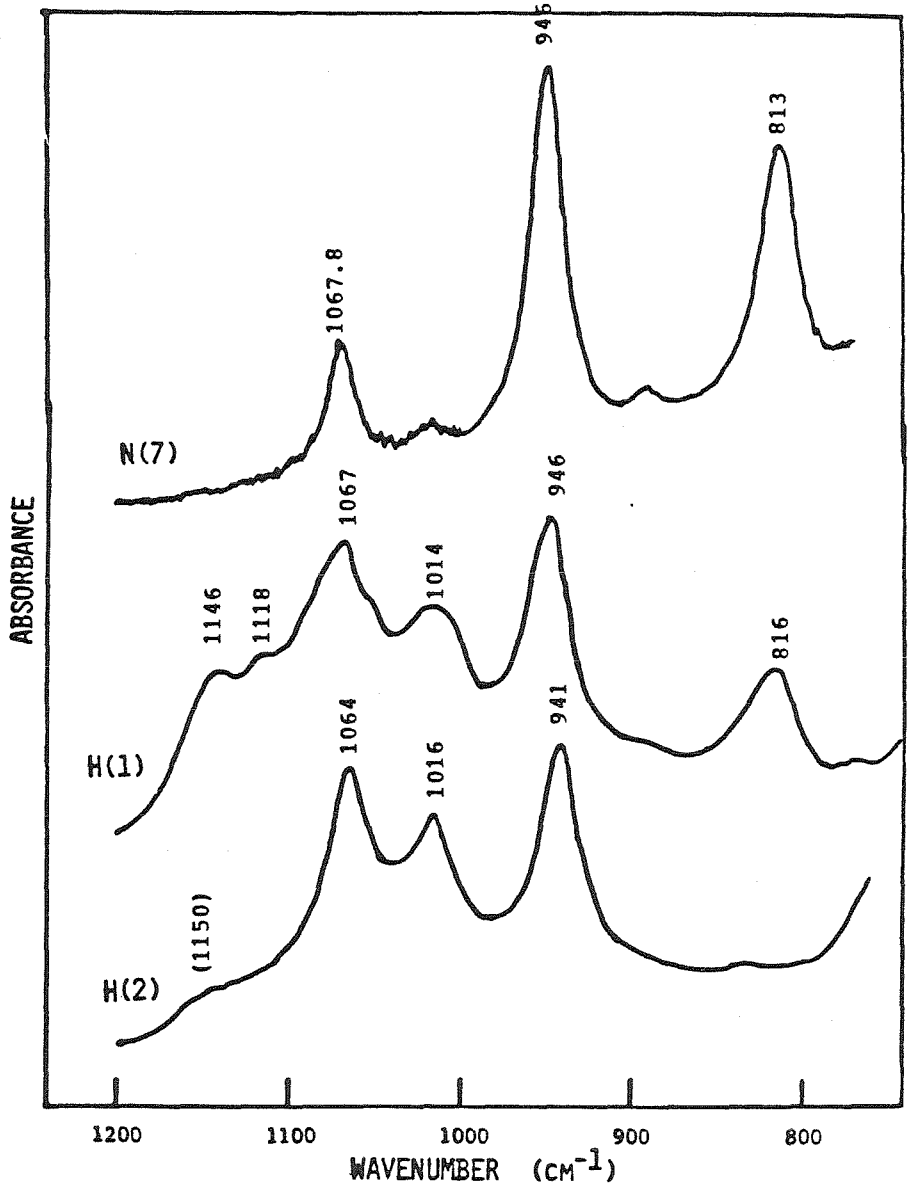

Figure 5.6 IR spectra of N(7),H(1), and H(2) in the region characteristic of Mn-OH groups.

in this region. Manganite peaks in the 800-1200 cm^{-1} region are quite faint, suggesting that other peaks may be obscured by feitknechtite absorbance.

Recorded sample spectra show little resemblance to reference spectra of hausmannite, groutite, partridgeite, pyrolusite, ramsdellite, and nsutite. Identification of principal peaks of buserite, rancieite, todorokite, and birnessite based on the 200 to 800 cm^{-1} region is made difficult by the strong absorbance of the manganese hydroxide (feitknechtite) component in this region. Variations in relative peak heights from sample to sample in this region also indicate that a mixed phase of variable composition is present in all samples. Characteristic peaks of rancieite and todorokite are not present in the oxide spectra. Two key birnessite bands (420-460 and 485-525 cm^{-1}) as well as a weak shoulder at 740-755 cm^{-1} are present in N(7) and N(8).

IR spectra of N(3), N(7), N(8), H(1), and H(2) contain manganese-hydroxide bands not found in available reference spectra. These bands are assigned to the phase feitknechtite, which has been identified in the samples by X-ray diffraction. Manganite has been tentatively identified in samples N(3) and H(1), and birnessite in samples N(7) and N(8). The low degree of crystallinity and presence of two or more phases make identification by IR necessarily tentative.

5.6 Surface Analysis

The particle size distribution of the oxide suspensions can be determined using the filtration technique described in Section 6.2.

Figures 6.2 and 6.3 show how the particle size distribution of suspensions N(7) and N(9) respectively change over a five month period. Freshly prepared suspensions contain particles that are between 0.2 and 0.4 microns in diameter. Coagulation slowly causes the particle size to increase with time, until most particles are larger than 1.0 microns after 5 months of aging.

5.6A. B.E.T. Analysis

Hem (1981) measured B.E.T. surface areas ranging from 48 to 99 m^2/gm for hausmannite and feitknechtite oxygenation products. In the present study, the surface area of suspension N(8) was measured using nitrogen as the adsorbate. The 140-day-old oxide sample was washed and ground to a fine powder as described in section 5.4A. The surface area of 58 m^2/gm determined by this procedure lies within the range mentioned above. Figure 5.7 shows the particle size distribution of the suspension as determined by filtration (Section 6.2).

5.6B. Determination of pH_{zpc}

The pH_{zpc} (zero proton condition) of the suspensions was determined so that the oxide surface charge during dissolution experiments would be known. In the absence of specifically adsorbing cations and anions (except for H^+ and OH^-) the oxide surface has a net positive charge at pH's below the pH_{zpc} and a net negative charge above the pH_{zpc}.

One liter of suspension was repeatedly filtered and washed using sonication as described in section 5.4A. After a final sonication to

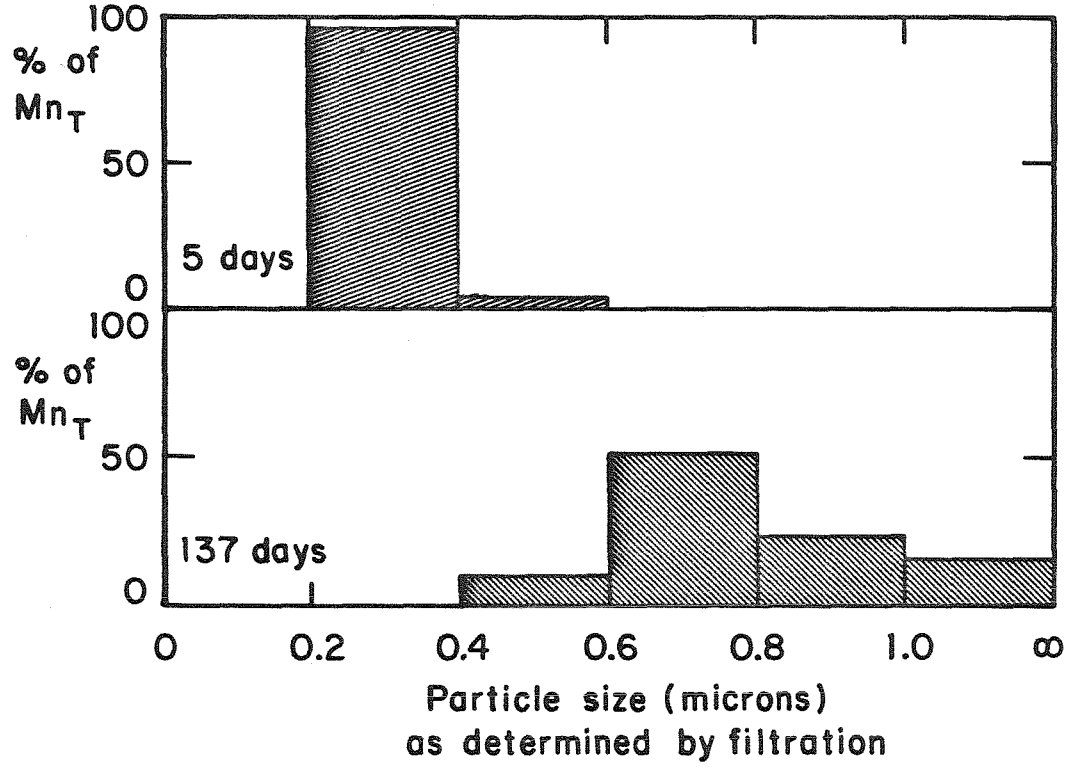

Figure 5.7 Particle size distribution of suspension N(8) as a function of age, determined by filtration.

resuspend the particles, the suspension was pipetted into a one liter jacketed beaker and diluted with D_2H_2O to 700 mls. Enough sodium nitrate was added to set the ionic strength at 0.10M.

The mean oxide surface charge was calculated at each point of an acidimetric titration using the following charge-balance equation (Stumm and Morgan, 1981):

$$C_A - C_B + [OH^-] - [H^+] = \text{Surface charge (equivs./liter)}$$
$$= [=MnOH_2^+] - [=MnO^-]$$

where $C_A - C_B$ = moles of strong acid minus moles of strong base.

$(C_A - C_B)$ was determined by titrating a blank solution.

Constant ionic strength was maintained throughout the titration, and temperature controlled using a constant temperature bath. Hydrogen ion concentrations required for the equations above were calculated from activity measurements (glass electrode, NBS buffers) using an ionic strength correction (Davies equation). Titrations were performed under HP nitrogen. The pH was first raised to about 10.2 by addition of 2 mls of 0.10N NaOH (Dilut-it standard, CO_2 free). Additions of 0.10N nitric acid (Dilut-it Standard) were made using a Gilson pipettor. Surface charge in equivalents/liter is plotted against p^cH for suspensions N(7) and N(9) in Figure 5.8. The p^cH at which the surface charge is zero is converted back to the corresponding p^aH value, providing the value of pH_{zpc}. The pH_{zpc} of the suspension is independent of the imposed ionic strength. The pH_{zpc}

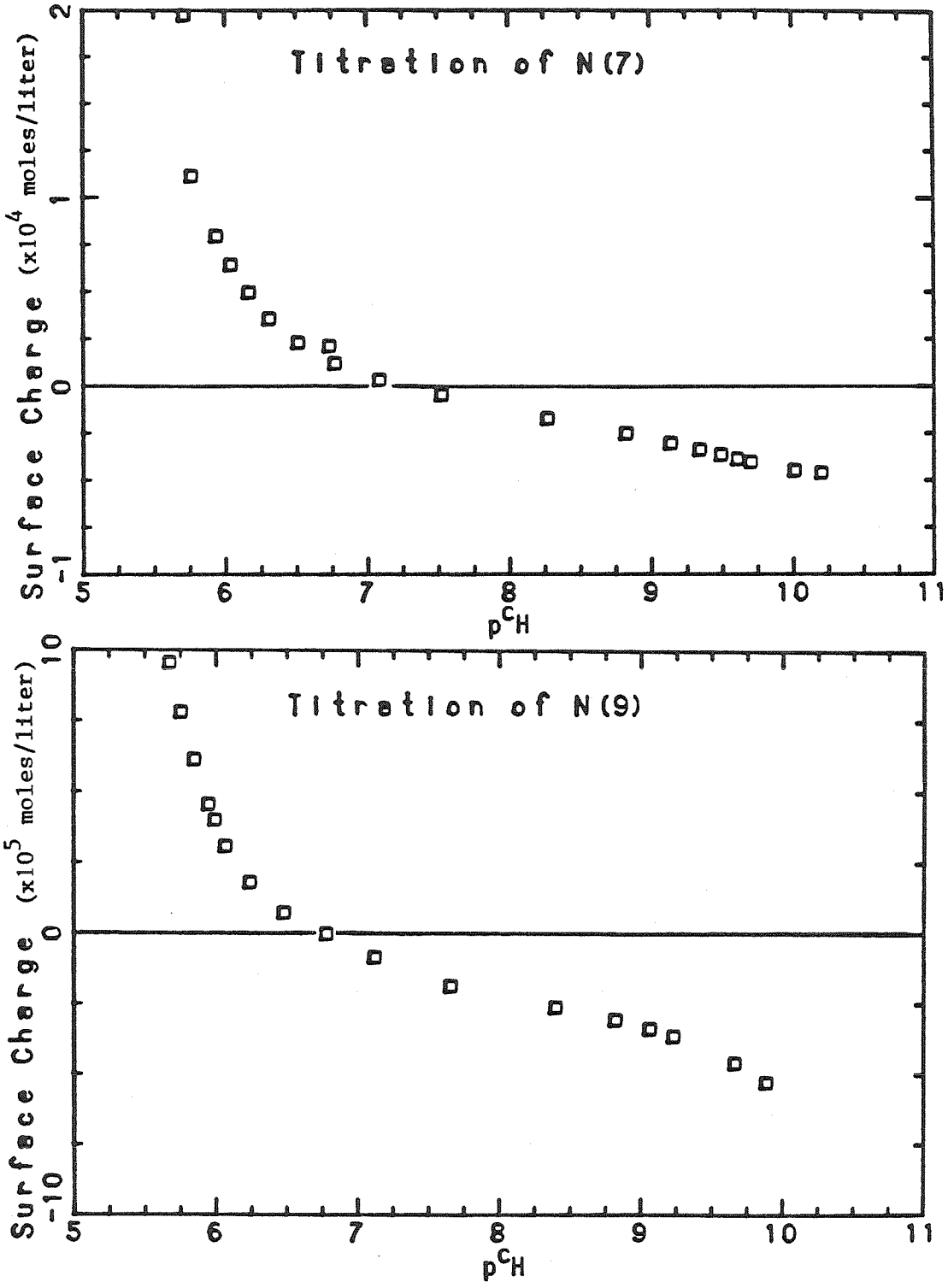

Figure 5.8 Surface charge of suspensions N(7) and N(9) as a function of pH determined by titration (equation 5.1).

values of 7.4 for N(7) and of 6.9 for N(9) are quite close to neutrality. The oxide surface charge is near neutral for most of the dissolution experiments described in the chapters that follow.

5.7 Conclusions

5.7A. Preparative Scheme

The suspensions used in the dissolution experiments were all prepared by the same procedure. A pyrochroite ($Mn(OH)_2(s)$) suspension was first formed by adding stock $MnCl_2$ to a rapidly stirred, deaerated ammonia solution. This was followed by rigorous bubbling with pure oxygen for an hour or more. X-ray diffraction and IR spectrometry indicate that the product is a mixed phase containing mostly feitknechtite and a small amount of manganite and birnessite.

The identification of feitknechtite as the principal product is consistent with the observations of Bricker (1965). The precipitation of pyrochroite before oxygenation and the rapid introduction of oxygen both favor the formation of feitknechtite over hausmannite. The small amounts of manganite and birnessite in the samples may have formed in the initial reaction or may be products of aging that occurred before analysis was performed.

5.7B. Product Characteristics

Suspensions prepared by this technique are stable with respect to settling for six months or more. Fresh suspensions consisted of particles between 0.2 and 0.4 microns in diameter. This was true even for preparation N(8), in which two separate additions of stock $MnCl_2$ were made in an effort to form larger particles. Coagulation

accompanied aging, raising the particle size to over 1.0 microns in five months.

The absence of the ammonia peak in the IR spectrum indicates that there are no cationic impurities in the oxide samples formed from the oxygenation of pyrochroite suspensions. The suspensions are a mixture of phases, which is somewhat undesirable with regard to the dissolution experiments.

5.7C. Resemblance to Natural Oxides

Since the oxide preparations are predominately feitknechtite, their mineralogy does not match that of oceanic nodules and crusts, or freshwater coatings, which are all principally Mn^{IV} oxides. The identification of manganite in lakewater particulates (Stumm and Giovanoli, 1976) provides one situation in which trivalent manganese oxides may be significant. The measurements of manganese oxidation state in Saanich Inlet (Emerson et al., 1982) indicate that lower valent oxides may be a significant fraction of natural oxides of low crystallinity.

The laboratory studies outlined in section 5.1B. all indicate that natural, freshly formed manganese oxides should be mostly hausmannite and feitknechtite. The low degree of crystallinity of fresh precipitates may be the reason that lower valence oxides are not commonly identified in natural samples. Although not commonly identified, hausmannite and feitknechtite may be significant phases of freshly formed, reactive manganese oxides.

The chemical conditions during oxide precipitation in nature are

somewhat different than those employed in the method described above. A solution pH of 10.5 was used, which is higher than in most environmental situations. This caused the oxidation to proceed more quickly. The method also involved saturation with respect to pyrochroite, which rarely occurs in natural systems. Medium effects are also different, since ammonium ions probably interacted less with the precipitating solid than cations like Na^+, K^+, Ca^{2+}, and Mg^{2+} found in natural waters.

Suspensions used in this study most closely resemble freshly precipitated, particulate manganese oxides in nature.

CHAPTER 6

EXPERIMENTAL METHODS

6.1 Introduction

Experimental methods used in the study of the dissolution reactions are summarized in this chapter. The removal of particulate manganese from solution is an important part of each procedure. The extent of dissolution is monitored by first removing particles and then measuring total manganese by atomic absorption spectrophotometry (AAS). Recording UV spectra of the organic substrates requires prior removal of particles, which interfere with absorbance measurements. Filtration is also used to determine the amount of adsorbate bound to the oxide surface.

6.2 Filtration Technique for Determining Dissolved Manganese

The separation of reduced, dissolved manganese from oxidized, particulate manganese by filtration is the most effective way of monitoring the progress of the redox reaction. For this technique to be meaningful, the filter must quantitatively retain the particulate oxide phase and allow free passage of dissolved manganese. This section will describe the filtration technique and examine whether it is successful in providing a quantitative separation.

6.2A. Choice of Filters

Preliminary experiments indicated that capillary pore polycarbonate membrane filters were superior to tortuous pore cellulosic filters in retaining the stock manganese oxide suspensions. Standard nucleopore disc membranes were chosen, and their properties

will now be described, as stated in the Nucleopore Products Catalog. Capillary pore filters are extremely thin porous films with pores randomly distributed over their surface. Particles larger than the pore size are typically captured by interception while those smaller than the pore size are captured by diffusion and inertial compaction. The high viscosities of liquids greatly lowers the efficiency with which diffusion and inertial compaction remove particles. This results in few particles below the pore size being retained.

Nucleopore Corporation states that the rated pore size of the filters is an estimate of the maximum pore diameter, which is from 0% to -20% of the actual maximum. The retention properties stated in the preceding paragraph are such that "Serial filtration ... can accomplish a sharp fractionation between particles and provide relatively precise size distribution data" (Nucleopore).

6.2B. Measurement of Particle Size Distributions

A series of 45 mm diameter nucleopore filters was used to provide an estimate of the size distribution of the manganese oxide stock suspensions. Membranes having pore sizes of 0.1, 0.2, 0.4, 0.6, 0.8, and 1.0 microns were used. High loading of the capillary pore membranes caused increased retention of particles smaller than the rated pore size due to buildup of particles larger than the rated pore size on the membrane surface. For this reason, stock suspensions were diluted by a factor of ten before filtration. Each membrane was rinsed twice with 15 mls. of the diluted suspension before 30 mls. were filtered for the final analysis. Oxalate and nitric acid stock

solutions were then added to portions of the filtrate for the determination of total manganese by AAS. The relative amount of manganese attributed to a particular size range was calculated by subtracting the total manganese concentration determined in successive membrane pore size filtrations. This procedure is illustrated in figure 6.1.

Total filtrate manganese from duplicate filtrations sometimes varied by as much as 44%. For this reason, successive filtration can only be used to discern broad shifts in particle size distribution as aging proceeds. Figure 6.2 shows how the particle size distribution of suspension N(7) changed over a five month period. Coagulation slowly transformed the particle distribution from one dominated by 0.2 to 0.4 micron particles to one in which all particles were in excess of 1.0 micron. Throughout this five month period, the 0.2 micron membrane effectively retained the particles in the stock suspension. The particle size distribution of suspension N(9) changed in a similiar manner, as shown in figure 6.3.

Addition of oxide suspension to the reaction medium used in the dissolution experiments results in rapid flocculation because of the increase in ionic strength and decrease in pH. The particle size distribution at the onset of dissolution is therefore different from that of the stock suspension. The measured distribution does, however, provide a lower size limit for particles at the onset of dissolution. The increase in size of particles in the stock suspension accompanying aging may result in a decrease in the surface area of the freshly

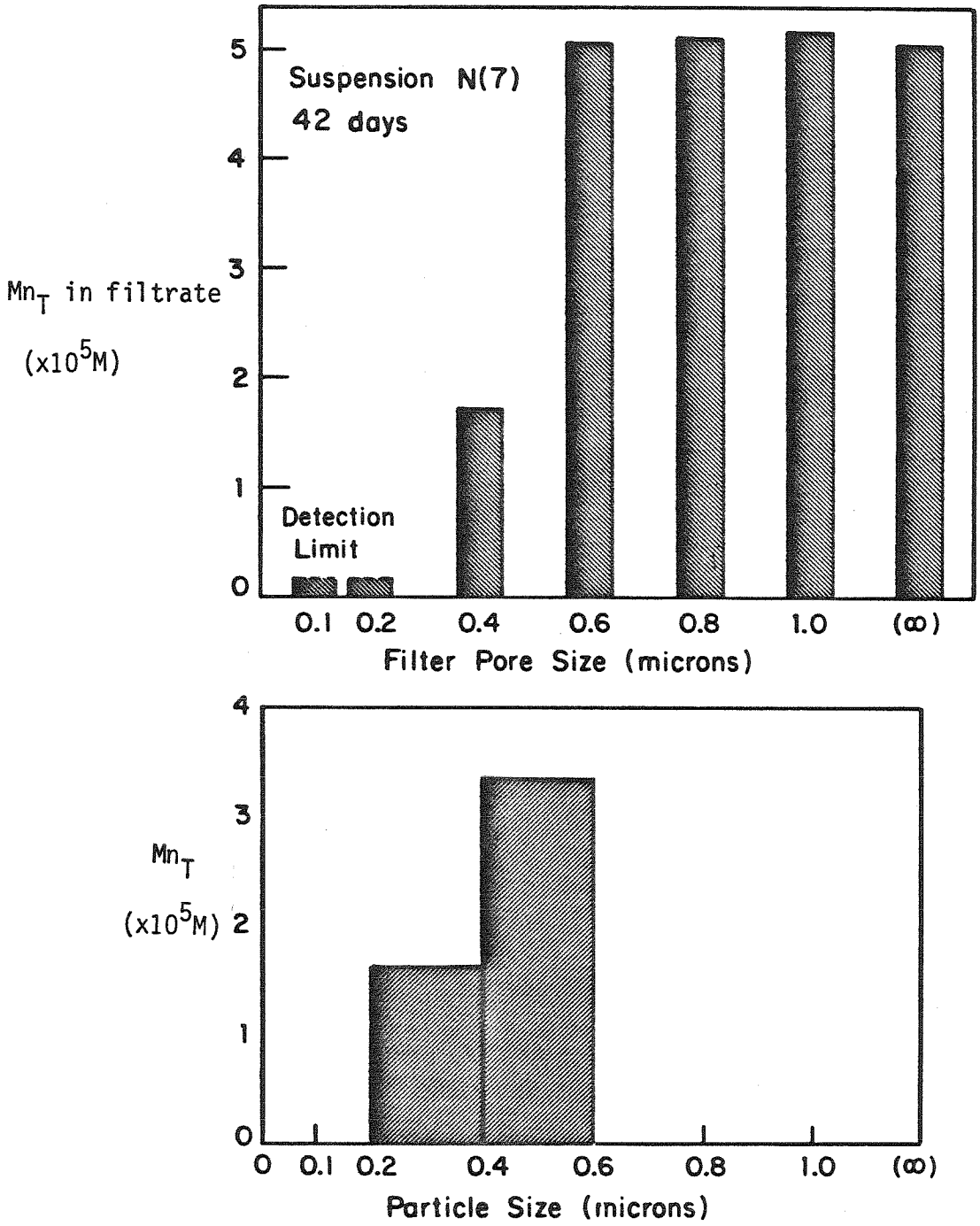

Figure 6.1 Calculation of particle size distribution using filtration. Manganese concentrations in the filtrates from filters of increasing pore size are first measured (A). Values from successive filters are then subtracted from one another to give the amount of manganese found in each particle size range (B).

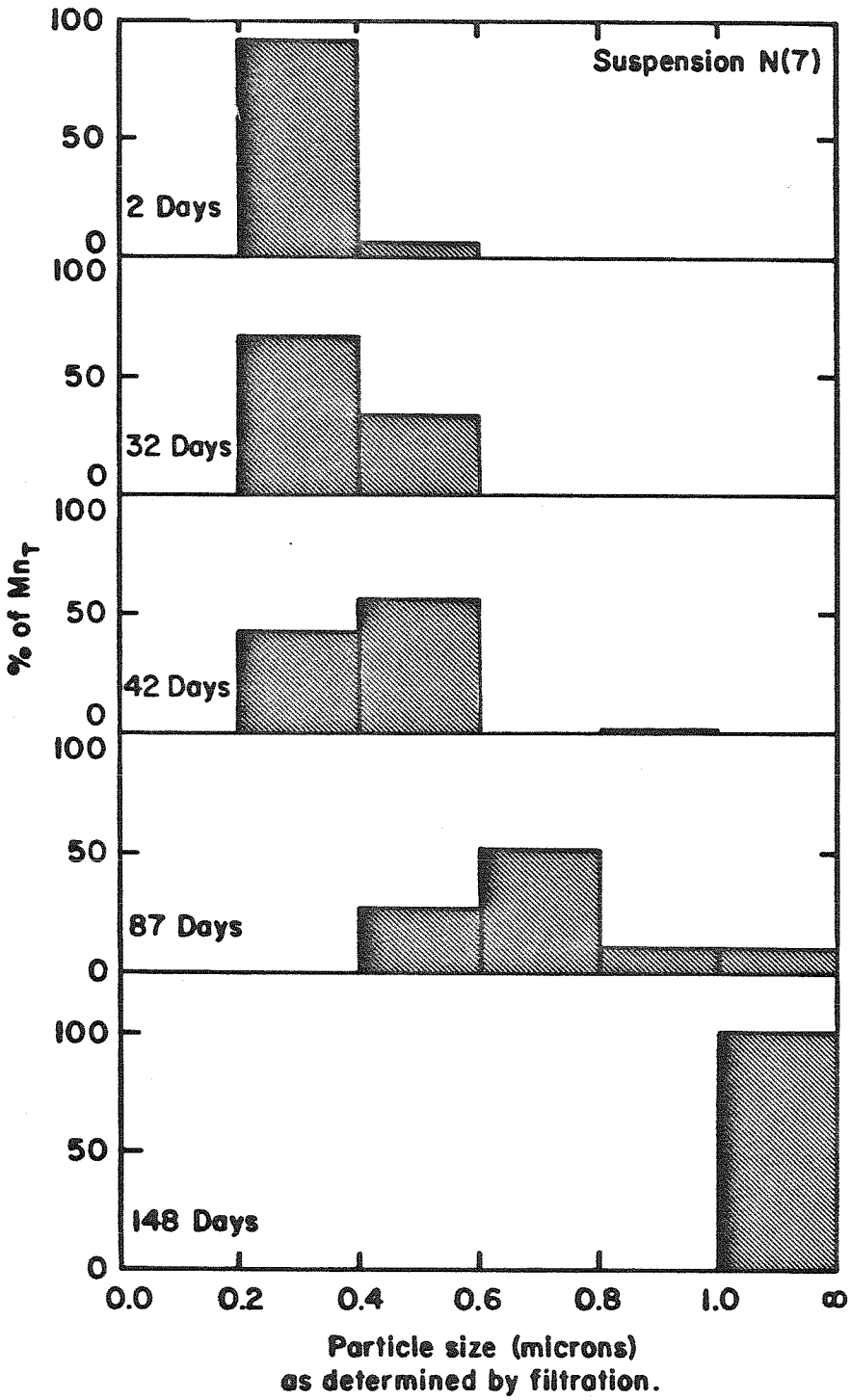

Figure 6.2 Particle size distribution of suspension N(7) as a function of age determined by filtration.

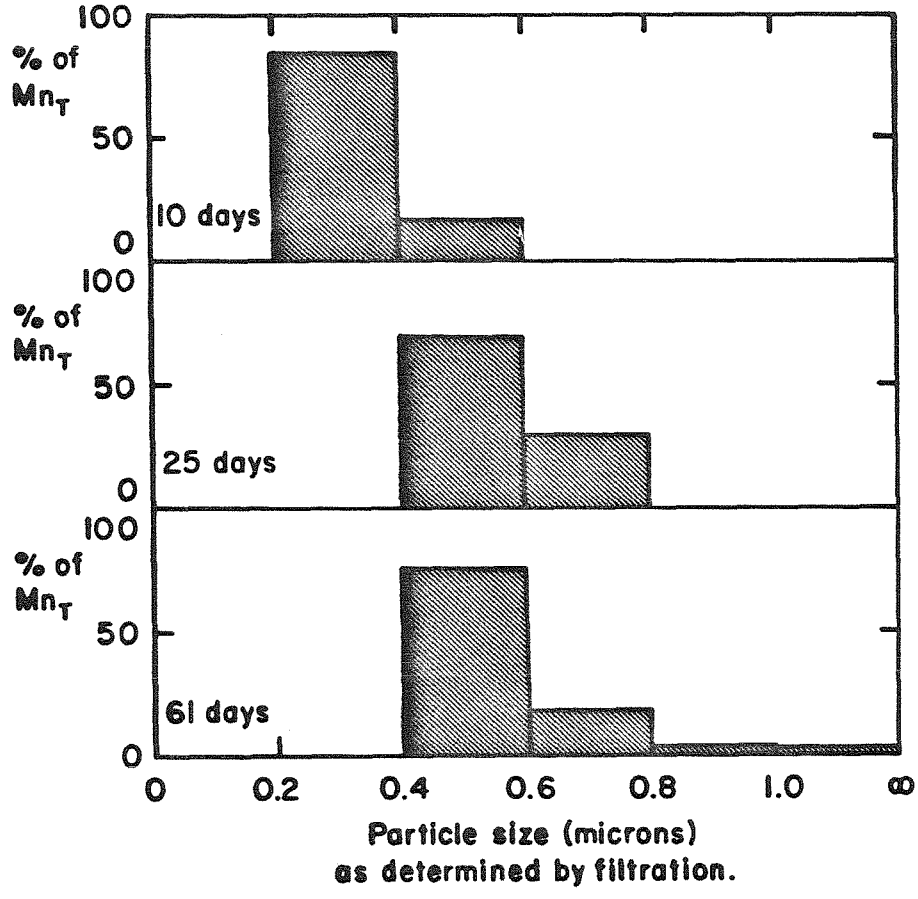

Figure 6.3 Particle size distribution of suspension N(9) as a function of age determined by filtration.

flocculated particles in the reaction medium, and may therefore influence the reaction rate.

6.2C. Effect of Dissolution on the Efficiency of Separation

Dissolution shifts the particle size distribution and modifies the efficiency of separation. For the most simple case, consider spherical particles of diameter D_0 dissolving uniformly over their entire surface area; the diameter is reduced to $.794D_0$ when 50% of the particle volume has been dissolved. The suspension particles in the experimental situation, however, are not monodispersed and may have geometries quite unlike spheres. Dissolution may etch out some regions of the particles more quickly than others.

Measuring the oxidation state of the filtrate manganese is the most direct way of determining separation efficiency. The low concentration of manganese in the filtrate requires using an analytical method based on the oxidation of a redox dye, such as leuco crystal violet (Section 5.3A). Unfortunately, the organic substrates used in the dissolution experiment interfere with the leuco crystal violet test. The pH 4.0 acetate buffer used in this test accelerates the reduction of manganese by unreacted substrate. The oxidant titer is therefore underreported when organic substrate is present.

The change in separation efficiency as dissolution occurs can be tested by filtering aliquots with both 0.1 and 0.2 micron filters at selected time intervals. The amount of manganese retained by the two filters can be compared as the suspension is dissolved. Figure 6.4 shows the results of such a dissolution experiment in which the

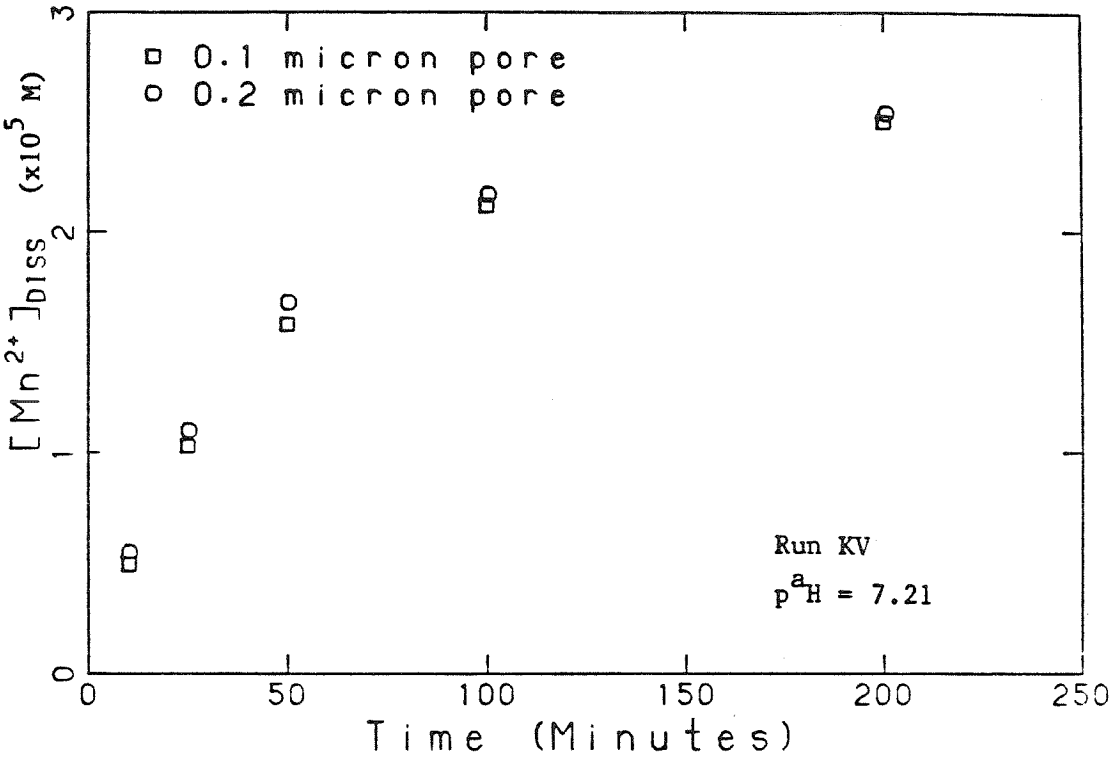

Figure 6.4 A dissolution experiment is performed where aliquots are filtered with both 0.1 and 0.2 micron filters. The plot shows the amount of manganese in the filtrate ($[Mn^{2+}]$diss.) from each filter pore size.

Table 6.1 Collection Efficiency of 0.2 Micron Filters

(Run KV)

Time (Minutes)	Mn Measured in Filtrate		$[MnO_x]_{underreported}$*
	0.1 Micron	0.2 Micron	
10.0	4.94x10-6M	5.48x10-6M	.023
25.0	1.03X10-5	1.10X10-5	.039
50.0	1.58X10-5	1.68X10-5	.081
100.0	2.12X10-5	2.17X10-5	.071
200.0	2.50X10-5	2.54X10-5	.125
400.0	2.68X10-5	2.65X10-5	-.214

* Define $[MnO_x]_{underreported}$ as the fraction of particulate manganese that the 0.2 micron filter fails to collect.

Define: Mp(t) = Particulate manganese at time t (moles/liter)

M(1) = Total manganese in 0.1 micron filtrate at time t (moles/liter)

M(2) = " " " 0.2 " " " " "

Assume that Mp(t) = Mp(0) - M(1). (0.1 micron filter retains all of the particulate manganese)

Then: $[MnO_x]_{underreported} = \frac{M(2) - M(1)}{Mp(t)} = \frac{M(2) - M(1)}{Mp(0) - M(1)}$

procedures outlined in section 6.4 were followed. For all but the last aliquot, more manganese passed through the 0.2 micron filter than through the 0.1 micron filter. Table 6.1 calculates the degree to which the 0.2 micron filter failed to separate particulate from dissolved manganese. The relative amount of particulate manganese that passed through the 0.2 micron filter increased as dissolution proceeded. During the first 75% of the reaction, the 0.2 micron filter retained 92% or more of the particulate manganese.

6.3 Analytical Methods for Monitoring the Reaction

6.3A. Atomic Absorption Spectrometry (AAS)

Atomic absorption spectrophotometry (AAS) was the method of choice for determining total manganese in the filtrate solutions. Aliquots taken from the reaction mixture contained the organic reductant being tested, so any method that relied upon complexation of manganese or upon a redox reaction with manganese was subject to interference. This ruled out the use of the formaldoxime colorimetric test for total manganese, since it involves the formation of a manganese formaldoxime complex (Bartusek and Okac, 1961; Becka and Jokl, 1971). AAS was quite sensitive for manganese, and required little sample. All samples for AAS analysis were made 0.10M in nitric acid. An excess of oxalate was added to the acidified samples if oxidized manganese was present. All solutions and manganese standards were made to the same concentration of supporting electrolyte on order to minimize matrix interference. Phosphate enhanced and calcium suppressed the absorbance readings, making their addition to the standard solutions particularly important.

Lanthanum chloride (1%) was added to all solutions containing calcium to minimize interference. Samples containing as low as 4.0×10^{-7}M manganese were analyzed by this procedure.

6.3B. UV Spectrometry

A number of the organic substrates examined for reactivity in the survey experiment (Chapter 8) have absorbance peaks in the UV that can be used to monitor their depletion as the reaction proceeds. Absorption and light scattering by suspension particles interfered with absorbance measurements of the unfiltered reaction solution. Filtration with 0.2 micron, 25 mm nucleopore filters effectively removed the particles and eliminated this interference.

Many of the organic substrates are reactive with oxygen in the pH range of the experiments. In some cases, autooxidation is enhanced by Mn^{2+} ions formed in the dissolution reaction. For these reasons it was important that spectra of filtered aliquots were measured immediately. In this way reaction with oxygen was minimized.

6.4 Design of the Dissolution Experiments

6.4A. Introduction

Reactions must be performed in such a way that parameters affecting the reaction rate are controlled and interference minimized. Oxygen reacts rapidly with dihydroxybenzoid compounds in basic solutions, and must therefore be prevented from oxidizing the organic substrates before the reaction with the oxide suspension is complete. It is desirable to keep pH constant during the course of a reaction by using buffers. Some buffers contain ions such as phosphate that can

interfere with the reaction by adsorbing to the oxide surface. Buffer solutions containing adsorbable ions should therefore be avoided. A constant ionic strength must be maintained so that species activities in different experiments can either be kept constant or varied for comparison.

6.4B. Preparation of Reaction Solutions

Chemical reagents were chosen to minimize the impurities present in the reaction mixture. Deionized distilled water (D_2H_2O) was used to prepare all stock solutions. Glassware was soaked in 5N nitric acid and repeatedly rinsed with D_2H_2O. All stock solutions were filtered with 0.2 micron nucleopore membrane filters to remove insoluble contaminants. Sodium nitrate, calcium nitrate, sodium bicarbonate, mono- and dibasic potassium phosphate were all analytical reagent grade, purchased from Mallinckrodt. Stock solutions of hydrochloric and nitric acids were prepared from Mallinckrodt (A.C.S. specifications) concentrated reagents. Dilut-it 0.1N sodium hydroxide and 0.1 N nitric acid standard solutions were also used.

Stock solutions of organic substrates were prepared slightly acidic to minimize oxidation by oxygen and were used within 24 hours of preparation. Stock hydroquinone solutions were prepared 1.00×10^{-1}M in hydroquinone (Sigma Chemical Company) and 1.0×10^{-2}M in HCl. Solutions of 1.50×10^{-2}M 2,5-dihydroxybenzoic acid (99%,Aldrich Chemical Company) were used without the addition of mineral acid.

A carbon dioxide/bicarbonate buffer was used to simulate natural reaction conditions. Carbonate and bicarbonate species are unlikely to

interfere with the surface reaction because their affinity for oxide surfaces is low. Carbon dioxide and nitrogen mixtures were purchased from Linde and Matheson gas. A mixture of 1.0% CO_2 was found most suitable for buffering in the pH range $6.5 < pH < 8.0$.

The reaction solution was prepared by adding stock sodium nitrate, sodium bicarbonate, and D_2H_2O by pipette to a dried, 1 liter jacketed beaker. Unless otherwise noted, solutions contained 5.00×10^{-2}M $NaNO_3$ when additions were complete. Solution pH was set by adding enough sodium bicarbonate stock solution to reach the necessary alkalinity.

6.4C. Experimental Procedure

Each jacketed beaker was sealed with a plexiglas faceplate and stirred using a 1.5 inch teflon stir bar (Figure 6.5). Stock manganese oxide suspension was added by pipette at this point and bubbling with the carbon dioxide/nitrogen mixture begun. A flow rate of 200 cc/minute was maintained using a six inch Pasteur pipette tip. Gas dispersion tubes were first used for this purpose, but the fritted glass quickly became coated with the manganese oxide particles. An Orion glass electrode and double junction reference electrode were calibrated using pHydrion N.B.S. standard buffers and used for pH measurement. Water from a constant temperature bath was circulated through the jacketed beakers to maintain a constant temperature within $0.5^{\circ}C$ of the stated value.

A minimum of one hour was required for the solution to equilibrate with the carbon dioxide/nitrogen mixture. Vessels were typically

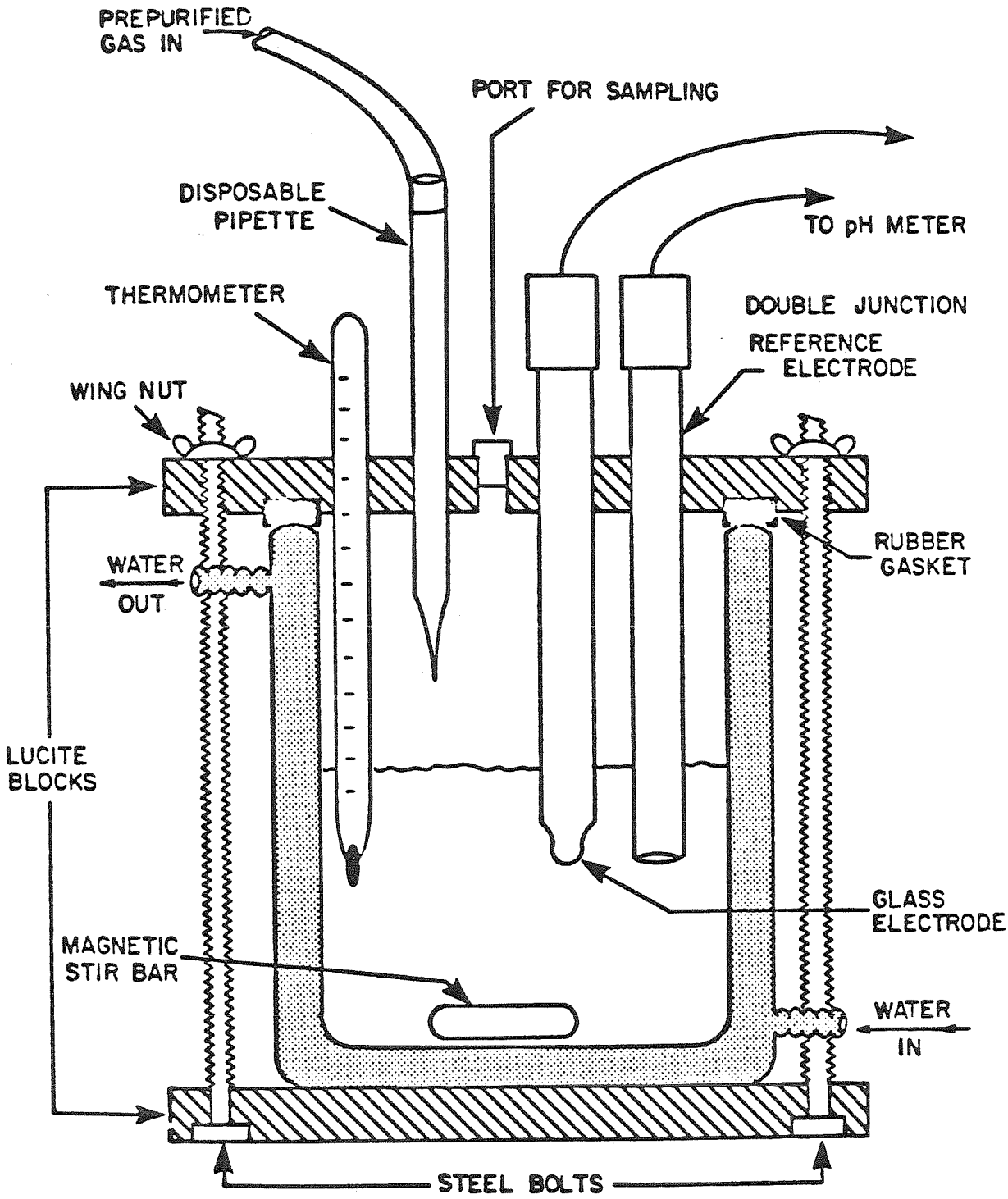

Figure 6.5 Diagram of the reaction chamber used in the dissolution experiments.

equilibrated 1.5 to 5 hours before the dissolution with organic substrate was begun. Suspension particles experienced an increase in ionic strength and decrease in pH upon addition to the solution medium, causing flocculation. Experiments therefore measured the dissolution rate of freshly flocculated suspensions.

The reaction was initiated by adding 10 mls of the stock organic substrate by pipette, and timed by stopwatch. In some cases, acidity introduced by the organic stock solution was neutralized by the prior addition of an equivalent amount of sodium hydroxide. Before use, the 0.2 micron, 25 mm diameter nucleopore membrane filters were rinsed once with 10 mls of 0.10M nitric acid and three times with 10 mls of D_2H_2O. Aliquots were taken with a six inch tube connected to a syringe, both polyethylene. For each sample, 5 mls were removed to rinse the filter, followed by 20 mls removed for filtration and analysis. Portions of the filtrate were added to 25 ml volumetric flasks containing enough stock nitric acid to make 0.10M solutions upon dilution, ready for AAS analysis.

At the end of each experiment an unfiltered aliquot of solution was taken and dissolved by addition of oxalate and nitric acid. This provided a final value of Mn_T (total manganese, in moles/liter) that could be compared to the amount initially added. The value of Mn_T at the end of the experiment was typically 5 to 10% lower than the amount added. This difference was caused by coagulated particles adhering to the glass walls of the vessel and becoming stranded as the solution level was lowered by the withdrawl of aliquots.

6.5 Adsorption Experiments

Experiments were performed to determine the amount of orthophosphate adsorbed by the manganese oxide suspension under the conditions of the dissolution experiments. The affinity of phosphate for the oxide surface was low, so it was not possible to determine the amount adsorbed by changes in the bulk solution concentration. Instead, the suspension particles were collected by filtration and phosphate desorbed and measured.

Each reaction solution was prepared in a 1-liter erlenmeyer flask following the procedures outlined in section 6.4B, and equilibrated with the CO_2 mixture. Phosphate was then added and equilibrated for the specified amount of time. The entire reaction solution was then filtered using rinsed 0.2 micron nucleopore filters. The filtrate was saved in some cases for determination of dissolved phosphate concentration. Filters were placed in 50 ml beakers containing 10 mls 1.00×10^{-2}M ascorbic acid and sonicated. This treatment completely dissolved the oxide suspension. The clear solutions were then diluted and analyzed for orthophosphate using the Molybdenum Blue Technique (Eisenreich, Bannerman, and Armstrong, 1975).

CHAPTER 7

REDUCTION AND DISSOLUTION OF MANGANESE OXIDES BY HYDROQUINONE

7.1 Introduction

This chapter presents the results of experiments in which manganese oxide suspensions are reduced and dissolved by hydroquinone. The rate of dissolution is found by measuring values of $[Mn^{2+}]_{diss.}$, the amount of dissolved manganese, against time. $[Mn^{2+}]_{diss.}$ is determined using the filtration technique described in Section 6.1. It is an operational definition of dissolved manganese which does not necessarily reflect the amount of manganese that has been reduced, only that which is not retained by a 0.2 micron filter. These data will be used to formulate a rate law for the reaction.

Oxidation of hydroquinone by manganese oxide forms p-benzoquinone, as verified by UV spectroscopy (Section 8.3B). Coupling and ring-cleavage reactions of hydroquinone are relatively insignificant, thus providing a simple system for studying how oxide properties and medium composition influence the reaction rate.

A rate law is an experimentally derived equation that describes the way in which the reaction rate depends upon the concentrations of component species. The rate law for many reactions can be written in the form:

$$7.1 \qquad \frac{dC_1}{dt} = kC_1^{n_1} C_2^{n_2} C_3^{n_3}$$

where C_i = Concentration of component i.

The order of the reaction is defined by the sum of the powers:

$$7.2 \qquad n = \text{order of the reaction} = n_1 + n_2 + n_3 + \ldots$$

The order of the reaction with respect to a specific component i is given by the exponent n_i. Experiments can be performed where the concentration of all reactants, except component i, are in excess. The reactions are then said to be pseudo-n_ith order, since all other component concentrations are constant (Frost and Pearson, 1961; Laidler, 1965).

An overall order of the reaction cannot be defined for all chemical reactions. Consider a rate law of the form:

$$7.3 \qquad \frac{dC_1}{dt} = k \frac{C_1 C_2 C_3^2}{(1 + k' C_2)}$$

Although the order of this reaction with respect to components (1) or (3) can be defined, the presence of C_2 in the denominator interferes with assignment of order to component (2). For this reason, an overall reaction order cannot be defined either.

7.2 Order with Respect to Manganese Oxide Loading

All experiments described in this section employed hydroquinone concentrations ten or more times higher than Mn_T (total manganese

concentration) added as the oxide suspension. Since hydroquinone is a two-equivalent reductant and the average oxidation state of the oxide is +3.3 (N(7),Table 5.2), the excess of hydroquinone in these experiments was:

$$7.4 \qquad \left(\frac{10 \text{ moles HQ}}{1 \text{ mole Mn}}\right)\left(\frac{2 \text{ equiv. Red.}}{\text{mole HQ}}\right)\left(\frac{1 \text{ mole Mn}}{1.3 \text{ equiv. Oxid.}}\right) = 15.4$$

Only about 1/15 th of the total reductant concentration was consumed by the oxide during dissolution. The reductant concentration can therefore be considered constant.

7.2A Experimental Design and Results

Five dissolution experiments were completed in which pH and hydroquinone concentration were kept constant, but different amounts of stock manganese oxide suspension were added. Experimental conditions are summarized in Table 7.1. Figure 7.1A shows the increase in $[Mn^{2+}]_{diss}$ observed with time for all five runs. Before the addition of hydroquinone, the amount of dissolved manganese was below the analytical range. Samples were taken until about 70% of the manganese oxide had been dissolved.

7.2B Initial Rate Method

At this point we cannot safely assume that the same reaction mechanism is followed throughout the course of the reaction. We proceed then, by first determining the order of the reaction with respect to manganese oxide suspension at the start of the experiment. The next section considers whether data collected throughout the entire

Table 7.1 Dissolution Experiments with Varying Suspension Loadings

Conditions common to all runs:

[Hydroquinone] = 4.29×10^{-4}M

[Alkalinity] = 1.00×10^{-3}M

$P_{CO_2} = 1.09 \times 10^{-2}$M

Supporting Electrolyte = 5.00×10^{-2}M $NaNO_3$

25°C

Trial	pH	Mn_T (M)	$[HQ]/Mn_T$	$\frac{\Delta[Mn^{2+}]}{\Delta t}$ **	Age (days)
X	7.71	1.44E-5	29.8	6.33E-7	69
Y	7.72	2.10E-5	20.4	9.65E-7	75
U	7.71	2.87E-5	14.9	1.36E-6	67
Z	7.78	3.51E-5	12.9	1.49E-6	75
QA	7.78	4.21E-5	10.2	2.00E-6	75

**Slope of line fitted through the first three points in units of (moles/liter/minute)

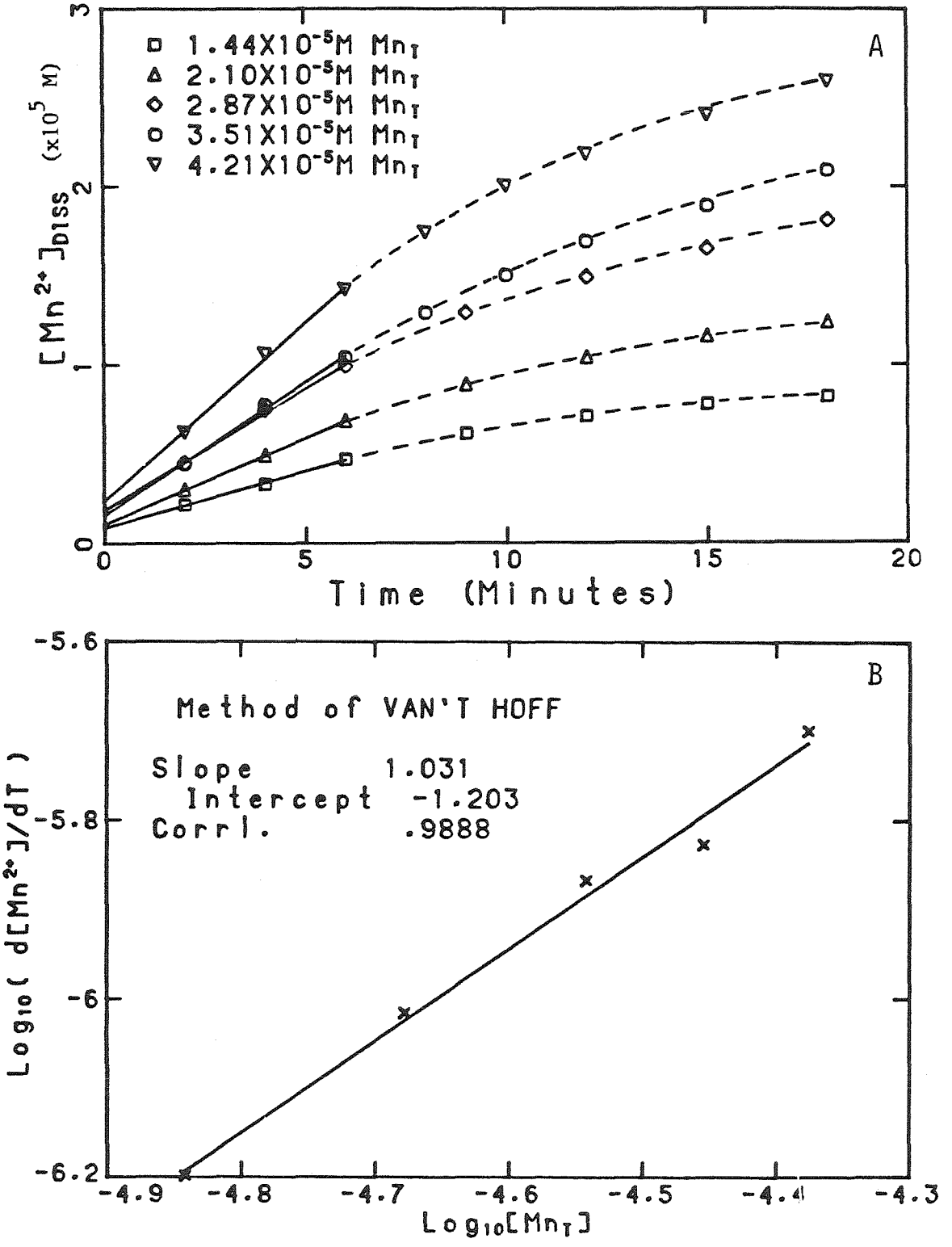

Figure 7.1 Vary the suspension loading. A. $[Mn^{2+}]$diss. against time for different suspension loadings. B. Method of van't Hoff to determine the order with respect to initial oxide loading.

course of the reaction are consistent with this order.

Van't Hoff's Method (Swinbourne,1971) can be used to find the order with respect to the concentration of a reactant near the start of the reaction. Given that the rate law can be written as:

$$7.5 \qquad \frac{d[Mn^{2+}]_{diss}}{dt} = k[Mn_T]^a$$

where $[Mn_T]$ = Total Added Manganese (as the solid oxide) in in moles/liter,

then:

$$7.6 \qquad \log\left(d[Mn^{2+}]_{diss}/dt\right) = \log(k) + a\log[Mn_T].$$

The initial reaction rate is estimated from the experimental data, and a plot of $\log(d[Mn^{2+}]_{diss}/dt)$ against $\log[Mn_T]$ provides the order with respect to Mn_T as the slope (a).

A line was fitted through the first three data points of each run, and its slope used as an estimate of the initial reaction rate (Figure 7.1A). Figure 7.1B plots the logarithm of the initial rate against the suspension loading expressed as Mn_T. The slope of this plot is the order with respect to manganese oxide loading. The experimentally derived slope of 1.03 indicates that the reaction was first order with respect to Mn_T.

7.2C Integral Method

This section examines whether the order with respect to manganese oxide loading is first order throughout the course of the reaction. As the reaction proceeds, manganese oxide is consumed, producing Mn^{2+}.

The amount of manganese oxide that remains at time t is found using the following mass balance equation:

7.7 $[MnO_x] = Mn_T - [Mn^{2+}]_{diss}$

where $[MnO_x]$ = Solid Mn oxide present at time t (moles/liter)

Mn_T = Total manganese (Dissolved and precipitated) at time t
= $[MnO_x]$ at t=0

$[Mn^{2+}]_{diss}$ = Dissolved manganese at time t (moles/liter), as determined by filtration.

$[MnO_x]$ is therefore the amount of manganese that is retained by the filter at time t.

The rate law can now be written:

7.8 $$\frac{d[Mn^{2+}]_{diss}}{dT} = k[MnO_x]^b = k(Mn_T - [Mn^{2+}]_{diss})^b$$

The integrated forms of this rate equation are:

7.9 for b=1, $$\ln\left(\frac{Mn_T - [Mn^{2+}]}{Mn_T}\right) = -kt$$

7.10 for b≠1, $$\frac{1}{(b-1)}\left(\frac{1}{(Mn_T - [Mn^{2+}]_{diss.})^{b-1}} - \frac{1}{Mn_T{}^{b-1}}\right) = kt$$

Values of b can be chosen by trial and error and used to plot the data according to equation 7.9. The value that produces the most linear plot is the order.

When t is near zero $Mn_T >> [Mn^{2+}]_{diss}$ and equation 7.8 becomes:

$$7.11 \qquad \frac{d[Mn^{2+}]_{diss}}{dt} = k(Mn_T)^b$$

In section 7.2B., (b) was found to be 1.0. This suggests plotting data for the entire reaction using equation 7.9. Figure 7.2 plots $\ln(Mn_T - [Mn^{2+}]_{diss}/Mn_T)$ against time to test the agreement with a first-order fit. Data plotted for the five runs during the first 50% of the reaction are quite linear, indicating good agreement with equation 7.9. Subsequent points curve progressively upward, indicating that the order is higher than one in this region.

The reaction is therefore first order with respect to remaining manganese oxide during the first 50% of the reaction. Deviation from first-order behavior after this time indicates that equation 7.9 is not strictly valid near completion of the reaction.

7.2D Calculation of Rate Constants

Rate constants must be calculated in a consistent manner so that reactions performed under different conditions can be reliably compared. The last section showed that the reaction is first order with respect to remaining oxide during the first half of the reaction. The fit becomes poorer as time increases, which may introduce a systematic error in calculated values of the rate constant.

To check this, two methods of calculating the pseudo-first-order rate constant can be compared. The first method defines an

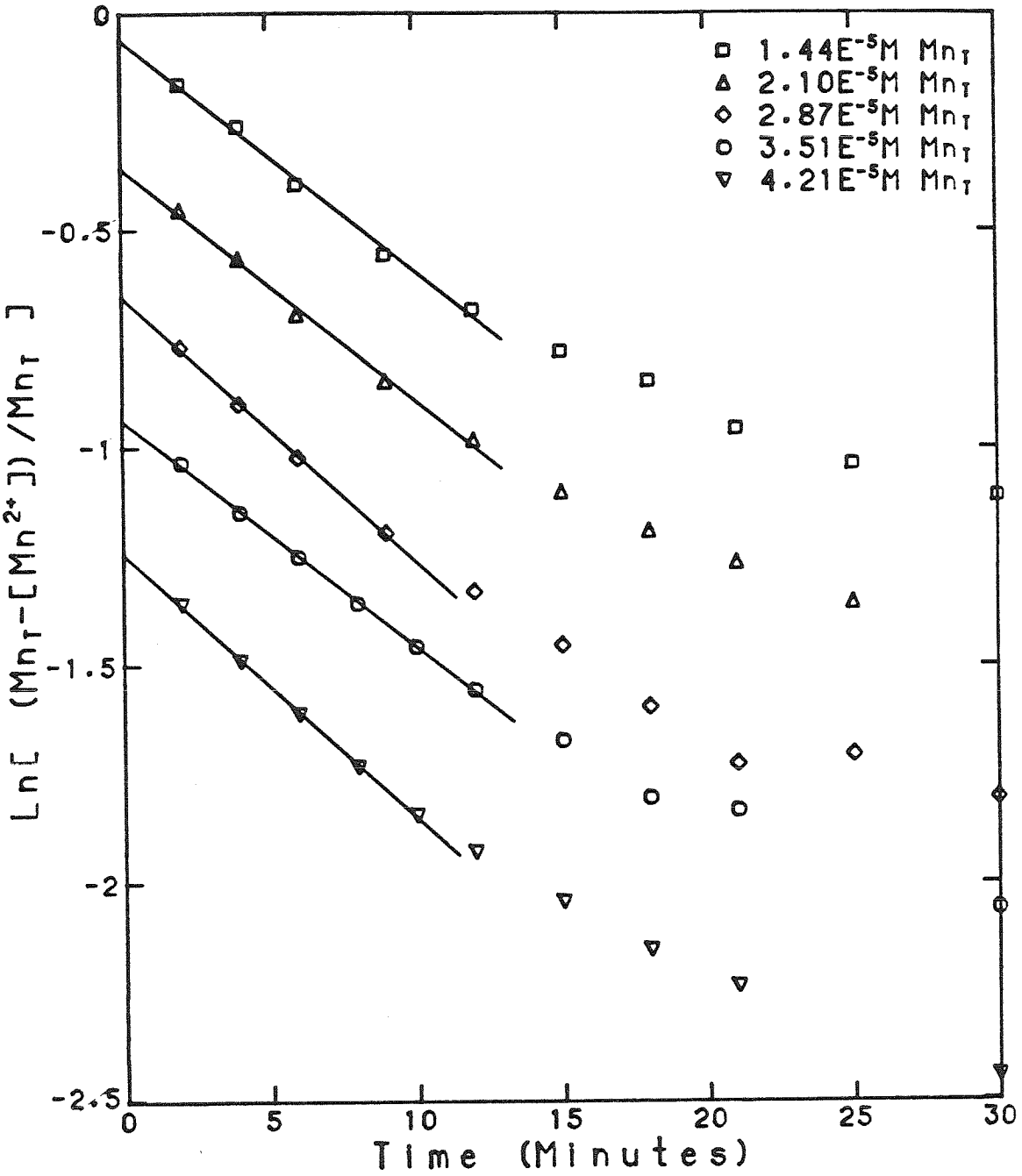

Figure 7.2 Equation 7.9 is used to fit experimental data from different suspension loadings. The scale of the abscissa is arbitrary.

experimental rate constant k_{exp} as the slope of $\ln(Mn_T - [Mn^{2+}]_{diss}/Mn_T)$ plotted against time for data collected in the first 50% of the reaction. The second method calculates a rate constant k_{pair} from successive pairs of points:

$$7.12 \quad k_{pair} = \frac{-1}{(t_2 - t_1)} \ln \left(\frac{Mn_T - [Mn^{2+}]_{t_2}}{Mn_T - [Mn^{2+}]_{t_1}} \right)$$

k_{pair} is calculated from only two experimental points whereas k_{exp} is found by fitting a line through all the points collected in the first 50% of the reaction. k_{exp} can therefore be considered the average of a group of k_{pair} values, and will be less sensitive than k_{pair} to small changes in order with time.

Table 7.2 lists values of k_{pair} calculated from consecutive data points and compares them with the value of k_{exp} determined as described above. The values of k_{exp} for the five runs are quite similiar, differing by only 16%. The k defined by equation 7.8 is independent of suspension loading when the correct value of b is used, lending support to the assignment of first-order. This can be further illustrated by plotting $(Mn_T - [Mn^{2+}]_{diss})/(Mn_T)$, the fraction of the original oxide that still remains at time t, against time. This is shown in figure 7.3. Data from five different suspension loadings plot on the same curve, indicating that equation 7.9 is a reasonable fit of the data.

Values of k_{pair} calculated using data collected before 50% of

Table 7.2 Calculated Values of k_{exp} and k_{pair} under Varying Initial Suspension Loadings

Run U
2.87E-5M Mn_T
k(exp)= 6.09E-2 (1/min.)

Time (Min.)	k(pair)	k(pair)/k(exp)	%
3.0	6.55E-2	1.076	+7.6
5.0	6.15E-2	1.010	+1.0
7.5	5.80E-2	.953	-4.7
10.5	4.50E-2	.739	-26.1
13.5	4.10E-2	.673	-32.7
16.5	4.70E-2	.772	-22.8
19.5	4.33E-2	.711	-28.9
23.0	-7.00E-3	-.115	-88.5
27.5	2.00E-2	.329	-67.2

t(1/2)

Run X
1.44E-5M Mn_T
k(exp)= 5.32E-2 (1/min.)

Time (Min.)	k(pair)	k(pair)/k(exp)	%
3.0	4.85E-2	.912	-8.8
5.0	6.70E-2	1.260	+26.0
7.5	5.40E-2	1.016	+1.6
10.5	4.23E-2	.796	-20.4
13.5	3.20E-2	.602	-39.8
16.5	2.27E-2	.427	-57.3
19.5	3.63E-2	.683	-31.7
23.0	2.03E-2	.382	-61.8
27.5	1.46E-2	.275	-72.5

Run Y
2.10E-5M Mn_T
k(exp)= 5.34E-2 (1/min.)

Time (Min.)	k(pair)	k(pair)/k(exp)	%
3.0	5.60E-2	1.049	+4.9
5.0	6.45E-2	1.209	+20.9
7.5	5.13E-2	.961	-3.9
10.5	4.50E-2	.843	-15.7
13.5	4.00E-2	.750	-25.1
16.5	2.97E-2	.557	-44.4
19.5	2.07E-2	.388	-61.2
23.0	2.30E-2	.431	-56.9
27.5	1.93E-2	.361	-63.8

t(1/2)

Run Z
3.51E-5M Mn_T
k(exp)= 5.20E-2 (1/min.)

Time (Min.)	k(pair)	k(pair)/k(exp)	%
3.0	5.65E-2	1.087	+8.7
5.0	5.15E-2	.991	-0.9
7.0	5.30E-2	1.019	+1.9
9.0	5.00E-2	.962	-3.8
11.0	4.95E-2	.952	-4.8
13.5	3.87E-2	.744	-25.6
17.5	4.40E-2	.846	-15.4
19.5	9.67E-3	.186	-81.4
25.5	2.50E-2	.481	-51.9

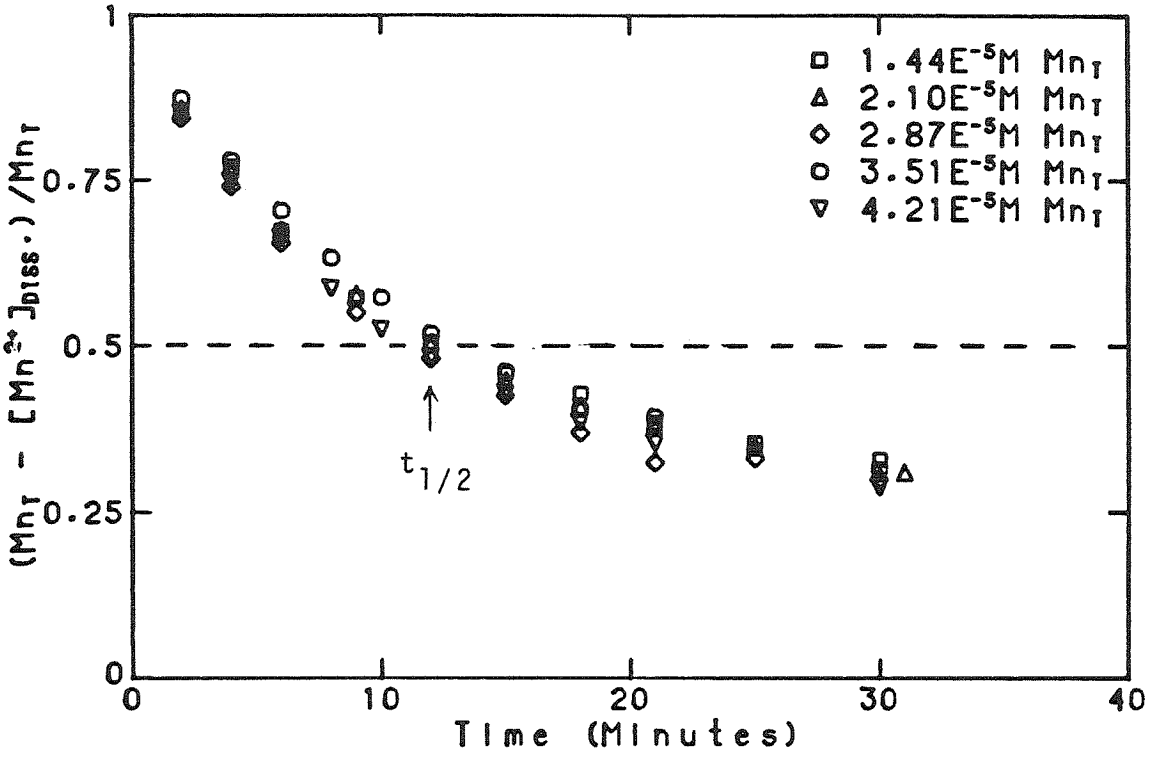

Figure 7.3 Data from different suspension loadings normalized using equation 7.9 and plotted against time.

the reaction is complete are within 30% of k_{exp}. The decrease in k_{pair} becomes quite significant after this time, with k_{pair} values quite a bit lower than k_{exp}. The value of the rate constant is therefore dependent upon how much of the dissolution data is included in the calculation. A value calculated with data collected during the first 25% of the reaction is larger than one using data from 75% of the reaction. Since the deviation in k_{pair} is smallest during the first half-life of the reaction, values of k_{exp} calculated over this interval minimize this variation.

7.2E. Duplicate Runs

Duplicate runs (I and J) were performed to determine the reproducibility of the experimental technique. Table 7.3 summarizes the results from the two runs. Values of $[Mn^{2+}]_{diss}$ differ between the two runs by less than 5% for all but the first values, which differ by 12%. This is reasonable since $[Mn^{2+}]_{diss}$ changes most rapidly early in the reaction, magnifying small differences in the time of aliquot removal. Values of k_{exp} calculated for both runs are in excellent agreement, differing by only 3.7%. Values of k_{pair} calculated from the two runs are quite close, both decreasing with respect to k_{exp} as the reaction proceeds. The trend away from equation 7.9 observed in all the runs after half of the reaction is complete is therefore reproducible and systematic.

7.2F. Summary

The reduction of manganese oxide suspensions by hydroquinone is first

Table 7.3 Duplicate Runs: Experimental Data and Calculated Rate Constants

Time (min.)	[Mn2+] I (M)	J (M)	Ave. (M)	(I-J)/Ave. (%)
2.0	3.87E-6	3.43E-6	3.65E-6	12.1
5.0	7.30E-6	6.98E-6	7.14E-6	4.5
8.0	9.74E-6	9.70E-6	9.72E-6	0.4
12.0	1.25E-5	1.23E-5	1.24E-5	1.6
15.0	1.40E-5	1.41E-5	1.41E-5	0.7
20.0	1.61E-5	1.61E-5	1.61E-5	0.0
25.0	1.77E-5	1.77E-5	1.77E-5	0.0
30.0	1.88E-5	1.91E-5	1.90E-5	-1.6
40.0	2.01E-5	2.03E-5	2.02E-5	1.0
50.0	2.07E-5	2.14E-5	2.11E-5	-3.3
60.0	2.18E-5	2.17E-5	2.18E-5	0.5

$t_{1/2}$

	$\frac{k_{exp}}{}$
I	4.06×10^{-2} min^{-1}
J	4.21×10^{-2}
Ave.	4.13×10^{-2}
(I-J)/Ave.	3.7%

Time (Min.)	k(pair) I	J (Minutes^{-1})	Ave.	$\frac{(I-J)}{Ave.}$	$\frac{k(pair)}{k(exp)}$	% Difference
3.5	5.00E-2	5.10E-2	5.05E-2	-2.0%	1.223	+22.3%
6.5	4.07E-2	4.50E-2	4.29E-2	-10.0	1.039	+3.9
10.0	3.98E-2	3.70E-2	3.84E-2	+7.3	.930	-7.0
13.5	3.27E-2	3.93E-2	3.60E-2	-18.3	.872	-12.8
17.5	3.14E-2	3.00E-2	3.07E-2	+4.6	.743	-25.7
22.5	3.24E-2	2.76E-2	3.00E-2	+17.3	.726	-27.4
27.5	2.14E-2	2.78E-2	2.46E-2	-26.0	.596	-40.4
35.0	1.44E-2	1.36E-2	1.40E-2	+5.7	.339	-66.1
45.0	7.40E-3	1.44E-2	1.09E-2	-64.2	.264	-73.6
55.0	1.52E-2	4.40E-3	9.80E-3	+10.2	.237	-76.3

order with respect to suspension loading using the initial rate method. The reaction is also first-order with respect to remaining manganese oxide within the first 50% of the reaction but deviates from this relation as the reaction comes closer to completion. Values of the experimental rate constant (k_{exp}) calculated using the first-order fit of data from the first 50% of reaction are independent of suspension loading and reproducible.

7.3 Kinetic Data

Reaction conditions for all experimental runs performed with hydroquinone, p-benzoquinone, and 2,5-dihydroxybenzoic acid are listed in Table 7.4. Values of k_{exp} are also included for reactions performed using excess hydroquinone.

7.4 Reaction Parameters that influence rate.

7.4A. Adsorption of Mn^{2+}

An experiment was performed to determine the extent to which Mn^{2+} produced by the reduction reaction adsorbs onto the remaining oxide surface. If such a process occurs, values of $[Mn^{2+}]_{diss}$ determined using filtration would underreport the amount of manganese oxide that has been reduced. Two manganese oxide suspensions (2.82×10^{-5}M MnO_x) were equilibrated with CO_2 under the same conditions of the dissolution experiments. Suspensions filtered at this point had manganese concentrations below the sensitivity of the AAS analysis procedure. Enough stock $MnCl_2$ solution was then added to make the suspensions 2.97×10^{-5}M in Mn^{2+}. Aliquots were removed, filtered, and analyzed during the first half hour after

Table 7.4: Summary of Kinetic Data

7.4A. Reduction of Suspension N(7) with Hydroquinone

Trial	pH	Mn_T (M)	[HQ] (M)	Age (Days)	kexp (min-1)	Comments
G	7.79	2.82E-5	2.86E-4	19	4.80E-2	
H	7.76	2.82E-5	1.43E-3	19	*1.50E-1*	
I	7.86	2.85E-5	2.86E-4	33	4.06E-2	
J	7.85	2.85E-5	2.86E-4	33	4.20E-2	
K	7.85	2.85E-5	2.86E-4	33	3.78E-2	IN DARK
L	7.83	2.89E-5	5.71E-4	53	7.02E-2	
M	7.80	2.89E-5	8.57E-4	53	*8.88E-2*	
N	7.79	2.89E-5	1.14E-3	53	*1.14E-1*	
O	7.8-8.9	2.87E-5	-	62	-	BLANK
P	7.82	2.87E-5	2.86E-4	63	4.24E-2	101 RPM
Q	7.81	2.87E-5	2.86E-4	63	3.72E-2	412 "
R	7.82	2.87E-5	2.86E-4	63	3.55E-2	1080 "
S	7.4-7.7	2.87E-5	4.29E-4	66		
T	9.06	2.87E-5	4.29E-4	66	2.48E-2	
U	7.71	2.87E-5	4.29E-4	66	6.09E-2	
V	6.98	2.87E-5	4.29E-4	69	*1.39E-1*	
W	7.29	2.87E-5	4.29E-4	69	*1.04E-1*	
X	7.71	1.44E-5	4.29E-4	69	5.32E-2	
Y	7.72	2.10E-5	4.29E-4	75	5.34E-2	
Z	7.78	3.51E-5	4.29E-4	75	5.20E-2	
QA	7.78	4.21E-5	4.29E-4	75	6.07E-2	
QB	8.58	2.81E-5	4.29E-4	79	3.67E-2	
QC	8.25	2.81E-5	4.29E-4	79	5.33E-2	
QD	7.87	2.81E-5	4.29E-4	79	8.52E-2	
QE	6.89	2.12E-5	2.14E-4	84	7.68E-2	.050 I
QF	6.90	2.12E-5	2.14E-4	84	6.65E-2	.011 I
QG	6.88	2.12E-5	2.14E-4	84	7.57E-2	.0062 I
QH	6.94	2.13E-5	2.14E-4	87	6.83E-2	.202 I
QJ	6.94	2.13E-5	2.14E-4	87	3.78E-2	15.0 C
QK	6.98	2.13E-5	2.14E-4	91	3.32E-2	15.0
QL	7.09	2.13E-5	2.14E-4	91	2.13E-2	5.0
QM	6.49	2.13E-5	2.14E-4	91	4.99E-2	20.0
QN	6.49	2.10E-5	2.14E-4	96	8.56E-2	
QO	7.29	2.10E-5	2.14E-4	96	4.88E-2	
QP	7.71	2.10E-5	2.14E-4	96	2.57E-2	
QQ	7.83	2.83E-5	2.86E-4	112	2.88E-2	
QS	7.49	2.83E-5	2.86E-4	112		.50M NaCl
QT	6.82	2.12E-5	2.15E-4	116	2.23E-2	1.0E-2PO4
QU	6.84	2.12E-5	2.15E-4	116	2.50E-2	1.0E-3PO4
QV	6.85	2.12E-5	2.15E-4	116	2.62E-2	1.0E-4PO4
QW	6.87	2.12E-5	2.14E-4	122	6.68E-2	
QX	6.87	2.12E-5	2.14E-4	122	5.76E-2	1.0E-4Ca
QY	6.87	2.12E-5	2.14E-4	122	6.30E-2	1.0E-5Ca
QZ	6.89	2.08E-5	2.14E-4	128	3.28E-2	1.0E-5PO4

*Fewer than 4 points used to calculate k_{exp}.

Table 7.4B: Reduction of Suspension N(7) with Hydroquinone

Trial	pH	Mn_T (M)	[HQ] (M)	Age (Days)	Kexp (min-1)	Comments
KA	6.82	2.08E-5	2.14E-4	128	4.80E-2	1.0E-2Ca
KB	6.87	2.08E-5	2.14E-4	128	5.01E-2	1.0E-3Ca
KC	7.68	2.13E-5	2.14E-4	132	6.66E-3	1.0E-2PO4
KD	7.68	2.13E-5	2.14E-4	132	7.98E-3	1.0E-4PO4
KE	7.68	2.13E-5	2.14E-4	132	2.75E-2	
KF	7.7		-	137		Blank
KG	6.91	2.13E-5	2.14E-4	141	2.10E-2	
KH	6.90	2.13E-5	2.14E-4	141	2.14E-2	22%Oxygen

Table 7.4C: Reduction of Suspension N(7) with 2,5-Dihydroxybenzoic Ac

Trial	pH	Mn_T (M)	[2,5-DIOH] (M)	Age (Days)	kexp (min-1)	Ionic Strength (M)	Comments
KI	6.55-6.78	2.13E-5	2.14E-4	141		5.0E-2	-
KJ	6.79	"	"	143	1.41E-2	"	1.00E-2M PO4
KK	6.66-6.80	"	"	143	2.05E-2	"	1.00E-4M PO4
KL	6.64-6.81	"	"	143	6.12E-2	"	-
KM	7.71	"	"	146	3.84E-3	"	1.00E-2M PO4
KN	7.56-7.68	"	"	146	5.53E-3	"	1.00E-4M PO4
KO	7.53-7.68	"	"	146	1.65E-2	"	-
KP	6.72	"	"	149	1.58E-2	1.0E-1	1.00E-2M PO4
KQ	6.62	"	"	149	1.62E-2	2.0E-1	1.00E-2M PO4
KR	6.70	"	"	149	1.37E-2	5.0E-1	1.00E-2M PO4
KS	6.52	"	"	151	2.06E-2	5.0E-2	1.00E-2M PO4
KT	7.27	"	"	151	7.79E-3	"	1.00E-2M PO4
KU	8.00	"	"	151	2.37E-3	"	1.00E-2M PO4

Table 7.4D: Reduction of Suspension N(9) with Hydroquinone and p-Benzoquinone

Trial	pH	Mn_T (M)	Reductant (M)	Age (Days)	Rate Constant	Comments
KV	7.21	2.82E-5	2.54E-5 HQ	26		
KW	7.19	2.82E-5	2.54E-5 HQ	26		3.00E-3 Sorbitol
KX	7.16	2.82E-5	-	24		3.00E-3 Sorbitol
KY	7.20	2.82E-5	-	24	Blank	2.98E-5M Mn2+
KZ	7.91	2.82E-5	-	24	Blank	2.97E-5M Mn2+
GH	7.68	3.43E-5	1.72E-5 HQ	33		
GO	7.25	3.54E-5	1.77E-5 HQ	38		
XK	7.75	2.85E-5	5.00E-5 HQ	112		
XL	7.74	2.85E-5	5.00E-5 HQ	112		7.14E-4 Quinone
XM	7.74	2.85E-5	-	112		7.14E-4 Quinone
XN	7.77	2.85E-5	-	114		1.00E-5 Quinone
XO	7.77	2.85E-5	-	114		5.00E-5 Quinone
XP	7.77	2.85E-5	-	114		2.00E-4 Quinone
XQ	7.79	2.87E-5	5.00E-5 HQ	117		2.00E-3 Salicylate
XR	7.78	2.87E-5	5.00E-5 HQ	117		5.00E-4 Salicylate
XS	7.79	2.87E-5	5.00E-5 HQ	117		5.00E-5 Salicylate
XT	7.79	2.87E-5	2.00E-4 Quinone	120		9.27E-6M Mn2+
XU	7.79	2.87E-5	2.00E-4 HQ	120		9.27E-6M Mn2+
XV	7.80	2.87E-5	2.00E-4 HQ	120		
XW	6.82	2.81E-5	2.00E-5 HQ	129		2.00E-3 Phthalate
XX	6.81	2.81E-5	2.00E-5 HQ	129		
XY	6.81	2.81E-5	-	129		2.00E-3 Phthalate
XZ	6.83	2.81E-5	2.00E-5 HQ	132		2.00E-3 Oxalate
AA	6.85	2.81E-5	2.00E-5 HQ	132		2.00E-3 EDTA
AB	6.9-7.1	2.81E-5	-	132		2.00E-3 EDTA
AC	6.80	2.89E-5	2.00E-5 HQ	138		5.00E-6 PO4
AD	6.80	2.89E-5	2.00E-5 HQ	138		1.00E-5 PO4
AE	6.79	2.89E-5	2.00E-5 HQ	138		1.00E-4 PO4
AF	6.80	2.89E-5	2.00E-5 HQ	141		1.00E-3 PO4
AG	6.80	2.89E-5	2.00E-5 HQ	141		3.00E-4 PO4
AH	6.80	2.89E-5	2.00E-5 HQ	141		
AJ	6.50	2.89E-5	-	145		Blank
AK	7.77	2.89E-5	2.00E-4 Quinone	145		2.00E-3 Sorbitol

mixing. Figure 7.4 shows that 98% of added Mn^{2+} remains in solution, which means that less than 2% was adsorbed. Loss of Mn^{2+} onto oxide surfaces is small enough that it does not interfere with the determination of reduced manganese.

7.4B. Oxygen

The sensitivity of the reaction to oxygen was examined to determine whether the steps taken to exclude oxygen were adequate. Low levels of oxygen may have been present in the carbon dioxide/nitrogen mixtures and may have been introduced when opening and closing the stoppered faceplate. A reaction performed in equilibrium with 21.8% oxygen was compared to one in equilibrium with an oxygen-free mixture. Both reactions had a 15-fold excess of hydroquinone and a pH of 6.9. Differences in $[Mn^{2+}]_{diss.}$ between the two reactions were negligible, as shown in figure 7.5A. It is safe to assume that any inadvertent introduction of oxygen into the sealed vessel had little effect on the reaction rate.

7.4C. Light

As discussed earlier, the reduction of manganese oxides by natural organics is catalyzed by solar radiation (Section 4.6B). It was therefore necessary to test whether laboratory fluorescent lights enhanced the reaction rate. Duplicate reactions were performed under normal laboratory lighting and under darkroom lights; the results are shown in figure 7.5B. Fluorescent light had a negligible effect on the reaction rate, so no effort was made to keep it out.

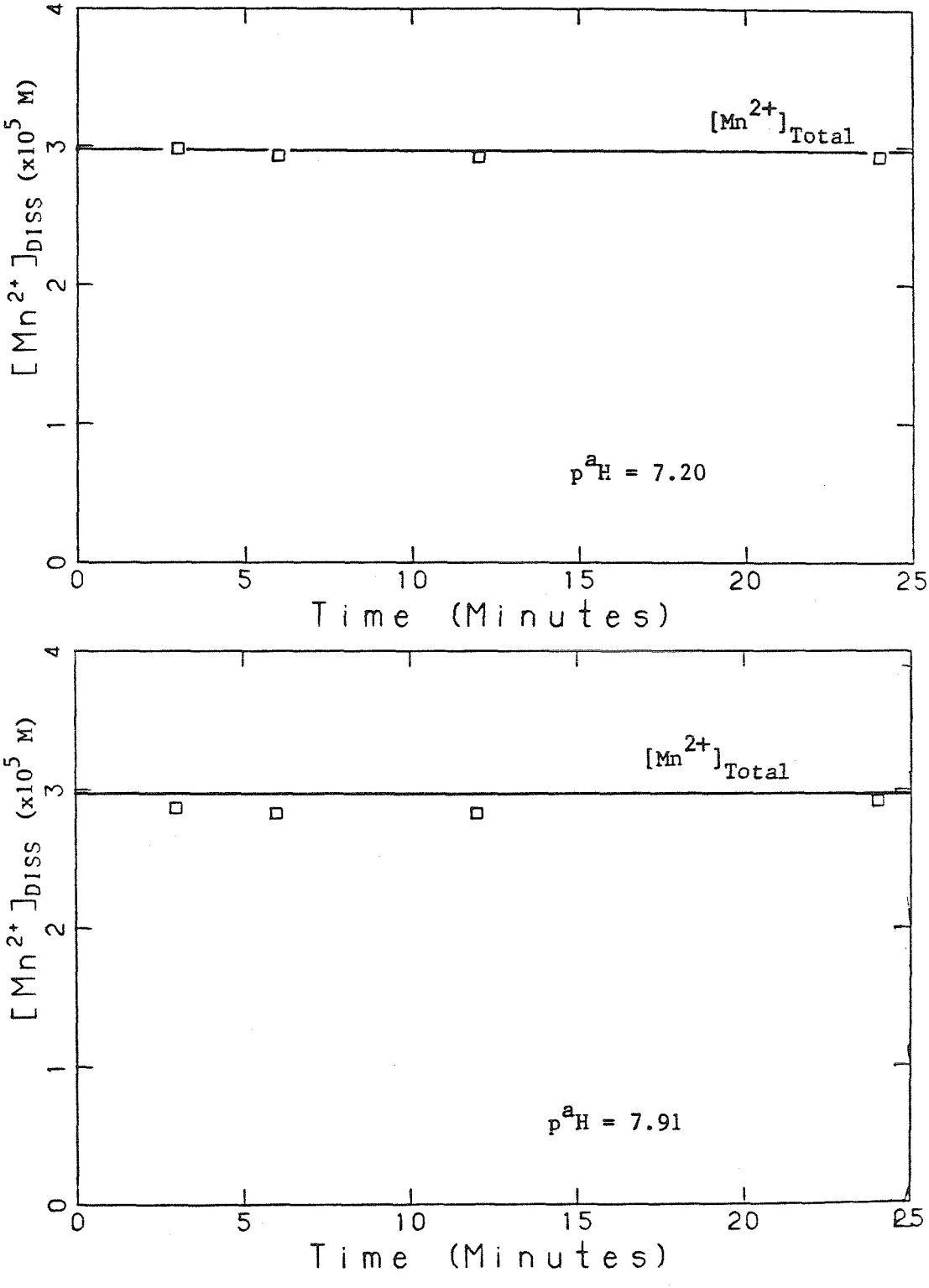

Figure 7.4 Adsorption of Mn^{2+} by the manganese oxide suspension at pH values of 7.20 and 7.91. The smooth line is the amount of $MnCl_2$ added to the suspension, and experimental points show the amount of manganese present in the filtrate.

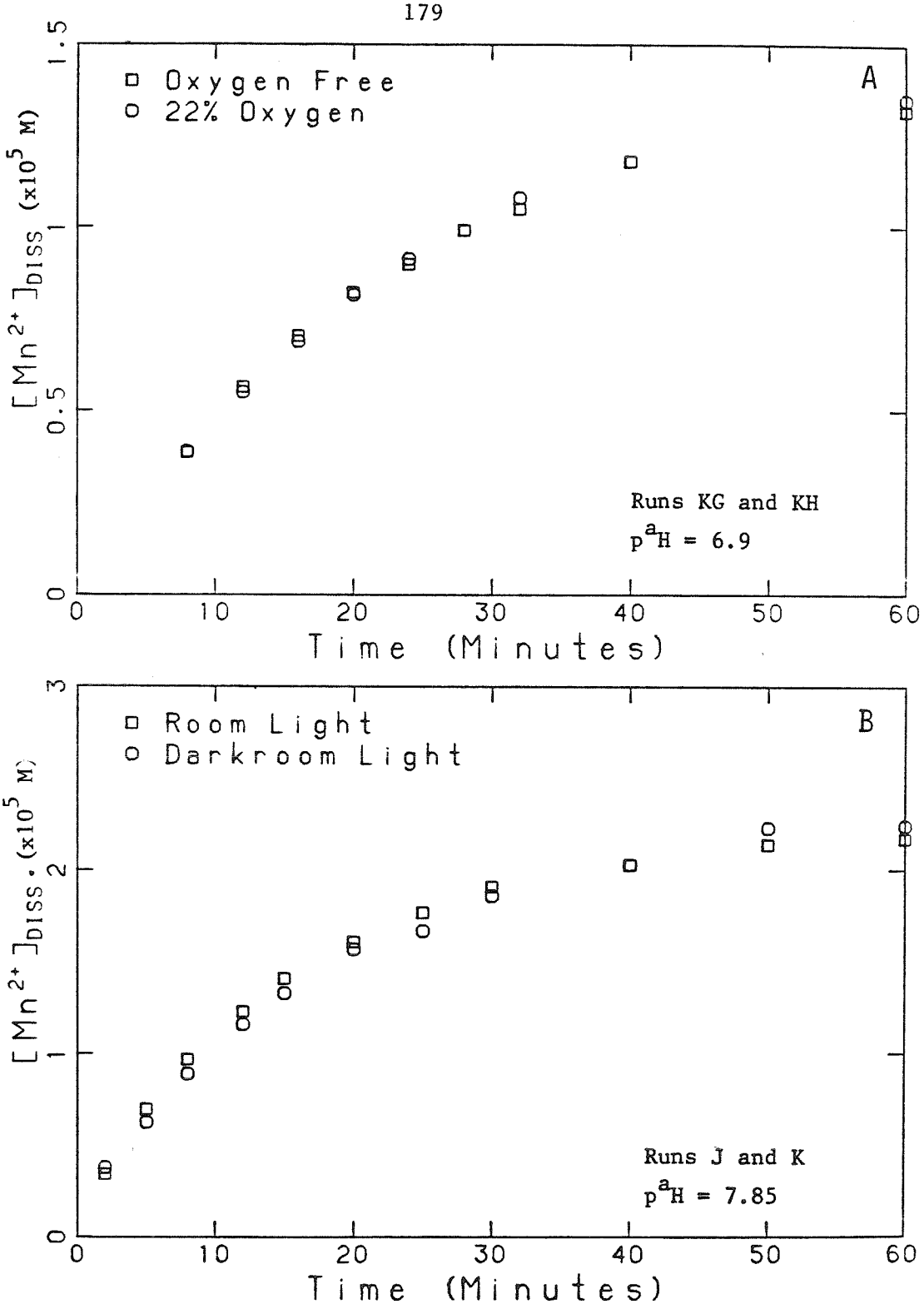

Figure 7.5 The effect of oxygen (A) and of light (B) on the dissolution of manganese oxide suspensions by hydroquinone.

7.4D. Stirring Rate

The dependence on stirring rate was measured by running the reaction at stirring rates of 100, 410, and 1100 rpm. Figure 7.6 shows that increasing the stirring rate did not increase the reaction rate; calculated rate constants (k_{exp}) actually decreased slightly when stirring was increased.

7.4E. Age of Suspension

In order to compare reaction rates from runs performed on different days, the influence of suspension age on the reaction must be known. The reactivity of the suspension may change upon aging due to gradual recrystallization of the oxide, or because of lowering of surface area caused by coalescence of particles.

Dissolution of suspension N(7) under the same experimental conditions was repeated several times during a three month period. As figure 7.7 shows, calculated k_{exp} values decreased 40% during the period studied, or by approximately 0.4% per day. For this reason, the relative suspension age must be considered when experiments performed on different days are compared.

7.5 Order with Respect to Hydroquinone

The order with respect to hydroquinone was derived from the runs summarized in Table 7.5. In each case, the initial hydroquinone concentration was 10 or more times greater than Mn_T and can therefore be considered constant for the entire reaction. Table 7.5 also includes the experimental rate constant k_{exp} and the rate constant k_p corrected for pH (see Section 7.6) for each run.

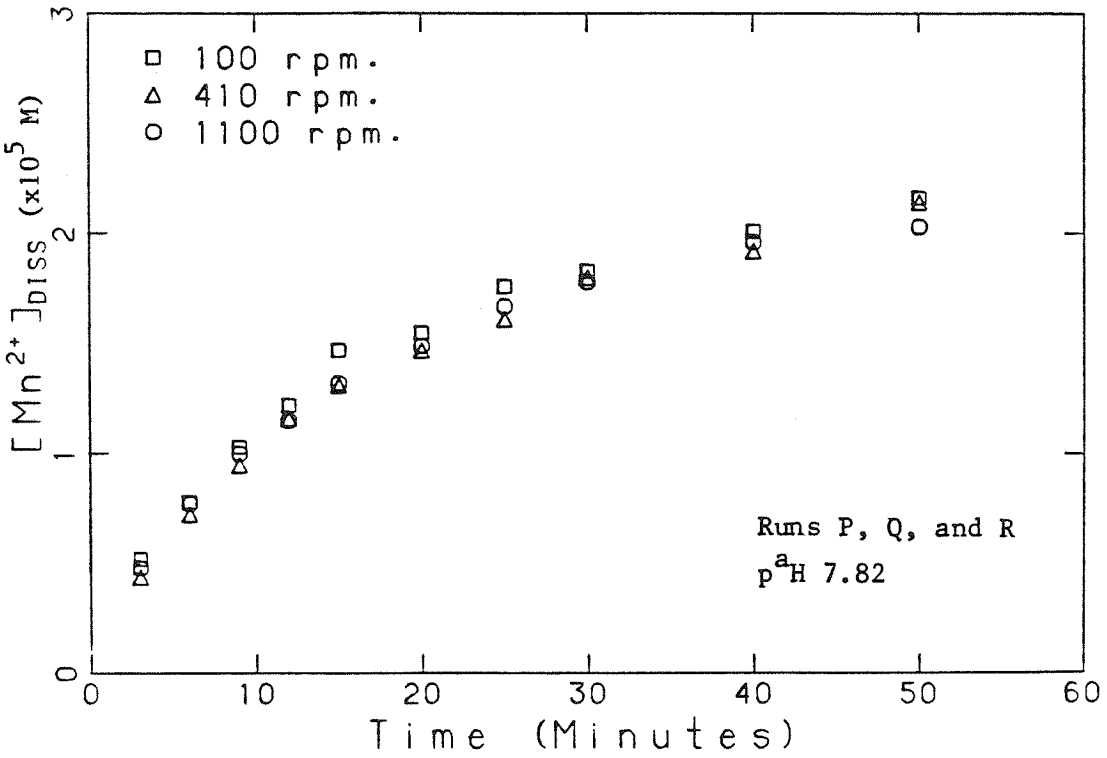

Figure 7.6 The effect of stirring rate on the dissolution reaction.

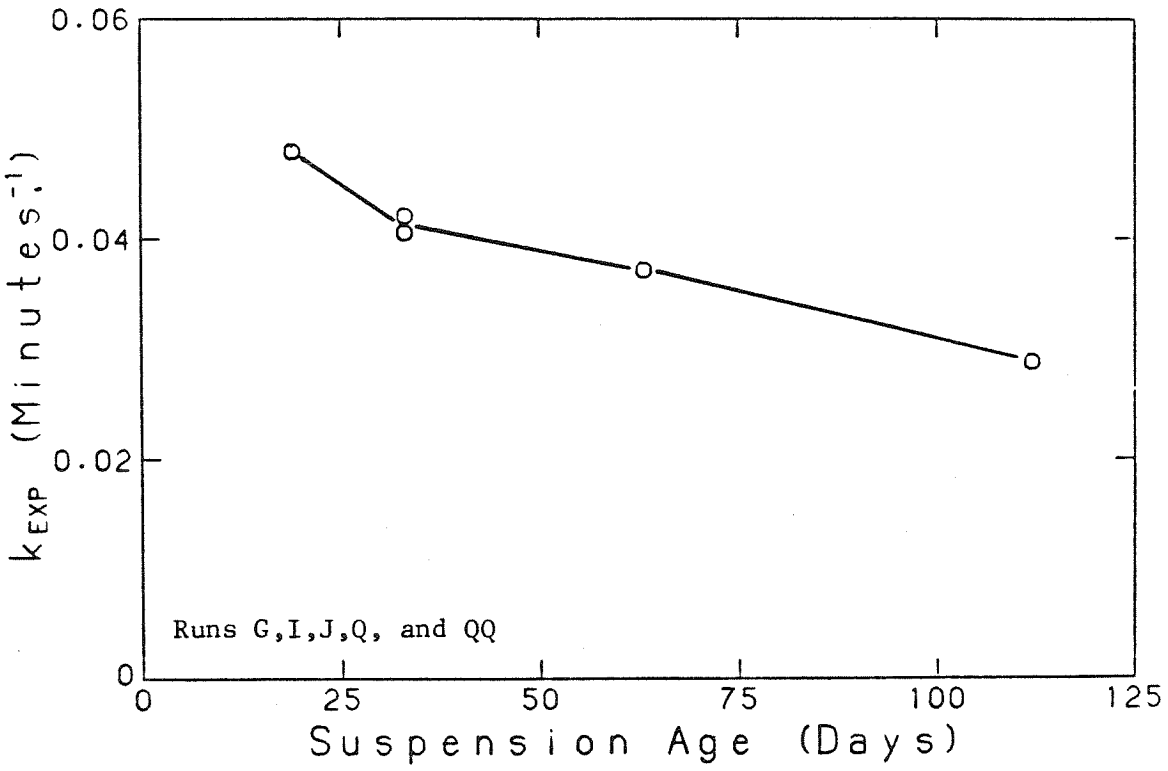

Figure 7.7 Rate constants determined for dissolution of manganese oxides under the same conditions performed on different days.

Table 7.5 Experimental Runs: Vary [Hydroquinone]

Trial	pH	Mn_T (M)	[HQ] (M)	[HQ]/Mnt	kexp (min-1)	kp	Age (days)
M	7.80	2.89E-5	8.57E-4	29.7	9.93E-2	4.61E+2	53
L	7.83	2.89E-5	5.71E-4	19.8	7.02E-2	3.37E+2	53
U	7.71	2.87E-5	4.29E-4	14.9	6.09E-2	2.57E+2	66
Q	7.81	2.87E-5	2.86E-4	10.0	3.72E-2	1.75E+2	63
R	7.82	2.87E-5	2.86E-4	10.0	3.55E-2	1.68E+2	63
Y	7.72	2.10E-5	4.29E-4		5.34E-2	2.26E+2	75
QP	7.71	2.10E-5	2.14E-4	10.2	2.57E-2	1.08E+2	96

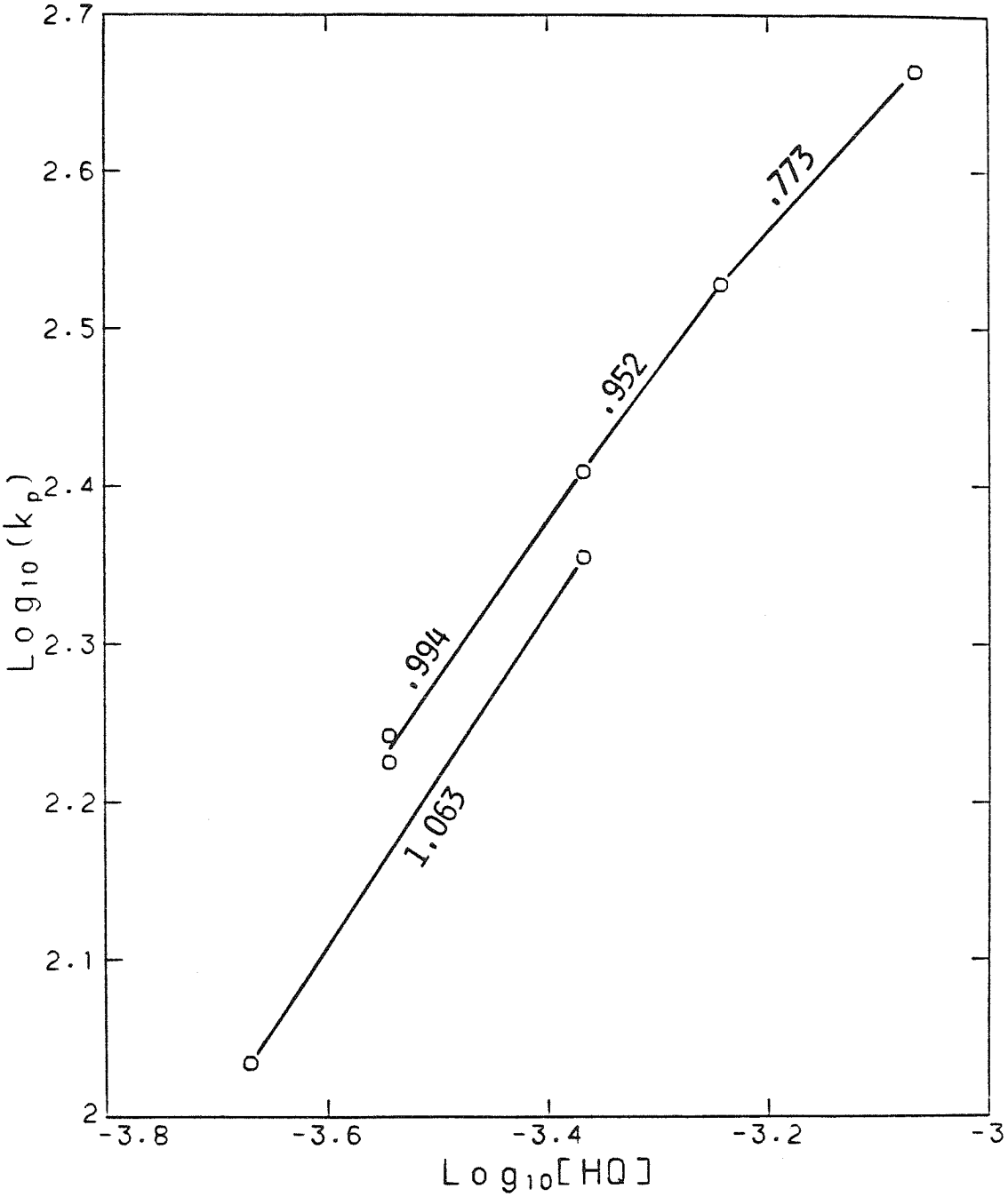

Figure 7.8 Determination of the order of the reaction with respect to hydroquinone. The order is found from the slope of $\log_{10}(k_p)$ plotted against $\log_{10}[HQ]$.

Figure 7.8 plots $\log(k_p)$ against log[Hydroquinone] using the data from Table 7.5. The slope of the plot is the order with respect to hydroquinone. A slope is calculated from successive pairs of points, so that any change in order as the concentration of hydroquinone is increased can be distinguished. Runs Y and QP were performed using suspension that had aged longer than the other experiments, which explains why the rate constants are smaller.

The order with respect to hydroquinone is close to 1.0 for all but one pair of points. An order of 0.77 was determined using k_p from runs performed at the highest hydroquinone concentrations. This slope may reflect uncertainty in the measurement of k_p, or may be an actual decrease in the order at high hydroquinone concentrations. If the decrease in slope is real, it is consistent with the adsorption model described in Section 4.3. According to this model, once the fraction of surface sites occupied by adsorbate becomes significant, the apparent order with respect to adsorbate becomes less than 1.0. Apparent order calculated from runs at still higher concentrations of hydroquinone should be even lower than 0.77, if this model is correct.

7.6 pH Dependence

The pH of a series of runs can be varied by either adding different amounts of sodium bicarbonate (changing [Alkalinity]) or by using gas mixtures with varying amounts of carbon dioxide. Reactions of interest are summarized in Table 7.6.

The order of the reaction with respect to $\{H^+\}$ is found by plotting $\log(k_{exp})$ against p^aH as shown in figure 7.9. All the

Table 7.6 Experimental Runs: Vary $\{H^+\}$

Trial	pH	Mn_T (M)	[HQ] (M)	[Alk] (M)	P(CO2) (atm.)	kexp (min-1)	Age (days)	
QN	6.49	2.10E-5	2.14E-4	<1E-3	1.09E-2	8.56E-2	96	
QE	6.89	2.10E-5	2.14E-4	9.8E-4	1.09E-2	7.68E-2	84	Set 1
QO	7.29	2.10E-5	2.14E-4	3.6E-3	1.09E-2	4.88E-2	96	
QP	7.71	2.10E-5	2.14E-4	1.0E-2	1.09E-2	2.57E-2	96	
V	6.98	2.87E-5	4.29E-4	9.6E-4	1.09E-2	1.39E-1	69	
W	7.29	2.87E-5	4.29E-4	3.0E-3	1.09E-2	1.04E-1	69	Set 2
U	7.71	2.87E-5	4.29E-4	1.0E-2	1.09E-2	6.09E-2	69	
QD	7.87	2.81E-5	4.29E-4	2.9E-3	2.14E-3	8.52E-2	79	
QC	8.25	2.81E-5	4.29E-4	5.7E-3	2.14E-3	5.33E-2	79	Set 3
QB	8.58	2.81E-5	4.29E-4	1.0E-2	2.14E-3	3.67E-2	79	
T	9.06	2.87E-5	4.29E-4	1.0E-2	3.20E-4	2.48E-2	66	

Set	Slope	Corrl.
1	-.44	.962
2	-.49	.997
3	-.45	.995

Average slope= -.46

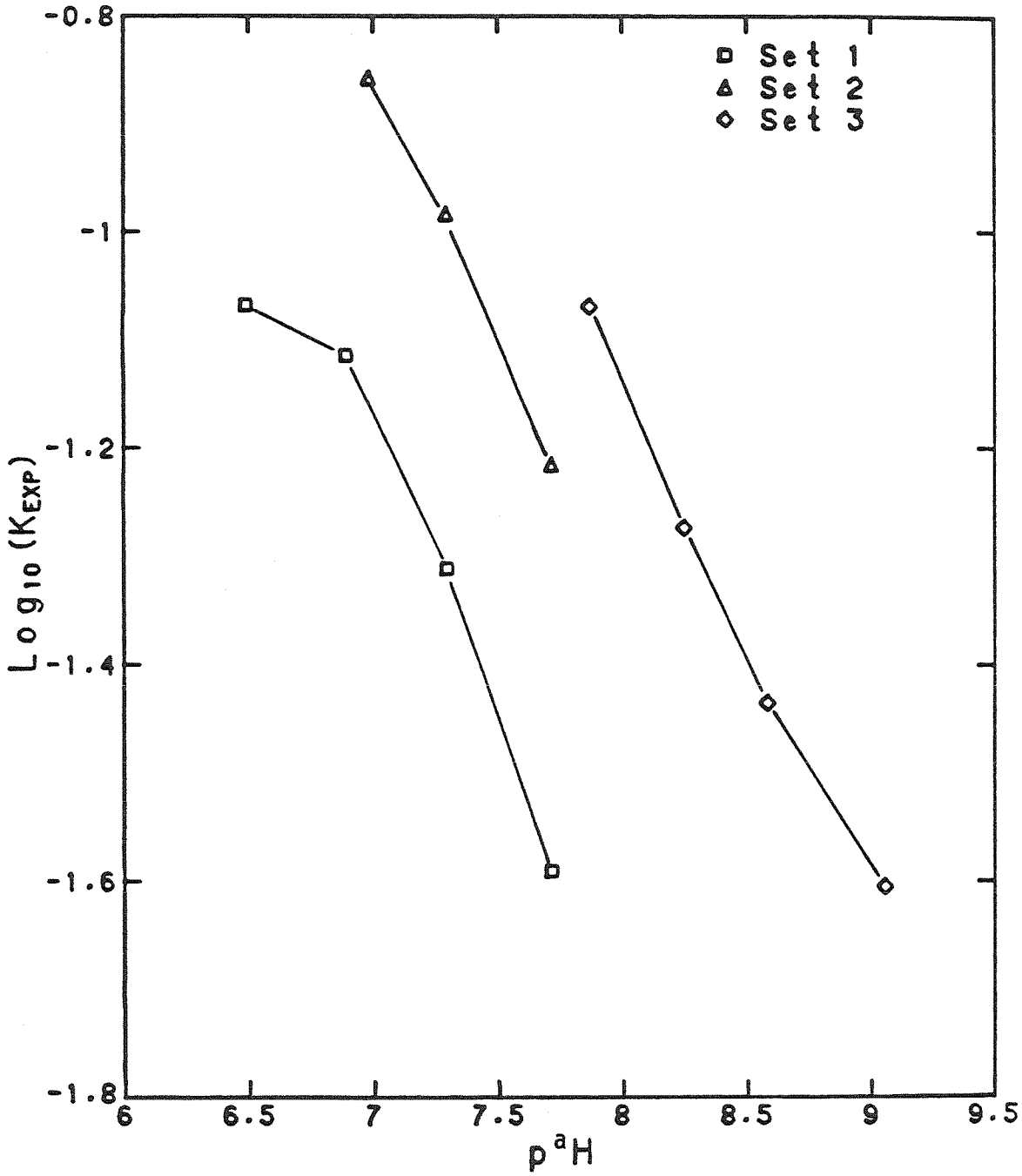

Figure 7.9 Effect of pH on the dissolution of manganese oxide suspensions with hydroquinone. See Table 7.6 for a description of the reaction conditions.

reactions were performed in the same ionic medium (5.00×10^{-2}M $NaNO_3$) so the slope found by plotting against p^aH is the same as that found by plotting against p^cH. Table 7.5 includes the slopes calculated from each set. The rate increases as $\{H^+\}$ increases; the average order from the three sets of data is 0.46. The pH dependence of k_{exp} can now be written as:

$$7.13 \qquad k_{exp} = k_p\{H^+\}^{0.46}$$

Values of k_p can be calculated which are independent of pH within the range studied and can be used to compare the rates under different experimental conditions.

7.7 Reaction with p-Benzoquinone

Since the oxidation of hydroquinone is known to form p-benzoquinone (Section 8.3B) it must be determined whether or not p-benzoquinone has any activity of its own. Figure 7.10 shows that quinone does reduce the manganese oxide suspension at an appreciable rate, and that the reaction is autocatalytic.

When hydroquinone is oxidized, the amount of p-benzoquinone formed is limited by the oxide loading. For a typical case, the maximum amount of p-benzoquinone that can form is:

$$\left(\frac{2.85\text{E-}5\text{moles Mnt}}{\text{liter}}\right)\left(\frac{1.3\text{ Equivs. Oxidant}}{\text{mole Mnt}}\right)\left(\frac{1\text{ mole quinone}}{2\text{ Equivs. Oxidant}}\right) = 1.85\times10^{-5}\text{M}$$

Reduction by p-benzoquinone in solutions containing excess hydroquinone

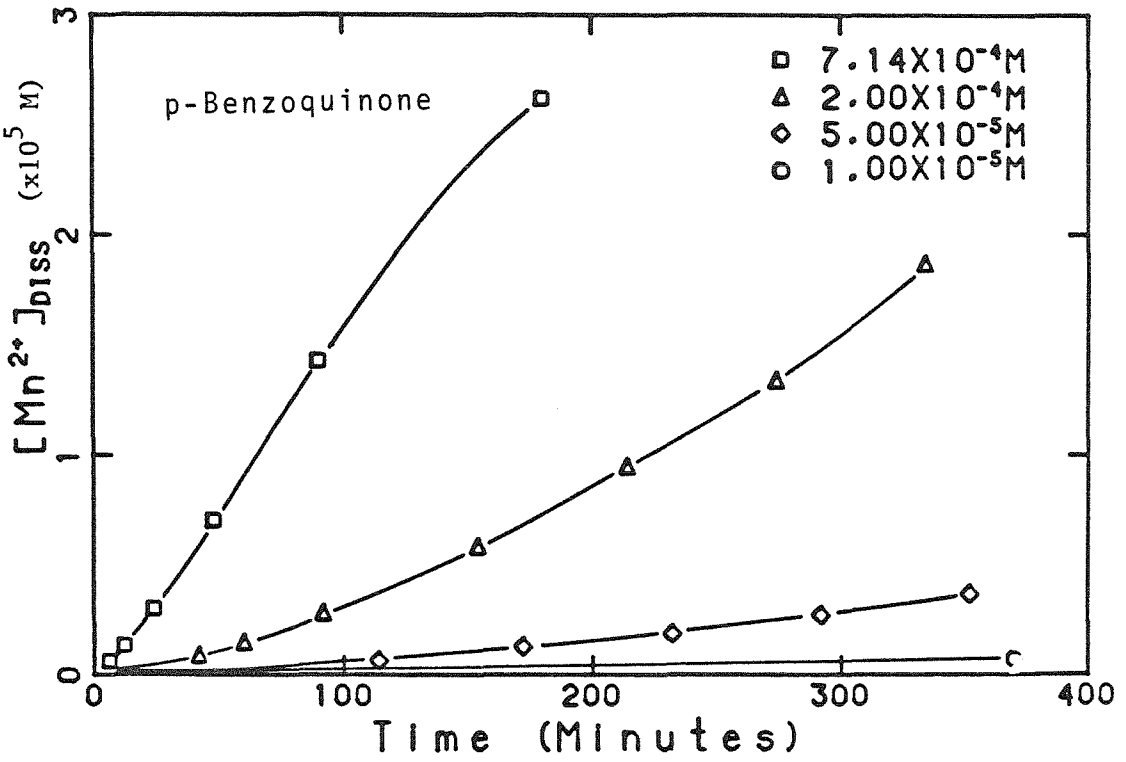

Figure 7.10 Dissolution of manganese oxides by p-benzoquinone under the following conditions:

2.85x10-5M Mn_T (as N(9))

5.00x10-2M $NaNO_3$, 1.00x10-2M $NaHCO_3$

p^aH 7.8 , 1.0% CO_2.

Runs XM,XN,XO, and XP.

is insignificant because its concentration is low and it reacts slowly. In solutions containing excess manganese oxide, however, reaction with p-benzoquinone causes more than two equivalents of manganese oxide to be reduced per mole of hydroquinone.

7.8 Effect of Mn^{2+}

As the dissolution reaction progresses, the amount of Mn^{2+} in solution increases. Its effect on the reaction can be observed by adding stock $MnCl_2$ prior to initiation of the dissolution reaction and comparing the reaction rate to the rate measured in its absence. The reaction can be monitored by the filtration technique only if the amount released by dissolution can be distinguished from the initial concentration. Figure 7.11 shows the effect of 9.3×10^{-6}M Mn^{2+} on the dissolution of the oxide suspension by hydroquinone and p-benzoquinone. The initial Mn^{2+} concentration has been subtracted out of the measured value so that $[Mn^{2+}]_{diss}$ represents only Mn^{2+} released by dissolution. As Figure 7.11 shows, this concentration of Mn^{2+} had no effect on the reaction rate.

7.9 Ionic Strength

The effect of ionic strength on the dissolution rate was studied using two reductants, hydroquinone and 2,5-dihydroxybenzoic acid (2,5-diOH). Reactions with hydroquinone were performed at pH 6.9, and with 2,5-diOH at pH 6.6. Ionic strength was set by addition of sodium nitrate. The neutral H_2L form of hydroquinone and negatively charged H_2L^{1-} form of 2,5-diOH are predominant species at this pH (see Table 8.1). Reactions with 2,5-diOH were performed in

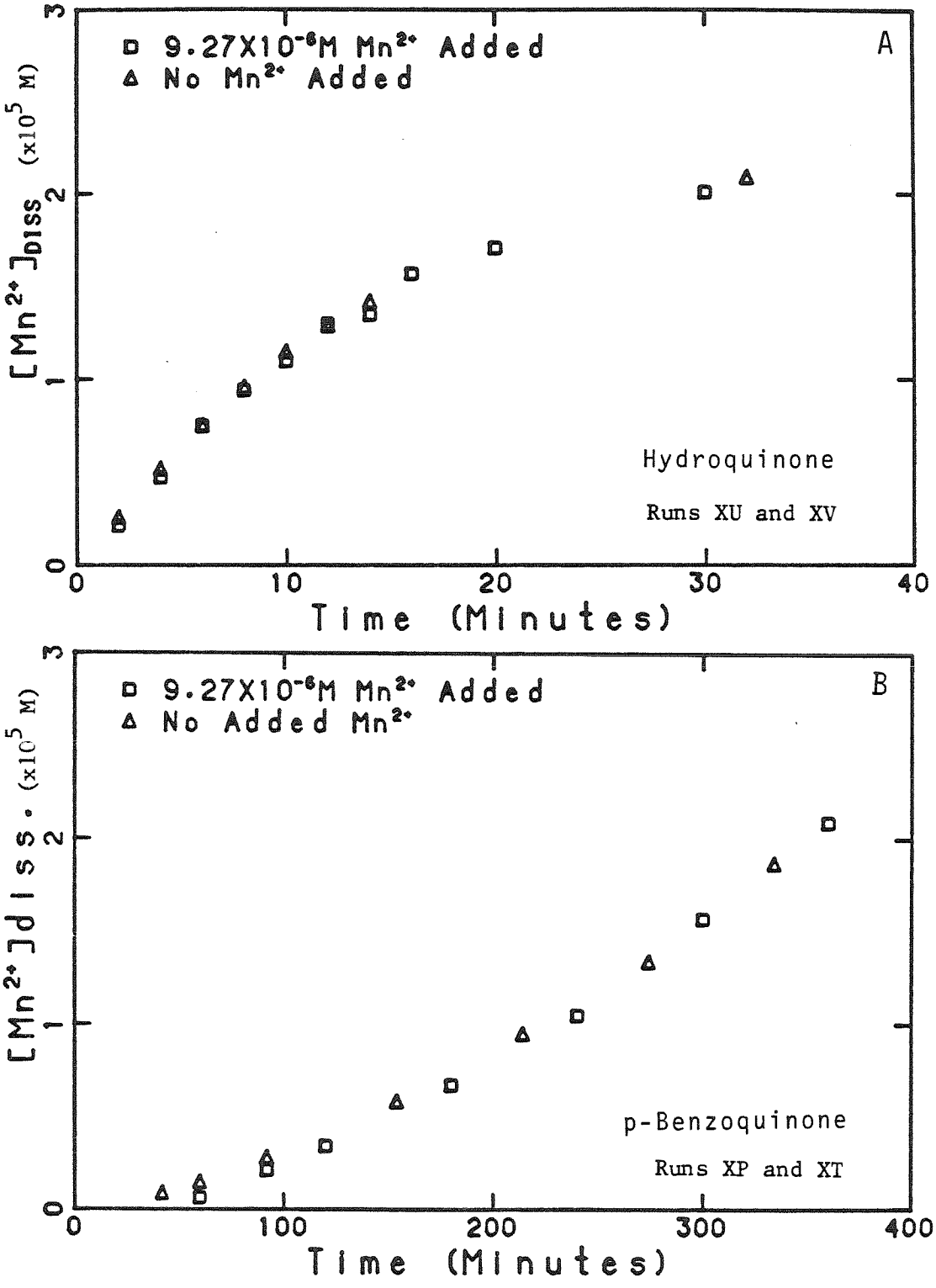

Figure 7.11 Effect of Mn^{2+} on dissolution of manganese oxide by hydroquinone (A) and by p-benzoquinone (B).

1.00×10^{-2}M phosphate buffer to minimize pH changes during the reaction. It should be noted, however, that phosphate lowers the reaction rate (Section 7.11).

Figure 7.12 plots values of k_p (pH independent rate constants) against ionic strength for the two reductants. Rate constants decreased with increasing ionic strength in both cases. Differences in rate with increasing ionic strength are small. Equation 4.60 and the Davies Equation for estimating activity coefficients (Stumm and Morgan, 1981) can be used to calculate the change in rate assuming two reactants of charge +1 and -1 based on the primary salt effect. If the ionic strength is increased from 5×10^{-2} to 2.0×10^{-1}M then the rate of reaction should decrease by 17%. The actual decrease was 18% for reaction with hydroquinone, and 10% for reaction with 2,5-diOH.

The pH_{zpc} of suspension N(7) used in these experiments was determined by titration to be 7.4 (Section 5.6B.). The reaction with hydroquinone at pH 6.9 therefore involved interaction of a neutral solute species with a slightly positive oxide surface. Reaction with 2,5-diOH was performed in phosphate solution; adsorption by phosphate onto the oxide surface probably made the surface charge more negative than in the reaction with hydroquinone (Section 7.11).

As outlined in Section 4.5C., adsorption of neutral adsorbate decreases with increasing ionic strength because of ion-pair formation between electrolyte ions and surface sites. The amount of decrease depends upon the affinity of the adsorbate for the surface, and of the stability constants for formation of surface ion-pairs with electrolyte

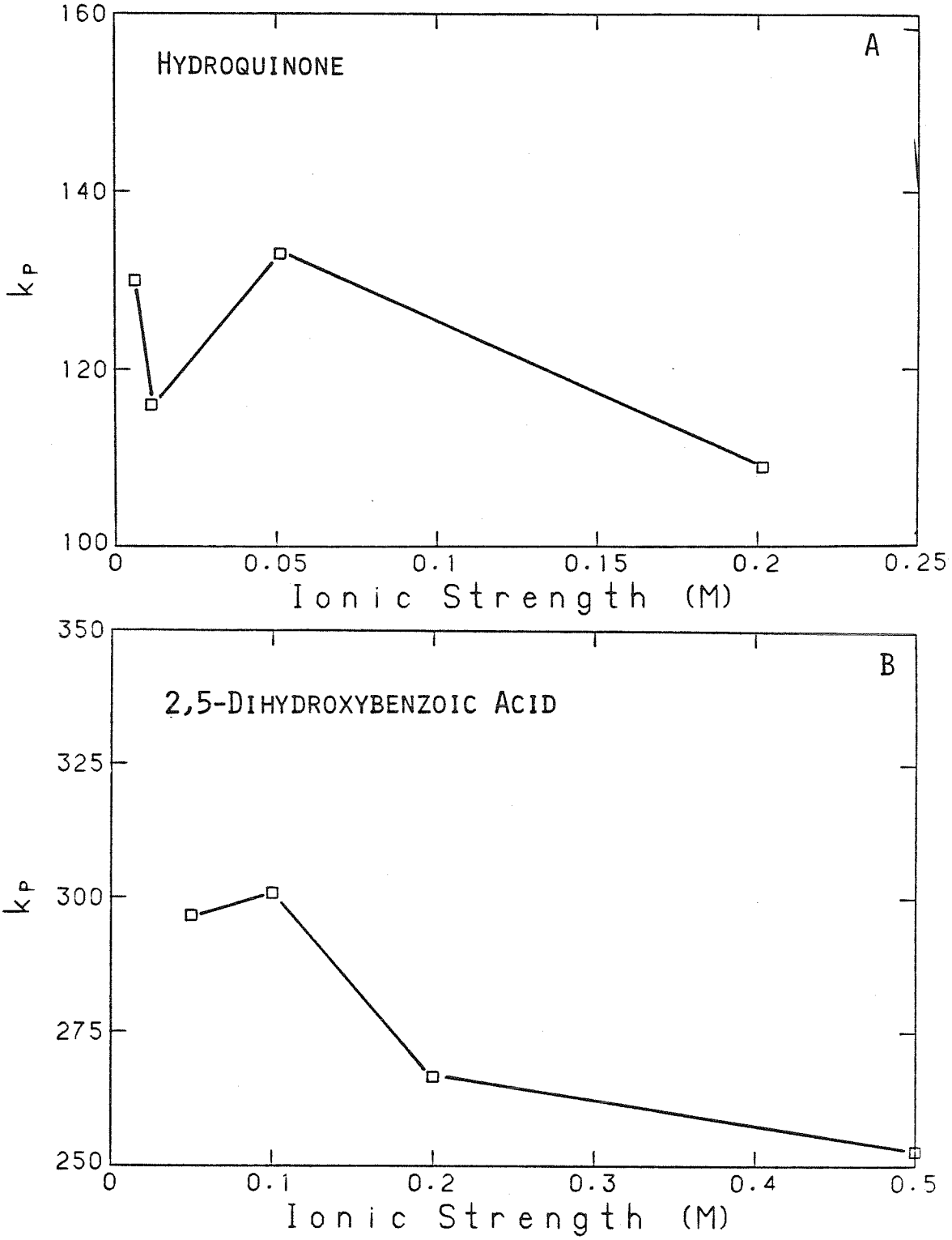

Figure 7.12 Effect of ionic strength on the rate constant for dissolution of manganese oxides by hydroquinone (A) and 2,5-dihydroxybenzoic acid (B).

ions. The decrease in reaction rate of hydroquinone with manganese oxide with increasing ionic strength may have been caused by this effect.

The effect of ionic strength on the reaction with anionic 2,5-diOH should be greater, assuming that the oxide surface charge is significant. If the surface is positive, the reaction rate should decrease with increasing ionic strength, since the solute species and surface are oppositely charged. The reaction rate with 2,5-diOH did decrease, but not any more than was observed for hydroquinone. The surface charge at this pH was probably very small, since little difference between the two substrates was observed.

7.10 Effect of Temperature

A series of dissolution reactions were performed at different temperatures in order to measure the apparent activation energy. A refrigerated constant-temperature bath was used to maintain the temperature to within $0.5^{0}C$ of the reported value. The conditions for the reactions were:

$Mn_T = 2.12 \times 10^{-5} M$

$[HQ] = 2.14 \times 10^{-4} M$

$5.00 \times 10^{-2} M\ NaNO_3$

$p^aH\ 6.9\text{-}7.1$

$9.8 \times 10^{-4} M$ [Alk.], 1.0×10^{-2} atm. P_{CO_2}

Figure 7.13 shows that k_p increases with increasing temperatures.

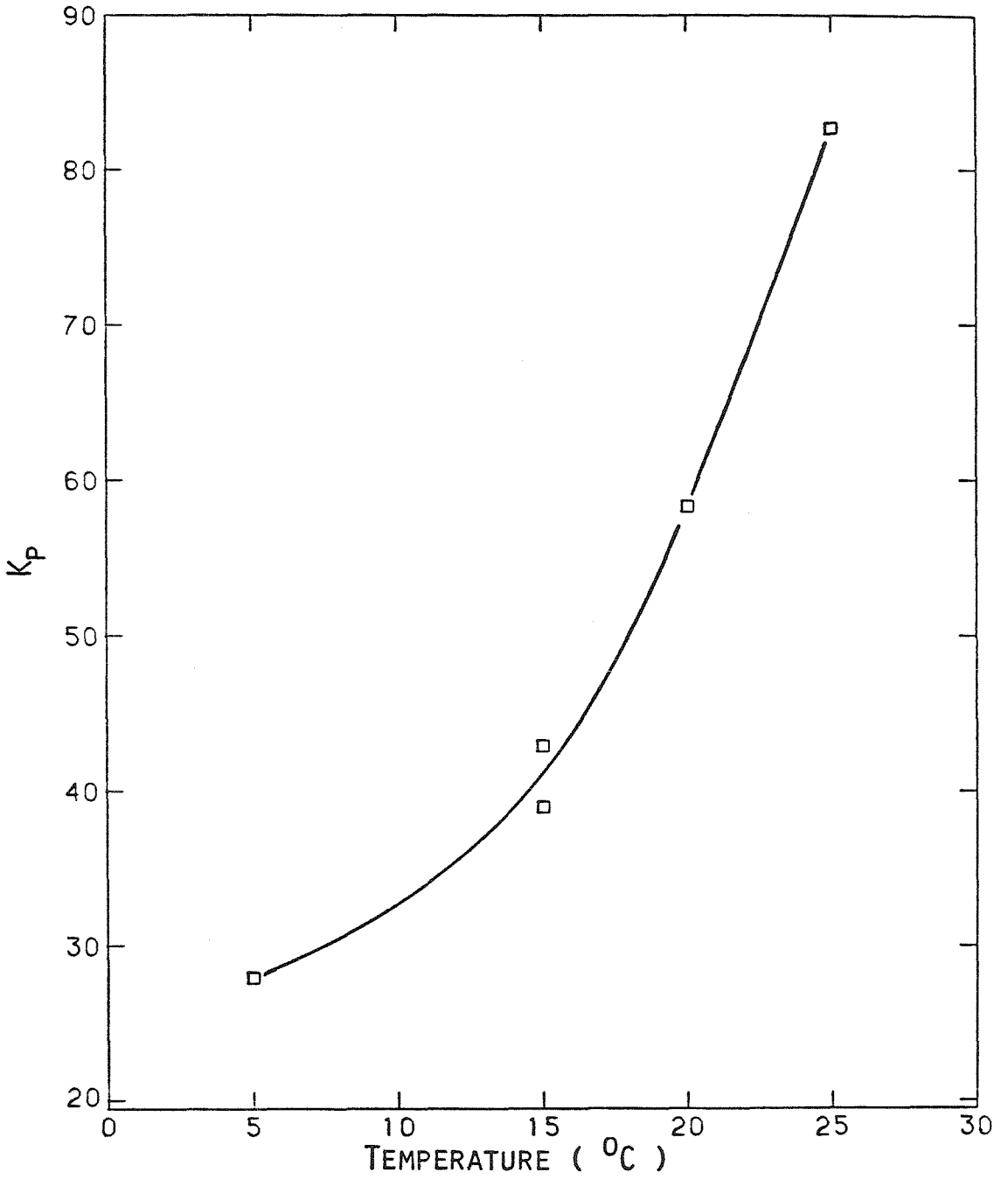

Figure 7.13 Effect of temperature on the rate constant for dissolution of the manganese oxide suspension by hydroquinone.

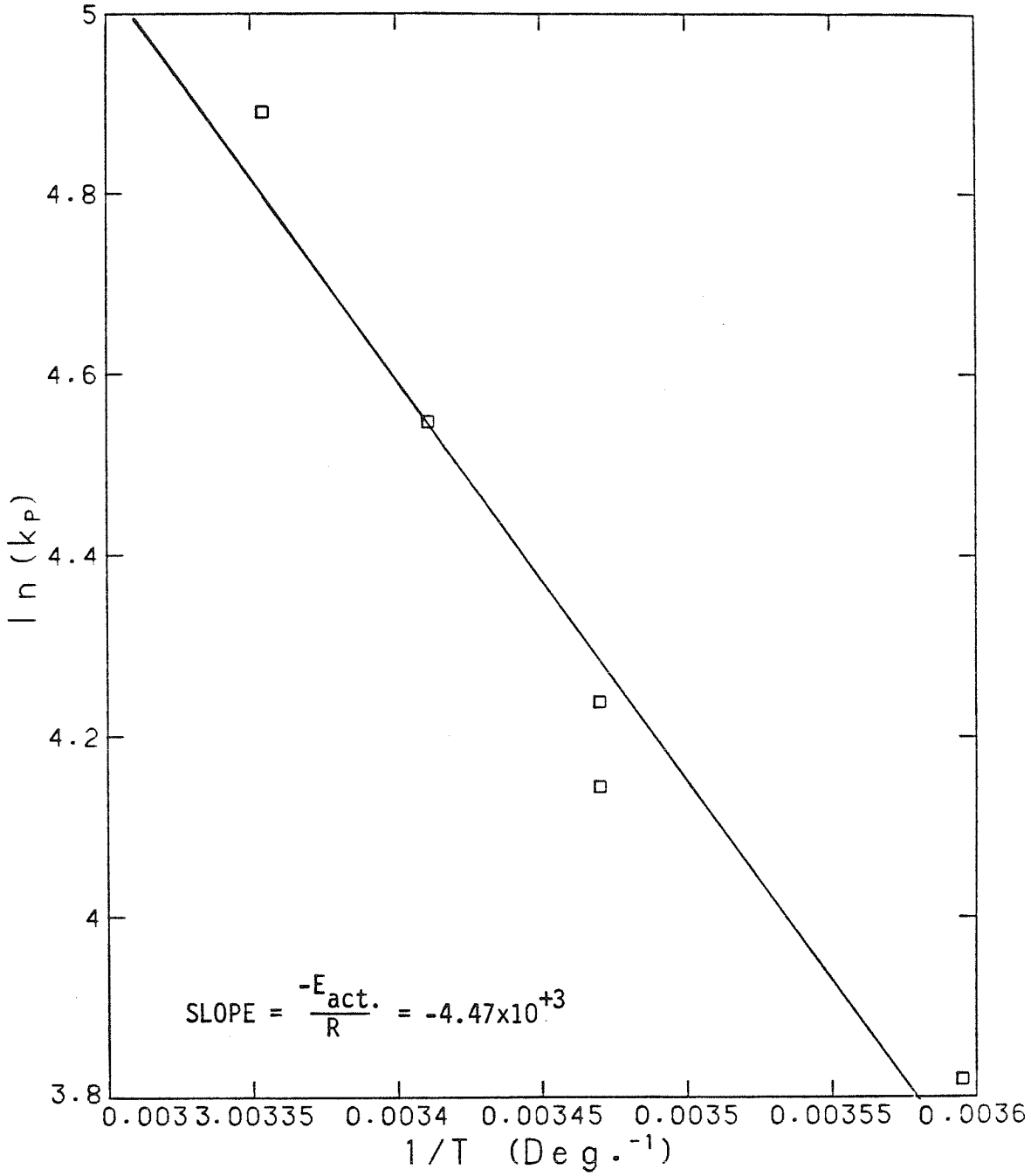

Figure 7.14 Arrhenius plot for the dissolution reaction. The activation energy of the reaction is found from the slope.

According to the Arrhenius Equation, a plot of the log of the rate constant against 1/T gives a slope equal to $-E_{act.}/RT$ (Figure 7.14). Using the slope from Figure 7.14, the apparent activation energy of the reaction with hydroquinone was found to be +37 kJ/mole. This agrees favorably with the value of +33±2 kJ/mole determined for the reaction of manganese oxide with hydroquinone measured by Ono et al. (1977) (Section 4.6C.).

7.11 Influence of Calcium and Phosphate

Specifically adsorbing cations and anions may lower the reaction rate by blocking adsorption sites (Section 4.3C.) or by interfering with the release of Mn^{II} into solution (Section 4.4). A series of experiments were performed in which varying amounts of calcium and phosphate were added to determine their effect.

Stock solutions of calcium nitrate ($Ca(NO_3)_2$) and potassium phosphate (a 50:50 mixture of KH_2PO_4 and K_2HPO_4) were added to reaction solutions prior to addition of stock suspension and equilibrated with the CO_2/N_2 mixture.

$k_{exp}(x)/k_{exp}(0)$ represents the pseudo first-order rate constant determined in the presence of the specified amount of phosphate or calcium divided by the rate constant measured in their adsence. Figure 7.15 shows that for reaction with excess hydroquinone, both phosphate and calcium lower the reaction rate. Inhibition by phosphate was much greater than by calcium, lowering the rate by 75% at the highest phosphate concentration examined. The rate was lowered by phosphate to a greater extent at pH 7.7 than at pH 6.8. Calcium,

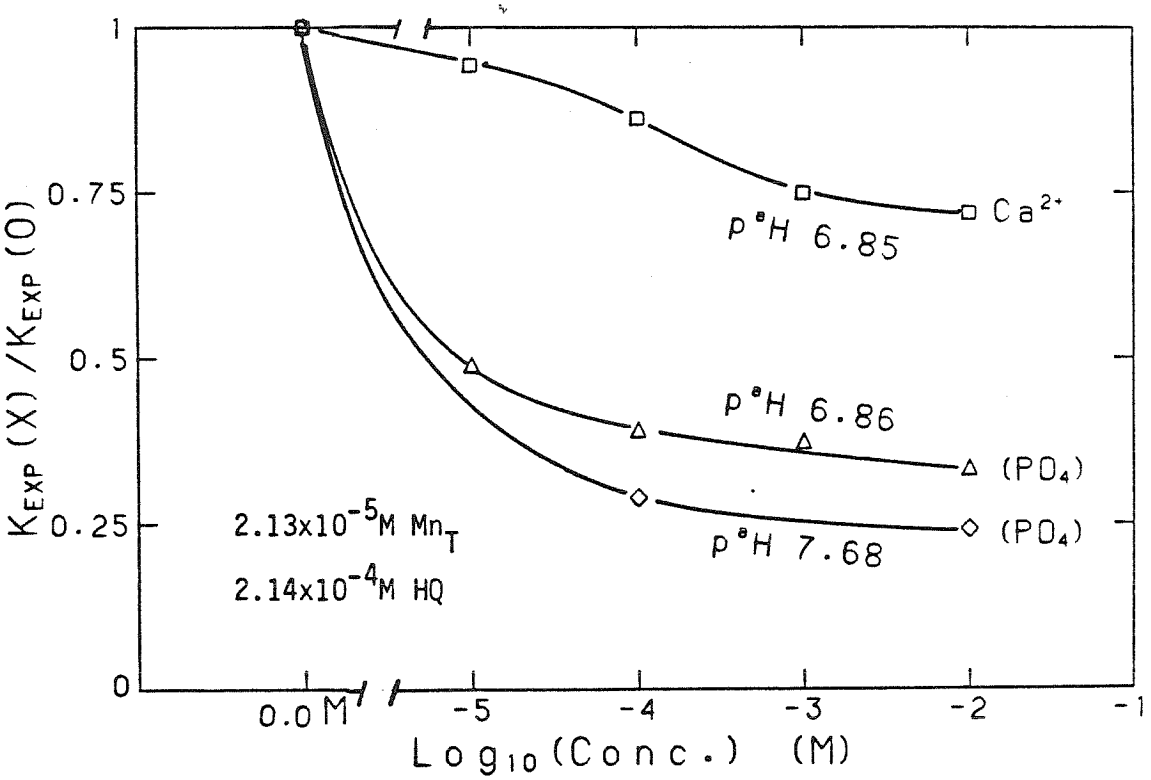

Figure 7.15 The effect of calcium and phosphate on the rate of dissolution by hydroquinone (in excess hydroquinone).

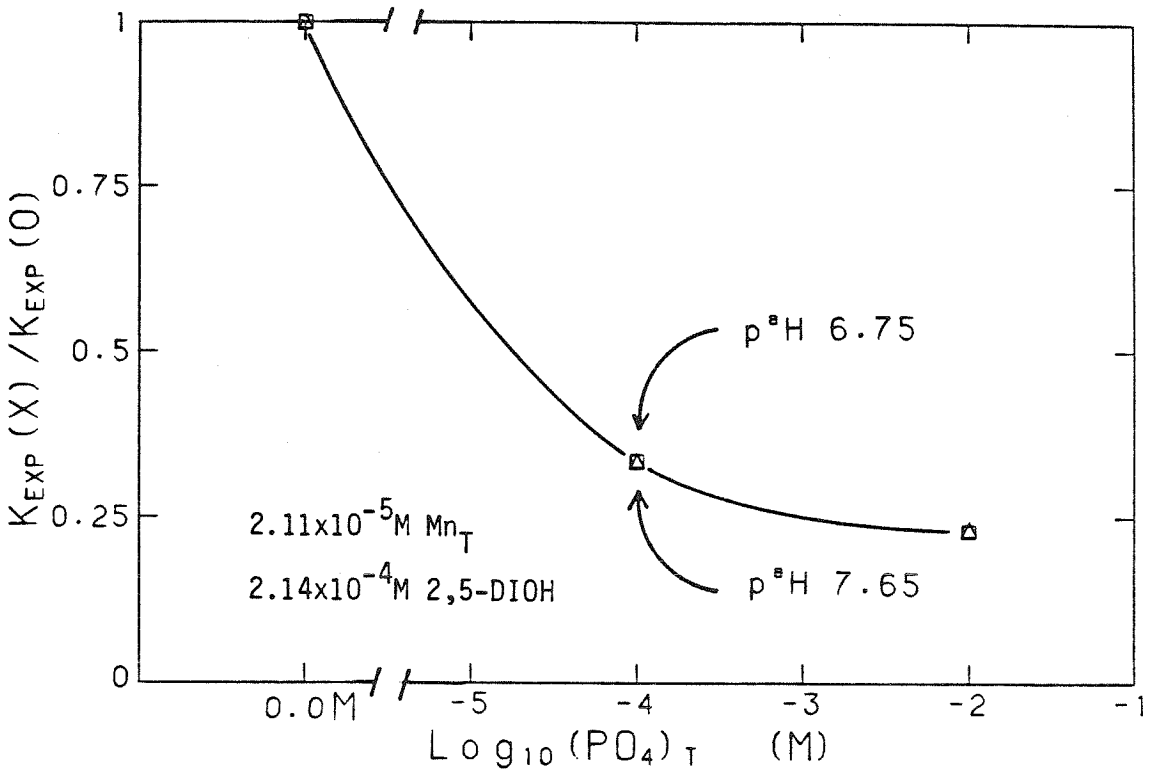

Figure 7.16 The effect of phosphate on the rate of dissolution by 2,5-dihydroxybenzoic acid.

even at a concentration of 10^{-2}M, lowered the rate by only 30%. Phosphate lowered the reaction rate with excess 2,5-diOH to the same degree as the reaction with hydroquinone (Figure 7.16). It is interesting to note, however, that no dependence on pH was observed, as seen with hydroquinone.

Figure 7.17 shows the effect of phosphate on the reaction rate when the hydroquinone concentration was close to Mn_T. A different suspension (N(9)) was used for this experiment, so the results cannot be directly compared with those described above. The amount of phosphate adsorbed in the absence of reductant was determined using the method described in Section 6.5. Second order rate constants (k_x) are calculated from the experimental data by taking into account the decrease in hydroquinone concentration during the reaction (see Section 8.2B). The amount of phosphate adsorbed per liter of suspension, as well as calculated rate constants, are listed in Table 7.7. Figure 7.18A plots the amount of phosphate adsorbed on the oxide after three hours of equilibration, under the same conditions. The amount of phosphate adsorbed was quite low throughout the range of phosphate concentrations tested, never exceeding 2.0×10^{-7}moles/liter. Saturation of the oxide surface with adsorbed phosphate did not occur; the amount of adsorbed phosphate continued to increase as the phosphate concentration was increased.

Figure 7.18B. shows the relation between the reaction rate and the amount of adsorbed phosphate. The amount of inhibition per mole of adsorbed phosphate was highest when surface coverage by phosphate was

Table 7.7: Effect of phosphate on the reaction of hydroquinone with manganese oxide suspension.

Conditions: 2.89×10^{-5}M Mn_T

2.00×10^{-5}M Hydroquinone

5.00×10^{-2}M $NaNO_3$

p^aH 6.80 (1% CO_2)

Trial	$[Phosphate]_T$ (moles/liter)	$\{Phosphate\}_{ads.}$ (moles/liter)	k_x (liters/mole sec.)	$\frac{k_x(X)}{k_x(0)}$
AH	0.00×10^{-0}	0.00×10^{-0}	4.39×10^{2}	-
AC	5.00×10^{-6}	2.29×10^{-8}	3.42×10^{2}	.779
AD	1.00×10^{-5}	3.15×10^{-8}	3.17×10^{2}	.722
AE	1.00×10^{-4}	8.17×10^{-8}	2.24×10^{2}	.510
AG	3.00×10^{-4}	1.23×10^{-7}	1.78×10^{2}	.405
AF	1.00×10^{-3}	1.73×10^{-7}	1.33×10^{2}	.303

Site Density	S_o	Source
4 to 10 sites/nm^2	1.0 to 2.6×10^{-6} moles/liter	Estimate based on Sigg and Stumm (1980)
8.5 sites/nm^2	2.2×10^{-6} moles/liter	Lower limit by acid/base titration

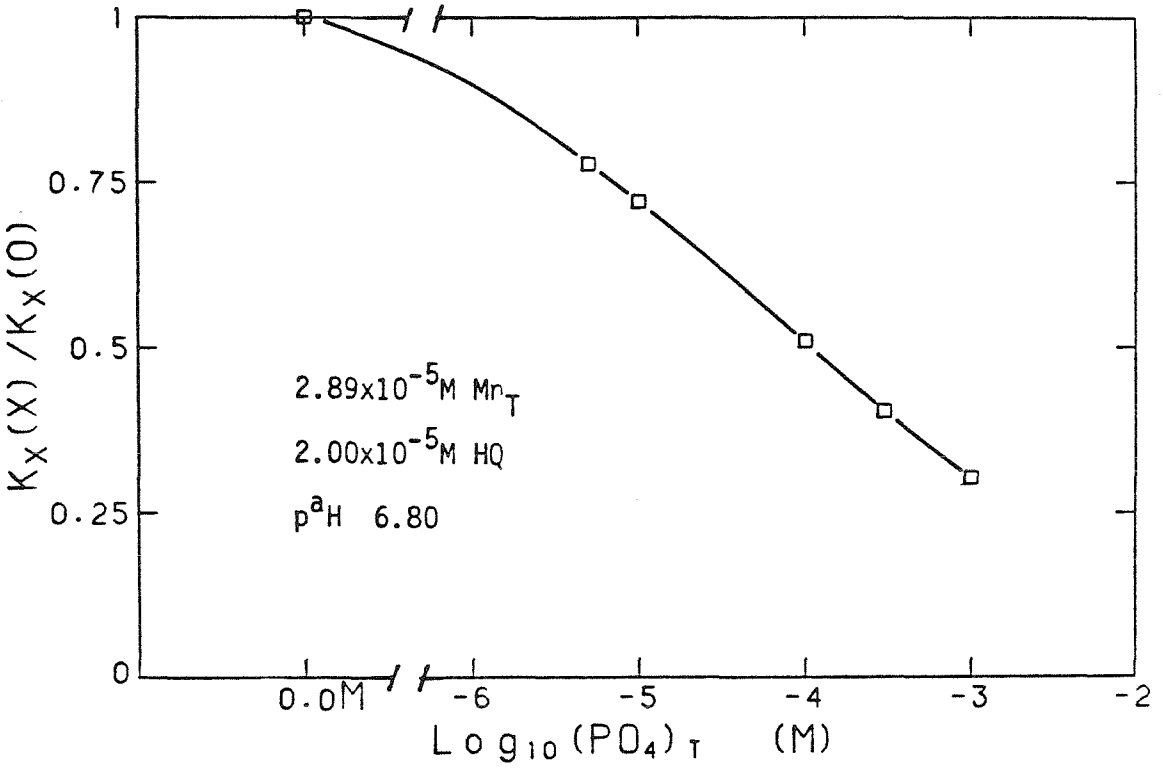

Figure 7.17 The effect of phosphate on the dissolution by hydroquinone (at low hydroquinone concentration). k_x is the second-order rate constant (see Section 8.2B.).

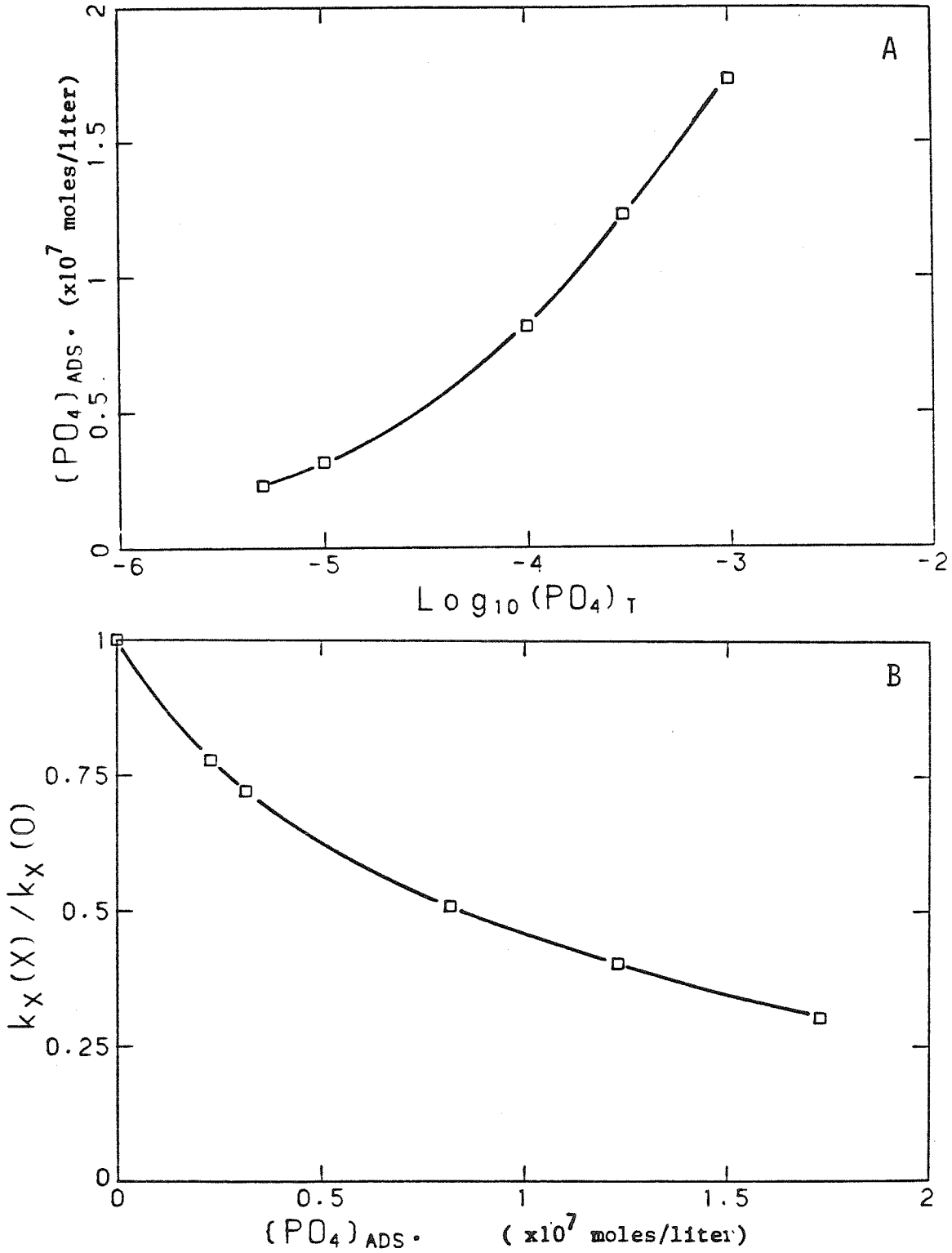

Figure 7.18 The amount of phosphate adsorbed on manganese oxide as a function of phosphate added (A) and the relationship between inhibition of the reaction and the amount of adsorbed phosphate (B).

low.

7.12 Conclusions

7.12A. Rate Law for Reaction with Hydroquinone

The results from previous sections in this chapter can be combined to give the following rate law:

$$7.14 \quad \frac{d[Mn^{2+}]}{dt}_{diss.} = k_1\{H^+\}^{0.46}[HQ]^{1.0}(Mn_T - [Mn^{2+}]_{diss.})^{1.0}$$

$$k_1 = 8\times10^3 \left(\frac{\text{liters}}{\text{mole}}\right)^{1.46}\left(\frac{1}{\text{sec.}}\right)$$

(Based on runs U,X,Y,Z, and QA)

where Mn_T is the oxide loading in moles/liter.

This rate law was determined in the following ranges of concentration:

$2\times10^{-4}M < [\text{Hydroquinone}] < 6\times10^{-4}M$

$6.5 < p^aH < 8.5$

$1.4\times10^{-5}M < Mn_T < 4.2\times10^{-5}M$

At higher concentrations of hydroquinone, the order with respect to hydroquinone becomes less than 1.0, as discussed in Section 7.7.

The rate law can also be expressed in terms of oxide surface area. Section 7.2B. described experiments performed using different oxide loadings. The initial rate of reaction increased in proportion to the increase in oxide loading, because of the corresponding increase in oxide surface area. The B.E.T. surface area of preparation N(8) (Section 5.6A.) can be used to estimate the surface area of suspension

N(7) at the start of the reaction. The rate law in terms of oxide surface area is written as:

$$7.15 \quad \frac{d[Mn^{2+}]}{dt}_{diss.} = k_A\{H^+\}^{0.46}[HQ]^{1.0}\, A(MnO_x)$$

$$k_A = 1x10^0\left(\frac{liters}{mole}\right)^{0.46}\left(\frac{liters_2}{meter}\right)\left(\frac{1}{sec.}\right)$$

(Based on runs U,X,Y,Z, and QA)

where A_{MnO_x} = Oxide surface area per liter, in units of (meters^2/liter).

k_A calculated in this manner is only approximate, since the B.E.T. surface area was determined with a different oxide preparation, and may not accurately reflect the area of the preparation used in the dissolution experiments.

Oxidation of hydroquinone by manganese oxide formed p-benzoquinone (Section 8.3B.). p-Benzoquinone dissolved manganese oxide via an autocatalytic reaction, but at a rate much slower than reaction with hydroquinone. In excess hydroquinone, the reaction with p-benzoquinone was negligible.

The reaction rate was found to be independent of $[Mn^{2+}]$ and oxygen partial pressure. The reaction rate did not increase when the stirring rate was increased, indicating that the reaction was not diffusion controlled. The apparent activation energy (+37 kJ/mole) supports this conclusion, since it is higher than expected for a transport-controlled reaction. The effect of ionic strength on the rate of dissolution by hydroquinone and 2,5-diOH was small, probably

because the oxide surface charge was small.

7.12B. Agreement with the Surface Site-Binding Model

The dependence of the reaction rate on hydroquinone concentration, manganese oxide loading, and pH provides clues concerning the mechanism of the reaction.

The data summarized in this chapter are sufficient to rule out reaction between Mn^{III} and organic substrate solely in the aqueous phase. Consider the following reactions in which $Mn^{3+}(aq)$ is released by the solid and reacts with hydroquinone in the overlying solution:

7.16 $MnOOH(s) + 3H^+ \rightleftharpoons Mn^{3+} + 2H_2O$

7.17 $Mn^{3+} + QH_2 \longrightarrow Mn^{2+} + {}^{\bullet}QH + H^+$.

The fastest rate at which reactions 7.16 and 7.17 can dissolve the oxide is controlled by the diffusion of Mn^{3+} away from the surface. The solubility of the oxide in the experiments should be similar to that of γ-MnOOH(s) (manganite). According to equations 3.5 and 3.8, the concentrations of Mn^{3+} and $MnOH^{2+}$ in equilibrium with γ-MnOOH(s) at pH 7.0 are 2×10^{-22}M and 2×10^{-15}M respectively. Thus, during dissolution, the concentration of $Mn^{III}(aq)$ at the surface is less than or equal to 2×10^{-15}M.

Using the diffusion equation 4.44 and the estimate of surface area

by B.E.T. (Section 5.6A.), the transport-controlled rate of dissolution can be calculated. The B.E.T. surface area of 58 m^2/gm gives 5.4×10^3 m^2 per mole of manganese. Setting Mn_T equal to 2×10^{-5}M, then there are 1×10^2 cm^2 of oxide per liter of suspension at the onset of dissolution. For a well-stirred solution the stagnant layer thickness δ can be taken to be about 0.001 cm. Using a value of 1×10^{-5} cm^2/sec for the diffusion coefficient, the initial rate of dissolution becomes:

$$7.18 \quad \frac{d[Mn^{2+}]}{dt} = \frac{(1 \times 10^3 \text{ cm}^2/\text{cm}^3)\ (1 \times 10^{-5} \text{cm}^2/\text{sec})\ (2 \times 10^{-15} \text{ moles/liter})}{(0.001 \text{ cm})}$$

$$= 2 \times 10^{-14} \text{ moles/liter/sec.}$$

Experimentally measured initial rates of dissolution were between 2×10^{-9} and 8×10^{-8} moles/liter/sec, much higher than possible by reactions 7.16 and 7.17. Dissolution must therefore involve reaction at the surface, which increases the solubility of manganese in the stagnant layer by reduction.

The order with respect to hydroquinone was found to 1.0, with the exception of the runs performed at the two highest hydroquinone concentrations, which gave an order below 1.0 (Section 7.5). The surface site-binding model developed in Section 4.3 predicts a first-order dependence on adsorbate concentration for two limiting cases. If the surface reaction is quite fast, then the adsorption step is rate-limiting, and the reaction is first order. If electron transfer within the surface complex is slow compared to adsorption and

the surface coverage is low, then the reaction is also first-order with respect to adsorbate. The apparent order becomes less than one when a significant fraction of surface sites are bound to adsorbate, as would happen at high adsorbate concentrations. The decrease in apparent order at high hydroquinone concentrations is consistent with electron transfer within the surface complex being rate limiting. This result, however, is not sufficient to rule out the possibility that the adsorption step is rate limiting. Results discussed in Chapter 8 are necessary to show that reaction within the surface complex is rate-limiting.

If the model developed in Section 4.3D. is correct, the order with respect to hydrogen ion concentration can be predicted from the pK_a's of the oxide surface and substrate. Formation of the surface complex can be written as:

$$7.19 \qquad \equiv MnOH + QH_2 \underset{k_{-1}}{\overset{k_1}{\rightleftharpoons}} \equiv MnQH + H_2O \qquad K_1^s$$

Assuming that electron-transfer, not adsorption, is the rate-limiting step, the concentration of surface complexes can be written as:

$$7.20 \qquad \{\equiv MnQH\} = K_1^s\{\equiv MnOH\}[QH_2]$$

The number of surface sites is highest when $[=MnOH][QH_2]$ is maximum. The pH_{zpc} of the oxide is 7.4, and therefore [=MnOH] is nearly constant within the pH range studied (the range is approximately one pH unit above and below the pH_{zpc}). The pK_{a1} of

hydroquinone is 10.01, so $[QH_2]$ is the predominant hydroquinone species, and its concentration is nearly constant within this pH range. If this adsorption model is correct, then the reaction rate should be nearly independent of pH in the range $6.5 < pH < 8.5$.

The experimentally determined order with respect to H^+ is low (0.46) but significant. The fractional order indicates that the adsorption model may be too simplistic. Surface complexes having stoichiometries different from the product of equation 7.19 may be important in the reaction, and may cause a different dependence on pH. Consider, for example, the following reactions:

7.21 $\equiv MnOH + QH_2 = \equiv MnQ^- + H_3O^+ \qquad K_2^s$

7.22 $\{\equiv MnQ^-\} = K_2^s\{\equiv MnOH\}[QH_2]/\{H^+\}$

7.23 $2\equiv MnOH + QH_2 = (\equiv Mn)_2Q + 2H_2O \qquad K_3^s$

7.24 $\{(\equiv Mn)_2Q\} = K_3^s\{\equiv MnOH\}^2[QH_2]$

Formation of a surface complex with the fully protonated adsorbate by equation 7.21 increases as the pH is increased, which was not observed experimentally. Formation of binuclear surface complexes by equation 7.23 is independent of pH, as was the case with formation of =MnQH.

If release of Mn(II) from the crystal lattice is slow, then the pH dependence may be caused by protons assisting in the release. Protonation of surface sites may weaken bonds between Mn(II) and lattice atoms, thereby lowering the activation energy of the

dissolution step.

$$7.25 \quad \equiv Mn^{II}OH^- + H^+ \underset{k_{-1}}{\overset{k_1}{\rightleftharpoons}} \equiv Mn^{II}OH_2$$

$$7.26 \quad \equiv Mn^{II}OH^- \longrightarrow MnOH^+(aq). \qquad \text{slow}$$

$$7.27 \quad \equiv Mn^{II}OH_2 \longrightarrow Mn(H_2O)^{2+}(aq.) \qquad \text{fast}$$

If this scheme is correct, then the rate of dissolution should increase as the pH is decreased. This is the trend observed experimentally.

The reaction rate is proportional to the amount of remaining oxide, (Mn_T - $[Mn^{2+}]$diss.) during the first half of the reaction. In Section 4.3C., it was found that such a relation arises when the ratio of oxide surface to volume remains constant during dissolution. In this case, S_T, the number of surface sites per liter available for reaction at time t, is related to the amount of undissolved oxide by the following equation:

$$7.28 \quad S_T = f(Mn_T - [Mn^{2+}]_{diss.}).$$

The constant f can be found by estimating S_o, the number of surface sites per liter at t=0. S_o can be estimated using acidimetric titrations of oxide surfaces described in Section 5.6B., or from values of the number of sites per unit area of oxide surface reported by other workers.

Sigg and Stumm (1980) stated that most oxides have between 4 and

10 surface hydroxyl groups per mm^2. The specific surface area of preparation N(8) was found to be 58 $meter^2/gm.$ in Section 5.6A., which gives between $3.5x10^{-2}$ and $9.0x10^{-2}$ moles of hydroxyl surface sites per mole of Mn_T. In the titration of suspension N(9), the largest calculated negative surface charge was $5.3x10^{-5}$ equivalents/liter for a solution containing $7.00x10^{-4}$ moles/liter Mn_T. There are, therefore, at least $8x10^{-2}$ moles of surface hydroxyl groups per mole of Mn_T.

According to either estimate, surface =MnOH sites make up less than 10% of Mn_T at the start of the reaction. The constant (f) in equation 7.28 thus has a value somewhere below 0.10.

7.12C. Inhibition by Calcium and Phosphate

Both calcium and phosphate inhibit reaction between manganese oxide and hydroquinone, but the effect of phosphate is more dramatic. The amount of phosphate adsorbed at given concentrations of phosphate was measured, and included in Table 7.7. Estimates of S_o from Section 7.12B. are also included for these reactions.

S_o was approximately $2x10^{-6}$ moles/liter for the reactions summarized in Table 7.7. In $1.00x10^{-3}$M phosphate, $1.7x10^{-7}$ moles/liter of phosphate were adsorbed on the oxide surface, less than 10% of S_o. This concentration of phosphate, however, lowered the reaction rate by 60%. According to Section 7.12B., the fraction of sites covered by hydroquinone was probably small, because of the observed first-order dependence on hydroquinone concentration. The maximum surface loading of phosphate or hydroquinone is not known. It

is probable that the maximum surface loading is less than S_o, because of the size of adsorbate molecules compared to protons, and because of more restrictive bonding requirements. Thus, although the moles of phosphate adsorbed are small compared to S_o, a large fraction of hydroquinone binding sites may have been blocked. Additional information about surface coverage by hydroquinone and phosphate molecules is necessary to determine whether or not phosphate inhibits the reaction in proportion to the fraction of hydroquinone adsorption sites it occupies.

Oxide surface sites that can bind hydroquinone may also differ in reactivity. If phosphate selectively adsorbs onto the sites that are most reactive with hydroquinone, then the amount of inhibition is greater than the fraction of surface sites bound to phosphate.

The observed inhibition may be caused by phosphate occupying a large area of the oxide surface per molecule, or by phosphate occupying surface sites that are most reactive with hydroquinone. Section 7.11B. noted that inhibition per mole of phosphate adsorbed decreased as the amount of phosphate adsorbed on the surface increased. Phosphate blocks the sites it is bound to, and may also interfere with adsorption at neighboring sites. Phosphate molecules adsorbed close to one another have some neighboring sites in common, lowering the amount of interference per molecule. This would be expected to happen when the surface coverage by phosphate is high. The amount of phosphate on the surface in these experiments was probably small, so it is unlikely that phosphate groups were bound so closely to one another. It is more

likely that inhibition was greatest for small amounts of adsorbed phosphate because surface sites most reactive with hydroquinone were preferentially occupied by phosphate.

CHAPTER 8

SURVEY OF ORGANIC SUBSTRATES

8.1 Introduction

The dissolution of manganese oxide suspensions by twenty-seven organic substrates was studied to determine the relative reactivity of different functional groups found in natural organics. UV and visible spectra of filtered reaction solution were recorded for a number of organics to provide information about the structures of oxidized products. For some substrates the rate of substrate consumption can be calculated from absorbance measurements and compared to the rate of oxide dissolution. Dissolution of the manganese oxide suspension by marine fulvic acid was studied to determine the reactivity of an important natural organic material. Reactions were also performed to determine whether or not organics inert to oxidation by manganese oxide interfere with the dissolution reaction.

8.1A. Selection of Organics

Organic substrates were chosen that resemble structural groups found in natural organics and that allow the reactivity of different functional groups to be distinguished. Figure 8.1 presents the aromatic substrates used in the dissolution experiments. Catechol, hydroquinone, resorcinol, and their substituted analogs were studied to determine the relative reactivities of ortho-, para-, and meta-dihydroxybenzenes and the effect that other substituents have on reactivity. Methoxy aromatic groups have been identified in natural

Figure 8.1 Aromatic substrates used in the dissolution experiments.

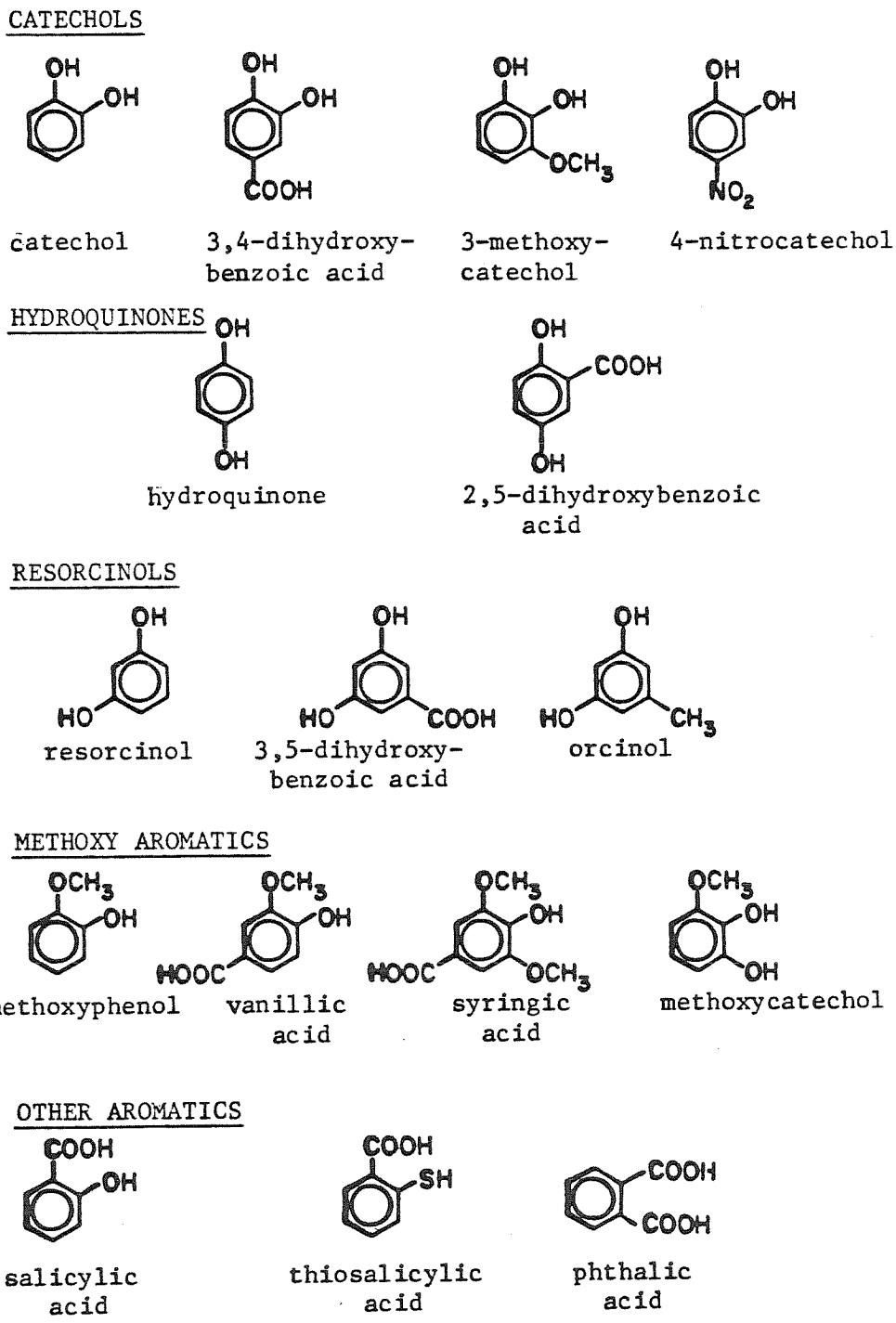

Figure 8.2 Aliphatic substrates used in the dissolution experiments.

Compound	Chemical Group	Structure
1-Propanol	Saturated Alcohol	$CH_3CH_2CH_2OH$
Propionaldehyde	Enolizable Aldehyde	CH_3CH_2CHO
Propionic Acid	Carboxylic Acid	CH_3CH_2COOH
Lactic Acid	α-Hydroxy Acid	$CH_3CH(OH)COOH$
Pyruvic Acid	α-Keto Acid	$CH_3COCOOH$
Glycerol	Poly Alcohol	$HOCH_2CH(OH)CH_2OH$
Sorbitol	" "	$HOCH_2CH(OH)CH(OH)CH(OH)CH(OH)CH_2OH$
Oxalic Acid	Dicarboxylic Acid	HOOC-COOH
Malonic Acid	" "	$HOOCCH_2COOH$
Fumaric Acid	Olefin	HOOCCH=CHCOOH
Formic Acid	Non-enolizable Aldehyde	HCOOH
Ascorbic Acid	Lactone with enediol structure	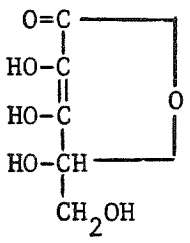

organics (Chapter 1) and were therefore included. Reactions with salicylic and thiosalicylic acids were also examined, to identify the differences in reactivity between hydroxy- and thio- substituted aromatics. Phthalic acid was included because it has been shown to adsorb onto oxide surfaces (Kummert and Stumm, 1980).

Figure 8.2 presents the aliphatic substrates included in this study. This set was chosen to represent a variety of oxygen-containing functional groups found in natural organics that may have reducing power. Many of these compounds have themselves been identified in natural waters and sediments.

8.1B. Chemical Properties of Organics

Acidity constants of the organic substrates are listed in Table 8.1. Most of the experiments described in this section were performed at a pH of 7.2. With the exception of 4-nitrocatechol, the aromatic hydroxy groups of all the phenolic compounds studied are fully protonated at this pH. One hydroxy group of 4-nitrocatechol is protonated and the other deprotonated at pH 7.2.

Table 8.2 lists redox equilibria of several organic substrates and Mn(III)/Mn(II), and their standard potentials (E^o). $E^{o'}$, the potential at pH 7.0, is also calculated for each reaction. Additional values of E^o for dihydroxybenzenes are listed in Table 2.2. $E^{o'}$ of manganite is greater than that of the organic substrates listed in the tables; redox reaction between the oxide and substrate is therefore thermodynamically favorable in each case.

Reaction with manganese oxide may form oxidized products similar

Table 8.1 Protonation Equilibria of the Organic Substrates

Compound	pKa(1)	pKa(2)	pKa(3)	pKa(4)	Source	Ionic Strength, Temp.
Ascorbic Acid	4.37	11.34			2	3.0M, 25°C
Catechol	9.34	12.6			2	0.1, 25
2,5-Dihydroxybenzoic Acid	2.97	10.21	13.90		2	0.1, 31
3,4-Dihydroxybenzoic Acid	4.26	8.64	13.13		2	0.25,25
3,5-Dihydroxybenzoic Acid	3.84	9.00	10.54		2	0.20,25
EDTA	1.994	2.674	6.17	10.26	3	0.1,20
Formic Acid	3.53				2	1.0,20
Fumaric Acid	3.02	4.45			4	0.04,18
Glycerol	14.9				1	
Hydroquinone	10.01	11.66			1	0.1,13
Lactic Acid	3.57				2	0.2,25
Malonic Acid	2.62	5.30			2	0.1,25
3-Methoxycatechol	9.20	11.99			5	0.1,25
2-Methoxyphenol	9.90				1	0.1,25
4-Nitrocatechol	6.70	10.85			2	0.1,25
Orcinol	9.36	11.66			1	0.1,20
Oxalic Acid	1.26	3.82			2	0.1,25
Phthalic Acid	2.76	4.92			2	0.1,22
Propanoic Acid	4.52				2	0.3,25
Pyruvic Acid	2.35				2	0.5,25

Compound	pKa(1)	pKa(2)	pKa(3)	pKa(4)	Source	Ionic Strength, Temp.
Resorcinol	9.30	11.06			1	0.1,20 to 25
Salicylic Acid	2.80	13.6			2	0.1,25
Sorbitol	13.00				1	?,60
Syringic Acid	4.34	9.49			1	?,25
Thiosalicylic Acid	3.6	8.2			2	0.1,25
Vanillic Acid	4.51	9.39			1	?,25

Sources

(1) Serjeant and Dempsey (1979)

(2) Perrin (1979)

(3) Anderegg (1977)

(4) Kortum et al. (1961)

(5) Martell and Smith (1977)

Table 8.2 Oxidation Potentials

Reactions	E^o (pH 0.0)	$E^{o'}$ (pH 7.0)	Reference
$2CO_2(g) + 2H^+ + 2e^- = H_2C_2O_4(aq)$ (Oxalic Acid)	-0.49v	-0.904v	1
$CO_2(g) + 2H^+ + 2e^- = HCOOH(aq)$ (Formic Acid)	-0.196	-0.610	1
$CH_3COCOOH + 2H^+ + 2e^- = CH_3CHOHCOOH$ (Pyruvic Acid) (Lactic Acid)	+0.20	-0.21	1
Dehydroxy-Ascorbate $+ 2H^+ + 2e^-$ = Ascorbate	+0.40	+0.063	2
Quinone $+ 2H^+ + 2e^-$ = Hydroquinone	+0.699	+0.285	3
$MnOOH(s) + 3H^+ + e^- = Mn^{2+} + 2H_2O$	+0.751	+0.613	4

Sources

(1) Latimer (1952)

(2) Clark (1960)

(3) Musso and Dopp (1967)

(4) Bricker (1965)

to those formed by reaction with other metal complexes. Catechols and hydroquinones can be oxidized by two one-equivalent steps to form the corresponding quinones, as discussed in Section 2.3. Resorcinols cannot form quinones, but will instead form a variety of oxidized products by radical reactions. Figure 2.5 shows that oxidation of orcinol by $Fe(CN)_6^{3-}$, for example, results in dimer and polymer formation.

Ortho- and para-methoxyphenols can also be oxidized to quinones. Oxidation of o-methoxyphenol by the two-equivalent oxidant Tl^{III} in acidic perchlorate medium forms methanol and o-benzoquinone (Mentasti et al.,1975):

8.1 Tl^{III} + o-methoxyphenol + H_2O =

Tl^{I} + o-benzoquinone + CH_3OH + $2H^+$.

Vanillic and syringic acids may also form o-benzoquinones by similar reactions.

Oxidation of thiosalicylate by $Fe(CN)_6^{3-}$ forms a dimer linked by a disulfide bond (Panpalia et al.,1974):

8.2 $$2R\text{-}SH + 2Fe(CN)_6^{3-} \longrightarrow R\text{-}SS\text{-}R + 2Fe(CN)_6^{4-} + 2H^+$$

Thiosalicylate in this reaction is a one-equivalent reductant.

Salicylate is oxidized by one equivalent to form a phenoxy radical. Since there are no additional hydroxy or methoxy substituents on the aromatic ring, the stability of the radical generated is low,

and for this reason oxidation is not as favorable as for the substrates discussed above. Phthalate is not expected to react at all.

Oxidations of aliphatic substrates listed in Figure 8.2 may proceed in different ways, depending on the oxidant employed. Mechanisms postulated for oxidation of aliphatics by Mn^{III} sulfate and pyrophosphate are reviewed in Section 3.5. Ascorbate is readily oxidized to dehydroxyascorbate, by the reversible reaction shown in Table 8.2.

8.1C. Experimental Methods

Dissolution experiments discussed in this chapter followed the procedures outlined in Chapter 6. The following two sets of experimental conditions were employed:

	Set 1	Set 2
Reductant Concentration	1.77×10^{-5} M	1.00×10^{-3} M
Mn_T	3.54×10^{-5} M	2.83×10^{-5} M
p^aH	7.2	7.2
Ionic Medium	5.0×10^{-2} M ($NaNO_3$ or $NaClO_4$)	5.0×10^{-2} M ($NaNO_3$)
		(10^{-3} M $NaHCO_3$, 1% CO_2)

For a two-equivalent reductant, the conditions of Set I are approximately stoichiometric. Set I conditions (using $NaClO_4$) were used when the spectral change accompanying substrate oxidation was monitored, since absorbance by unreacted substrate interferes with the measurement when it is in great excess (as in Set II conditions).

Sodium perchlorate was substituted for sodium nitrate when spectra were recorded because sodium nitrate absorbs in the UV. Reactions were monitored for three hours following substrate addition. Set II conditions were employed when the reactivity of the substrate was low. Increased substrate concentration accelerates the dissolution rate, so that measurable change in $[Mn^{2+}]_{diss.}$ could be observed after three hours of reaction time.

8.2 Measurement of $[Mn^{2+}]diss.$

8.2A. Experimental Results

Table 8.3 summarizes reactions performed with the different substrates. In experiments marked NR (no reaction) the amount of manganese dissolved by reaction with substrate after 3 hours could not be distinguished from background levels. In blank reactions, experimentally determined $[Mn^{2+}]_{diss.}$ is less than 3% of Mn_T. Dissolution was not observed under Set II conditions when formate, fumarate, glycerol, lactate, malonate, phthalate, propanol, propionaldehyde, propionate, or sorbitol were used as substrate. The amount of dissolution under the same conditions was quite small when pyruvate, oxalate, and salicylate were used, barely rising above $[Mn^{2+}]$ measured in blank solutions. A reaction was performed in which the pyruvate concentration was increased to 10^{-2}M to verify that pyruvate was indeed dissolving the oxide. The amount of oxide dissolved after 3 hours was greater in the solution containing the higher pyruvate concentration, even though less than 10% of the oxide was dissolved. This verifies that pyruvate is dissolving manganese

Table 8.3 Survey Experiment: Reduction of Suspension N(9) by Selected Organics

Trial	pH	Mn_T (M)	Age (Days)	Reductant		Results
GA	7.19	2.82E-5	29	1.00E-3	Propanol	NR
GB	7.19	"	29	"	Propionaldehyde	NR
GC	7.19	"	29	"	Propionic Acid	NR
GD	7.20	"	30	"	Glycerol	NR
GE	*7.37	"	30	"	Lactate	NR
GF	7.19	"	30	"	Pyruvate	5.6% Dissolved
GG	7.19	"	31	"	Malonate	NR
GH	7.68	3.43E-5	33	1.72E-5	Hydroquinone	Rxn.
GI	7.73	"	33	"	Catechol	Rxn.
GJ	7.70	"	33	"	Resorcinol	NR
GK	7.16	3.54E-5	36	1.77E-5	3,5-diOH	NR
GL	7.17	"	36	"	2,5-diOH	Rxn.
GM	7.17	"	36	"	3,4-diOH	Rxn.
GN	7.24	"	38	"	Orcinol	NR
GO	7.25	"	38	"	Hydroquinone	Rxn.
GP	7.26	"	38	"	Catechol	Rxn.
GQ	7.20	"	40	"	Syringic Acid	Rxn.
GR	7.19	"	40	"	o-Methoxyphenol	<5% Dissolved
GS	7.22	"	40	1.76E-5	3-methoxycat.	Rxn.
GT	7.13	2.83E-5	45	1.00E-3	Salicylate	3% Dissolved
GU	7.11	"	45	"	Vanillate	Rxn.
GV	6.5-7.6	"	45	"	Fumarate	NR
GW	7.15	"	47	"	Orcinol	Rxn.
GX	7.14	"	47	"	3,5-diOH	Rxn.
GY	7.15	"	47	"	Resorcinol	Rxn.
GZ	7.29	3.54E-5	50	1.77E-5	4-Nitrocatechol	Rxn.
XA	7.30	"	50	"	Ascorbate	Rxn.
XB	7.28	"	50	"	Thiosalicylate	Rxn.
XC	7.17	2.63E-5	52	1.00E-3	o-Methoxyphenol	Rxn.
XD	7.17	"	52	"	Oxalate	3.5% Dissolved
XE	7.26	3.29E-5	52	1.69E-5	Formate	NR
XF	7.20	2.64E-5	68	9.90E-4	Formate	NR
XG	7.21	"	68	1.00E-2	Pyruvate	Rxn.
XH	*6.85	"	68	2.63E-4	2,5-diOH	Rxn.
XI	7.65-7.74	2.85E-5	110	199 mg/l	Fulvic Acid	<2.5% Dissolved
AB	6.90-7.11	2.81E-5	132	2.00E-3	EDTA	Rxn.
AI	6.35	2.89E-5	145	201 mg/l	Fulvic Acid	Rxn.
AJ	6.50	2.89E-5	145	Blank		6.8% Dissolved

NR: No reaction (no measurable dissolution).

Rxn.: $[Mn^{2+}]_{diss.}$ at end of experiment is greater than 10% of Mnt.

* An approximate value.

oxide, but at a very slow rate. Figure 8.3 shows the results of dissolution experiments using pyruvate and oxalate.

The results from experiments with phenolic substrates and with ascorbate are shown in Figures 8.4 through 8.6. The most reactive substrates reduced a significant amount of oxide under Set I (low substrate concentration) conditions. The greatest dissolution rates were measured with catechols and ascorbate. Figure 8.4A. shows that rates of dissolution by 3-methoxycatechol, 3,4-dihydroxybenzoate (3,4-diOH), and catechol were approximately the same. The rate of dissolution by 4-nitrocatechol, substituted with a strong electron-withdrawing group, was one-fourth that of other catechols. Hydroquinone and 2,5-dihydroxybenzoate (2,5-diOH), both para-dihydroxybenzenes, dissolved the oxide under Set I conditions, although more slowly than catechols. Figure 8.4B. shows that dissolution by hydroquinone was slightly faster than by 2,5-diOH. Given sufficient time ortho- and para- dihydroxybenzenes dissolved most of the manganese oxide suspension. Each mole of substrate reduced two or more equivalents of manganese oxide.

Dissolution by ascorbate and thiosalicylate under Set I conditions is shown in Figure 8.5A. As mentioned earlier, ascorbate dissolved the oxide as quickly as any of the substrates tested. Thiosalicylate initially reacted at an appreciable rate, but only dissolved 1.2×10^{-5}M manganese. This amount of manganese oxide was dissolved in about an hour. The equivalents of oxidant consumed per mole of thiosalicylate can be calculated:

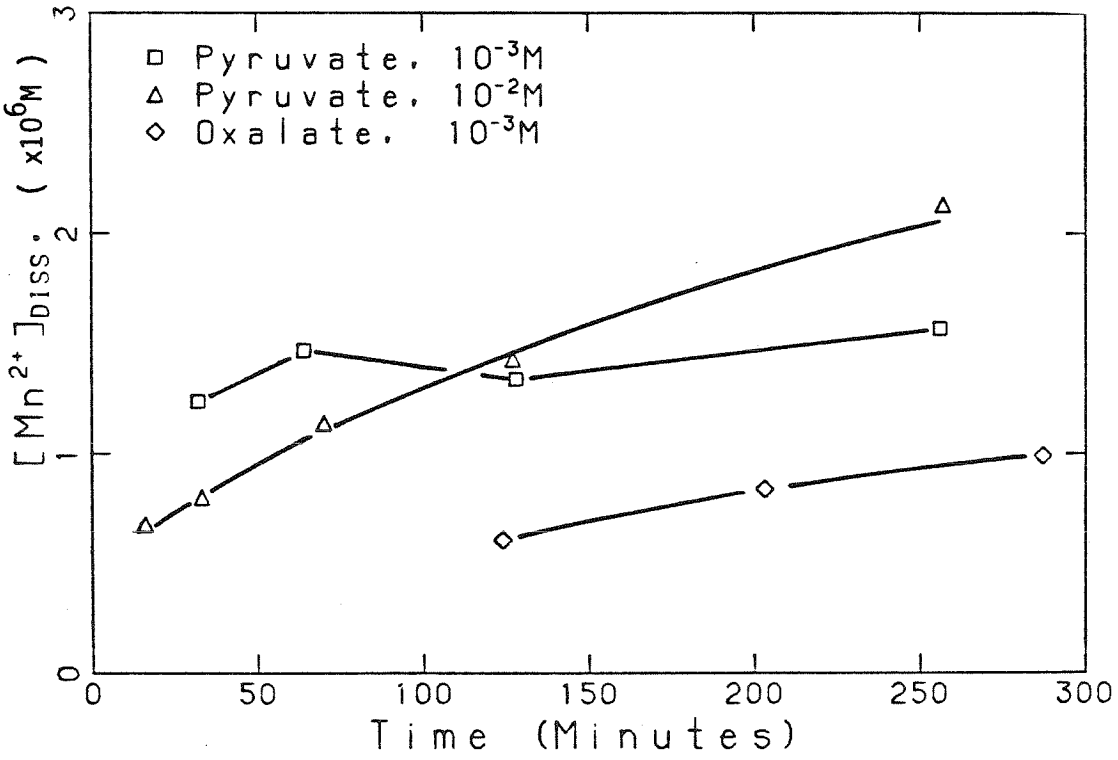

Figure 8.3 Dissolution of manganese oxide suspensions by pyruvate and oxalate (Runs GF,XD, and XG).

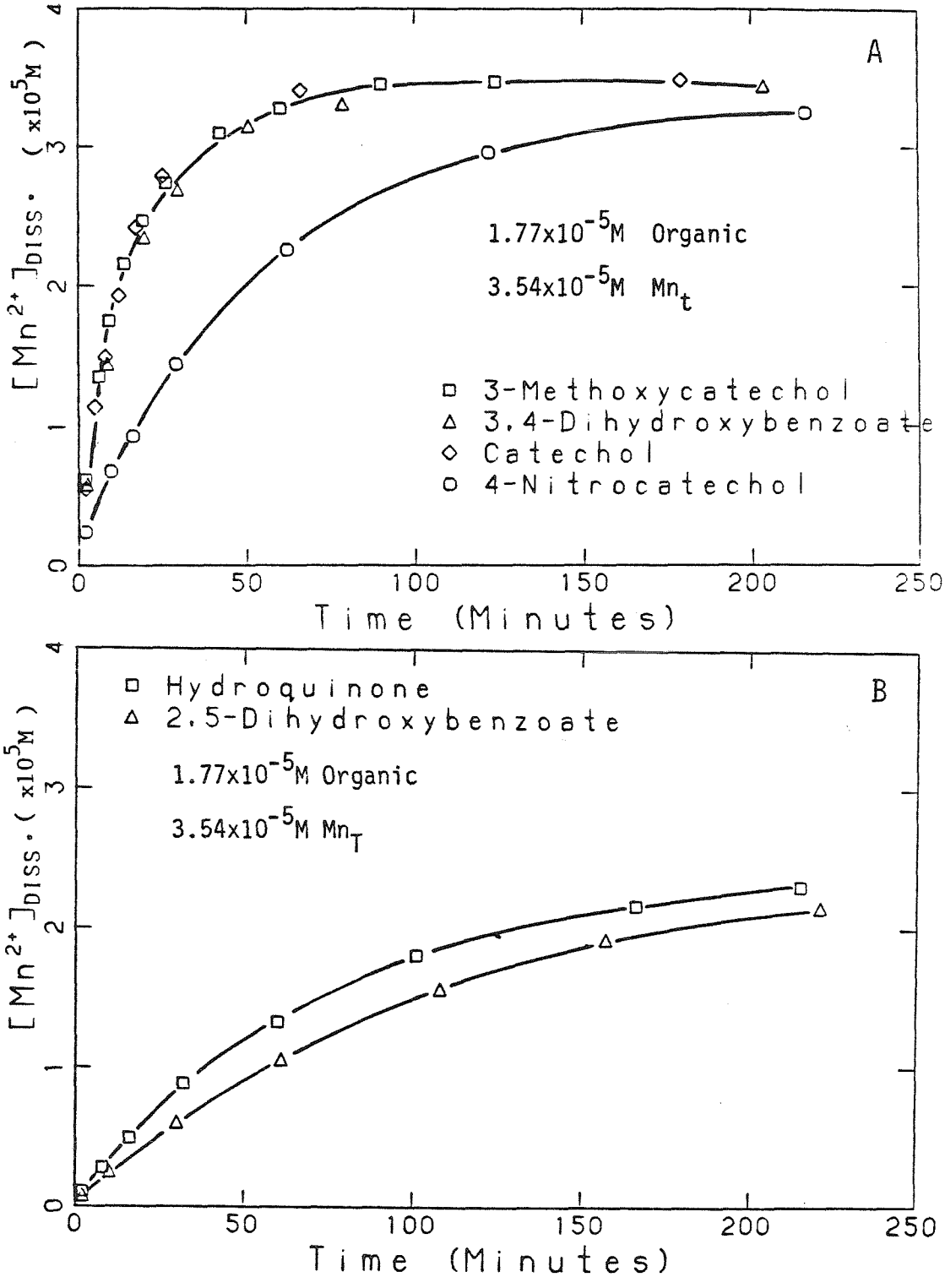

Figure 8.4 Catechols and Hydroquinones: Dissolution of manganese oxide suspensions by 3-methoxycatechol, 3,4-dihydroxybenzoic acid, catechol, and 4-nitrocatechol (A), and by hydroquinone and 2,5-dihydroxybenzoic acid (B). (Runs GL,GM,GO,GP,GS, and GZ).

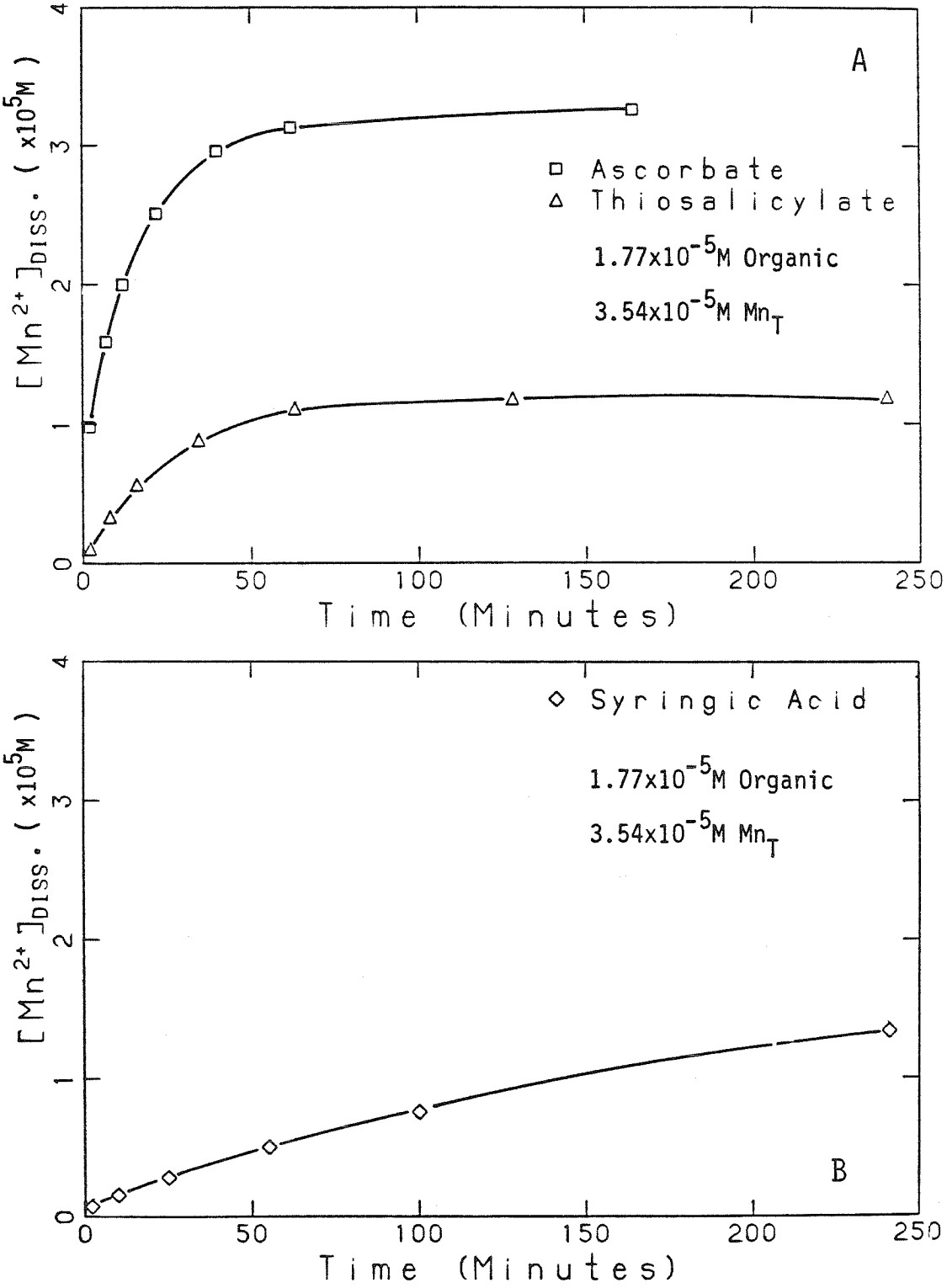

Figure 8.5 Dissolution by ascorbate and thiosalicylate (A), and by syringic acid (B). (Runs GQ,XA, and XB).

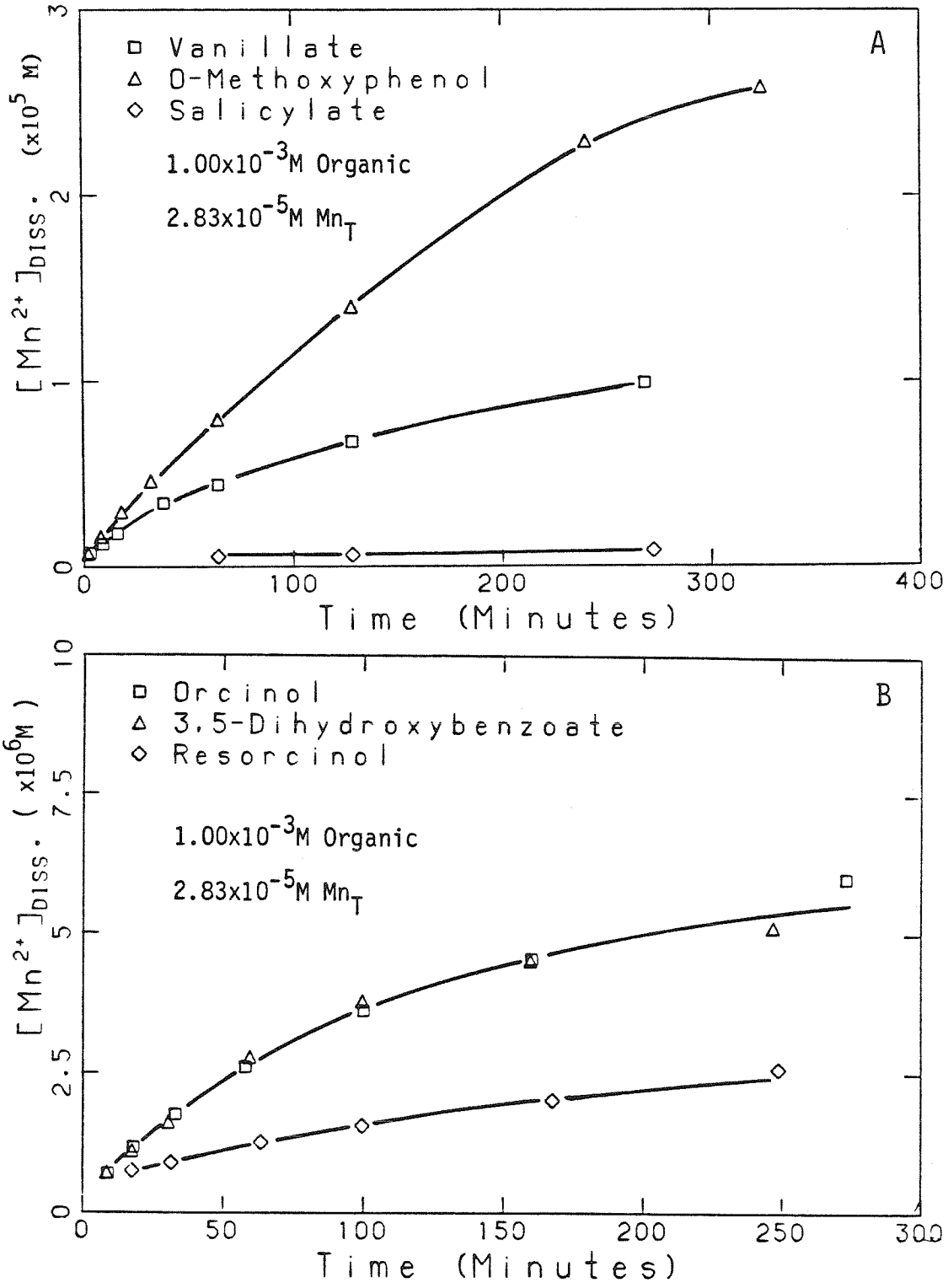

Figure 8.6 Methoxyphenols and resorcinols: Dissolution of manganese oxide suspensions by vanillate, o-methoxyphenol, and salicylate (A), and by orcinol, 3,5-dihydroxybenzoic acid, and resorcinol (B). (Runs GT,GU,GW,GX,GY, and XC).

$$8.3 \quad \frac{\left(\frac{1.2\times10^{-5}\text{ moles Mn}}{\text{liter}}\right)\left(\frac{1.3\text{ Equiv.'s Oxidant}}{\text{mole Mn}}\right)}{\left(\frac{1.77\times10^{-5}\text{ moles Thiosal.}}{\text{liter}}\right)} = 0.87\ \frac{\text{Equivalents}}{\text{mole of Thiosal.}}$$

A little less than one equivalent of oxidant was therefore reduced per mole of thiosalicylate.

Syringic acid, a dimethoxyphenol, reacted slowly under Set I conditions (Figure 8.5B.). The reactivity of other mono-phenols (o-methoxyphenol, vanillate, and salicylate) was still lower, with very little dissolution occurring under Set I conditions. When the concentration of substrate was increased 50-fold, dissolution by o-methoxyphenol and vanillate was appreciable (Figure 8.6A.). The reactivity of o-methoxyphenol was lower than syringic acid, but greater than vanillate, which has a carboxyl group para to the hydroxy substituent. After three hours of reaction, $[Mn^{2+}]_{diss.}$ measured in the solution containing salicylate was scarcely greater than the amount measured in blank solutions. The reactivity of phenols is therefore greatly enhanced by each methoxy substituent added to the ring.

Resorcinol, 3,5-dihydroxybenzoate (3,5-diOH), and orcinol all reacted more slowly than methoxy-substituted phenols, but still at a measurable rate (Figure 8.6B.). Under Set II conditions (high substrate concentration) less than 20% of the oxide was dissolved by these substrates within the first three hours. The methyl and carboxyl substituted derivatives reacted at the same rate, which was more than

twice the rate of reaction with resorcinol.

8.2B. Order of Reactivity

In order to compare the reactivities of the substrates, rate constants independent of substrate concentration and suspension loading must be calculated. Two assumptions are required to calculate such rate constants. The first assumption is that the reaction is first order with respect to reductant and remaining oxide concentration for all substrates, as was observed in the reaction with hydroquinone (Section 7.12A). The rate law for each substrate at constant pH can therefore be written as:

$$8.4 \qquad \frac{d[Mn^{2+}]}{dt}_{diss.} = k_x[Red.]^{1.0}(Mn_T - [Mn^{2+}]_{diss.})$$

Under the conditions of Set II, $[Red.] \sim [Red.]_{t=0}$ and integration of equation 8.2 gives:

$$8.5 \qquad \ln\left(\frac{Mn_T - [Mn^{2+}]_{diss.}}{Mn_T}\right) = k_x t[Red.]$$

For reactions under Set II conditions, the slope of $\ln(Mn_T - [Mn^{2+}])$ against t is calculated and divided by the reductant concentration to give k_x.

For reactions performed under Set I conditions, a second assumption must be made concerning the stoichiometry of the reaction, since both reductant and oxide are being depleted. Assuming that all substrates are two-equivalent reductants, then:

8.6 $[\text{Red.}]_t = [\text{Red.}]_{t=0} - 1/2[Mn^{2+}]_{diss.}$.

Since $[\text{Red.}]_{t=0} = 1/2Mn_T$, equation 8.4 becomes:

8.7 $$\frac{d[Mn^{2+}]_{diss.}}{dt} = \frac{k_x}{2}(Mn_T - [Mn^{2+}]_{diss.})^2$$

and integration yields:

8.8 $$\frac{1}{(Mn_T - [Mn^{2+}]_{diss.})} - \frac{1}{Mn_T} = \frac{k_x}{2}t$$

In this case, the slope of $1/(Mn_T - [Mn^{2+}]_{diss.})$ against t is equal to $k_x/2$.

Values of k_x calculated for each substrate are listed in order of reactivity in Table 8.4. Each value of k_x was calculated from points collected before half the oxide had been consumed. The assumption that the substrate is a two-equivalent reductant is clearly incorrect for the reaction with thiosalicylate and possibly incorrect for some of the other substrates, but k_x is calculated the same way for the sake of comparison. Using Table 8.4, the following generalities can be made concerning the reactivity of substrates:

i. For dihydroxybenzenes, the order of reactivity is:

Catechols > Hydroquinones >> Resorcinols.

ii. For methoxy-substituted phenols, the order of reactivity is:

Table 8.4 Apparent Second-Order Rate Constants for Dissolution of Manganese Oxide Suspensions.

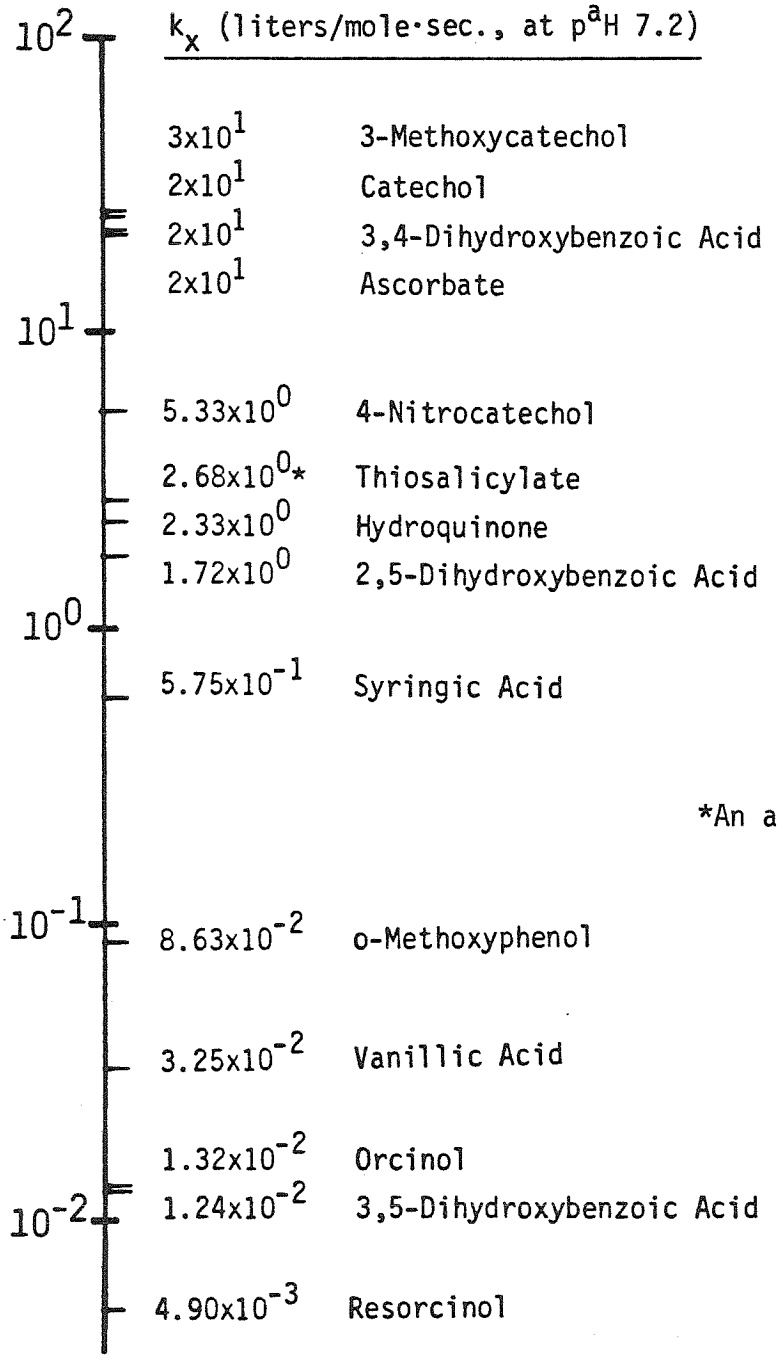

Oxalate, Pyruvate, Salicylate

Formate, Fumarate, Glycerol, Lactate, Malonate

Phthalate, Propanol, Propionaldehyde, Propionic Acid, Sorbitol

Dimethoxyphenols >> Monomethoxyphenols >> Phenols.

iii. Strong electron-withdrawing substituents (such as $-NO_2$) lower substrate reactivity.

iv. Substitution by a carboxyl group can either promote or inhibit reaction, depending on the other ring substituents.

8.3 Spectral Analysis

8.3A. Introduction

Electronic transitions responsible for ultraviolet (UV) and visible absorption bands are of the same order of magnitude as the energies of chemical bonds (Brown, 1980). UV and visible spectra are therefore useful in monitoring chemical transitions in molecules. In practice, only near-UV and visible spectra (200 to 800 nanometers) are accessible for routine study. Organic molecules that absorb appreciably in this spectral region contain delocalized electrons; fully saturated molecules do not have strong near-UV or visible absorption bands.

The purpose of measuring spectra during oxidation is to monitor the consumption of substrate by the oxide and to help identify the oxidized products. If the substrate is in great excess, the change in absorbance accompanying the reaction is quite small compared to the total absorbance, and the consumption of substrate is difficult to calculate. Excess substrate swamps the spectrum of oxidized product, making identification more difficult.

Spectra were recorded in runs performed under Set I conditions

(see Section 8.1C.). For two-equivalent substrates, stoichiometric amounts of reductant and oxidant were present in solution, and complete oxidation of substrate was possible. Reactions were followed for only three hours, which was not enough time for much oxidation of low reactivity substrates to occur. Little spectral change was observed in these cases. Spectra were recorded during oxidation of substrates listed in Table 8.5. Absorption bands of unoxidized substrates were measured in 1.4×10^{-2}M phosphate buffer(pH 7.2) and are also listed in the table.

Light scattering from particles lowers the intensity of light transmitted through the sample, causing an increase in absorbance. The amount of absorbance caused by light scattering depends on the wavelength of measurement, the refractive index of the solution, and the number density and size of particles (Hiemenz, 1977). Rayleigh Theory is used to model light scattering of particles that have dimensions 1/20th or less of the wavelength of incident light. Larger particles are in the region covered by Debye or Mie Theory. Light scattering increases as the wavelength of light decreases by the factor $1/\lambda^4$ (Hiemenz, 1977). The absorbance spectrum of solutions containing small particles therefore slope progressively upward at decreasing wavelengths.

The absorbance spectrum of the manganese oxide suspension is caused by a combination of absorption and light scattering. Suspension particles are between 0.2 and 1.0 microns in diameter, comparable to the wavelengths of UV and visible light. Figure 8.7 shows the

Table 8.5 Absorbance Spectra of Substrates

(in 1.40×10^{-2}M phosphate buffer, pH 7.2)

Substrate	$\lambda_{max.}$(nm.), ε (liters/mole·cm.)	
Hydroquinone	288(2.56×10^3)	
2,5-Dihydroxybenzoic Acid	320(4.07×10^3)	
Catechol	275(2.31×10^3)	
3,4-Dihydroxybenzoic Acid	250(8.30×10^3)	287(3.79×10^3)
3-Methoxycatechol	267(8.03×10^2)	
4-Nitrocatechol	264(4.99×10^3)	426(1.30×10^4)
Syringic Acid	261(9.22×10^3)	
Thiosalicylic Acid	252(Shoulder)	303(Shoulder)
Ascorbic Acid	266(1.45×10^4)	

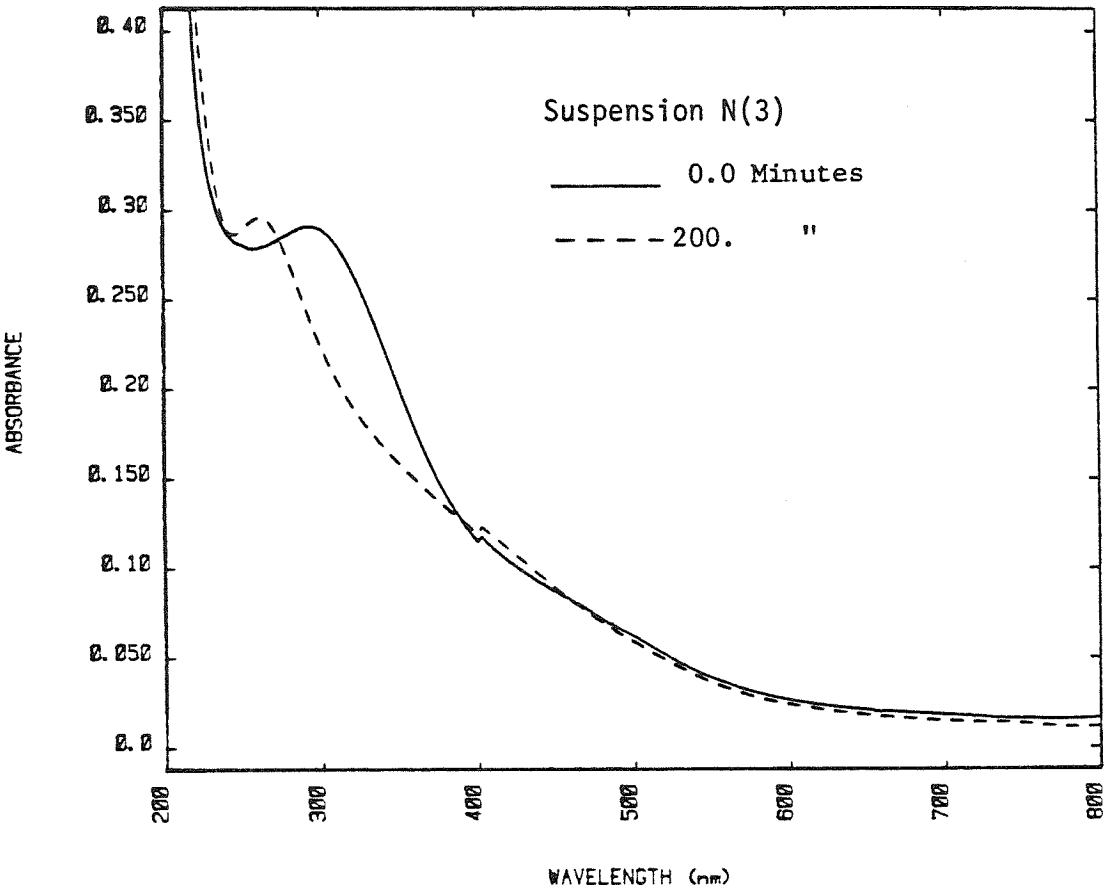

Figure 8.7 Absorbance spectrum of suspension N(3) upon mixing with 0.10M phosphate buffer (pH 6.84). Mn_T = 6.70×10^{-6}M. (Path length of cell = 10 cm.)

absorbance spectrum of suspension N(3) immediately upon mixing with a 0.10M phosphate buffer (pH 6.8) and after 200 minutes. Lowering the pH causes particles to grow by flocculation, changing absorbance.

Spectra of unfiltered reaction solution contain an absorbance contribution from the manganese oxide suspension. The absorbance due to the suspension does not remain constant, since dissolution and flocculation are continually changing the particle size distribution. For this reason, all solutions were filtered with 0.2 micron nucleopore filters prior to the measurement of absorbance. Interference by the suspension was thereby eliminated.

Polymerization of organic substrates forms large molecules that scatter light. Since polymers generated by the reaction may be smaller than 0.2 micron, the filtration step will not remove all of them.

Identification of an oxidized product on the basis of UV and visible absorption bands requires that the component responsible for those particular absorption bands has been identified by an independent method. In this study, the product spectra are compared to spectra of possible oxidation products found in the literature.

Reference spectra for some oxidized products do not exist, so that the product cannot be directly identified by its spectrum. The spectrum provides other information, however. The observation that absorbance increases with time over a wide wavelength range and slopes upward towards the UV, for example, indicates polymer formation.

In some cases, the overall spectrum changes as the reaction progresses, but the absorbance at particular wavelengths remains

constant. These locations are called isosbestic points, and are observed at wavelengths where substrate and product have the same molar absorptivity (Brown, 1980). Figure 8.8A. shows spectra recorded during the oxidation of hydroquinone to p-benzoquinone by manganese oxide. An isosbestic point is found at 266 nm, the wavelength at which the molar absorptivities of hydroquinone and p-benzoquinone are equal. It is very unlikely that a wavelength exists for three or more species where molar absorptivities of all species are the same. Isosbestic points, therefore, indicate that the observed spectrum is caused by a mixture of only two absorbing species (Brown, 1980).

8.3B. Experimental Results

The spectra of hydroquinone and 2,5-dihydroxybenzoic acid (2,5-diOH) recorded during oxidation by manganese oxide suspension are shown in Figure 8.8. Consumption of hydroquinone lowered absorbance at $\lambda_{max.}$ (288 nm). The absorption band appearing at 244 nm in the reaction with hydroquinone is ascribed to p-benzoquinone (Davies and Kustin, 1969). The isosbestic point at 266 nm verifies that two species are responsible for the observed spectra. p-Benzoquinone did not absorb appreciably at the 288 nm absorption band of hydroquinone, thus absorbance at this wavelength can be used to calculate the amount of hydroquinone consumed (Section 8.3C.).

Spectra collected during oxidation of 2,5-diOH are similar to those of hydroquinone. 2,5-DiOH ($\lambda_{max.}$ = 320 nm) was oxidized to the corresponding p-benzoquinone product ($\lambda_{max.}$ = 244 nm). The isosbestic point at 291 nm confirms that a single oxidized product is

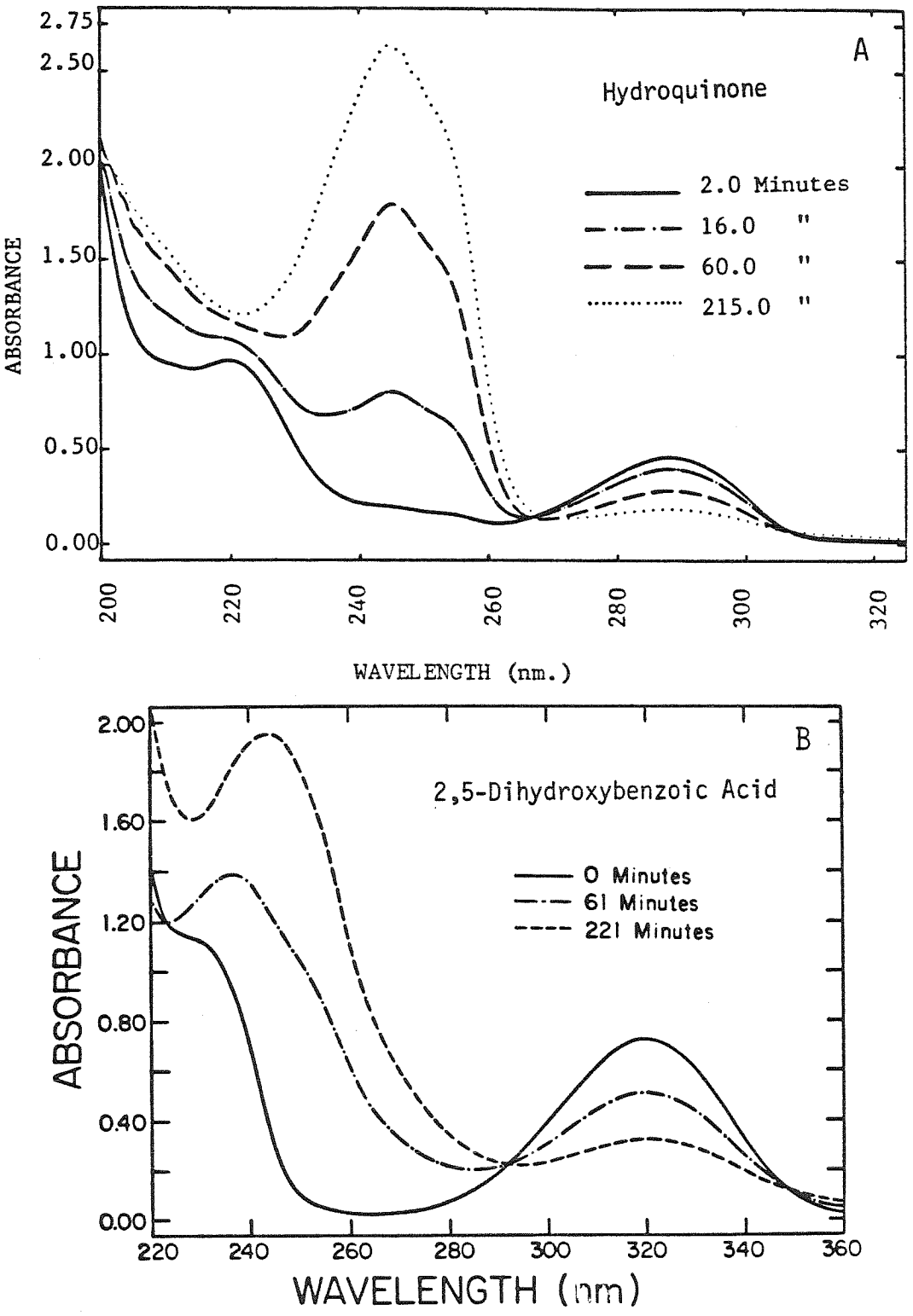

Figure 8.8 Spectra of hydroquinone (A) and 2,5-dihydroxybenzoic acid (B) recorded during oxidation by manganese oxide suspension. (Runs GL and GO).

formed. Absorbance at 320 nm is used to calculate consumed substrate.

Spectra showing the oxidation of catechol and its substituted derivatives are shown in Figures 8.9, 8.11, 8.13, and 8.15. Oxidation of catechol, 3,4-dihydroxybenzoic acid (3,4-diOH), and 3-methoxycatechol caused an increase in absorbance with time over a wide wavelength range that increased in the direction of decreasing wavelengths. This indicates polymerization of oxidized substrate.

Spectra of solutions containing catechol or 3,4-diOH show a decrease in absorbance at $\lambda_{max.}$ of the substrate relative to the rest of the spectrum. Figures 8.10 and 8.12 show absorbance values from selected wavelengths and $[Mn^{2+}]_{diss.}$ plotted against time for these reactions. Increases in absorbance at different wavelengths were in proportion to the increase in $[Mn^{2+}]_{diss.}$. The rates of polymerization reactions were therefore tied in some manner to the amount of remaining manganese oxide.

Oxidation of o-methoxycatechol initially formed an intermediate oxidized product with an absorbance maximum at 374 nm, and a shoulder near 500 nm. (Figure 8.13). Subsequent reactions, including polymerization, consumed this intermediate. Figure 8.14 shows that absorbance at 374 nm increased quickly at the start of the reaction, reached a maximum, then slowly decreased. Absorbance measured at 316 and 484 nm increased throughout the time period studied, even after $[Mn^{2+}]_{diss.}$ leveled out. Thus, changes in absorbance were not in proportion to the amount of oxide reduced. Organic molecules continued to polymerize even after most of the oxide had been consumed.

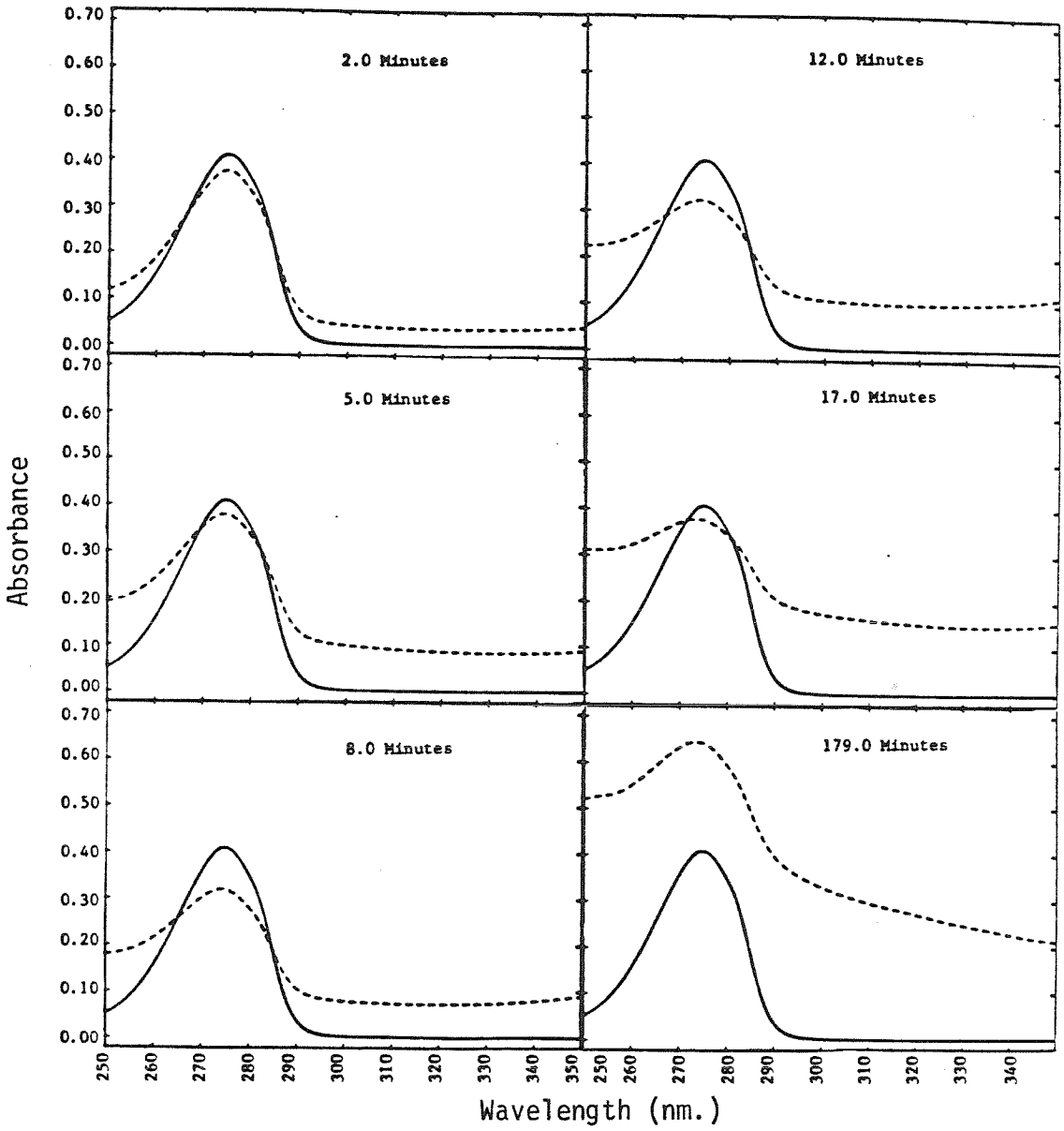

Figure 8.9 Spectra of catechol recorded during oxidation by manganese oxide suspension (Run GP). Smooth curves represent the spectrum at t=0, calculated from the spectrum of a standard solution (in phosphate buffer). Dashed curves are the spectra taken at the times stated.

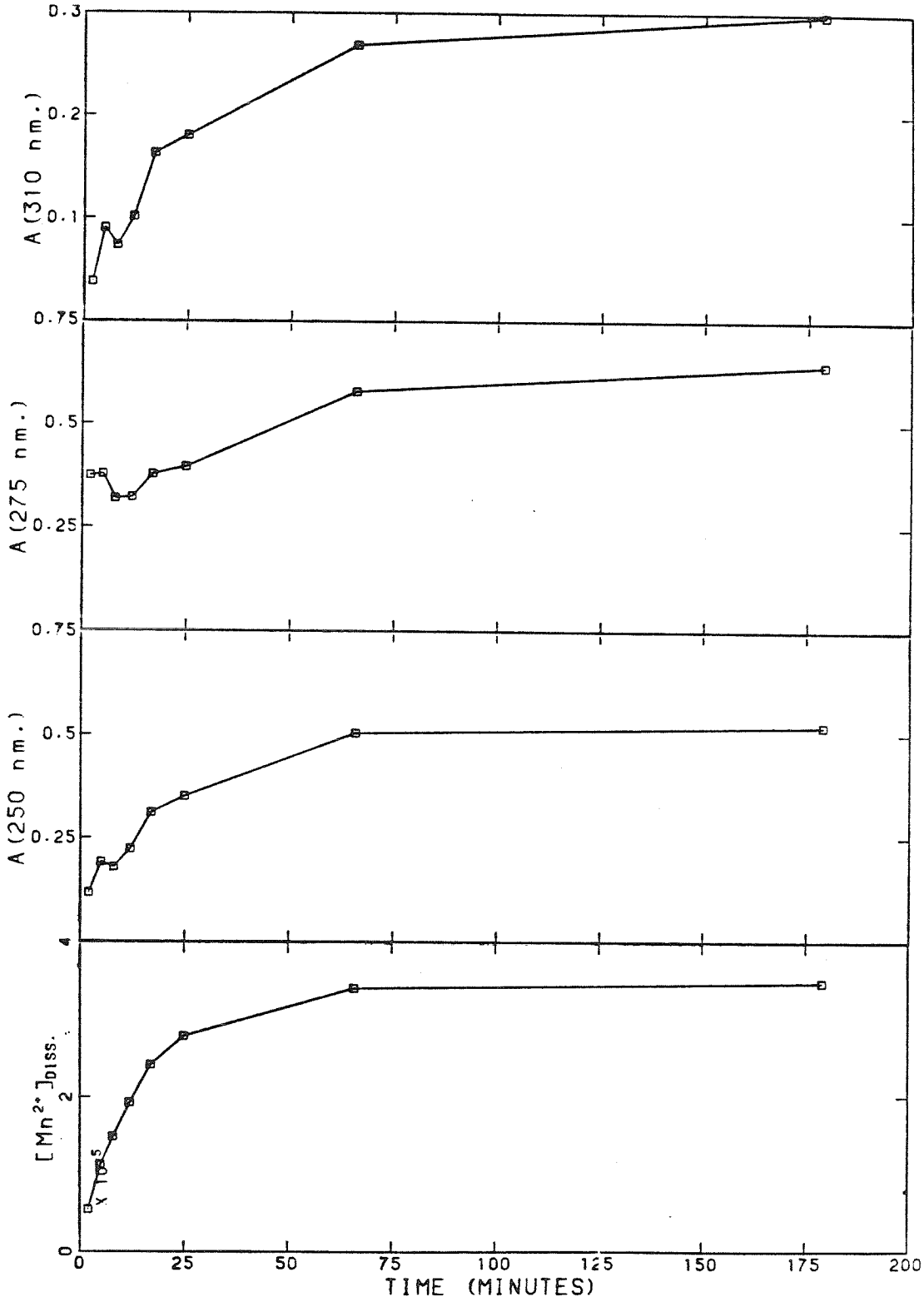

Figure 8.10 Absorbance of catechol at selected wavelengths during oxidation by manganese oxide suspension (Run GP). Dissolved manganese as a function of time is presented for comparison.

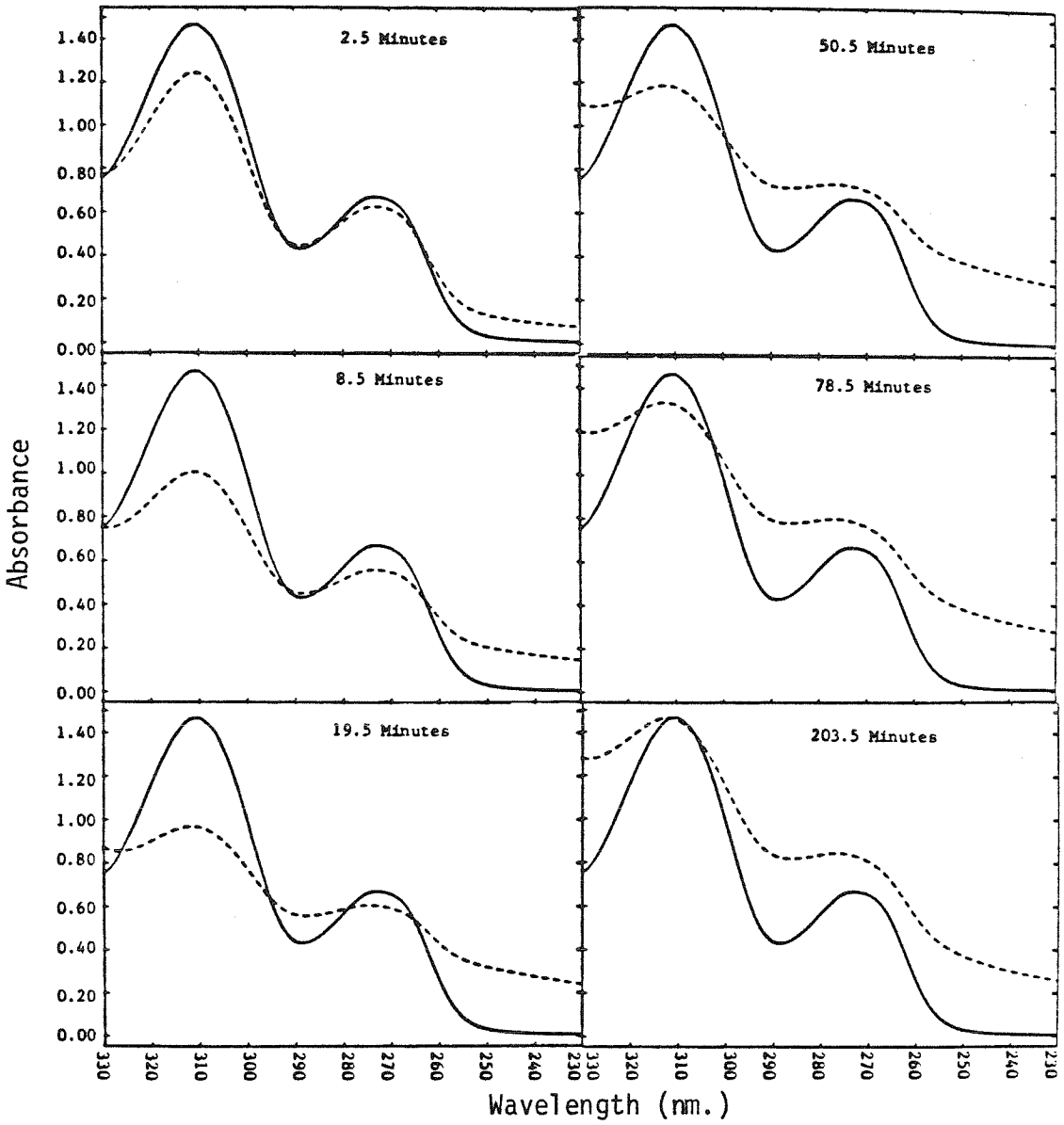

Figure 8.11 Spectra of 3,4-dihydroxybenzoic acid recorded during oxidation by manganese oxide suspension (Run GM). Smooth curves represent the spectrum at t=0, calculated from the spectrum of a standard solution (in phosphate buffer). Dashed curves are spectra taken at the times stated.

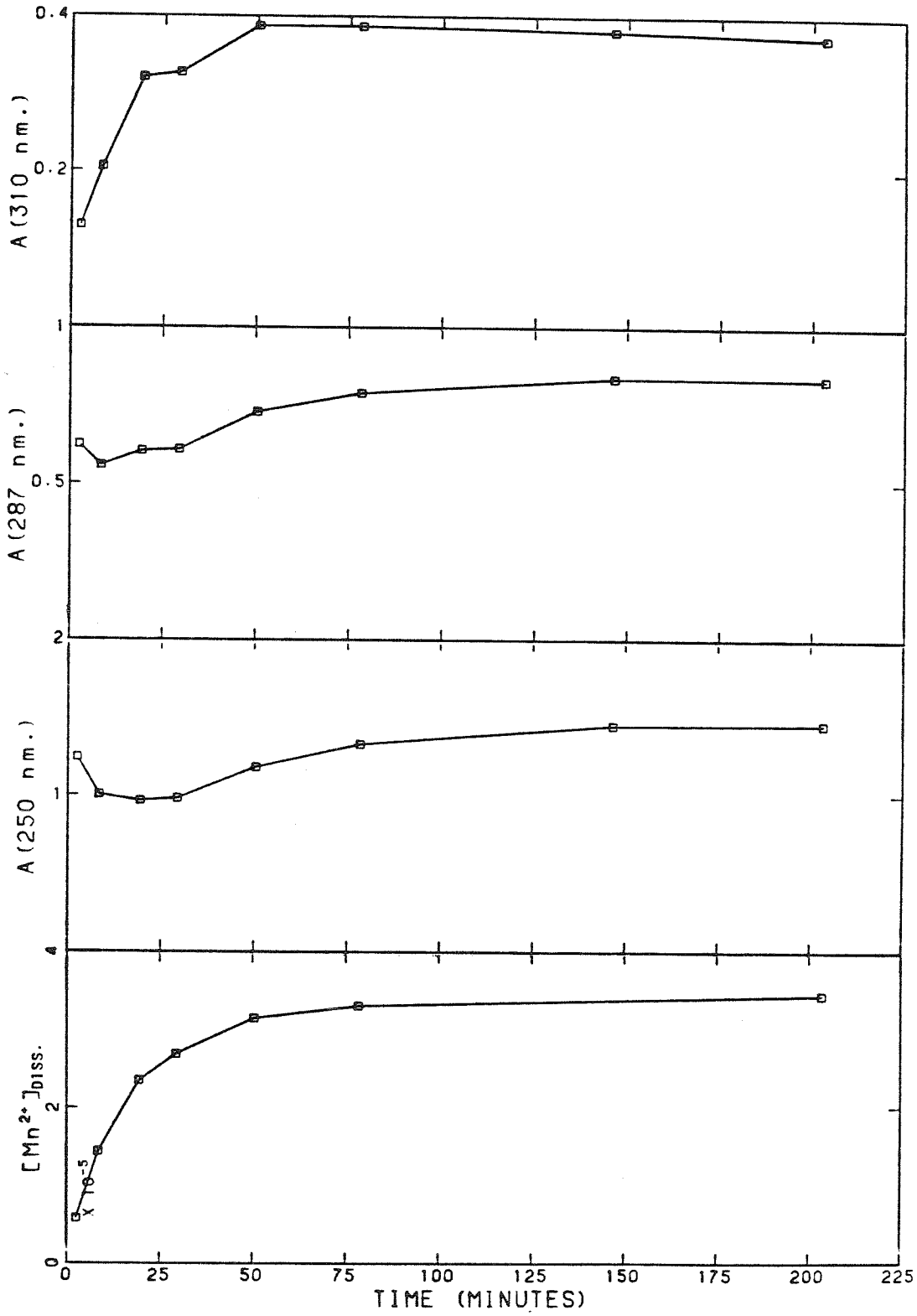

Figure 8.12 Absorbance of 3,4-dihydroxybenzoic acid at selected wavelengths during oxidation by manganese oxide suspension (Run GM). Dissolved manganese as a function of time is presented for comparison.

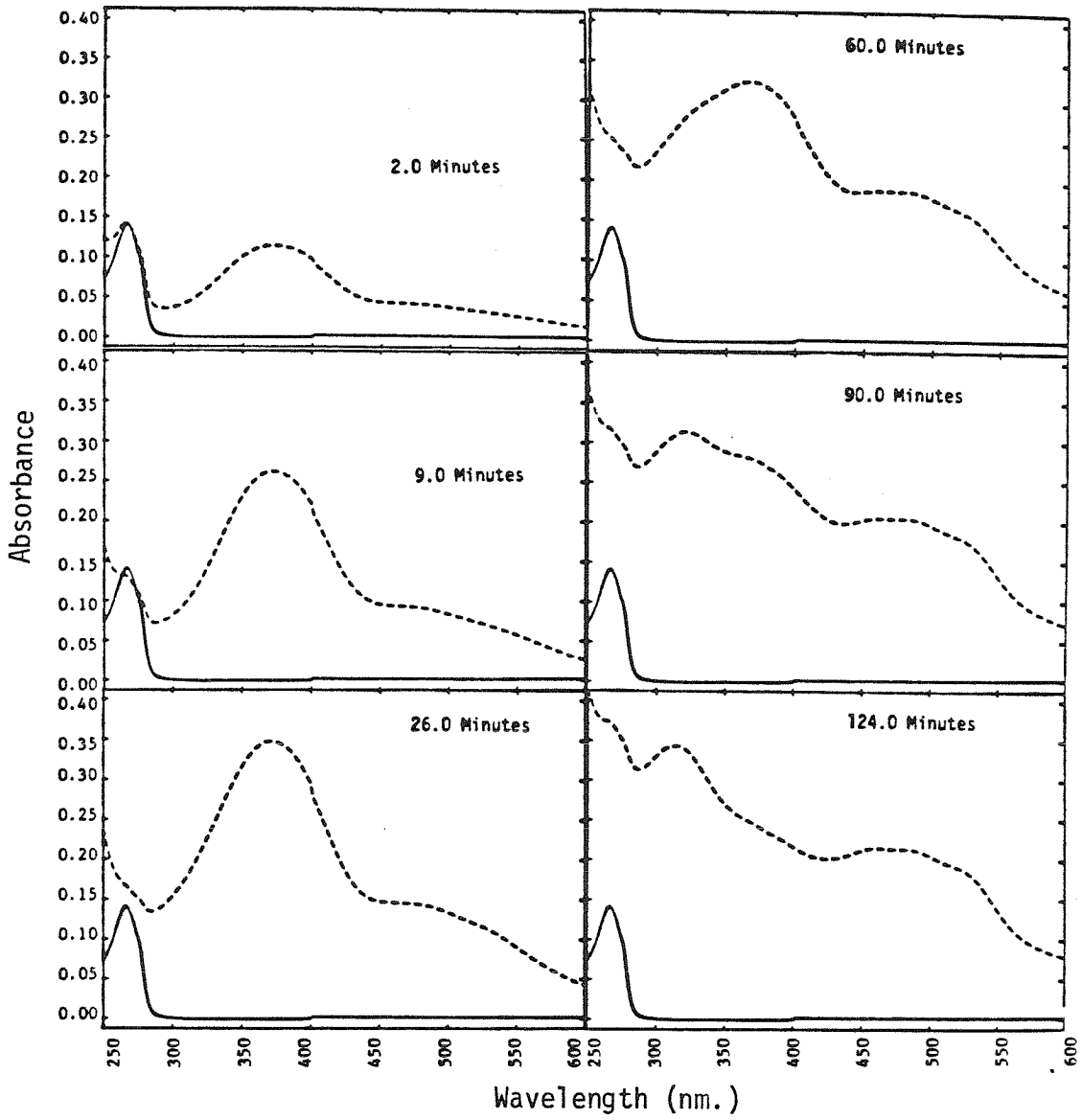

Figure 8.13 Spectra of 3-methoxycatechol recorded during oxidation by manganese oxide suspension (Run GS). Smooth curves represent the spectrum at t=0, calculated from the spectrum of a standard solution (in phosphate buffer). Dashed curves are spectra taken at the times stated.

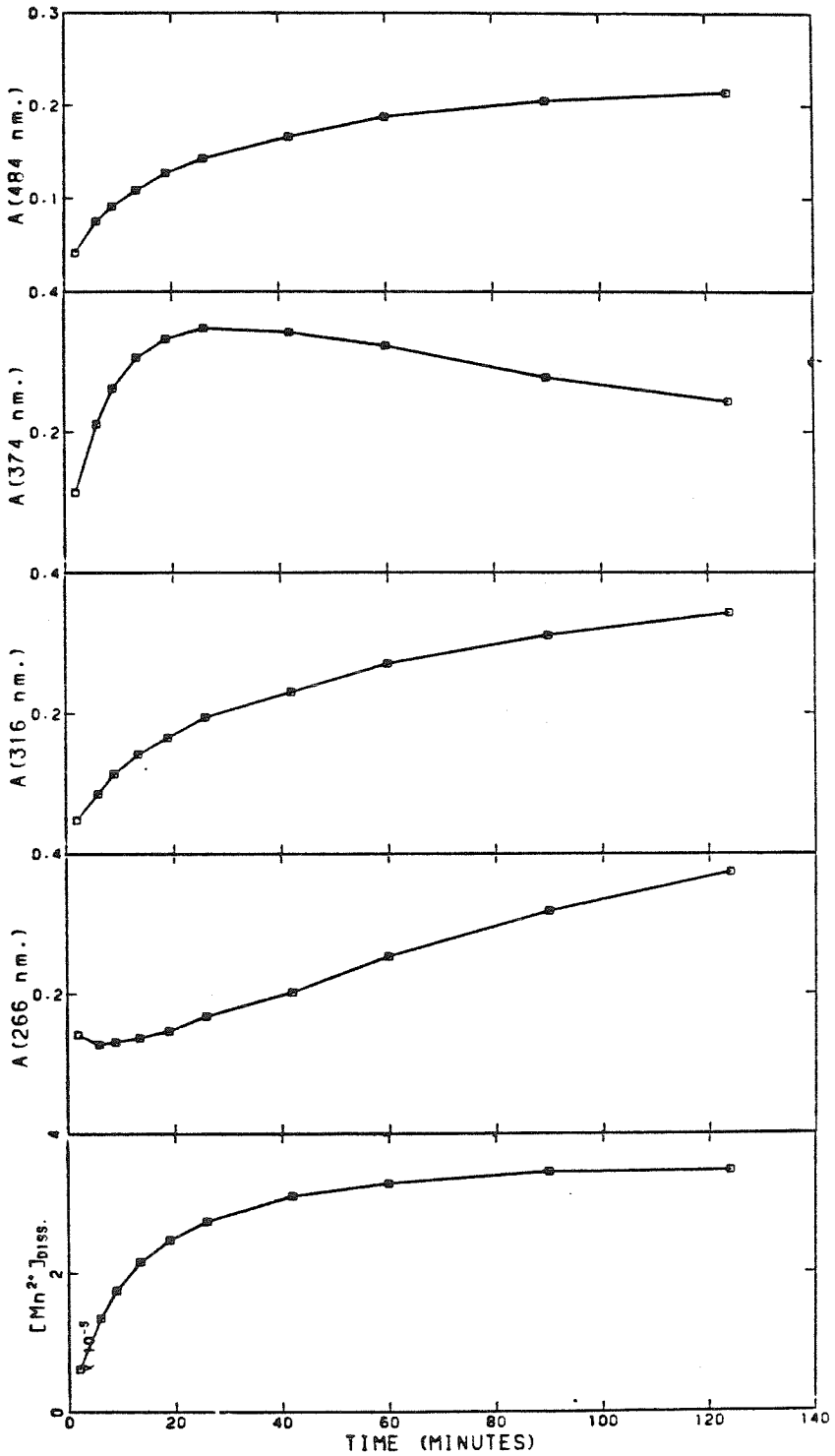

Figure 8.14 Absorbance of 3-methoxycatechol at selected wavelengths during oxidation by manganese oxide suspension (Run GS). Dissolved manganese as a function of time is presented for comparison.

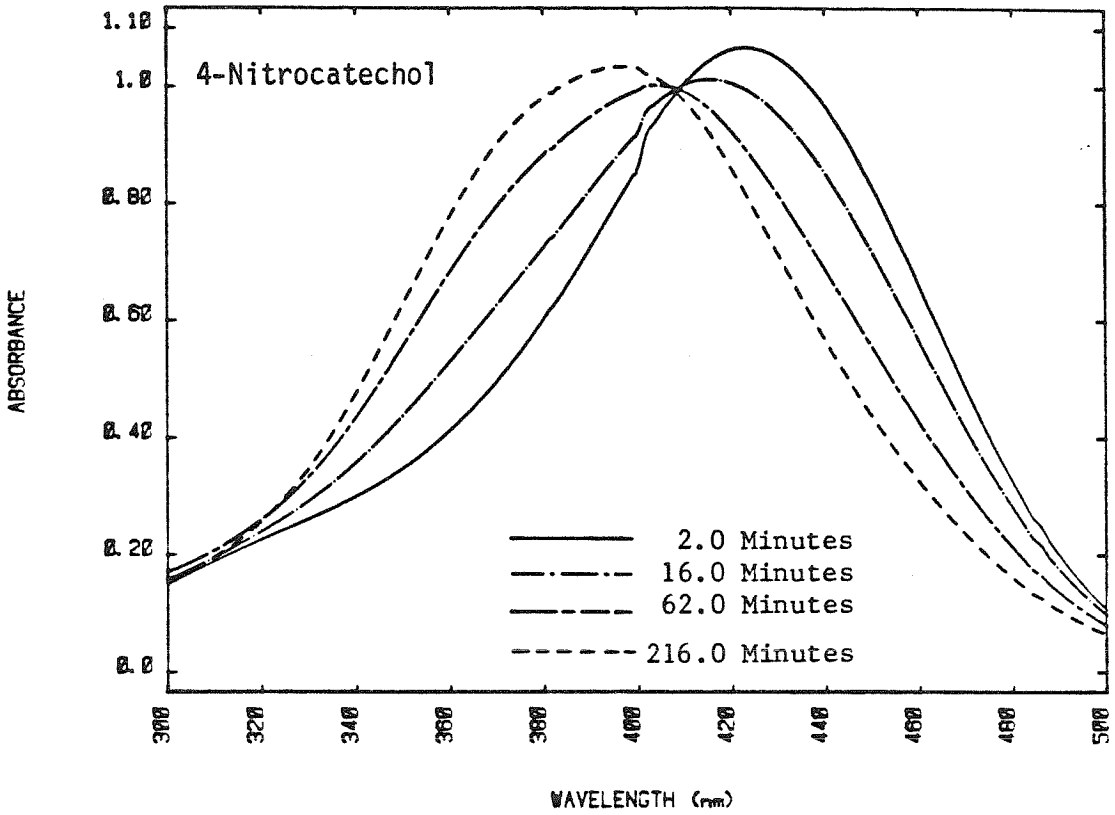

Figure 8.15 Spectra of 4-nitrocatechol recorded during oxidation by manganese oxide suspension (Run GZ).

Spectra recorded during the oxidation of 4-nitrocatechol exhibit an isosbestic point, indicating that one oxidized product was formed (Figure 8.15). Nitro-substitution effectively blocked reactions that led to polymer formation with other catechols.

Oxidation of thiosalicylate resulted in the growth of a peak at 296 nm (Figure 8.16). Section 8.2A. noted that thiosalicylate behaved as a one-equivalent reductant in the reaction with manganese oxide. All spectra save the first pass through two isosbestic points at 267 and 280 nm, indicating that a single oxidation product was formed. Both of these observations are consistent with disulfide bond formation, generating dimer. The first recorded spectrum does not pass through the isosbestic points, indicating that either the reaction is more complicated than just described, or that contaminant was present in the first sample that was absent in later samples.

Figure 8.17 shows the spectrum of syringic acid during oxidization by manganese oxide. The reaction with syringic acid was slow, such that only 40% of the oxide was dissolved after 4 hours of reaction. Isosbestic points at 242 and 284 nm. indicate that a single oxidized product was formed.

The oxidation of ascorbate can be readily monitored by measuring the absorbance at 266 nm, $\lambda_{max.}$ of the substrate. Absorbance by the oxidized product was quite low at wavelengths greater than 240 nm (Figure 8.18) such that product formation did not interfere with the determination of ascorbate concentration.

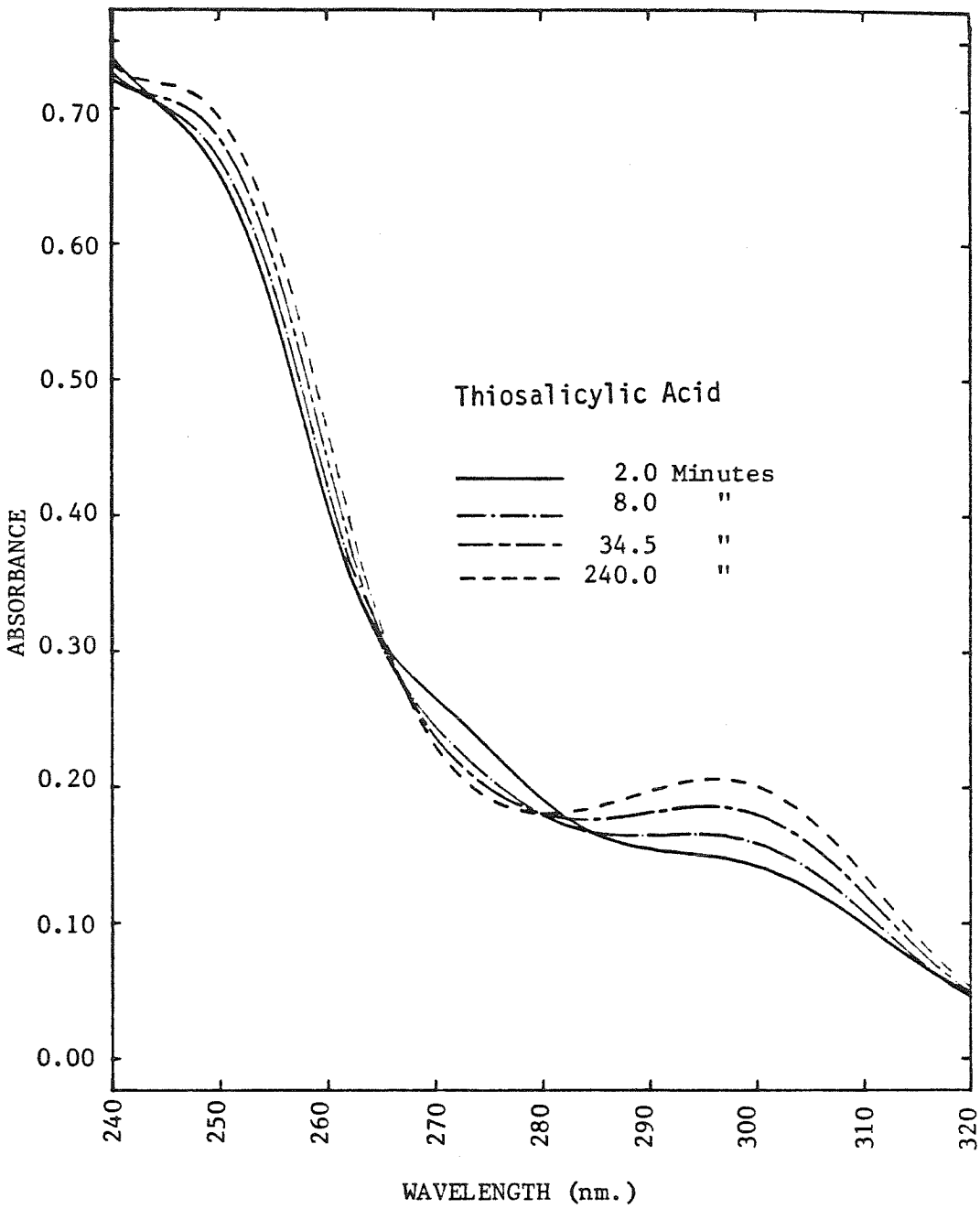

Figure 8.16 Spectra of thiosalicylate recorded during oxidation by manganese oxide suspension (Run XB).

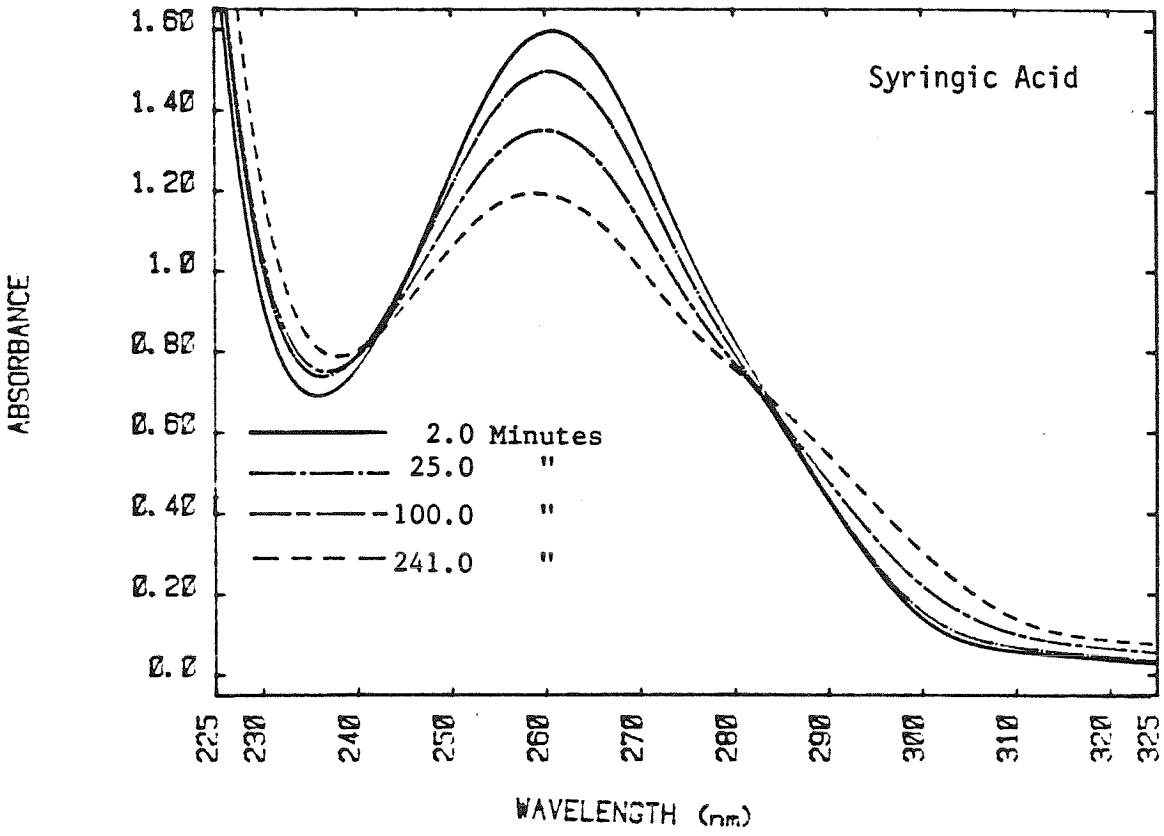

Figure 8.17 Spectra of syringic acid recorded during oxidation by manganese oxide suspension (Run GQ).

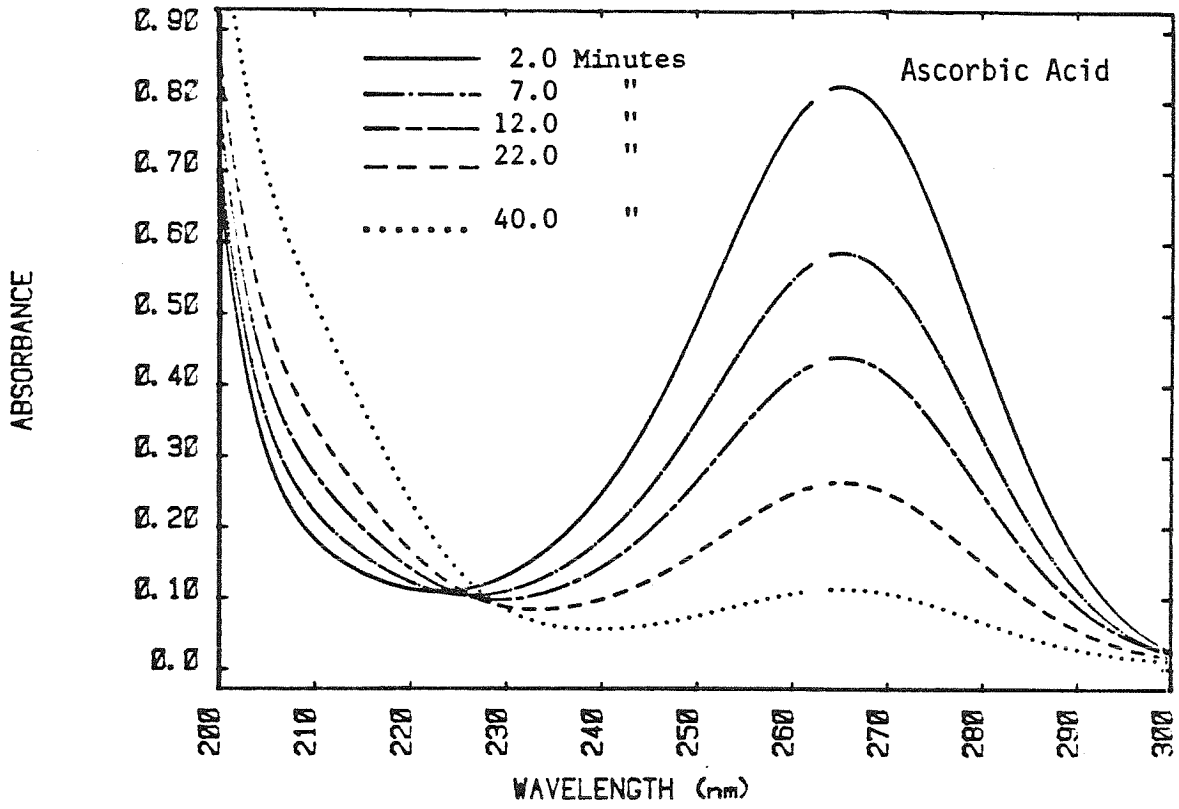

Figure 8.18 Spectra of ascorbate recorded during oxidation by manganese oxide suspension (Run XA).

8.3C. Reaction Stoichiometry

As mentioned in the previous section, the amount of hydroquinone, 2,5-diOH, and ascorbate consumed by the reaction with manganese oxide can be calculated from the wavelength maximum of the substrate. All three substrates are two-equivalent reductants, so the amount of Mn^{2+} formed per mole of substrate consumed should be:

$$8.9 \quad \left(\frac{2 \text{ Equivs. Reductant}}{1 \text{ mole Reductant}}\right) \left(\frac{1 \text{ mole Mn}}{1.28 \text{ Equiv. Oxidant}}\right) = 1.56.$$

Since the reactions were performed using stoichiometric concentrations of oxidant and reductant, the relation between $[Mn^{2+}]_{diss.}$ and consumed substrate at the completion of the reaction is not very meaningful. Instead, R_t, the ratio of $[Mn^{2+}]$diss. to consumed reductant at time t, is calculated as the reaction progresses. In Section 5.3B. it was determined that the manganese oxides used in the experiments are mixed phases containing between 20 and 36% Mn^{IV}, the remainder being Mn^{III}. If the ratio of Mn^{IV} to Mn^{III} is the same throughout the particles, then R_t should be constant and equal to 1.56 during the entire reaction. If Mn^{IV} is unevenly distributed within the particles, then this ratio may change once outer layers are dissolved. If Mn^{IV} is located mainly at particle centers, for example, then R_t would be close to two at the beginning of the reaction, but would drop to near one once outer layers have been removed. Changes in R_t with time therefore indicate that

the particles are inhomogeneous.

Accurate determination of consumed reductant requires making a calibration curve and deciding whether Beer's Law is obeyed in the concentration range studied. Values of consumed reductant reported here were calculated using only one standard solution (substrate in 1.40×10^{-2}M phosphate solution), and the assumption was made that Beer's Law was obeyed. Small error in the measurement of absorbance of this standard can result in larger errors in the calculation of [Consumed Reductant] and R_t. Calculated values of these two quantities are therefore only approximate.

Figures 8.19, 8.20, and 8.21 show the amount of consumed reductant, $[Mn^{2+}]_{diss.}$, and R_t plotted against time for reaction with hydroquinone, 2,5-diOH, and ascorbate. For hydroquinone and 2,5-diOH, R_t was greater than 2 throughout the reaction, indicating that more than two moles of manganese were dissolved for every mole of substrate consumed. [Consumed Reductant] at t=0 was, however, slightly less than zero. This means that calculation of substrate concentration from absorbance measurements gives values that are too high. Values of R_t are therefore overreported.

The results of the reaction with ascorbate are in closer agreement with equation 8.9 (Figure 8.21). The average value for the ratio was 1.75, and less fluctuation in the ratio as the reaction progresses was observed.

Taken as a whole, the three reactions give values of R_t greater than the predicted value. One explanation is that the filters

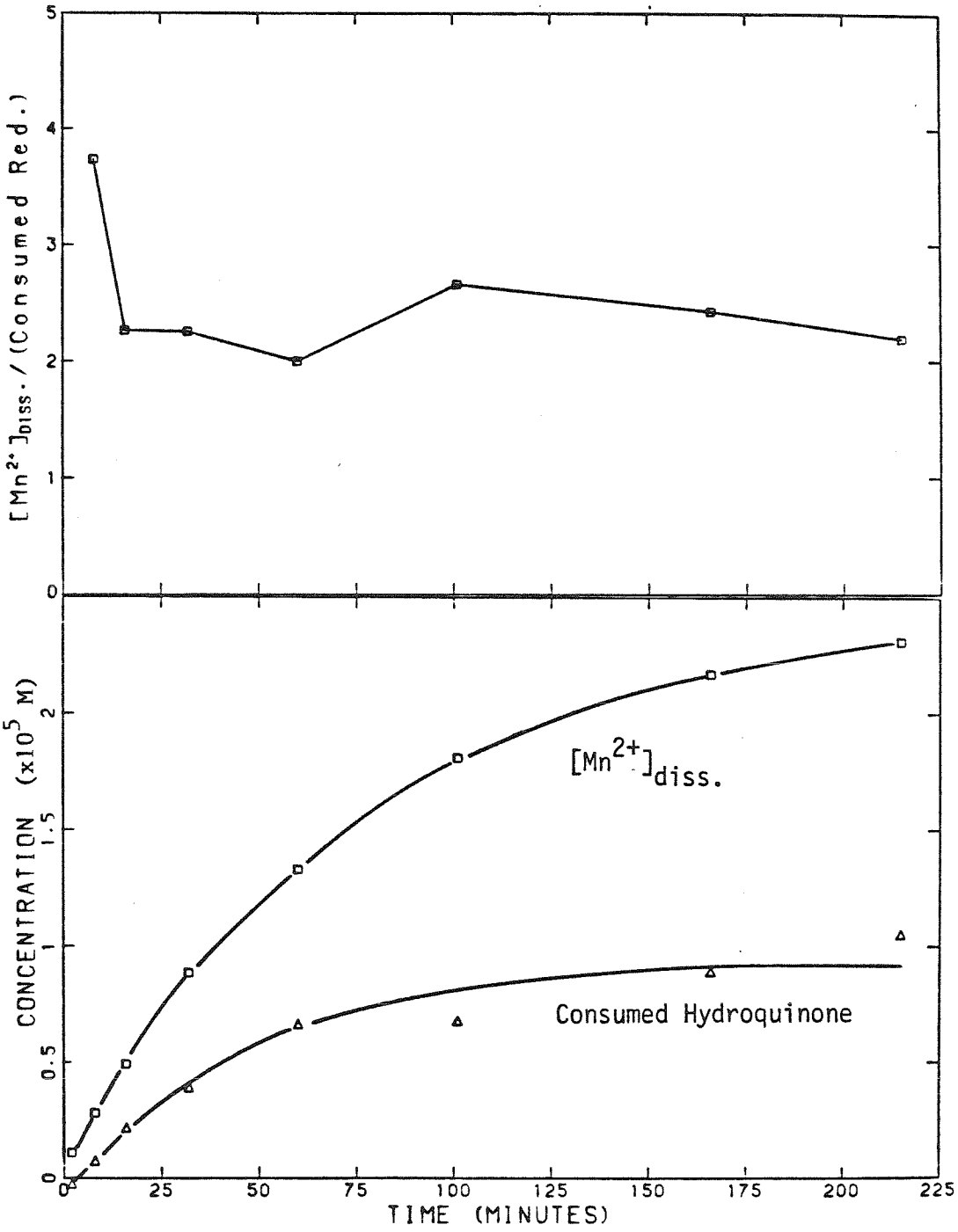

Figure 8.19 Consumed hydroquinone and $[Mn^{2+}]$diss. plotted as a function of time (Run GO). The ratio ($[Mn^{2+}]$diss./Consumed Reductant) gives the stoichiometry of the reaction. (Run GO).

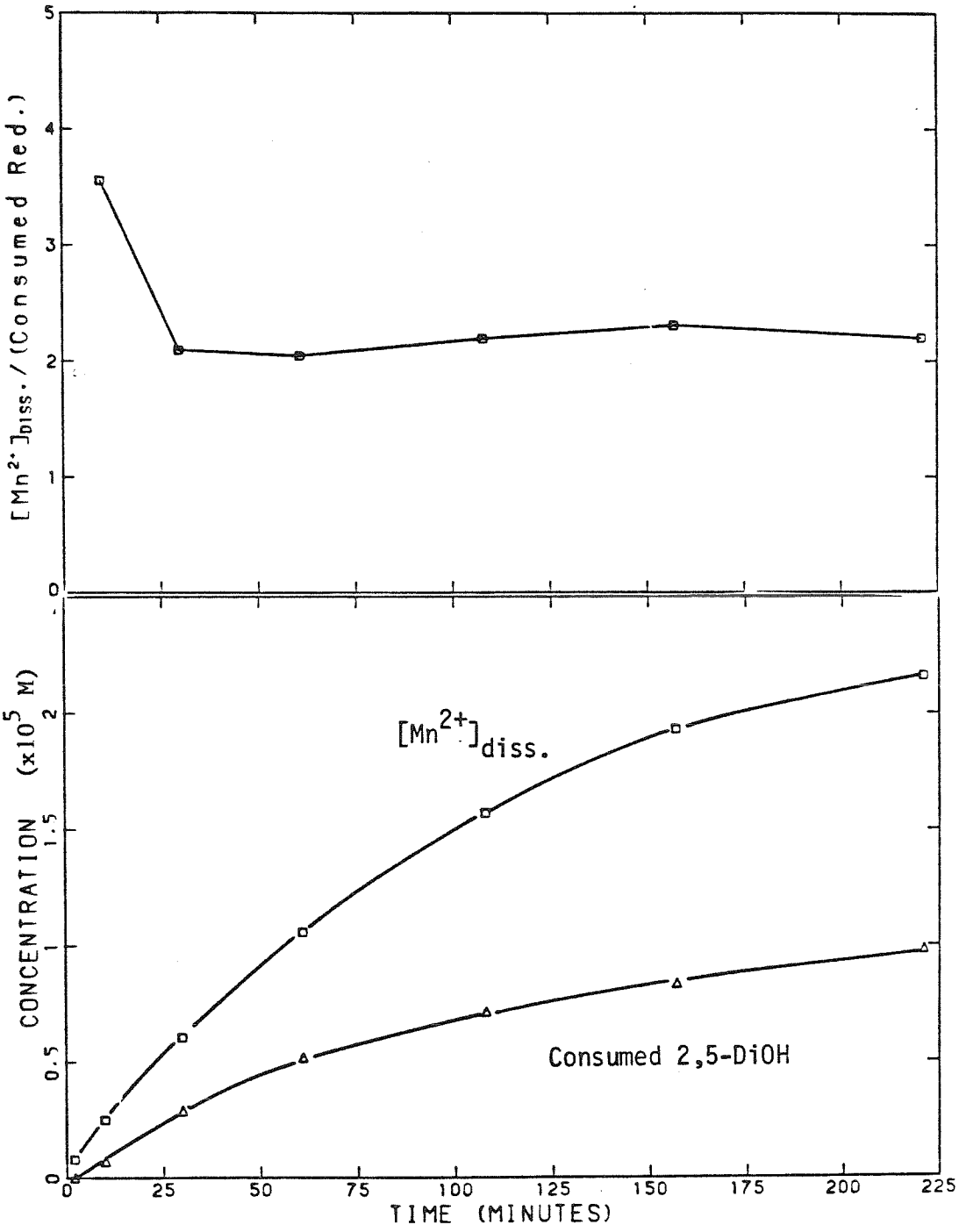

Figure 8.20 Consumed 2,5-dihydroxybenzoate and $[Mn^{2+}]$diss. plotted as a function of time (Run GL). The ratio ($[Mn^{2+}]$diss./Consumed Reductant) gives the stoichiometry of the reaction. (Run GL).

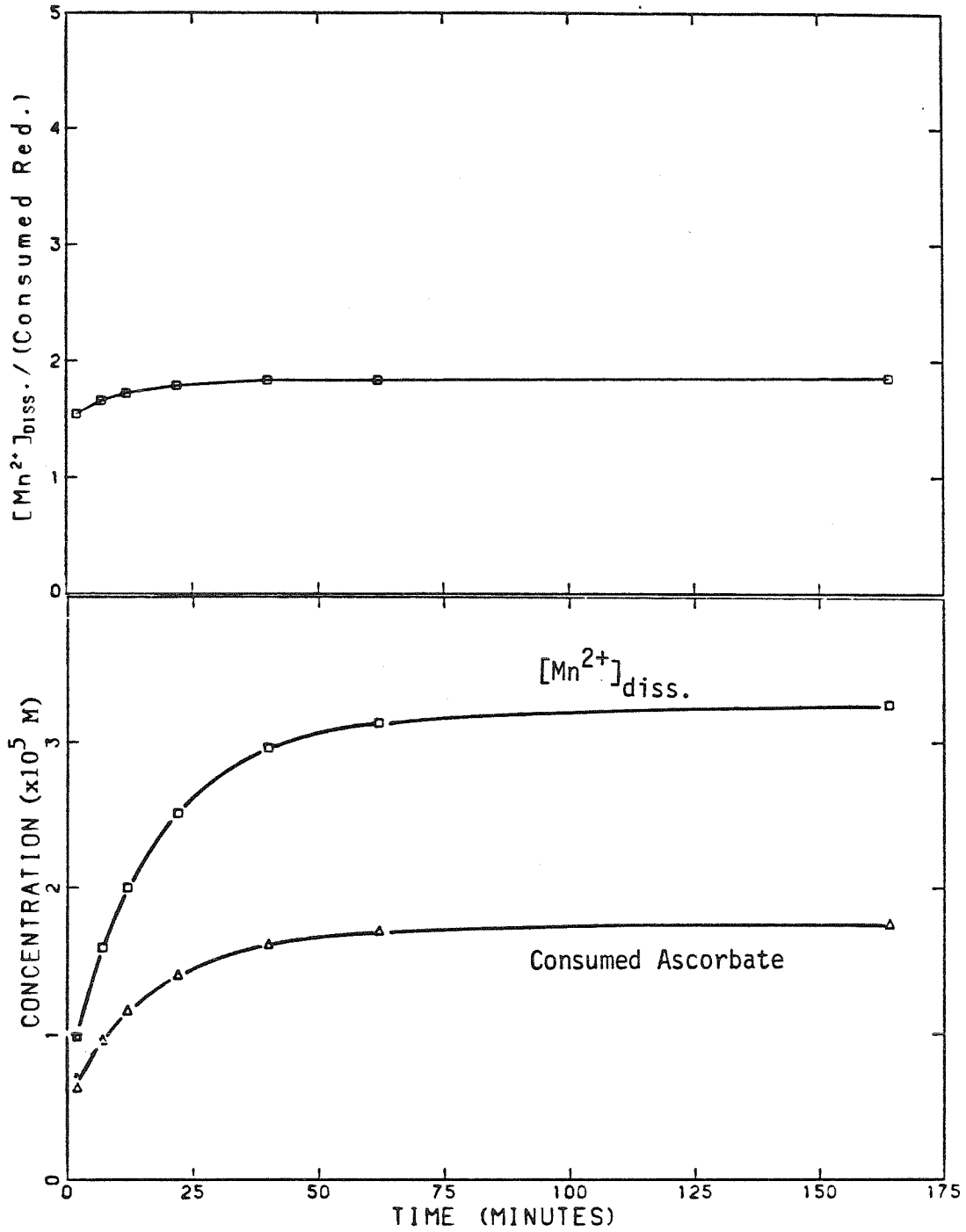

Figure 8.21 Consumed ascorbate and $[Mn^{2+}]$diss. plotted as a function of time (Run XA). The ratio ($[Mn^{2+}]$diss./Consumed Reductant) gives the stoichiometry of the reaction. (Run XA).

do not retain all the oxide, and that $[Mn^{2+}]$diss. values are therefore overreported. This possibility was addressed in Section 6.2C. by filtering partially dissolved suspensions through both 0.1 and 0.2 micron filters, and comparing differences in $[Mn^{2+}]$diss. The amount of oxide that passes through the 0.2 micron filters was found to be less than 10% in most cases, and therefore not large enough to cause R_t to be as high as reported here. Besides, values reported for ascorbate are only slightly larger than the predicted value, while those for hydroquinone and 2,5-diOH are much larger. It is more likely that values of [Consumed Reductant] for hydroquinone and 2,5-diOH are underreported, because of errors in the calibration technique.

Values of R_t for ascorbate are quite constant, indicating that the distribution of Mn^{IV} within the oxide particles is quite uniform. Although R_t values for hydroquinone and 2,5-diOH do fluctuate, the overall change in R_t is small, also indicating that oxide particles are relatively homogeneous.

8.4 Dissolution by Marine Fulvic Acid

Sunda et al. (1982) determined that marine organic matter reduces manganese oxides by a photocatalyzed reaction (see Section 4.6B.). The purpose of the experiments described in this section was to confirm these observations under the same experimental conditions employed in studying the model compounds.

Marine fulvic acid was provided by G.R. Harvey of the Atlantic Oceanographic and Meteorological Laboratories (NOAA). The sample was collected from the Gulf of Mexico in December 1979. The fulvic acid

was adsorbed on activated carbon from seawater that had passed through an XAD-2 resin. Characterization of similar material has been reported by Harvey et al. (1981).

Experiments performed in this work and those performed by Sunda et al. (1982) are summarized in the following table:

Experiment	Mnt	Organic Matter	pH	Ionic Medium
Sunda et al.	1.0x10-8M	5 mg/l	8.1	Seawater and Estuarine Water
XI	2.85x10-5	199 mg/l	7.65-7.74	5x10-2M $NaNO_3$
AI	2.89x10-5	201 mg/l	6.35	"
AJ	2.89x10-5	-	6.50	"

Manganese oxide loadings in this experiment were 3 orders of magnitude higher than employed in the Sunda experiment, and the concentration of fulvic acid was 40 times higher than their most concentrated solution. Manganese oxide used in the Sunda experiment was prepared by oxidizing $MnCl_2$ with $KMnO_4$, whereas the suspension used in the experiments described here was formed by oxygenation. The mineral phases of the two preparations are therefore different, and differences in reactivity may result.

Dissolution reactions were performed following procedures outlined in Chapter 6. In each experiment, reaction was initiated by adding fulvic acid stock solution to manganese oxide suspension equilibrated with bicarbonate buffer in a 1-liter jacketed beaker. The reaction was followed under room light for a given length of time (3.6 hours for XI,

6.0 hours for AI) after which the solution was illuminated with a 450 watt, filtered quartz-mercury arc lamp. This is an intense lamp that provides light of intensity greater than sunlight throughout the UV/visible spectrum.

The amount of manganese oxide dissolved in reaction XI, even after 3 hours of mercury lamp illumination, was negligible (<3% of Mn_T). Reaction AI was performed at a lower pH (pH 6.35), and measurable amounts of oxide were dissolved (Figure 8.22). At this low pH, the amount of dissolved manganese in the blank solution was also significant (7% of Mn_T). Figure 8.22 shows that $[Mn^{2+}]_{diss.}$ was not much higher than that in the blank solution until the quartz-mercury arc lamp was turned on. The dissolution rate under illuminated conditions was significant, verifying that the reaction is photocatalyzed.

Unfortunately, the reaction was not followed to completion, so the amount of oxide dissolved per weight of fulvic acid cannot be calculated.

8.5 Two-Substrate Experiments.

8.5A. Introduction

This section considers the situation where two organic substrates are added to a manganese oxide suspension, one which dissolves manganese oxide when added alone, and the other inert to reaction. The rate of dissolution by the reactive, or primary substrate (HA) may depend upon the concentration of the unreactive, secondary substrate (HB). The secondary substrate can interfere with the reaction through

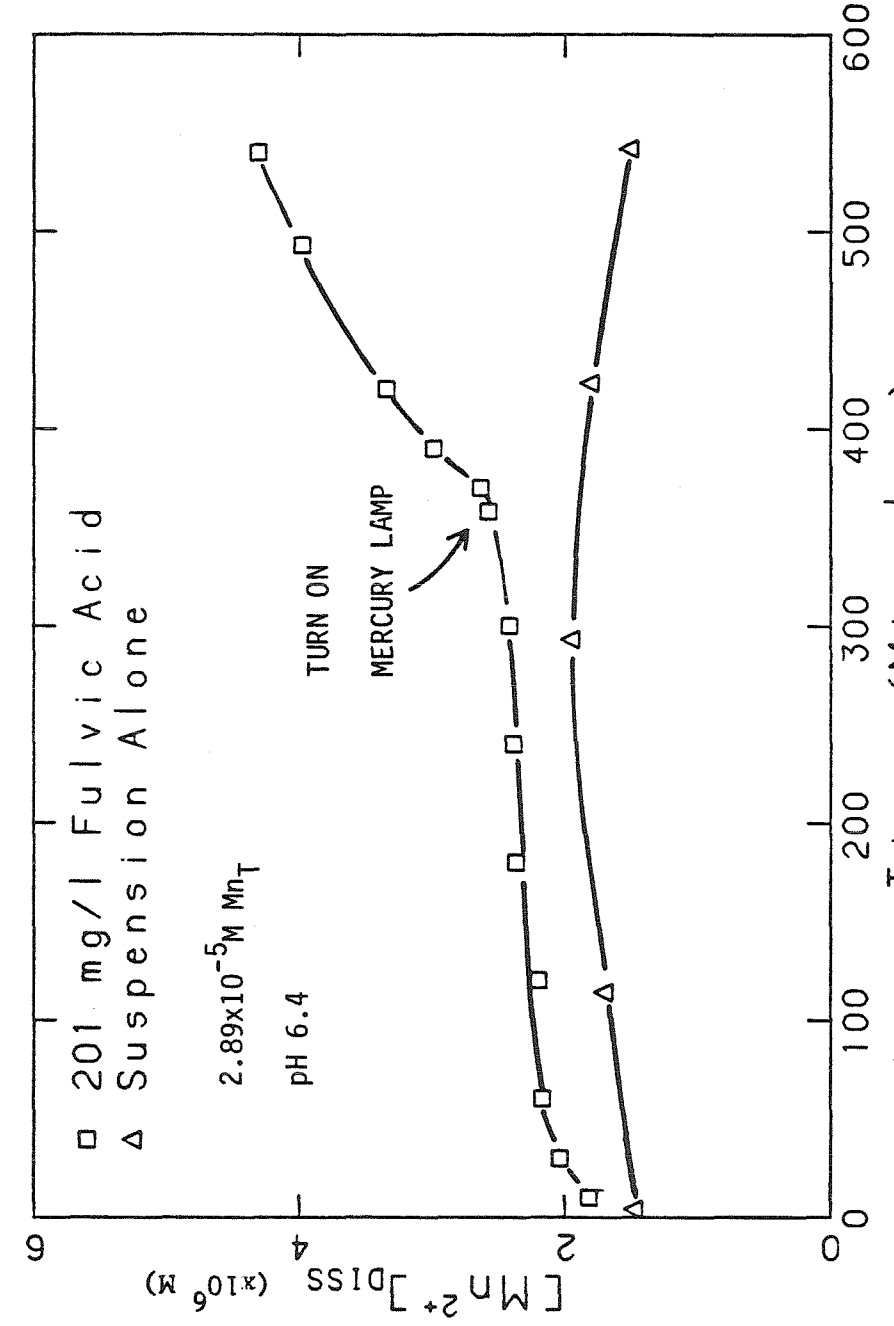

Figure 8.22 Dissolution of manganese oxide by marine fulvic acid. (Runs AI and AJ).

a number of mechanisms:

(i) Competitive Absorption.

If a surface complex (≡MnA) must form prior to electron transfer, and if substrate HB successfully competes for surface sites, then HB can block sites from reaction with HA, and inhibit the reaction. (See Section 4.3B.).

(ii) Enhancement/Inhibition of Mn^{II} Dissolution.

If release of Mn^{II} from the oxide surface is rate limiting, HB may facilitate dissolution by binding Mn^{II} on the surface and lower the energy required for its release. Surface complexes may also form that block dissolution. (See Section 4.4).

(iii) Radical Reaction.

In some cases, reaction of the primary substrate with manganese oxide generates free radicals, that also reduce the oxide:

8.10 $$\equiv Mn^{III}OH + HA \xrightarrow{k_a} \equiv Mn^{II}OH_2 + A^{\cdot}$$

8.11 $$\equiv Mn^{III}OH + A^{\cdot} \xrightarrow{k_b} \equiv Mn^{II}OH^{-} + A^{+}$$

The secondary substrate, although inert to reaction with manganese oxide, may react with radical $A^{\cdot}$ to generate new radicals that are reactive with manganese oxides. Table 2.1 lists a number of radical

reactions that can occur in such a system. Consider the case where the following two reactions compete with reaction 8.11:

$$8.12 \quad A^{\bullet} + HB \xrightarrow{k_c} B^{\bullet} + HA$$

$$8.13 \quad \equiv Mn^{III}OH + B^{\bullet} \xrightarrow{k_d} \equiv Mn^{II}OH^{-} + B^{+}.$$

Reactions 8.11 and 8.13 are in general faster than other steps in the dissolution reaction. If radical $B^{\bullet}$ is reactive with the oxide, its formation has little effect on the rate. If $B^{\bullet}$ does not reduce manganese oxides, then reaction 8.12 slows down the dissolution reaction. If that is the case, then the secondary substrate acts to quench the reactions of radical $A^{\bullet}$.

8.5B. Experimental Results

Secondary (unreactive) substrates were chosen from the organics discussed in Section 8.2 that did not dissolve appreciable amounts of oxide. Stock solutions of secondary substrate were added to manganese oxide suspensions a few minutes before the primary substrate (either hydroquinone or p-benzoquinone) was added. Table 8.6 summarizes experiments performed using two substrates and lists values of the second-order rate constant (k_x) calculated when measurable amounts of dissolution occurred.

The secondary substrate employed, its concentration relative to the primary substrate, and the pH all determine the extent to which the secondary substrate interferes with the reaction with primary

Table 8.6 Two-Substrate Experiments

Trial	pH	Mn_T	Primary Substrate	Secondary Substrate	Secondary Primary	k_x (1/mole min.)
KX	7.16	2.82E-5M	-	3.00E-3M Sorbitol	-	-
KV	7.21	2.82E-5M	2.54E-5M HQ	-	-	3.96E+2
KW	7.19	2.82E-5M	2.54E-5M HQ	3.00E-3M Sorbitol	118.	2.64E+2
XP	7.77	2.85E-5M	2.00E-4M Q	-	-	@4.68E-8
AK	7.77	2.89E-5M	2.00E-4M Q	2.00E-3M Sorbitol	10.0	@4.72E-8
GT	7.79	2.83E-5M	-	1.00E-3M Salicylate	-	-
XK	7.75	2.85E-5M	5.00E-5M HQ	-	-	1.38E+2
XQ	7.79	2.87E-5M	5.00E-5M HQ	2.00E-3M Salicylate	40.1	1.36E+2
XR	7.78	2.87E-5M	5.00E-5M HQ	2.00E-4M Salicylate	4.01	1.48E+2
XS	7.79	2.87E-5M	5.00E-5M HQ	2.00E-5M Salicylate	.401	1.42E+2
XY	6.81	2.81E-5M	-	2.00E-3M Phthalate	-	-
XX	6.81	2.81E-5M	2.00E-5M HQ	-	-	4.39E+2
XW	6.82	2.81E-5M	2.00E-5M HQ	2.00E-3M Phthalate	100.	3.27E+2
XD	7.17	2.63E-5M	-	1.00E-3M Oxalate	-	-
XX	6.81	2.81E-5M	2.00E-5M HQ	-	-	4.39E+2
XZ	6.83	2.81E-5M	2.00E-5M HQ	2.00E-3M Oxalate	100.	4.69E+2

HQ = Hydroquinone

Q = p-Benzoquinone

@ = $\frac{\Delta[Mn^{2+}]}{\Delta t}$diss. (for the first 3 points)

substrate. If an absorption mechanism is operative, then increasing the concentration of secondary substrate relative to the primary substrate causes a greater fraction of surface sites to be bound to the secondary substrate, slowing the reaction down. Since the pK_a's of the primary and secondary substrates are different, a change in pH affects the amount of each substrate adsorbed differently. Inhibition is therefore a function of pH.

Concentrations of sorbitol or phthalate 100 times higher than hydroquinone substrate lowered the dissolution rate by 30%. Oxalate at similar concentrations had no effect on the reaction rate; values of k_x that are within 10% of one another are not significantly different. Sorbitol does not interfere with dissolution by p-benzoquinone, or salicylate with dissolution by hydroquinone, but lower concentrations of secondary substrate were employed in those experiments.

In any case, inhibition by sorbitol, salicylate, phthalate, and oxalate was quite small under the conditions examined. High concentrations of secondary substrate relative to the reactive substrate were necessary to observe any effect. Most likely, the affinity of these substrates for surface sites was low, probably lower than hydroquinone and p-benzoquinone. Substrates that form strong surface complexes are expected to have a much greater effect on the reaction rate. Phosphate, for example, strongly inhibited the reaction, even at concentrations lower than the reactive substrate (Section 7.11B.). It should be possible to find organic adsorbates

inert to oxidation that have the same effect.

8.6 Conclusions

8.6A. Reaction Mechanism

Relative reactivities of twenty-seven organic substrates with manganese oxide were reported in this chapter, and can be used to distinguish between different possible reaction mechanisms.

Apparent second-order rate constants for dissolution by catechol, hydroquinone, and resorcinol differ by more than three orders of magnitude. Since all three substrates have similar pK_a's, their ability to form metal-hydroxy bonds are similar. They differ, however, in their ability to form a second bond to the central metal ion and the ease with which they are oxidized. The overall activation enthalpies required to form surface complexes are similar for these substrates, and it is therefore unlikely that the large differences in second-order rate constants are caused by the adsorption step being rate-limiting. Instead, reaction within the surface complex, such as electron transfer, must be rate-limiting.

A number of arguments can be developed to show that electron transfer occurs via a bonded, rather than a non-bonded mechanism. Oxidation of catechols and hydroquinones by $Fe^{III}(bipy)_3$, a substitution inert complex, was studied by Mentasti and Pelizzetti (1976). This reaction occurs by a non-bonded mechanism. Five of the substrates examined in their work were also studied here; the second-order rate constants for oxidation by each oxidant and the potential (for the reaction $Q + 2H^+ + 2e^- = QH_2$) of each

organic substrate are listed in Table 8.7. Figure 8.23 plots the log of the second-order rate constant for reaction with each oxidant against the potential of the organic substrate. A linear relationship between the log of the rate constant and the substrate potential is observed for oxidation by $Fe^{III}(bipy)_3$, consistent with Marcus Theory. The energy required to distort substrate molecules to form the transition state for reaction with $Fe^{III}(bipy)_3$ has been found to be approximately the same for the catechols and hydroquinones examined (Mentasti and Pelizzetti, 1976).

There is no relation between the potential of the substrate and the reaction rate with manganese oxide suspensions for these five substrates. The assumption is made that the pH dependence of the potential is the same for all five substrates; otherwise, relative differences in standard potential (at pH=0) would not be representative of changes in overall free energy of reaction at pH 7.2.

Catechols, having hydroxy substituents ortho to one another, react more quickly than hydroquinones, despite less favorable overall free energy of reaction for quinone formation (E^o for catechol is higher than for hydroquinone). Ortho-hydroxy substituents can chelate metal ions, whereas para-hydroxy substituents of hydroquinone cannot. Chelation may enhance surface complex formation with catechols relative to hydroquinones. Increased surface coverage by catechols would allow them to dissolve the oxide more quickly, assuming that rates of electron transfer within surface complexes of different substrates are approximately equal.

Table 8.7 Correlation between reaction rate and substrate potential.

Substrate	E^{0*} (volts) (1)	Manganese Oxide k_x (l./mole·sec.) (2)	$Fe^{III}(bipy)_3$ κ (l./mole·sec.) (3)
Hydroquinone	.699	2.33×10^{0}	1.0×10^{7}
2,5-diOH	.77	1.72×10^{0}	3.5×10^{5}
Catechol	.792	2×10^{1}	6.4×10^{5}
3,4-diOH	.883	2×10^{1}	1.3×10^{4}
4-Nitrocatechol	.95	5.33×10^{0}	1.1×10^{3}

(1) From Table 2.2.

(2) This Study
(Ionic Strength = 5.00×10^{-2}M, $p^aH = 7.2$)

(3) From Mentasti and Pelizzetti (1976)
(Ionic Strength = 1.00M, 1.00M $HClO_4$).

* E^0 is for the reaction Quinone + $2H^+$ + $2e^-$ = Dihydroxybenzene

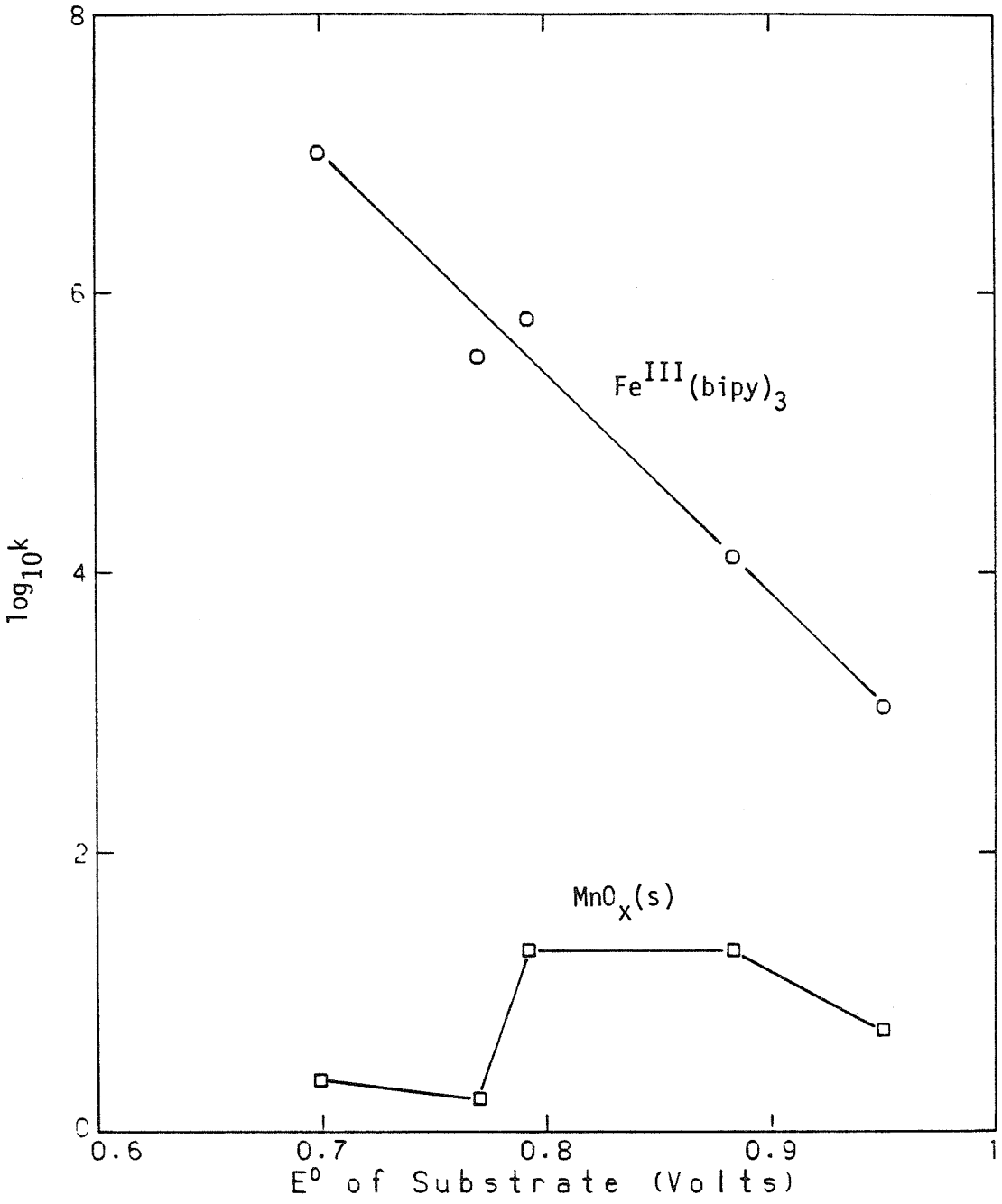

Figure 8.23 Oxidation of ortho- and para-dihydroxybenzenes by $Fe^{III}(bipy)_3$ (Mentasti and Pelizzetti, 1976) and by manganese oxide suspensions (this study). The graph shows the relationship between the log of the rate constants and the oxidation potentials of the substrates.

If the functional groups that bind metal ions are the same for two substrates, their relative reactivities reflect their relative potentials:

Functional Groups	Reactivity with Manganese Oxides
ortho-dihydroxy	Catechol (E^o .792v) > 4-Nitrocatechol (E^o .95v)
	Catechol (E^o .792v) $\approx$ 3,4-diOH (E^o .883v)
para-dihydroxy	Hydroquinone (E^o .699v) > 2,5-diOH (E^o .77v)
meta-dihydroxy	Orcinol ($E_{1/2}$ .700v) > Resorcinol ($E_{1/2}$ .800v)

For each pair, the reaction rate was greater for the substrate with the lower potential, for which the overall free energy of reaction was more favorable. The only exception was the catechol/3,4-diOH pair; despite a difference in potential of 0.1 volts, the two substrates were oxidized at approximately the same rate.

The following observations are consistent with a bonded mechanism for the oxidation of organics by manganese oxides:

(i) The order of the reaction with respect to hydroquinone was 1.0, possibly decreasing to lower values at high concentrations of hydroquinone. This is consistent with adsorption of substrate prior to electron transfer (Section 7.12A.,B.).

(ii) Adsorption of calcium and phosphate on the surface caused a decrease in the reaction rate, most likely by blocking surface sites

(Section 7.12C.).

(iii) The rate of oxidation of organic substrates bears no clear relation to the potentials of the substrate redox couples (which are related to the overall free energy of reaction).

(iv) Oxidation of organics by Mn^{III} solute complexes occurs via bonded mechanisms, and reaction with oxide surface sites should occur via a similar mechanism.

If the bonded mechanism is correct, then differences in reactivity among the organic substrates are caused by different affinities for the oxide surface; the reaction proceeds more quickly when the surface coverage is high. Cases were described above in which substrates with lower potentials reacted more quickly. In these cases, ring substituents which increased the potential may have also made them weaker complexing agents.

8.6B. Oxidation Products

The oxidation products formed by reaction with manganese oxide can be compared to those from other oxidants. Absorbance spectra recorded during oxidation of hydroquinone, 2,5-diOH, 4-nitrocatechol, and syringic acid all indicate that only one oxidized product is formed, probably the corresponding benzoquinone. Oxidation of thiosalicylate and ascorbate also produced single products, most likely dithiosalicylate dimer and hydroxyascorbate, respectively (Section

8.1B.).

Catechol, 3,4-diOH, and 3-methoxycatechol polymerize when oxidized by manganese oxide. This is evident from the increase in absorbance over a wide range wavelength range. Polymerization probably occurred by addition of semiquinone radical to either unreacted substrate or to the o-benzoquinone product.

Dissolution of manganese oxide by hydroquinone and p-benzoquinone was studied in the presence of organic substrates that by themselves did not react with the oxide. A slight inhibitory effect was observed in a few cases (Section 8.5B.). In order for the secondary substrate to compete for surface sites, it must either be a relatively strong complexing agent or must be present in considerable excess.

8.6C. Reaction with Natural Organics

The dissolution of manganese oxide by marine fulvic acids was observed in this chapter to be a photocatalyzed reaction, confirming the results of Sunda et al. (1982). Experiments with the 27 substrates shown in Figures 8.1 and 8.2 were performed only in room light, so it is not known whether more intense light also would enhance dissolution by those substrates. In any case, the flux of solar radiation under natural conditions is probably important in determining the rate of dissolution.

Dempsey (1981) studied the adsorption of fulvic acid on manganese oxides that were prepared by permanganate oxidation. The amount adsorbed increased with decreasing pH. In Section 8.4 it was noted that measurable photo-assisted reduction occurred at pH 6.35, but not

at pH 7.7. This probably reflects greater adsorption of fulvic acid at the lower pH.

Under natural conditions, the concentration of actively reducing organics may be quite low compared to the total concentration of organics. The surface sites may be blocked by organics inert to oxidation. The affinity of non-reactive natural organics for the surface and their relative concentration must be known before the dissolution rate can be accurately predicted.

8.6D. Solubilization of Manganese Oxides in Nature

The results reported in this chapter can be used to predict rates of solubilization of manganese oxides in natural systems. Ionic strength, pH, anionic and cationic adsorbates, and temperature are known to influence the reaction rate with hydroquinone (Chapter 7). Rates of dissolution by different organic substrates differ considerably; rate constants listed in Table 8.4 differ by more than 3 orders of magnitude. Bacterial exudates, short-lived radical species, and other reactive organics may be present, along with more refractory compounds. Estimates of the dissolution rate require some knowledge of the relative concentrations of these compounds.

Dissolution by marine fulvic acid was described in Section 8.4. In the presence of the mercury-arc lamp, 200 mg/l of marine fulvic acid at pH 6.4 dissolved manganese oxide at a rate comparable to that caused by 110 mg/l ($1x10^{-3}$M) resorcinol at pH 7.2. Taking into account the relative differences in pH and organic substrate concentration, photoactivated fulvic acid was less reactive than resorcinol. The

reaction without illumination was still slower. This fulvic acid sample, however, may be less reactive than is typical for natural organics. Given that catechol, vanillic acid, and syringic acid have been identified in chemical degradation products of humic material (Section 1.4), the reactivity of most natural organics may in fact lie somewhere in the middle of Table 8.4.

As discussed in Section 1.4, low molecular-weight aliphatic acids (Barcelona, 1980) as well as glycolic, lactic, oxalic, and succinnic acids (Peltzer and Bada, 1981) may make up a significant fraction of dissolved organic matter in anoxic pore waters. Reactivities of the simple aliphatic alcohols and acids examined in this chapter were low.

The rate constant for reaction with resorcinol will be used to estimate the rate of dissolution of manganese oxides in natural systems. If the reactivity of the marine fulvic acid is representative of natural organic material, then calculations based on resorcinol provide an upper limit for the rate of dissolution. If this sample is unusually refractory, the rate of dissolution under natural conditions may be faster than calculated.

(i) Solubilization of Manganese Oxide Crusts

The experimentally derived rate law (equation 7.15) will now be used to estimate the flux of dissolved manganese from near-shore sediments, which can then be compared to rates actually measured. Balzer (1982) found that the flux of dissolved manganese from reducing sediments was as high as 1.13×10^{-3} moles/meter^2/day. The source of this manganese was mainly the 3 cm thick manganese oxide

crust. Eaton (1979) observed an even higher flux (7.0×10^{-3} moles/meter^2/day) from anoxic Chesapeake Bay sediment.

Consider the dissolution of a 3 cm-thick oxide crust, such as the one described by Balzer (1982), at the onset of reducing conditions. This layer contained about 1.9×10^{-4} moles of solid manganese oxides per liter of sediment. If the oxide surface area was about 50 meter^2/gm, then there were 8.2×10^{-3} meters^2 of oxide surface per liter of sediment. k_A can be calculated for reaction with resorcinol by assuming that the reaction orders with respect to reductant substrate and H^+ concentrations for resorcinol are the same as for hydroquinone. The value of k_A is 2×10^{-3} $(\text{liters/mole})^{0.46}(1/\text{sec.})(\text{liters/meter}^2)$.

An estimate of the DOC (dissolved organic carbon) in sediment pore waters is necessary to find the rate of dissolution. DOC pore water concentrations were not measured by Balzer (1982) or by Eaton (1979). Barcelona (1982) measured DOC (dissolved organic carbon) values in anoxic Santa Barbara Basin sediment in the range 75 to 150 mg/l. The flux of dissolved manganese from a square meter of sea floor can be calculated using equation 7.15 for different DOC values in the sediment pore water (pH 8.0).

DOC	[Resorcinol]	Flux from Sediment
10 mg/l	1.4×10^{-4}M	1.31×10^{-3} moles/meter^{2}day
50	6.9×10^{-4}	6.48×10^{-3}
100	1.4×10^{-3}	1.31×10^{-2}

The fluxes calculated for 10 and 50 mg/l DOC are within the range measured from actual sediments.

(ii) Solubilization of Oxide Particles in Anoxic Bottom Waters

In basins where the oxic/anoxic boundary is in the water column, particles settling down past the boundary are dissolved. The time required for dissolving half of the particle volume ($t_{1/2}$) can be estimated using equation 7.14, making the same assumptions as for dissolution in sediments. An additional assumption is made, namely that the area to volume ratio of the particles in the water column is the same as for the particles used in the dissolution experiments, so that equation 7.14 is valid. k_1 for resorcinol is 2×10^1 $(\text{liters/mole})^{1.46}(1/\text{sec})$. Values of $t_{1/2}$ are calculated for reaction at pH 8.

DOC	[Resorcinol]	$t_{1/2}$
10mg/l	1.4×10^{-4}M	16 Days
50	6.9×10^{-4}	3.3
100	1.4×10^{-3}	1.6

Similar calculations for reaction with 10 mg/l (DOC) of 3-methoxycatechol and hydroquinone gave $t_{1/2}$ values of 4.5 minutes and 49 minutes respectively.

CHAPTER 9

CONCLUSIONS

9.1 General Comments

Generalities about the reaction of organic substrates with manganese oxide surfaces can now be proposed based on experimental results from preceding chapters. Given information about the structures of natural organics, rates of solubilization of manganese oxides under different environmental situations can be estimated. Oxidation by iron and manganese oxides may be an important degradative mechanism for some natural organics.

9.2 Reaction between Manganese Oxide Surfaces and Organic Substrates.

Conclusions from the experiments discussed in Chapters 7 and 8 are summarized below.

9.2A. Surface Site-Binding Model

(i) Dissolution of manganese oxides by organics was surface-reaction controlled; the reaction was too fast to be explained by release of Mn^{3+} into solution prior to reduction.

(ii) The reaction was first order with respect to hydroquinone concentration below 6×10^{-4}M. At higher concentrations, the order dropped below unity. Rate constants for organics having similar functional groups varied by more than 3 orders of magnitude, too wide a

range for reactions limited by the rate of adsorption. Reaction within the surface complex, most likely electron transfer, was therefore the rate-limiting step.

(iii) A fractional dependence (below 0.5) with respect to hydrogen ion concentration was observed. According to the surface site-binding model, formation of the surface complex ≡MnQH prior to electron transfer would result in a zero-order dependence on H^+. If the complex $\equiv MnQ^-$ was formed, the reaction would be first-order. The fractional order observed may be caused by involvement of H^+ in the electron-transfer step, or in the dissolution of Mn(II) surface sites.

(iv) Phosphate and calcium inhibited the dissolution of manganese oxides by adsorbing on oxide surface sites.

(v) The reaction rate was proportional to $(Mn_T - [Mn^{2+}]diss.)$, the amount of undissolved manganese oxide at time t, during the first half of the reaction. According to the surface site-binding model, this implies that the ratio of oxide surface sites to undissolved manganese oxide was constant.

9.2B. Reactivity of Organic Substrates

(i) Two of the fifteen aromatic substrates and eight of the twelve aliphatic substrates did not dissolve appreciable amounts of manganese

oxide under the conditions studied (see section 8.2A). Saturated alcohols, aldehydes, ketones, and carboxylic acids showed no reactivity, except for pyruvic and oxalic acids.

(ii) Catechols, hydroquinones, methoxyphenols, and resorcinols, as well as ascorbate, reduced and dissolved manganese oxide suspensions at appreciable rates. With the exception of ascorbate, molecules such as these have been shown to form the core structure of humic substances. Humic substances should therefore dissolve manganese oxides under natural conditions.

(iii) Differences in the ability of organic substrates to form surface complexes appear to be more important in determining relative reactivities than differences in the overall free energy of reaction.

(iv) Electron-withdrawing substituents on aromatic substrates lower the reaction rate with manganese oxides, while electron-donating groups increase the reaction rate.

(v) Photoreduction of manganese oxides by marine humic substances, first observed by Sunda et al. (1982) has been confirmed. Dissolution by marine fulvic acid was faster at lower pH values, most likely caused by greater adsorption of fulvic acid on the oxide surface.

9.3 Implications for Manganese Geochemistry

Estimates of rates of dissolution of manganese oxides by organics in different environments can be made based on this work, as shown in Section 8.6D. The surface site-binding model can be used to predict how changes in chemical and physical parameters influence the reaction rate.

The shortcomings of the present state of knowledge are evident in the broad uncertainties in these estimates. Accurate estimates require knowing the concentrations and reactivities of natural organics in the location of interest. Field measurements of DOC and the relative amounts of humics, low molecular-weight acids, and bacteria metabolites would make these calculations more meaningful. Better documentation of the valence and physical characteristics of natural manganese oxides would also be useful.

The results are sufficient to conclude that dissolution of manganese oxides is enhanced when the concentration of organics (especially phenolic compounds) is high, the pH is low, and coverage of oxides by specifically adsorbing ions is low. Dissolution in deep-sea sediments is slow because organics are present at low concentrations, and possibly resistant to oxidation. Dissolution occurs much more quickly in coastal waters because of the large flux of fresh organic material.

9.4 Implications for Degradation of Organics in Natural Waters

The importance of manganese oxides in the degradation of organic matter in natural systems depends upon the rate of reaction with

manganese oxides relative to rates of oxidation by oxygen and other inorganic species, and to rates of organic decomposition by organisms. As Table 8.4 shows, the susceptibility of different classes of organics to reaction with manganese oxide varies by more than three orders of magnitude. Oxidation by manganese oxides may be a significant degradative pathway for some organic compounds, but not for others.

Manganese oxides are reduced by marine humics in the presence of oxygen (Sunda et al., 1982), indicating that at least a fraction of natural organics are oxidized at an appreciable rate by manganese oxides. In solutions containing 5 mg/l marine humic acid, 10^{-6}M Mn^{2+}, and 10^{-8}M manganese oxide at pH 8.1, the rate of dissolution was 1.6×10^{-13} moles/liter/sec in sunlight and 5.7×10^{-14} moles/liter/sec in the dark (Sunda et al., 1982). Under these conditions, the rate of oxidation of Mn^{2+} by oxygen is approximately 1.2×10^{-11} moles/liter/sec, using rate constants determined by Matsui (1973). Because oxidation of Mn^{2+} by oxygen and reduction of manganese oxides by natural organics is occurring simultaneously, manganese can catalyze the oxidation of organics.

Iron has been shown to catalyze the oxygenation of humics in surface waters illuminated by sunlight (Miles and Brezonik, 1981). Oxidation of Fe(II) is considerably faster than oxidation of Mn(II) under the same conditions (Stumm and Morgan, 1981). For this reason, iron oxides are regenerated by oxygenation at a faster rate than are manganese oxides. As long as reduction by organics is not rate-limiting, catalysis of organic matter oxygenation by iron will be

faster. This is probably the case in surface waters, since iron is readily photoreduced by natural organics.

In both deep-sea and coastal marine sediments, manganese oxides are dissolved at higher E_h values than iron oxides (Froelich et al., 1979; Balzer, 1982). Once oxygen is depleted, oxidation by manganese oxides is predominant. Within the region of active manganese oxide reduction, the relative concentrations of different natural organic compounds may be determined by their susceptibility to oxidation by manganese oxides.

Microbial mediation is an important factor in many redox reactions in nature. Hydroxylation and ring-cleavage of phenolic compounds, for example, can be performed by bacteria (Chapman, 1972). The presence of molecular oxygen, however, is required; in anoxic conditions, other reactions take place instead, such as the formation of chlorophenols (Chapman, 1972). Non-biological reactions predominate either when substrates necessary for microbial degradation are unavailable, or when microbes lack pathways necessary to degrade particular compounds. Under such conditions, oxidation by iron and manganese oxides may be important in degrading some natural organics.

9.5 Suggestions for Future Research

The experimental system described in this thesis can be used to provide new information not just about the reactions of manganese oxides, but also about reactions at oxide-water interfaces in general. Understanding how an adsorbate binds to an oxide surface and how electron transfer occurs within the surface complex can prove valuable

in understanding other heterogeneous reactions.

The relationship between adsorption equilibria and chemical reactions at surface sites should be studied in more detail. This was difficult to do for the reaction of hydroquinone with the manganese oxide surface, since surface sites were continually being lost by dissolution following electron transfer. Adsorbate species inert to reaction are useful in examining surface coverage, as illustrated by the study of dissolution in the presence of phosphate (Chapter 7). A careful study of adsorption kinetics and equilibria of inert adsorbates should aid in understanding how such adsorbates inhibit the dissolution reaction.

Dissolution of a manganese oxide surface can be considered a surface-site dependent reaction, because surface complexes must form in order for electron-transfer reactions leading to dissolution to occur. Surface microstructure models are also used to describe how physical surface structure (such as ledges and kinks) affects the rate of dissolution (Section 4.4C.). The surface site-binding model accommodates effects due to surface microstructure by allowing a distribution of the energies of surface sites.

The distribution of surface site energies can be found by measuring the apparent activation energy of reaction with reductant substrate as the concentration of inert adsorbate is increased. As the fraction of surface sites bound to inert adsorbate is increased, the apparent activation energy should increase, since a greater fraction of the most reactive sites are occupied by inert adsorbate. Only less

reactive sites are available to the reductant substrate.

Release of reduced manganese from the crystal lattice may be a slow step in the overall dissolution reaction. If the concentration of organic substrate is increased and the pH lowered, the rate of the surface redox reaction may be fast enough that dissolution is rate-limiting. Under these conditions, it could be determined whether or not H^+ or other solute species aid in the release of reduced manganese.

The rates of reduction of different manganese oxide mineral phases may vary considerably, and merits further study. The pH_{zpc} values of oxides used in this work were higher than those of manganese oxides used in most adsorption studies to date, which have pH_{zpc} values below 3 (Balistrieri and Murray, 1982). Adsorption of organics onto oxides having widely different pH_{zpc} values will be quite different. Because the lattice structure of different phases are not the same, the geometry of the surface sites will differ as well, and will modify the reactivity of the surface. The distribution of Mn(II), Mn(III), and Mn(IV) within the lattice may also have an effect on the reaction rate. Suspensions of different phases can be prepared and reacted with organic substrates. Differences in rate may be shown to be a function of surface properties and crystal structure.

Little time was spent in this study identifying the oxidized organic products. As mentioned in Section 9.4, iron and manganese oxides may decompose organic compounds that are resistant to reaction with oxygen or to microbial action. If the kinds of oxidized products

formed from these reactions are known, then shifts in the distribution of organic compounds during oxidation can be understood. Reactions with iron and manganese oxides may also create unique products that are not formed by other processes.

Dissolution by fulvic acid was enhanced by illumination with the mercury arc lamp. Illumination activated the fulvic acid molecules, making them more reactive reductants. Radicals generated by other reactions in natural waters (such as autoxidation) may be particularly reactive with manganese oxide surfaces. Activation mechanisms may have to be taken into account when estimating the rate of dissolution of manganese oxides in some situations, and should therefore be studied more carefully.

In order to make predictions about the rate of solubilization of manganese oxides under natural conditions, more must be known about the reactivity of natural organics from different locations. The fulvic acid sample used in Chapter 8 may prove to be more refractory than organics found in anoxic sediments. Dissolved organic matter in anoxic pore waters may be quite unlike organic matter collected in oxic zones. Comparing the reactivities of organics from different locations would not only make calculations of rates of solubilization more realistic, it would also aid in identifying the structures of organics, since the reactivities of different structural groups are known from reactions with model compounds.

APPENDIX: PREPARATION OF MANGANESE OXIDE SUSPENSIONS

B(1) 1/26 81

3000 mls D_2H_2O	3.10×10^{-4} M Mn_T (Total Manganese)
2 mls 15M NH_4OH	9.3×10^{-3} M NH_4OH
100 mls 9.5×10^{-3} M $MnCl_2$	p^aH before reaction: 9.0
3102 mls	

3000 mls of deaerated D_2H_2O (deionized,distilled water) and 2 mls of 15M NH_4OH were added to a four liter jacketed beaker. Concentrated HCl was added until the pH was 8.4. The solution was aerated with pure oxygen, using a pasteur pipette, and stirred with a Teflon stir bar. The reaction vessel was thermostated to 25°C. After addition of stock $MnCl_2$, NH_4OH was added dropwise until the pH was 9.0. The solution turned a light brown, opaque color after about one hour. A coating of brown particles formed on all glass surfaces, which could be disturbed by jarring. Oxygen aeration, thermostating, and stirring were turned off after nine hours, and the vessel sealed. After 9 days, the vessel contained a clear, colorless solution overlying settled dark brown floc.

N(2) 4/18/81

8000 mls D_2H_2O	5.62×10^{-4} M Mn_T
45 mls 0.10M $MnCl_2$, 0.10M HCl	3.7×10^{-2} M NH_4OH
20 mls 15M NH_4OH	p^aH before reaction: 10.8
8065 mls	

20 mls of 15M NH_4OH were added to 8000 mls of D_2H_2O in a 10 liter separatory funnel and stirred with a plastic paddle. The solution was vigorously bubbled with pure oxygen using a 10 cm long cylindrical gas dispersion tube (glass). After 20 minutes, 45 mls of stock $MnCl_2$ solution were quickly added. Stirring and bubbling were continued for another hour, after which the solution was sealed. A deep brown suspension was formed, that rapidly settled out.

N(3) 4/18/81

8000 mls D_2H_2O	3.76×10^{-4} M Mn_T
30 mls .10M $MnCl_2$, 0.10M HCl	9.3×10^{-3} M NH_4OH
5 mls 15M NH_2OH	p^aH before reaction: 10.4
8035 mls	p^aH after two weeks: 10.0

5 mls of 15M NH_4OH were added to 8000 mls of D_2H_2O in a 10 liter separatory funnel and stirred with a plastic paddle. HP (high purity) nitrogen was bubbled in at a moderate rate for 20 minutes before $MnCl_2$ addition using the 10 cm gas dispersion tube. Prior to addition, stirring was turned up to maximum and nitrogen flow rate increased. The solution turned opaque, light brown upon addition of 30 mls of $MnCl_2$ stock solution. One minute after addition, gas flow

was switched to pure oxygen, and bubbled vigorously. After 15 minutes, gas flow and stirring were turned down to moderate rates. Gas bubbling and stirring were turned off after one hour and the vessel sealed. A rust-brown suspension was formed by this procedure. Although a small portion settled out within a day, most of the particles remained in suspension for a number of months.

N(7) 11/13/81

7890 mls QH_2O
80 mls 2.0M NH_4OH
100 mls 4.0×10^{-2}M $MnCl_2$
7970 mls

4.93×10^{-4}M Mn_t
2.0×10^{-2}M NH_4OH
p^aH before reaction: 10.7
p^aH after reaction: 10.5

80 mls of 2.0M NH_4OH were added to 7890 mls of QH_2O (milli-Q water) in a 10 liter separatory funnel. HP nitrogen was bubbled in using a 10 cm long cylindrical gas dispersion tube (glass) at a rate of 1500cm^2/min. The sealed vessel was stirred at a moderate rate for one hour. Immediately before addition of stock $MnCl_2$ solution, the nitrogen flow rate was increased to 7000 cm^2/min and stirring turned up to maximum. 100 mls of stock $MnCl_2$ were quickly poured in from a graduated cylinder; one wash with QH_2O was also added. After two minutes, the nitrogen purging was replaced by pure oxygen, bubbled at a rate of 10,000 cm^2/min for ten minutes. Bubbling of 5000 cm^2/min at a moderate stirring rate followed for an additional 90 minutes. After this time stirring was turned off and the solution sealed. The suspension consisted of finely dispersed, dark brown

particles. No settling had occurred.

N(8) 11/20/81

7720 mls QH_2O	4.97×10^{-4}M Mn_T
80 mls 2.0M NH_4OH	2.0×10^{-2}M NH_4OH
100 mls 8.0×10^{-3}M $MnCl_2$	p^aH before reaction: 10.8
100 mls 3.2×10^{-2}M $MnCl_2$	
8000 mls	

This experiment was an attempt to produce particles of larger diameter than those produced in N(7). The procedure followed in N(7) was followed except that $MnCl_2$ was added in to the vessel in two additions. The first 100 ml addition 8.0×10^{-3}M $MnCl_2$ was followed in two minutes by the addition of 100 mls of 3.2×10^{-2}M $MnCl_2$. It was hoped that Mn^{2+} added in the second addition would precipitate onto particles formed by the first addition.

N(9) 4/11/82

7890 mls QH_2O	4.96×10^{-4}M Mn_T
80 mls 2.0M NH_4OH	2.0×10^{-2}M NH_4OH
100 mls 4.0×10^{-2}M $MnCl_2$	p^aH before reaction: 10.8
7970 mls	

The procedure outlined for the preparation of suspension N(7) was followed.

H(1) 7/26/81

2000 mls QH_2O	4.32×10^{-4} M Mn_T
100 mls 0.46M NH_4OH	2.0×10^{-2} M NH_4OH
100 mls 9.9×10^{-3} M $MnCl_2$	1.0×10^{-2} M H_2O_2
100 mls 0.23M H_2O_2	p^aH before reaction: 10.5
2300 mls	

100 mls of .46M NH_4OH were added to 2000 mls QH_2O in a 3 liter round bottom flask and stirred at a moderate rate with a plastic paddle. HP nitrogen was bubbled in at 2300 cm^2/min using the 10 cm gas dispersion tube for one hour. Five minutes before $MnCl_2$ addition, bubbling was increased to 3900 cm^2/min and stirring set to maximum. 100 mls of stock $MnCl_2$ solution were then added; the solution turned light brown in color, which did not intensify appreciably after the first minute. Five minutes later, nitrogen bubbling was turned off and 100 mls of hydrogen peroxide (in excess) were added. The solution slowly turned a deep orange-brown color. After an additional hour of moderate stirring the vessel was sealed. The suspension was stable with respect to settling for over six months.

H(2) 7/26/81

	4.32×10^{-4} M Mn_T
2000 mls QH_2O	1.0×10^{-2} M H_2O_2
100 mls 9.9×10^{-2} M $MnCl_2$	2.0×10^{-2} M NH_4OH
100 mls .23M NH_4OH	p^aH before NH_4OH addition: 5.3
2300 mls	p^aH after NH_4OH addition: 10.3

100 mls of stock $MnCl_2$ and H_2O_2 solutions were added to

2000 mls of QH_2O in a 3 liter round bottom flask. The solution was stirred at a moderate rate using a plastic paddle and bubbled with 2300 cm^2/min of HP nitrogen (using the 10 cm gas dispersion tube). Throughout this time, the solution remained clear and colorless. Stirring was increased to the maximum and nitrogen bubbling turned off before stock NH_4OH solution was added. Upon addition of NH_4OH, the solution immediately turned black brown. After one hour, the stirring was turned off and the vessel sealed. The suspension was stable with respect to settling for over six months.

REFERENCES

Adamson, A.W. (1976) The Physical Chemistry of Surfaces, 3rd. edit.. John Wiley & Sons, NY.

Anderegg, G. (1977) Critical Survey of Stability Constants of EDTA Complexes. IUPAC Chemical Data Series #14, Pergamon Press, Oxford.

Atkinson, R.J., A.M. Posner, and J.P. Quirk (1971) Proc. Roy. Soc. London, Series A 324:247.

Atkinson, R.J., A.M. Posner, and J.P. Quirk (1972) J. Inorg. Nucl. Chem. 34:2201-2211.

Baker, W.E. (1973) Geochim. et Cosmochim. Acta 37:269-281.

Balistrieri, L.S. and J.W. Murray (1982) Geochim. et Cosmochim. Acta 46:1041-1052.

Balzer, W. (1982) Geochim. et Cosmochim. Acta 46:1153-1161.

Barcelona, M.J. (1980) Geochim. et Cosmochim. Acta 44:1977-1984.

Bard, A.J. and L.R. Faulkner (1980) Electrochemical Methods. John Wiley & Sons, NY.

Barnes, M.A., and W.C. Barnes (1978) Organic Compounds in Lake Sediments. In: Lakes: Chemistry, Geology, Physics. A. Lehrman, edit., Springer-Verlag, NY.

Bartusek, M. and A. Okac (1961) Collect. Czech. Communs. 26:883,2174. As cited in: A. F. Trotman-Dickenson, execut. edit. (1973) Comprehensive Inorganic Chemistry. Compendium Publ., Elmsford, NY.

Becka, J. and J. Jokl (1971) Collect. Czech. Communs. 36:2467,3263.

Benson, D. (1972) Oxidation-Reduction Reactions between Complexes of Different Metals. Chapter 3 in: Comprehensive Chemical Kinetics, Vol 7. C.M. Banford and C.F.H. Tipper, edits., Elsevier, Amsterdam.

Benson, D.(1976) Mechanisms of Oxidations by Metal Ions. Elsevier, Amsterdam.

Berner, R.A. (1980) Early Diagenesis: A Theoretical Approach. Princeton University Press, Princeton, NJ.

Berner, R.A. and J.W. Morse (1974) Am. J. Sci. 274:108-134.

Bishop, L.A. and L.K.J. Tong (1965) J. Am. Chem. Soc. 87:501-505.

Bricker, O. (1965) Am. Mineral. 50:1296-1354.

Brown, S.B. (1980) Ultraviolet and Visible Spectroscopy. Chapter 2 in: Spectroscopy for Biochemists. S.B. Brown, edit., Academic Press, London.

Burns, R.G. and V.M. Burns (1977) Mineralogy In: Marine Manganese Deposits. G.P.Glasby, edit. Elsevier, Amsterdam.

Burns, R.G. and V.M. Burns (1979) Manganese Oxides. In: Marine Minerals. R.G. Burns, edit., MSA Short Course Notes, Vol.6.

Buser, W. and P. Graf (1955) Helv. Chem. Acta 38:810-829. As cited in Giovanoli (1980).

Carey, F.A. and R.J. Sundberg (1977) Advanced Organic Chemistry, Parts A and B. Plenum, NY.

Castellan, G.W. (1971) Physical Chemistry, 2nd. Edit.. Addison-Wesley, Reading, MA.

Chapman, P.J. (1972) An Outline of Reaction Sequences Used for the Bacterial Degradation of Phenolic Compounds. In: Degradation of Synthetic Organic Molecules in the Biosphere. Nat. Acad. Sci.

Christman, R.F. and M. Ghassemi (1966) J. Am. Water Works Assoc. 58:723-741.

Clark, W.M. (1960) Oxidation-Reduction Potentials of Organic Systems. Williams & Wilkins Co., Baltimore, MD.

Cotton, F.A., and G. Wilkinson (1980) Advanced Inorganic Chemistry, 4 th. Edit.. John Wiley & Sons, NY.

Cranwell, P.A. (1975) Environmental Organic Chemistry of Rivers and Lakes, both Water and Sediment. In: Environmental Chemistry, Vol. 1:22-54. G. Eglinton, edit., The Chemical Society, Burlington House, London.

Crerar, D.A. and H.L. Barnes (1974) Geochim. et Cosmochim. Acta 38:279--300.

Davies, G. (1969) Coord. Chem. Rev. 4:199-224.

Davies, G. (1975) Inorg. Chim. Acta 14:L13-L14.

Davies, G., L.J. Kirschenbaum, and K. Kustin (1968) Inorg. Chem. 7:146-154.

Davies, G., and K. Kustin (1969) Trans. Farad. Soc. 65:1630-7.

Davis, J.A. and R. Gloor (1981) Environ. Sci. Technol. 15:1223--1229.

Davis, J.A., R.O. James, and J.O. Leckie (1978) J. Colloid. Interfac. Sci. 63:480-499.

Davis, J.A. and J.O. Leckie (1978) Environ. Sci. Technol. 12:1309--1315.

Degens, E.T. (1965) Geochemistry of Sediments; A Brief Survey. Prentice-Hall, Englewood Cliffs, NJ.

Dempsey, B.A. (1981) The Protonation, Calcium Complexation, and Adsorption of a Fractionated Aquatic Fulvic Acid. Ph.D. Thesis, University of North Carolina, Chapel Hill, NC.

Diebler, H. and M. Eigen (1966) Proc. 9th. Intern. Conf. Coord. Chem., St. Moritz, Switzerland, p.360.

Diebler, H. and N. Sutin (1964) J. Phys. Chem. 68:174-180.

Drummond, A.Y. and W.A. Waters (1953A) J. Chem. Soc. (1953):435-443.

Drummond, A.Y. and W.A. Waters (1953B) J. Chem. Soc. (1953):2836-37.

Drummond, A.Y. and W.A. Waters (1953C) J. Chem. Soc. (1953):3119-23.

Drummond, A.Y. and W.A. Waters (1954) J. Chem. Soc. (1954):2456-67.

Drummond, A.Y. and W.A. Waters (1955) J. Chem. Soc. (1955):497-504.

Drummond, A.Y. and W.A. Waters (1958) J. Chem. Soc. (1958):2129-2133.

Eaton, A. (1979) Geochim. et Cosmochim. Acta 43:429-432.

Eisenreich, S.J., R.T. Bannerman, and D.E. Armstrong (1975) Environ. Lett. 9:43-53.

Elderfield, H. (1976) Mar. Chem. 4:103-132.

Emerson, S., R.E. Cranston, and P.S. Liss (1979) Deep-Sea Research 26A:859-878.

Emerson, S., S. Kalhorn, L. Jacobs, B.M. Tebo, K.H. Nealson, and R.A. Rossen (1982) Geochim. et Cosmochim. Acta 46:1073-1079.

Feitknecht, W.,P. Brunner, and H.R. Oswald (1962) Z. Anorg. Allg. Chem. 316:154-160.
As cited in Stumm and Giovanoli (1976).

Fleischer, M. (1980) Glossary of Mineral Species. Mineralogical Record, Tucson, AZ.

Froelich, P.N., G.P. Klinkhammer, M.L. Bender, N.A. Luedtke, G.R. Heath, D. Cullen, P. Dauphin, D. Hammond, B. Hartman, V. Maynard (1979) Geochim. et Cosmochim. Acta 43:1075-1090.

Frost, A.A. and R.G. Pearson (1961) Kinetics and Mechanism, 2nd. Edit.. John Wiley & Sons, NY.

Fukuzumi, S., Y. Ono, and T. Keii (1973) Bull. Chem. Soc. Jap. 46:3353-3355.

Fukuzumi, S., Y. Ono, and T. Keii (1975) Int. J. of Chem. Kinetics 7:535-546.

Gadsden, J.A. (1975) Infared Spectra of Minerals and Related Inorganic Compounds. Butterworths, Essex, Great Britian.

Gardiner, W.C. (1972) Rates and Mechanisms of Chemical Reactions. W.A. Benjamin, Menlo Park, CA.

Giovanoli, R. (1980) On natural and synthetic manganese nodules. In: Geology and Geochemistry of Manganese, Vol.1.. I.M. Varentsov and Gy. Grasselly, edits., Budapest.

Giovanoli, R., P. Burki, M. Giuffredi, and W. Stumm (1975) Chimia 29:517-520.

Giovanoli, R. and U. Leuenberger (1969) Helv. Chim. Acta 52:2333-47.

Giovanoli, R., E. Stahli, and W. Feitknecht (1970) Helv. Chim. Acta 53:209-220.
As cited in Burns and Burns (1979).

Gjessing, E.T. (1976) Physical and Chemical Characteristics of Aquatic Humus. Ann Arbor Science, Ann Arbor, MI.

Goodman, B.A. and M.V. Cheshire (1975) Geochim. et Cosmochim. Acta

39:1711-1713.

Gordon, G. and H. Taube (1962) Inorg. Chem. 1:69-75.

Guy, R.D. and C.L. Chakrabarti (1976) Canad. J. Chem. 54:2600-2611.

Harvey, G.R., D.A. Boran, L.A. Chesal, and J.M. Tokar (1982) Submitted to Mar. Chem..

Hayward, D.O. and B.M.W. Trapnell (1964) Chemisorption. Butterworths, London.

Hem, J.D. (1965) USGS Water Supply Paper 1667-D.

Hem, J.D. (1981) Geochim. et Cosmochim. Acta 45:1369-1374.

Hiemenz, P.E. (1977) Principles of Colloid and Surface Chemistry. Marcel Dekker, NY.

Hingston, F.J. (1981) A Review of Anion Adsorption. Pages 51-90 in Adsorption of Inorganics at Solid-Liquid Interfaces. M.A. Anderson and A.J. Rubin, edits., Ann Arbor Science, Ann Arbor MI.

Huyser, E.S. (1970) Free Radical Chain Reactions. Wiley-Interscience, NY.

Kemp, T.J. (1972) Oxidation-Reduction Reactions between Covalent Compounds and Metal Ions. In: Comprehensive Chemical Kinetics, Vol. 7. C.H. Bamford and C.F.H. Tipper, edit., Elsevier, Amsterdam.

Kemp, T.J. and W.A. Waters (1964A) J. Chem. Soc. (1964):339-347.

Kemp, T.J. and W.A. Waters (1964B) J. Chem. Soc. (1964):1192-1194.

Kemp, T.J. and W.A. Waters (1964C) J. Chem. Soc. (1964):1489-93.

Kessick, M.A., J. Vuceta, and J.J. Morgan (1972) ES&T 6:642-644.

Kochi, J.K. (1973) Oxidation-Reduction Reactions of Free Radicals and Metal Complexes. Chapter 11 in: Free Radicals, Vol. 1. J.K. Kochi, edit., Wiley-Interscience, NY.

Kortum, G., W. Vogel, and K. Andrussow (1961) Dissociation Constants of Organic Acids in Aqueous Solution. IUPAC Section of Analytical Chemistry, Commission on Electrochemical Data, Butterworths, London.

Kummert, R. and W. Stumm (1980) J. Colloid. Interfac. Sci. 75:373--385.

Laidler, K.J. (1965) Chemical Kinetics, 2nd. Edit.. McGraw-Hill, NY.

Land, H. and W.A. Waters (1958) J. Chem. Soc. (1958):2129-2133.

Larson, R.A. and J.M. Hufnal (1980) Limno. Oceanogr. 25:505-512.

Latimer, W.M. (1952) Oxidation Potentials, 2nd. edit.. Prentice-Hall Inc., Englewood Cliffs, NJ.

Levesley, P, and W.A. Waters (1955) J. Chem. Soc. (1955):217-221.

Li, Y.H., J. Bischoff, and G. Mathieu (1969) Earth and Planet. Sci. Lett. 7:265-270.

Liao, W., R. Christman, J.D. Johnson, D.S. Millington, and J.R. Hass (1982) Environ. Sci. Technol. 16:403-410.

Littler, J.S. (1970) The Mechanisms of Oxidation of Organic Compounds with One-Equivalent Metal-Ion Oxidants: Bonded and and Non-Bonded Electron-Transfer. Chapter 15 in: Essays on Free-Radical Chemistry. Chem. Soc. Spec. Publ. 24.

Martell, A.E., and R.M. Smith (1977) Critical Stability Constants, Vol. 3: Other Organic Ligands. Plenum Press, NY.

Matsui, I. (1973) Catalysis and kinetics of manganese ion oxidation oxidation in aqueous solution and adsorbed on the surfaces of solid oxides. Ph.D. Thesis, Lehigh University, Bethlehem, PA.
As cited in W. Sung (1981).

McDonald, P.D. and G.A. Hamilton (1973) Mechanisms of Phenolic Oxidative Coupling Reactions. Chapter II in: Oxidation in Organic Chemistry. W.S. Trahanosky, edit., Academic Press, NY.

Mentasti, E. and E. Pelizzetti (1976) Transit. Met. Chem. 1:281-284.

Mentasti, E., E. Pelizzetti, E. Pramauro, and G. Giraudi (1975) Inorg. Chim. Acta 12:61-65.

Mentasti, E., E. Pelizzetti, E. Pramauro, and G. Giraudi (1975) J. Inorg. Nucl. Chem. 37:537-540.

Mihailovic, M.L. and Z. Cekovic (1971) Oxidation and Reduction of

Phenols. Chapter 10 in: The Chemistry of the Hydroxyl Group, Part 1. S. Patai, edit., Interscience Publ., London.

Miles, C.J. and P.L. Brezonik (1981) Environ. Sci. Technol. 15:1089--1095.

Miller, F.A. and C.H. Wilkins (1952) Anal. Chem. 52:1253-1294.

Mopper, K., R. Dawson, G. Liebezeit, and V. Ittekkot (1980) Mar. Chem. 10:55-66.

Mopper, K. and K. Larsson (1978) Geochim. et Cosmochim. Acta 42:153--163.

Morgan, J.J. (1964) Chemistry of Aqueous Manganese (II) and (IV). Ph.D. Thesis, Harvard University, Cambridge, MA.

Morgan,J.J. (1967) Chemical Equilibria and Kinetic Properties of Manganese in Natural Waters. In: Principles and Applications of Water Chemistry. S.D. Faust and J.V. Hunter, edit., John Wiley & Sons, NY.

Murray, J.W. and P.G. Brewer (1977) Mechanisms of Removal of Manganese, Iron, and Other Trace Metals from Seawater. In: Marine Manganese Deposits. G.P. Glasby, edit., Elsevier, Amsterdam.

Musso, H. (1967) Phenolic Coupling. Chapter 1 in: Oxidative Coupling of Phenols. W.I. Taylor and A.R. Battersby, edits., Marcell Dekker, NY.

Musso, H. and H. Dopp (1967) Chem. Ber. 100:3627.
As cited in Mihailovic and Cekovic (1971).

Musso, H., U. von Gizycki, H. Kramer, and H. Dopp (1965) Chem. Ber. 98:3952-63.

Norwood, D.L, J.D. Johnson, R.F. Christman, J.R. Hass, and M.J. Bobenrieth (1980) Environ. Sci. Technol. 14:187-190.

O'Connor, J.T. (1971) Iron and Manganese. Chapter 11 in: Water Quality and Treatment. H.B. Crawford and D.N. Fischel, edits., Amer. Water Works Assoc., McGraw-Hill, NY.

Ono, Y., T. Matsumura, and S. Fukuzumi (1977) J. Chem. Soc. Perkin II (1977):1421-1424.

Pankow, J.F. (1978) The Dissolution Rates and Mechanisms of Tetragonal Ferrous Sulfide (Mackinawite) in Anoxic Aqueous

Systems. Ph.D. Thesis, California Institute of Technology, Pasadena, CA.

Panpalia, S.S., R.N. Mehrotra, and R.C. Kapoor (1974) Indian J. Chem. 12:1166-70.

Parfitt, R.L., A.R. Fraser, and V.C. Farmer (1977) J. Soil Sci. 28: 289-296.

Pe´ligot, E. (1844) Ann. Chim. Physique 12:533.
" " (1845) " " " 14:240.
As cited by Valverde and Wagner (1976).

Pelizzetti, E. and E. Mentasti (1977) Z. Phys. Chem. 105:21-34.

Pelizzetti, E., E. Mentasti, and G. Giraudi (1975) Inorg. Chim. Acta 15:L1-L3.

Peltzer, E.T. and J.L. Bada (1981) Geochim. et Cosmochim. Acta 45: 1847-1854.

Perrin, D. (1979) Stability Constants of Metal-Ion Complexes, Part B: Organic Ligands. IUPAC Chemical Data Series #22, Pergamon Press, Oxford.

Pickering, W.F. (1966) Rev. Pure and Appl. Chem. 16:185-208.

Pitt, W.W., R.L. Jolley, and C.D. Scott (1975) Environ. Sci. Technol. 9:1068-1073.

Potter, R.M. (1979) The tetravalent manganese oxides: Clarification of their structural variations and relationships and characterization of their occurrence in the terrestrial weathering environment as desert varnish and other manganese-oxide concentrations. Ph.D. Thesis, California Institute of Technology, Pasadena, CA.

Potter, R.M. and G.R. Rossman (1979A) Am. Mineral. 64:1199-1218.

" " (1979B) " " 64:1219-1226.

Purcell, K.F. and J.C. Kotz(1977) Inorganic Chemistry. W.B. Saunders, Philadelphia, PA.

Rinehart, K.L. (1973) Oxidation and Reduction of Organic Compounds. Prentice-Hall, Englewood Cliffs, NJ.

Ronlan, A. (1976) Hydroxy Compounds: Phenols. Chapter XI-2(2.3) in: Encyclopedia of Electrochemistry of the Elements. A.J. Bard

and H. Lund, edit., Marcell Dekker, NY.

Rosseinsky, D.R. (1963) J. Chem. Soc. (1963):1181-1186.

Schindler, P.W. (1981) Surface Complexes at Oxide/Water Interfaces. In: Adsorption of Inorganics at Solid-Liquid Interfaces. M.A. Anderson and A.J. Rubin edits., Ann Arbor Science, Ann Arbor, MI.

Schnitzer, M. and S.U. Kahn (1972) Humic Substances in the Environment. Marcell Dekker, NY.

Schnitzer, M. and S.U. Kahn (1978) Soil Organic Matter. Elsevier, NY.

Schoettle, M. and G.M. Friedman (1971) Bull. Geol. Soc. Am. 82:101-110.

Schwarzenbach, G. and H. Flaschka (1961) Complexometric Titrations. Methuen & Co., London.

Scott, A.I. (1967) Some Natural Products Derived by Phenol Oxidation. Chapter 2 in: Oxidative Coupling of Phenols. W.I. Taylor and A.R. Battersby edits., Marcell Dekker, NY.

Senesi, N., Y. Chen, and M. Schnitzer (1977) Soil Biol. Biochem. 9: 397-403.

Serjeant, E.P. and B. Dempsey (1979) Ionization Constants of Organic Acids in Aqueous Solution. IUPAC Chemical Data Series #23, Pergamon Press, Oxford.

Sheldon, R.A. and J.K. Kochi (1973) Oxidat. and Combust. Rev. 5:135-242.

Sheldon, R.A. and J.K. Kochi (1981) Metal-Catalyzed Oxidations of Organic Compounds. Academic Press, NY.

Sigg, L. and W. Stumm (1980) Colloids and Surfaces 2:101-117.

Skogerboe, R.K. and S.A. Wilson (1981) Anal. Chem. 53:228-232.

Skoog, D.A. and D.M. West (1976) Fundamentals of Analytical Chemistry. Holt,Rinehart, & Wilson, NY.

Smith, I.C.P. and A. Carrington (1967) Mol. Phys. 12:439-448.

Spencer, D.W. and P.G. Brewer (1971) J. Geophys. Res. 76:5877-5892.

Steelink, C. (1977) J. Chem. Educ. 54:599-603.

Stewart, R.(1964) Oxidation Mechanisms. W.A. Benjamin Inc., NY.

Stumm, W. G. Furrer, and B. Kunz (1982) VI th. Internat. Summer Conference on the Chemistry of Solid/Liquid Interfaces, Cavtat, Yugoslavia, pp. 66-70.

Stumm, W. and R. Giovanoli(1976) Chimia 30:423-425.

Stumm, W., R. Kummert, and L. Sigg (1980) Croat. Chem. Acta 53:291-312.

Stumm, W. and J.J. Morgan (1981) Aquatic Chemistry, 2nd. edit.. Wiley-Interscience, NY.

Sunda, W.G., S.A. Huntsman, and G.R. Harvey (1982) Nature, in press.

Sung, W. (1981) Catalytic effects of the -FeOOH (lepidocrocite) surface on the oxygenation removal kinetics of Fe(II) and Mn(II). Ph.D. thesis, California Institute of Technology, Pasadena, CA.

Sung, W. and J.J. Morgan (1981) Geochim. et Cosmochim. Acta 45:2377-2383.

Swinbourne, E.S. (1971) Analysis of Kinetic Data. Appleton-Century-Crofts, NY.

Theis, T.L. and P.C. Singer (1974) Environ. Sci. Technol. 8:569-573.

Tipping, E. (1981A) Chem. Geol. 33:81-89.

Tipping, E. (1981B) Geochim. et Cosmochim. Acta 45:191-199.

Valverde, N. (1976) Ber. Bunsenges. Phys. Chem. 80:333-340.

Valverde, N. and C. Wagner (1976) Ber. Bunsenges Phys. Chem. 80:330-333.

Vetter, K.J. (1967) Electrochemical Kinetics; Theoretical Aspects. Academic Press, NY.

Waters, W.A. (1958) Quart. Rev. 12:277-300.

Waters, W.A. (1964) Mechanisms of Oxidation of Organic Compounds. John Wiley & Sons, NY.

Waters, W.A. and J.S. Littler (1965) Oxidation by Vanadium(V), Cobalt(III), and Manganese(III). Chapter III in: Oxidation in Organic Chemistry, Vol. 5. K.B. Wiberg edit., Academic

Press, NY.

Wells, C.F. (1965) Nature 205:693-694.

Wells, C.F. and C. Barnes (1968) J. Chem. Soc.(A) (1968):1626-1630.

Wells, C.F. and C. Barnes (1971A) J. Chem. Soc.(A) (1971):1405-1408.

Wells, C.F. and C. Barnes (1971B) Trans. Farad. Soc. 67:3297-3305.

Wells, C.F., C. Barnes, and G. Davies (1968) Trans. Farad. Soc. 64: 3069-3076.

Wells, C.F. and G. Davies (1965) Nature 205:692-693.

Wells, C.F. and G. Davies (1967) Trans. Farad. Soc. 63:2737-44.

Wells, C.F. and L.V. Kuritsyn (1970) J. Chem. Soc. A (1970):676.

Wells, C.F. and D. Whatley (1972) J. Chem. Soc. Faraday I. 68:434.

Wilson, D.E. (1980) Geochim. et Cosmochim. Acta 44:1311-1317.

Wilson, S.A. and J.H. Weber (1979) Chem. Geol. 26:345-354.

Yates, D.E. and T.W. Healy (1975) J. Colloid. Interfac. Sci. 52: 222-228.

Yates, D.E., S. Levine, and T.W. Healy (1974) J. Chem. Soc. Farad. Trans. I 70:1807-1818.

Zabin, B.A. and H. Taube (1964) Inorg. Chem. 3:963-968.

Zutic, V. and W. Stumm (1981) Unpublished manuscript.